

# ***In vivo* analysis of endocytic and biosynthetic transport to the plant vacuole**

## **Dissertation**

der Mathematisch-Naturwissenschaftlichen Fakultät  
der Eberhard Karls Universität Tübingen  
zur Erlangung des Grades eines  
Doktors der Naturwissenschaften  
(Dr. rer. nat.)

vorgelegt von  
Florian Fäßler  
aus Reutlingen

Tübingen  
2018

Gedruckt mit Genehmigung der Mathematisch-Naturwissenschaftlichen Fakultät der  
Eberhard Karls Universität Tübingen.

Tag der mündlichen Qualifikation:	30.07.2018
Dekan:	Prof. Dr. Wolfgang Rosenstiel
1. Berichterstatter:	Prof. Dr. Peter Pimpl
2. Berichterstatter:	Prof. Dr. Gerd Jürgens

## **Danksagung**

Zum Ende meiner Doktorarbeit wird es nun auch Zeit allen Danke zu sagen, die mich während meiner Zeit am ZMBP unterstützt haben.

Zu allererst will ich mich bei Herrn Prof. Dr. Peter Pimpl für das spannende Forschungsthema, seine Begeisterung für die Entwicklung neuer Methoden und den mir überlassenen wissenschaftlichen Freiraum herzlich bedanken. Vielen Dank außerdem, für all das vermittelte Wissen, sei es handwerklich oder fachlich und die Möglichkeit an mehreren internationalen Konferenzen sowie an einem wissenschaftlichen Austauschprogramm mit der chinesischen Universität Hong Kongs teilzunehmen.

Ich danke Herrn Prof. Dr. Gerd Jürgens für seine konstruktive Kritik und die erteilten Ratschläge sowie für die Erstellung des Zweitgutachtens dieser Arbeit.

Vielen Dank auch an die gesamte ehemalige AG PP. Danke Simone Frühholz, Fabian Künzl, Diana Vrajkovic und Jasmin Ehrismann für die großartige Zusammenarbeit, das tolle Arbeitsklima und alles, was ich von euch gelernt habe. Außerdem danke ich Richard Gavidia und Natalie Gerling für die technische Unterstützung. An unsere Hiwis Kerstin Balke, Elisabeth Lang und Anna Zucker: Es hat mich gefreut, mit euch zu arbeiten und euch auch das ein oder andere beizubringen.

Ich danke allen Kolleginnen und Kollegen der Entwicklungsgenetik für die gute Arbeitsatmosphäre, jede Hilfe und eine schöne Zeit im Labor als auch abseits davon.

Abschließend möchte ich mich noch bei meiner Familie und meinen Freunden dafür bedanken, dass sie mich über die gesamte Promotion hinweg unterstütz, motiviert und, wenn notwendig, auch vom Forschungsalltag abgelenkt haben.

## Contents

Danksagung.....	3
1. Summary .....	6
2. Zusammenfassung .....	7
3. Publication List .....	9
3.1 Receptor-mediated sorting of soluble vacuolar proteins ends at the <i>trans</i> -Golgi network/early endosome.....	9
3.2. Nanobody-triggered lockdown of VSRs reveals ligand reloading in the Golgi ..	9
3.3. <i>In vivo</i> interaction studies by measuring Förster resonance energy transfer through fluorescence lifetime imaging microscopy (FRET/FLIM) .....	9
3.4. Dissection of the ESCRT-II assembly and recruitment by nanobody-based <i>in vivo</i> precipitation (iVIP) .....	9
4. Personal Contribution.....	10
4.1. Receptor-mediated sorting of soluble vacuolar proteins ends at the <i>trans</i> -Golgi network/early endosome.....	10
4.2. Nanobody-triggered lockdown of VSRs reveals ligand reloading in the Golgi	10
4.3. <i>In vivo</i> interaction studies by measuring Förster resonance energy transfer through fluorescence lifetime imaging microscopy (FRET/FLIM) .....	11
4.4. Dissection of the ESCRT-II assembly and recruitment by nanobody-based <i>in vivo</i> precipitation (iVIP) .....	11
5. Introduction.....	12
5.1. The plant endomembrane system and the plasma membrane .....	12
5.1.1. The endoplasmic reticulum .....	12
5.1.2. The Golgi apparatus .....	13
5.1.3. The plasma membrane.....	14
5.1.4. The <i>trans</i> -Golgi network .....	15
5.1.5. The multivesicular body.....	16
5.1.6. The vacuole .....	16



5.2. The secretory pathway .....	17
5.2.1. Secretion .....	17
5.2.2. Receptor-mediated vacuolar sorting .....	19
5.3. The endocytic pathway .....	22
5.3.1. Endocytosis .....	23
5.3.2. Endosomal sorting complexes required for transport (ESCRT-) mediated vacuolar sorting .....	24
6. Objectives .....	27
7. Results and discussion .....	30
7.1. Compartment-specific analysis of the interaction between vacuolar sorting receptors and their cargo .....	30
7.1.1 <i>In vivo</i> interaction studies by measuring Förster resonance energy transfer through fluorescence lifetime imaging microscopy (FRET/FLIM) .....	34
7.1.2 Receptor-mediated sorting of soluble vacuolar proteins ends at the <i>trans</i> -Golgi network/early endosome .....	36
7.2. Nanobody-triggered lockdown of VSRs reveals ligand reloading in the Golgi	39
7.3. Dissection of the ESCRT-II assembly and recruitment by nanobody-based <i>in vivo</i> precipitation (iVIP) .....	42
7.3.1 Localization of Vacuolar Protein Sorting 22 (VPS22), VPS25 and VPS36	42
7.3.2 VPS22, VPS25 and VPS36 interact <i>in vivo</i> .....	43
7.3.3 Establishing the indirect <i>in vivo</i> precipitation (iVIP) in plant cells .....	45
7.3.4 The plant ESCRT-II complex contains two VPS25 subunits .....	48
7.4. Closing remarks .....	50
8. References .....	54
9. Appendix .....	73
Receptor-mediated sorting of soluble vacuolar proteins ends at the <i>trans</i> -Golgi network/early endosome .....	73

## 1. Summary

Proteins in the plasma membrane allow a cell to exchange molecules and information with its environment. This, however, urges for a stringent regulation of these proteins. A mechanism to regulate them is their degradation. This process involves their ubiquitination, endocytosis and transport into the lumen of a vacuole. The degradative function of vacuoles depends on proteolytic enzymes, which reach that very organelle via a different route. They are synthesized in the endoplasmic reticulum and transported via the endomembrane system. Vacuolar transport of those soluble proteins depends on sorting receptors separating vacuolar from secretory cargo. To get a better understanding on how the trafficking of membrane-bound and soluble cargo to the vacuole is spatially and temporally coordinated, we aimed at characterizing the machinery mediating those processes. Therefore we employed nanobody-epitope interactions to create intra-cellular setups, which allow for transport- and interaction-analyses of proteins via confocal microscopy.

We revealed that vacuolar sorting receptors interact with their ligands in the endoplasmic reticulum and the Golgi apparatus but not in the *trans*-Golgi network and the multivesicular body, by performing Fluorescent Lifetime Imaging to measure Förster Resonance Energy Transfer (FRET-FLIM; Künzli et al., 2016). To create suitable reporters for compartment-specific FRET-FLIM measurements, we exploited the nanobody-epitope interaction. This allowed us to link the ligand binding domain of vacuolar sorting receptors to membrane markers for the individual compartments of the endomembrane system. We were further able to not only demonstrate that those sorting receptors recycle but also to identify the *cis*-Golgi as the destination of their retrograde transport (Frühholz et al., 2018). These discoveries were based on the combination of two nanobody-epitope pairs that we used for post-translational labelling and trapping of vacuolar sorting receptors. Concerning the machinery, which mediates transport of to-be-degraded plasma membrane proteins, we analyzed the Endosomal Sorting Complex Required For Transport II (ESCRT-II). Here, we employed FRET-FLIM to show that Vacuolar Protein Sorting 22 (VPS22), 25 and 36 interact to form this complex of interest. We pushed the limits of nanobody-based approaches by employing membrane-anchored nanobodies to import the co-immune precipitation approach into living cells. This enabled us to perform *in vivo* studies, which showed that ESCRT-II contains two VPS25 moieties (Fäßler et al., prepared manuscript).

## 2. Zusammenfassung

Die Proteine in ihrer Plasmamembran ermöglichen es einer Zelle Moleküle und Informationen mit ihrer Umgebung auszutauschen. Diese wichtige Funktion erfordert allerdings auch eine stringente Regulation. Ein Kontrollmechanismus ist hierbei der gezielte Abbau beteiligter Proteine in einem lytischen Kompartiment. Diese werden dabei ubiquitiniert, endozytiert und zur Degradation in das Lumen einer Vakuole transportiert. Um die lytische Funktion der Vakuole aufrecht zu erhalten, muss diese über einen anderen Weg mit Hydrolasen versorgt werden. Diese Enzyme werden im endoplasmatischen Retikulum synthetisiert und durch das Endomembransystem transportiert. Der zugrundeliegende vakuoläre Transport löslicher Proteine hängt von Sortierungsrezeptoren ab, die vakuoläre von sekretorischer Fracht trennen.

Um besser zu verstehen wie der Transport von membrangebundener und löslicher vakuolärer Fracht räumlich und zeitlich koordiniert wird, hatten wir es uns zum Ziel gesetzt die Maschinerie, die diese beiden Transportwege aufrechterhält, zu charakterisieren. Um dies umzusetzen, verwendeten wir Nanobody-Antigen Paare, die es uns erlaubten Versuchsbedingungen innerhalb von lebendigen Zellen zu schaffen, welche Transport- und Interaktionsstudien mittels konfokaler Mikroskopie ermöglichten.

Wir zeigten, dass vakuoläre Sortierungsrezeptoren ihre Fracht ausschließlich im endoplasmatischen Retikulum und im Golgi-Apparat nicht aber im *trans*-Golgi Netzwerk oder in den multivesikulären Körpern binden, indem wir FRET-FLIM anwendeten (Künzl et al., 2016). Um die entsprechenden Reporter zu generieren, verwendeten wir Interaktion zwischen einem Nanobody und seinem Antigen, welche die Liganden bindende Domäne der vakuolären Sortierungsrezeptoren an die Membranmarker für die unterschiedlichen Kompartimente des pflanzlichen Endomembransystems koppelte. Zudem konnten wir beweisen, dass diese Rezeptoren rezyklieren und identifizierten die *cis*-Cisterne des Golgi-Apparats als Zielkompartiment des rückwärtsgerichteten Transports von vakuolären Sortierungsrezeptoren (Frühholz et al., 2018). Diese Entdeckungen basierten auf der Kombination von zwei Nanobody-Antigen Paaren, die genutzt wurden, um vakuoläre Sortierungsrezeptoren post-translational zu markieren und gezielt ihren Weitertransport zu verhindern. Bezüglich des Transports von zu degradierenden Plasmamembranproteinen zur Vakuole konzentrierten wir uns auf einen der

endosomalen Sortierungskomplexe (ESCRT-II). Mittels FRET-FLIM zeigten wir, dass dieser aus den drei Untereinheiten „Vacuolar Protein Sorting“ 22 (VPS22), 25 und 36 aufgebaut ist. Durch die Verwendung von an Membranen verankerten Nanobodies konnten wir sogar die Co-Immun-Präzipitation, einen klassischen biochemischen Ansatz, in lebenden Zellen implementieren. Dies erlaubte es uns *in vivo* Studien durchzuführen, welche aufzeigten, dass ein einzelner ESCRT-II Komplex zwei VPS25 Untereinheiten besitzt (Fäßler et al., vorbereitetes Manuskript).

### 3. Publication List

This dissertation is built upon the following four manuscripts.

#### Publications:

#### **3.1 Receptor-mediated sorting of soluble vacuolar proteins ends at the *trans*-Golgi network/early endosome**

Fabian Künzl, Simone Frühholz, **Florian Fäßler**, Beibei Li and Peter Pimpl

*Nature Plants* 2, Article number: 16017 (2016), doi:10.1038/nplants.2016.17

#### **3.2. Nanobody-triggered lockdown of VSRs reveals ligand reloading in the Golgi**

Simone Frühholz, **Florian Fäßler**, Üner Kolukisaoglu and Peter Pimpl

*Nature Communications* 9, Article number: 643 (2018), doi:10.1038/s41467-018-02909-6

#### **3.3. *In vivo* interaction studies by measuring Förster resonance energy transfer through fluorescence lifetime imaging microscopy (FRET/FLIM)**

**Florian Fäßler** and Peter Pimpl

In: Jiang L. (eds) Plant Protein Secretion. Methods in Molecular Biology, vol 1662. Humana Press, New York, NY, doi: 10.1007/978-1-4939-7262-3\_14

#### Prepared manuscripts:

#### **3.4. Dissection of the ESCRT-II assembly and recruitment by nanobody-based *in vivo* precipitation (iVIP)**

**Florian Fäßler**, Yonglun Zeng, Jasmin S. Ehrismann, Simone Frühholz, Carsten-Leo Greve, Liwen Jiang and Peter Pimpl (prepared manuscript)

## **4. Personal Contribution**

### **4.1. Receptor-mediated sorting of soluble vacuolar proteins ends at the *trans*-Golgi network/early endosome** (Künzli et al., 2016)

I designed, cloned and characterized the membrane anchors, the Nanobody-Luminal-Binding-Domain Fusion (LBD-Nb) and the vacuolar reporter used as acceptor for FRET-FLIM assays. Using the GFP-based membrane anchors, I applied FLIM to relatively compare the compartments of the endomembrane system regarding their pH. This enabled us to make predictions concerning which compartments should allow for VSR-ligand interaction and showed that fluorescence-lifetime-based approaches, such as FRET-FLIM, are applicable within the plant endomembrane system. I co-developed the strategy to link a soluble LBD-Nb via an antibody-antigen interaction to compartmental membrane anchors, which ultimately allowed for localization-specific interaction studies. Furthermore, FRET-FLIM measurements were established in the laboratory together with F.K. and experiments were designed and analyzed in collaboration with F.K., S.F. and P.P.

### **4.2. Nanobody-triggered lockdown of VSRs reveals ligand reloading in the Golgi** (Frühholz et al., 2018)

I co-developed the concept of post-translationally labelling recycling receptors at the TGN via endocytosis of fluorescent proteins. This strategy was applied to show that retrogradely transported vacuolar sorting receptors are targeted to the *cis*-Golgi. The anchors used to lock down recycled proteins within specific compartments are based on a membrane marker system devised by me. Furthermore, I provided data indicating that truncated VSRs lacking the LBD, which have been commonly used to study VSR-trafficking, are not recycled. This caused us to employ markers based on full-length receptors to visualize recycling and prevented possible false-negative results. Experimental design and analysis was performed together with S.F., Ü.K. and P.P.

### **4.3. *In vivo* interaction studies by measuring Förster resonance energy transfer through fluorescence lifetime imaging microscopy (FRET/FLIM)**

(Fäßler and Pimpl 2017)

The strategy to employ an RFP-anti-GFP-nanobody fusion as universal acceptor for a GFP-tagged donor in FRET-FLIM applications was devised by me. I designed the experiment, performed FRET-FLIM measurements and CLSM imaging and conducted the statistical analysis. The article was written together with P.P.

### **4.4. Dissection of the ESCRT-II assembly and recruitment by nanobody-based *in vivo* precipitation (iVIP)** (Fäßler et al., prepared manuscript)

I developed the concept of the Indirect *In Vivo* Precipitation (iVIP) and performed all experiments. This includes localization of fluorescently tagged ESCRT-II subunits by CLSM analysis and interaction studies performed via FRET-FLIM and iVIP. The ultrastructural localization studies and the segregation analysis were conducted in cooperation with Y.Z. and J.S.E., respectively. Furthermore, I produced the antigens for the immunization program that generated the polyclonal antisera against *Arabidopsis thaliana* VPS22, VPS25 and VPS36. I characterized these sera as well as the anti- $\alpha$ -synuclein-nanobody-peroxidase fusion protein for their possible applications via co-immune precipitation and Western blot. The experiments were designed and analyzed in collaboration with J.S.E., S.F., C.G., L.J and P.P. and the article was written together with P.P.

## **5. Introduction**

Survival of cells depends on the efficient management of a plethora of chemical reactions at the very same point in time. Many of those reactions require different physicochemical conditions to take place at a sufficient rate. Eukaryotic cells evade this predicament by providing several different reaction chambers, which are separated by membranes and are called compartments. Each of them harbors specific internal conditions, such as fine-tuned ion concentrations or characteristic sets of metabolites and enzymes. Furthermore, compartments exhibit a distinct lipid and protein composition in their limiting membranes, which can be recognized on a molecular level. Such a recognition is necessary for targeted transport of molecules between different compartments. This transport between compartments allows for the coordinated conduction of extensive multi-step reactions, which could not be performed within a single reaction chamber.

### **5.1. The plant endomembrane system and the plasma membrane**

The plant endomembrane system is one framework of several individual compartments interconnected by highly specific transport events. It consists of the Endoplasmic Reticulum (ER), the different stacks of the Golgi apparatus, the *Trans*-Golgi Network (TGN), which functions also as Early Endosome (EE), the Multivesicular Body (MVB), which is also referred to as Late Endosome (LE), and the different types of vacuoles. The Plasma Membrane (PM), even though not being an “endo”-membrane is also closely linked to this system, via multiple transport routes.

#### **5.1.1. The endoplasmic reticulum**

The ER is a dynamic network of interconnected tubular and cisternal structures. Classically, the ER is considered to consist of three sub-compartments: The smooth ER, the rough ER and the nuclear envelope (Staehein, 1997). The smooth ER is tubular and is a location of lipid synthesis. The cisternal rough ER is decorated with ribosomes and allows for co-translational translocation of proteins into the endomembrane system. The nuclear envelope forms together with the nuclear pore complexes the barrier that separates the nucleus from the cytosol. Regarding its chemical properties, the ER possesses a neutral pH of about 7, is likely to be enriched in  $\text{Ca}^{2+}$ -ions and provides an oxidative environment, which allows for the formation of



intra- and intermolecular di-sulfide bonds between the cysteine residues of proteins (Hiatt et al., 1989; Hwang et al., 1992; Frand et al., 2000; Stael et al., 2012; Martiniere et al., 2013; Shen et al., 2013).

The common pathway for soluble proteins to enter the ER lumen and for single- and multi-spanning transmembrane proteins to be inserted into the ER membrane is the co-translational translocation. This process starts with the recognition of an N-terminal signal sequence, which is present in a nascent peptide chain, by the signal recognition particle (SRP) and leads to a temporary stop of translation (Walter et al., 1981; Meyer et al., 1982; Wiedmann et al., 1987). Translation is reinitiated after recruitment of the ribosome-peptide-SRP complex to the ER membrane and occurs through the translocation pore into the lumen of the ER, where the signal peptide is cleaved off (Blobel and Dobberstein, 1975; Walter and Blobel, 1981b, a). One central role of the ER is to provide appropriate conditions for native folding and initial N-glycosylation of newly synthesized proteins (Liu and Howell, 2016). For this, the Binding Proteins (BiPs) bind preferentially to non-polar regions of peptides during translocation. They thereby prevent premature folding and aggregation during synthesis (Flynn et al., 1991; Vitale et al., 1995). BiPs, together with other chaperones like calreticulin and calnexin, further facilitate folding until native protein configurations are achieved (Hammond et al., 1994; Hammond and Helenius, 1994; Jin et al., 2007). The latter two are part of an ER-specific quality control mechanism that targets misfolded proteins for further rounds of refolding or the ER-Associated Degradation Pathway (ERAD; Hammond et al., 1994; Muller et al., 2005; Jin et al., 2007; Quan et al., 2008; Huttner et al., 2014). Proteins handed over to ERAD are relocated to the cytosol, ubiquitinated and ultimately degraded by the proteasome. Released native proteins will, if they are not ER-resident, be further transported to their respective destinations (Muller et al., 2005; Stevenson et al., 2016).

### **5.1.2. The Golgi apparatus**

The Golgi apparatus is a direct downstream compartment of the ER. It consists of individual stacks of cisternae. Those stacks are polarly organized and single cisternae are accordingly categorized into being part of the *cis- medial-* or *trans-*Golgi. In mammalian cells, the *trans-*most cisterna serves as the TGN sorting proteins either towards the PM or the lysosome (Griffiths and Simons, 1986). However, this is not the

case in plants. Here, the Golgi apparatus and the TGN are different entities (Viotti et al., 2010). While individual stacks and TGNs can be associated with each other, both of those highly motile organelles can also move independently within the cell (Nebenführ et al., 1999; Foresti and Denecke, 2008; Viotti et al., 2010; Uemura et al., 2014). The plant TGN is, furthermore, not only involved in sorting proteins towards the PM or endosomal compartments, it also acts as an early endosome (Dettmer et al., 2006; Viotti et al., 2010).

The Golgi apparatus, itself, is involved in modifying the glycosylations, which are attached to glyco-proteins in the ER, the synthesis of complex polysaccharides, which are deployed as building blocks for the plant cell wall, and protein transport towards the PM as well as the TGN (Driouich et al., 1993; Crowell et al., 2009; Viotti et al., 2010). In this regard, earlier steps in the saccharide remodeling reaction chains occur in the *cis*-cisternae, while latter steps occur in the *medial*- and the *trans*-cisternae (Zhang and Staehelin, 1992). The total amount of stacks per cell and the organization of individual stacks vary dependent on the developmental stage and the physiological conditions of a cell. Additionally, this variation seems to correlate with the demand for molecules, which are produced or modified by the Golgi (Iijima and Kono, 1992; Lynch and Staehelin, 1992).

Even though the individual cisternae types of the stack exhibit different morphologies and harbor different sets of enzymes, they all seem to have a rather similar pH of 6.8 to 6.9 and are enriched in calcium, since their initial source of luminal content is the ER and they furthermore possess thapsigargin-sensitive ion pumps accumulating  $\text{Ca}^{2+}$ -ions (Zhang and Staehelin, 1992; Ordenes et al., 2002; Ordenes et al., 2012; Martiniere et al., 2013; Shen et al., 2013).

### **5.1.3. The plasma membrane**

The PM is one downstream compartment of the Golgi apparatus. Here, soluble proteins and oligo-saccharides are secreted into the extracellular space, where they are involved in a plethora of functions like cell wall formation, pathogen defense and seed germination (Harris and Northcote, 1971; Gubler et al., 1986; Moore and Staehelin, 1988; Subbarao et al., 1998; Oh et al., 2005). Membrane proteins, however, are retained in the PM. They mediate the transport of molecules across this lipid bilayer and the perception of extracellular signals as well as their transduction into the

cell (Noguchi et al., 1997; Zipfel et al., 2004). The PM is thus the primary site of interaction between a cell and its surrounding. It is also able to adjust its protein composition rapidly to allow for timely reactions to environmental cues. This is mediated by protein delivery from and protein disposal via the endomembrane system (Paez Valencia et al., 2016).

In between the PMs of neighboring cells lies the apoplast. This extracellular space is generally considered to be acidic (Yu et al., 2000). Recent measurements performed on the apoplast of *Arabidopsis* roots indicate pH values of roughly 5.5 in the tip as well as in the elongation zone and slightly below 4.5 in the differentiation zone (Barbez et al., 2017).

#### **5.1.4. The *trans*-Golgi network**

Since the TGN is the first compartment reached by endocytosed molecules, it is also referred to as the early endosome (EE; Dettmer et al., 2006). It is a tubulo-vesicular structure that is often localized in close proximity to *trans*-most Golgi cisternae but can also be observed in complete spatial separation from the stack (Staehelin et al., 1990; Viotti et al., 2010; Kang et al., 2011; Uemura et al., 2014). The TGN/EE is considered to be the central sorting hub of the plant cell. It receives cargo from the Golgi apparatus and the PM and directs transport towards the PM and to the vacuole via the MVB/LE (Scheuring et al., 2011; Uemura, 2016). Additionally, TGN-derived vesicles transport the lipids, the cell wall components and membrane proteins, which form the nascent cell plate during cytokinesis (Samuels et al., 1995).

Another characteristic of the TGN/EE is the presence of Vacuolar H<sup>+</sup>-ATPases (V-ATPases), which acidify its lumen, resulting in pH values of 5.7 to 6.2 (Dettmer et al., 2006; Martiniere et al., 2013; Shen et al., 2013; Luo et al., 2015). V-ATPase activity appears to be vital for TGN function, since application of its specific inhibitor concanamycin A has severe effects on the transport capabilities and the structure of the TGN (Dettmer et al., 2006).

### **5.1.5. The multivesicular body**

The MVB matures from the TGN (Scheuring et al., 2011). It is characterized by Intraluminal Vesicles (ILVs), which are pinched off from its limiting membrane into its lumen by the activity of the Endosomal Sorting Complexes Required For Transport (ESCRTs; Jensen, 1965; Spitzer et al., 2009; Wollert et al., 2009). Due to the MVB being the penultimate compartment on the vacuolar route for endocytic and biosynthetic cargo, it is also referred to as the Late Endosome (LE) and the Prevacuolar Compartment (PVC; Tanchak and Fowke, 1987; Tse et al., 2004).

The structure of the ILVs-containing MVB allows for the parallel transport of membrane proteins to the limiting membrane of the vacuole (tonoplast) and of soluble as well as membrane-bound proteins to the vacuolar lumen: Proteins targeted to the tonoplast are in the outer membrane of the MVB, membrane proteins and soluble proteins targeted for vacuolar delivery are in the ILVs or in the lumen of the PVC, respectively (Spitzer et al., 2009; Bottanelli et al., 2011). Transport via the PVC is ultimately accomplished by the fusion of the MVB's limiting membrane with the tonoplast. This process causes the release of its lumen and of the ILVs into the vacuole (Murphy et al., 1984; Scheuring et al., 2011).

The progressive acidification of endosomes during their maturation, which is typical in mammals, does not occur in plants, as the pH values calculated for the MVB/LE are in between 6.2 and 6.9 and thus higher than in the TGN/EE (Murphy et al., 1984; Martinieri et al., 2013; Shen et al., 2013).

### **5.1.6. The vacuole**

Plant cells can contain two archetypes of vacuoles: Protein Storage Vacuoles (PSVs) and Lytic Vacuoles (LVs; Paris et al., 1996). PSVs are densely packed with proteins (Shewry et al., 1995). Their function is the storage of fixed nitrogen and carbon. They typically accumulate within cells of seeds and storage organs but are also present in the vegetative tissues of plants (Horner and Arnott, 1965; Paris et al., 1996).

LVs make by far the largest contribution to the volume of most fully developed cells (Owens and Poole, 1979). LVs drive the hydrolysis of macromolecules, provide the turgor pressure needed for cell elongation and are involved in detoxification (Thayer and Huffaker, 1984; Vögeli-Lange and Wagner, 1990; Kutschera and Köhler, 1994; Chaumont et al., 1998; Sergeeva et al., 2006). The individual tasks of PSVs and LVs

necessitate different protein compositions, which in turn cause their distinct morphologies (Shewry et al., 1995; Paris et al., 1996; Carter et al., 2004). Changing these protein compositions can cause vacuoles to shift from one archetype to another. This occurs for example during germination, when hydrolases are delivered to PSVs turning them into LVs that are capable of degrading storage proteins and supplying the seedling with amino acids (Bethke et al., 1998).

pH differences can only be assumed since measurements have only been performed for LVs. In compliance with their function in protein hydrolysis, those exhibit varying pH values of 6 and below (Jochem et al., 1984; Martiniere et al., 2013; Shen et al., 2013).

## **5.2. The secretory pathway**

The secretory pathway comprises of the ER, the PM, the vacuole and the compartments passed by the transport routes leading from the former one to the latter two. Transport leading from the ER to the PM is termed secretion. It is the default route for soluble proteins synthesized in the ER (Denecke et al., 1990). To divert them towards the vacuole or retain them within a given compartment *en-route* to the PM, sorting events are necessary (Semenza et al., 1990; Lee et al., 1993; Shimada et al., 2003).

### **5.2.1. Secretion**

Soluble proteins in the ER lumen, whether they are actually ER-resident or not, are transported to the *cis*-Golgi by default (Pimpl et al., 2000). This process is mediated by vesicular carriers in the following sequence of actions: First, formation of a coat, in this case Coat-Proteins (COP)-II, which deforms the membrane, leads to the formation of a vesicle (Barlowe et al., 1994; Saito et al., 1998). After fission, the coat is disassembled rendering the vesicle competent for fusion with a target compartment (Barlowe et al., 1994; Saito et al., 1998; Takeuchi et al., 2000). Target-specificity of vesicular transport depends on Soluble NSF Attachment Protein Receptors (SNAREs), which are present in characteristic sets on the surface of vesicular carriers and organelles (Jahn and Scheller, 2006). Only if the SNAREs of a given vesicle match with the ones of a target membrane a *trans*-SNARE complex, which first links both

entities and then exerts the mechanical force to cause membrane fusion, is formed (Jahn and Scheller, 2006).

Fusion of COP-II derived vesicles with a *cis*-cisterna of the Golgi then releases the transported soluble proteins into the lumen of the Golgi. After their arrival in the *cis*-cisternae of the Golgi, however, ER-resident soluble proteins, which possess the ER retrieval signal [KH]DEL (Lys or His followed by Asp-Glu-Leu) at their very C-terminus, are sequestered from anterograde transport by ER-Retention Defective 2 (ERD2) and are redirected to the ER (Munro and Pelham, 1987; Semenza et al., 1990; Denecke et al., 1992; Lee et al., 1993; Montesinos et al., 2014). This retrograde transport is mediated by COP-I-coated vesicles (Pimpl et al., 2000; Montesinos et al., 2014). Thus, retention of soluble ER-resident proteins is achieved by active retention, while proteins destined for down-stream compartments are transported further. Different mechanisms mediate ER-retention and -export of membrane proteins: ER export signals present in some proteins allow for interaction with COP-II and facilitate active transport to the Golgi (Nishimura and Balch, 1997; Hanton et al., 2005). C-terminal KKXX/KXKXX (either Lys-Lys or two Lys residues interspaced by a random amino acid, followed by the two most C-terminal residues of the protein) retrieval signals of other proteins mediate ER-retention via retrograde transport back from the Golgi to the ER (Letourneur et al., 1994; Benghezal et al., 2000). Proteins of the p24 family, which effect Golgi structure and the transport of ERD2, possess both, ER export and ER retrieval signals (Langhans et al., 2008; Montesinos et al., 2014; Pastor-Cantizano et al., 2018). They are thus able to interact with COP-II and COP-I coats allowing them to cycle between the ER and the Golgi (Contreras et al., 2004a; Contreras et al., 2004b; Langhans et al., 2008).

Soluble proteins lacking an ER retrieval signal appear to just pass through the stack and no soluble Golgi-resident proteins have yet been described in plants (Phillipson et al., 2001). In contrast, Golgi-resident transmembrane proteins, like glycan modifying enzymes, have been described. Those localize specifically to certain cisternae types (Schoberer and Strasser, 2011). The underlying targeting mechanism is thought to be dependent on anterograde maturation of individual cisternae in *cis* to *trans* direction coupled with selective COP-I-dependent retrograde transport (Nakano and Luini, 2010; Gao et al., 2012). This would result in transmembrane proteins actually “staying” in the same type of cisternae. However, COP-I is not exclusively mediating retrograde

transport as data from the mammalian field supports a role of COP-I also in anterograde intra-Golgi transport (Park et al., 2015).

Export from the Golgi stack can occur directly towards the PM. This is for example the case for the cellulose synthase complexes (Crowell et al., 2009). Yet, other cargoes destined for the PM or the apoplast, like complex saccharides, secretory Green Fluorescent Protein (GFP) and fluorescently tagged Brassinosteroid Insensitive 1 (BRI1) seem to transit the TGN/EE (Zhang and Staehelin, 1992; Viotti et al., 2010; Kang et al., 2011). Transport from the stack to the TGN/EE is postulated to be mediated by maturation of the *trans*-most cisterna accompanied by the retrograde transport of Golgi-resident proteins (Staehelin and Moore, 1995; Kang et al., 2011). Secretory vesicles (SVs) clad by a yet unknown coat perform the final transport step towards the PM (Kang et al., 2011). However, not only newly synthesized molecules are secreted from the TGN/EE, also the GNOM-mediated recycling of previously endocytosed transmembrane proteins back to the PM occurs in part via this compartment (Geldner et al., 2003). By generating MVBs via maturation, the TGN/EE also forms the carriers mediating transport to the vacuolar lumen and the tonoplast (Spitzer et al., 2009; Bottanelli et al., 2011; Scheuring et al., 2011). Thus, several different transport routes pass through the TGN/EE. To allow for specific delivery of cargoes from such a complex transport hub, efficient sorting processes are critical.

### **5.2.2. Receptor-mediated vacuolar sorting**

The apoplast is the default destination of soluble proteins transported within the secretory pathway (Denecke et al., 1990). Thus, diverting proteins towards the vacuole necessitates a sorting event. One of the best described biological sorting processes is the lysosomal sorting in mammals. Here, Mannosyl 6-Phosphate (MP6) Receptors (MPRs) shuttle soluble proteins destined for lysosomal delivery from the TGN to the EE (Sahagian et al., 1981; Geuze et al., 1985; Hoflack and Kornfeld, 1985; Brown et al., 1986). Since in this system these two are actually independent compartments, this equals a sorting from the secretory to the endocytic pathway that leads from the PM via EE and LE to the lysosome (Huotari and Helenius, 2011). The receptor-ligand interaction occurs in the TGN after an uncovering enzyme 'reveals' terminal MP6 residues, which act as the sorting signal in the glycosylation pattern of the cargo proteins (Sahagian et al., 1981; Hoflack and Kornfeld, 1985; Rohrer and Kornfeld,

2001). The receptor-ligand complex is then sorted into vesicular carriers, which ultimately fuse with the EE (Geuze et al., 1985; Brown et al., 1986; Zhu et al., 2001). Here, MPRs and their cargo disassociate due to the acidification that parallels the maturation from early to late endosomes and reduces the pH in these compartments below the pH values found in the TGN (Sahagian et al., 1981; Murphy et al., 1984; Hoflack and Kornfeld, 1985; Brown et al., 1986). The soluble proteins in this compartment are delivered to the lysosome (Geuze et al., 1985). MPRs are recycled back to the TGN via tubular membranous carriers formed by the retromer coat and engage in further rounds of transport (Geuze et al., 1985; Seaman, 2004).

In plants, there are two families of sorting receptors mediating transport of soluble cargo to the vacuole: The Vacuolar Sorting Receptor (VSR) family with its seven members VSR1-7 and the Receptor Homology-Transmembrane-RING H2 (RMR) proteins (Miao et al., 2006; Lousa et al., 2012; Li et al., 2013). The dimer forming RMRs sort storage proteins into the PSV and it is thought, that they are not recycled but are rather transported into the vacuole together with their cargo (Park et al., 2005; Shen et al., 2011; Occhialini et al., 2016). In contrast to the RMRs, VSRs have been suggested to recycle in order to be employed in several rounds of receptor-mediated transport (daSilva et al., 2005; Niemes et al., 2010b; Kang et al., 2012).

While MPRs recognize their cargo via post-translational modifications, VSRs bind directly to the protein backbone(s) of their cargoes (Sahagian et al., 1981; Kirsch et al., 1994; Watanabe et al., 2002). Typical VSR ligands display one of three types of Vacuolar Sorting Signals (VSS): Sequence-specific, C-terminal and structural sorting signals. Sequence-specific VSS are amino acid stretches of the consensus motif NPIR (Asn-Pro-Ile-Arg; Holwerda et al., 1992; Matsuoka and Neuhaus, 1999). C-terminal VSS, on the contrary, exhibit no consensus motif but have the common feature that they must be situated at the very C-terminus of a protein to be functional (Bednarek et al., 1990; Dombrowski et al., 1993; Matsuoka and Neuhaus, 1999). Structural VSS are not based on a single amino-acid stretch but are epitopes formed by the tertiary or quaternary structure of proteins (Saalbach et al., 1991; Von Schaewen and Chrispeels, 1993).

The VSRs themselves are type-I transmembrane proteins. They possess a short Cytosolic Tail (CT) at their C-terminus, a Transmembrane Domain (TMD) and an N-terminal Luminal Binding Domain (LBD) that again contains a protease associated and



a VSR-specific domain as well as 3 Epidermal Growth Factor (EGF) repeats, of which at least one can bind  $\text{Ca}^{2+}$  (Paris et al., 1997; Cao et al., 2000).

The LBD alone is capable of cargo recognition and binding (Watanabe et al., 2004; Niemes et al., 2010a; Luo et al., 2014). In this context, *in vitro* VSR-ligand interaction has been shown to persist at pH values at around 6.5 and to be gradually abolished under increasingly acidic or alkaline conditions (Kirsch et al., 1994). This pH dependency, however, can be overwritten by elevated calcium levels. It was shown, that a concentration of 1 mM  $\text{Ca}^{2+}$  prevents dissociation even at a pH of 4 (Watanabe et al., 2002).

The TMD links the LBD and potentially bound ligands to the CT, which in turn seems to be able to interact with several components of the transport machinery (daSilva et al., 2006). The CT contains several motifs necessary for VSR-transport. Notably, a tyrosine motif TXX $\phi$  (Tyr and  $\phi$  interspaced by two random amino acids with  $\phi$  being a bulky hydrophobic amino acid) that has been shown to interact with adaptor complexes *in vitro* (Happel et al., 2004). These complexes are able to recruit clathrin triskelia consisting of three clathrin light chain molecules and three clathrin heavy chain moieties (Kirchhausen and Harrison, 1981; Ford et al., 2002; Chidambaram et al., 2008; Fan et al., 2013). Their recruitment, in turn, leads to the formation of a clathrin-coated membrane protrusion, which can be pinched off by the action of Dynamin-Related Proteins (DRPs) giving rise to Clathrin-Coated Vesicles (CCVs; Roth and Porter, 1964; Sweitzer and Hinshaw, 1998; Hinrichsen et al., 2006; Fujimoto et al., 2010). In addition to harboring a signal for CCV-mediated transport, the CT of VSRs also seems to contain a motif for retromer-dependent transport, as VSR1 and the Vacuolar Protein Sorting 35 (VPS35) subunit of the retromer coat were shown to interact (Oliviusson et al., 2006).

In several aspects VSRs are similar to MPRs: They exhibit a pH dependency of receptor-ligand interaction *in vitro*, are associated with CCV- as well as retromer-dependent transport and were localized at the Golgi, the TGN/EE and the MVB (Kirsch et al., 1994; Paris et al., 1997; Happel et al., 2004; Miao et al., 2006; Hinz et al., 2007). This led to the conclusion that VSR-mediated transport paralleled the MPR transport in mammals. Anterograde transport was thought to occur from the Golgi or TGN to an endosomal compartment via CCVs. This endosomal target compartment was considered to be MVB/LE, in which a putatively lower pH would trigger ligand release.

From there on, retromer would recycle the VSRs back to the TGN (Paris et al., 1997). This model, however, has more recently been challenged by two major findings: First, the sorting nexins, which are considered to be a part of retromer complex, have been shown to localize at the TGN and second, the MVB is more alkaline than the TGN/EE, which is actually the most acidic compartment *en-route* to the vacuole (Niemes et al., 2010b; Martiniere et al., 2013; Shen et al., 2013). This implies that if recycling of VSRs is indeed mediated by retromer and there is an acidity-driven release of ligands, the TGN/EE is the most likely location for ligand unloading and thus the target compartment of receptor-mediated vacuolar transport. Yet, if this was actually the case, where would VSRs then be recycled to? Possible recycling targets are the ER and the Golgi. Since VSR-ligand interaction does not depend on post-translational modifications of the cargo, VSR-ligand interaction could, as was recently suggested, already occur in the ER (Kirsch et al., 1994; Watanabe et al., 2002; Watanabe et al., 2004; Niemes et al., 2010a).

Furthermore, how would a ligand release in the TGN/EE fit to the current model of secretion, which implies default PM delivery of soluble molecules from the very same compartment (Moore and Staehelin, 1988; Dettmer et al., 2006)? A better understanding of vacuolar transport, in particular of the whereabouts of VSR-ligand interaction and receptor recycling is needed for the construction of a more comprehensive model of the transport processes within the endomembrane system.

### **5.3. The endocytic pathway**

Proteins in the PM mediate the transfer of molecules and information into the cell (Noguchi et al., 1997; Zipfel et al., 2004). To control the uptake of substances, some of which can, if present in excess, be toxic, or to stop signaling events, a cell needs to be able to adapt its protein composition at the PM accordingly. A general mechanism to downregulate PM proteins fast during such an adaptation is transporting them to the vacuole via the endocytic pathway (Kasai et al., 2011; Lu et al., 2011; Martins et al., 2015). However, endocytosis does not necessarily lead to vacuolar delivery. Some PM proteins, like the auxin efflux carrier Pin-Formed 1 (PIN1), are constitutively endocytosed and recycled back to the PM from endosomal structures via a pathway that depends on the ADP-Ribosylation-Factor Guanine-Nucleotide exchange-factor (ARF-GEF) GNOM (Geldner et al., 2003).

### 5.3.1. Endocytosis

Formation of endocytic vesicles can be clathrin-mediated or clathrin-independent. Clathrin-Mediated Endocytosis (CME) is a multi-step process (McMahon and Boucrot, 2011; Paez Valencia et al., 2016). The first step in CME is the formation of a nucleation module. In opisthokonta, this module consists of the muniscin FCH Domain Only (FCHo) proteins, intersectins and EGFR Pathway Substrate 15 (EPS15; Stimpson et al., 2009; Henne et al., 2010). Plants, however, do not possess a known homolog of muniscin FCHo. Here, the TPLATE complex is thought to act as a nucleation module, since its subunits harbor some functional domains found in muniscins, EPS15 and intersectins (Gadeyne et al., 2014). Furthermore, TPLATE recruitment to the PM precedes the one of the Adaptor Complex 2 (AP2), which is the hetero-tetrameric adaptor interacting with clathrin triskelia during endocytosis (Fan et al., 2013; Gadeyne et al., 2014).

Nucleation is followed by recruitment of adaptors and the selection of cargoes. Signals marking proteins for endocytosis include a tyrosine motif and an acidic di-leucine signal [DE]xxxL[LI] (ASP or GLU and LEU-LEU or LEU-ILE interspaced by three random amino acids). The 3D-structures of these amino acid sequences are recognized by the subunits of AP2 (Hunziker and Fumey, 1994; Ohno et al., 1995; Pond et al., 1995; Ortiz-Zapater et al., 2006; Kelly et al., 2008; Wakuta et al., 2015). Furthermore, ubiquitination, which is the covalent attachment of one or more ubiquitin molecules to lysine residues of a protein, also trigger endocytosis. In this regard, the addition of a single ubiquitin to a protein seems to be insufficient to link a protein to the endocytosis machinery. Instead, the addition of ubiquitin chains (poly-ubiquitination) or of several individual ubiquitins to different lysine residues (poly mono-ubiquitination) is needed for efficient endocytic uptake (Pickart and Eddins, 2004; Barberon et al., 2011; Leitner et al., 2012; Scheuring et al., 2012). In plants, the Tom1-Like (TOL) proteins have been suggested to link ubiquitination to CME, since they are able to bind ubiquitin *in vitro*, are partially present at the PM and are involved in the degradation of the PM-localized auxin efflux carrier PIN2 (Korbei et al., 2013).

After cargo selection, which leads to an initial deformation of the PM due to the membrane modelling capabilities of adaptors, the clathrin coat induces membrane protrusions and CCVs are ultimately released by the action of DRPs (Sweitzer and

Hinshaw, 1998; Ford et al., 2002; Hinrichsen et al., 2006; Chidambaram et al., 2008; Fujimoto et al., 2010; Fan et al., 2013).

The CCVs then deliver their cargo by fusing with the TGN/EE (Dettmer et al., 2006; Dhonukshe et al., 2007). Endocytosed membrane proteins can, from here on, either be recycled to the PM or be sorted into ILVs during the maturation of MVBs from the TGN/EE (Geldner et al., 2001; Spitzer et al., 2009; Scheuring et al., 2011).

While there is evidence that also clathrin-independent endocytosis exists in plants, very little is known about the putative mechanisms of this process (Li et al., 2012).

### **5.3.2. Endosomal sorting complexes required for transport (ESCRT-) mediated vacuolar sorting**

In yeast and mammals, ubiquitination serves as the central sorting signal that is recognized by the ESCRT machinery, which consists of five protein complexes, namely ESCRT-0, ESCRT-I, ESCRT-II, ESCRT-III and the Vacuolar Protein Sorting 4 (VPS4) complex (Henne et al., 2011). ESCRT-0 is formed by VPS27 and Has Symptoms Of Class E Mutants 1 (Hse1; Bilodeau et al., 2002). VPS23, VPS28, VPS37 and Multivesicular Body 12 (Mvb12) form ESCRT-I. ESCRT-II consists of VPS22, two VPS25 moieties and VPS36. VPS20, Sucrose Non-Fermenting 7 (SNF7), VPS24 and VPS2 in varying stoichiometric ratios assemble ESCRT-III (Babst et al., 2002a). 12 VPS4 subunits form a complex together with 6 VPS Twenty Associated 1 (Vta1) proteins (Babst et al., 1997; Yu et al., 2008). After recognizing ubiquitinated proteins, the ESCRT machinery concentrates them and sorts them into budding ILVs of its own making.

Localization-specificity of the ESCRTs is conferred by the lipid-binding preferences of ESCRT-0 and ESCRT-II. Their subunits VPS27 and VPS36, respectively, are able to bind to Phospho-Inositol-3-Phosphate (PI3P), which is enriched in endosomal membranes (Raiborg et al., 2001; Gillooly et al., 2003; Petiot et al., 2003; Slagsvold et al., 2005). ESCRT-I and ESCRT-III subunits lack this kind of lipid-specificity. They are recruited by ESCRT-0 and ESCRT-II, respectively (Katzmann et al., 2003; Lu et al., 2003; Teo et al., 2004; Im et al., 2009) and maintain membrane attachment via the basic N-terminus of ESCRT-I's VPS37 and the myristoylation of ESCRT-III's VPS20 (Babst et al., 2002a; Kostelansky et al., 2007).

Ubiquitin-binding is performed by both ESCRT-0 subunits, the ESCRT-I subunits VPS23 and Mvb12 as well as ESCRT-II's VPS36 (Katzmann et al., 2001; Slagsvold et al., 2005; Teo et al., 2006; Shields et al., 2009; Ren and Hurley, 2010). Since ESCRT-0 interacts with ESCRT-I, which in turn interacts with ESCRT-II, the resulting super-complex is able to accumulate several ubiquitinated cargo molecules (Katzmann et al., 2003; Lu et al., 2003; Teo et al., 2006). The recruitment of two VPS20 moieties by the two VPS25 subunits of ESCRT-II links ubiquitin recognition and accumulation to the ILV formation performed by ESCRT-III (Teo et al., 2004; Wollert et al., 2009; Teis et al., 2010). For ILV formation, the participation of both of these VPS20 moieties followed by the assembly of two VPS24-capped poly-Snf7 filaments is necessary (Teis et al., 2008; Saksena et al., 2009; Teis et al., 2010).

The combined action of ESCRT-0-III ultimately sorts ubiquitinated cargo into nascent ILVs (Wollert and Hurley, 2010). Prior to budding, the following steps are performed to keep ESCRT-mediated sorting efficient, as they allow for the complexes to participate in multiple rounds of transport: First, de-ubiquitination enzymes remove ubiquitin from to-be-degraded proteins, thereby maintaining the ubiquitin level within the cell (Swaminathan et al., 1999; Amerik et al., 2000). This further allows ESCRT-0-II to escape vacuolar delivery (Wollert and Hurley, 2010). Then, ESCRT-III is disassembled and released into the cytosol by the action of the VPS4 complex (Babst et al., 1998; Wollert and Hurley, 2010).

In plants, the knowledge concerning the ESCRTs is comparatively limited. Homologs for most subunits have been identified in *Arabidopsis*, interactions have almost exclusively been studied by initial screens and a few selected subunits have been characterized in more detail (Spitzer et al., 2006; Richardson et al., 2011; Shahriari et al., 2011; Gao et al., 2014). Nevertheless, it has become evident, that the overall function of ESCRT at endosomal membranes is conserved, as perturbations of the machinery lead to miss-sorting of ubiquitinated proteins (Spitzer et al., 2009; Richardson et al., 2011; Cai et al., 2014; Gao et al., 2014). However, this is not the case for the underlying molecular mechanisms, as the FYVE Domain Protein Required For Endosomal Sorting 1 (FREE1) substitutes for the absence of ESCRT-0 and might even be completely integrated in a putative ESCRT-I complex (Gao et al., 2014).

Especially concerning plant ESCRT-II, information is scarce, and findings have been controversial. While fluorescently tagged VPS22 was reported to localize to

endosomal membranes (Scheuring et al., 2011), overexpressed and epitope-tagged VPS36 had been found to be present almost exclusively at the PM in an immunofluorescence-based localization screen (Richardson et al., 2011). Here, further studies are necessary to explore whether an ESCRT-II homologous complex actually exists in plants, which proteins this putative complex would consist of and what its plant-specific functions at the PM might be.

## 6. Objectives

Transport to the lumen of the lytic vacuole occurs differently for membrane-bound and soluble proteins. Membrane proteins that are to-be-degraded in this organelle are sorted by the ESCRTs into ILVs during endosomal maturation. These ILVs are released into the vacuole upon fusion of the limiting membrane of the MVB/LE with the tonoplast. Soluble proteins including the acidic hydrolases that mediate protein degradation in the vacuole are transported within the lumen of the compartments of the endomembrane system. Their vacuolar delivery depends on the sorting function of the VSRs, which sequester them from default secretion.

To grasp the over-all functionality of the plant endomembrane system, a thorough understanding of both, VSR- and ESCRT-mediated sorting events, especially concerning how they are spatially and temporally coordinated and intertwined, is needed.

For this, it is mandatory to understand where the VSRs bind and release their cargo and whether they are recycled to engage in multiple rounds of sorting. For the assessment of the whereabouts of VSR-cargo binding and release we aimed at characterizing the physicochemical conditions of the individual compartments of the endomembrane system regarding whether they allow for receptor-ligand interaction. Therefore we had to target pH sensitive probes precisely to the organelles of interest. We chose to employ GFP, which allowed for pH measurements via Fluorescent Lifetime Imaging (FLIM), as probe and translationally fused it to different compartment-specific markers to stir it to locations within the endomembrane system. The results of these recordings hinted towards VSR-ligand interaction being established in the ER and Golgi and being abolished in the TGN/EE. To confirm this, we next sought to perform compartment-specific VSR-ligand interaction studies *in vivo*. However, those necessitated directing the VSRs to individual compartments. As this was not feasible for the full-length receptors, we chose to employ just the LBD, which mediates ligand binding. This allowed us to translationally fuse only the LBD to a GFP-Nanobody (Nb<sub>G</sub>), resulting in LBD-Nb<sub>G</sub>. Via a nanobody-epitope interaction LBD-Nb<sub>G</sub> could be attached to the earlier described GFP-marker fusions, which would then guide the assembled sensors to the desired localization. With the sensors already containing GFP, we aimed at employing a ligand-RFP protein fusion to allow for assessing

interaction between the LBD and its ligand via Förster Resonance Energy Transfer (FRET) monitored by FLIM.

Due to the different GFP-lifetimes recorded for the individual compartments during the pH measurements, controls to assess the base fluorescent lifetime of the sensor at a given location had to be established. Furthermore, there was a lack of suitable biological positive controls, which could prove the general possibility of FRET induced reduction of the fluorescent lifetime of the sensor within the plant endomembrane system. To overcome this, a set of generally applicable controls had to be designed before FRET-FLIM could be used to monitor where ligand binding and release occur during VSR-mediated sorting.

After analyzing anterograde VSR-mediated sorting, we aimed at visualizing the putative retrograde transport of VSRs. To be able to directly observe the recycling of VSRs and identify the target compartment of retrograde transport, we had to establish a strategy to discriminate between receptors in two different states: First, VSRs which were newly synthesized and thus on the anterograde route and second, those which had already recycled. It was, furthermore, necessary to be able to halt the movement of VSRs in every single compartment *en-route* to the vacuole to test for the presence of recycled receptors at that specific location. We envisaged tackling both issues by exploiting two different nanobody-epitope interactions and monitoring the system by confocal microscopy. In this regard, we employed a first nanobody-epitope interaction to post-translationally label VSRs, which had already been anterogradely transported, with a fluorescent protein containing the two different epitopes in the TGN/EE, which is their assumed recycling point. This dual-epitope linker would then also be used to bind specifically recycled receptors to membrane markers in upstream compartments via the second nanobody-epitope interaction pair.

To get more insights into the other route leading into the vacuole and possibly gather hints on how the transport of membrane-bound and soluble proteins to this organelle might be intertwined, we sought to further characterize the ESCRTs. Here, we focused on three plant proteins homologous to the subunits of the *Saccharomyces* ESCRT-II, which reassembles the heart of the yeast ESCRT machinery. At the time, however, it was unclear, whether they would form a complex in plants, since heterologously expressed VPS22 and VPS36 had been found to localize at different compartments. We set out to clarify this and provide fundamental knowledge about a putative plant



ESCRT-II complex, concerning its localization, composition and function. In this regard, we planned to raise antibodies against VPS22, VPS25 and VPS36 to employ them in immune electron microscopy, ultimately localizing these endogenous proteins *in situ*. We aimed, furthermore, at verifying putative intra-complex interactions *in vivo* via FRET-FLIM and at analyzing the importance of ESCRT-II functions for plant life.

## 7. Results and discussion

### 7.1. Compartment-specific analysis of the interaction between vacuolar sorting receptors and their cargo

After their co-translational translocation into the ER lumen, proteins destined for vacuolar delivery are sorted out of the secretory bulk flow that leads to the PM and the apoplast. This active transport depends on Vacuolar Sorting Receptors (VSRs). Yet, the identities of donor- and acceptor-compartments interconnected by VSR-mediated sorting were a matter of speculation: First, even though *in vivo* studies elegantly demonstrated that VSRs interact with their cargo in the ER, neither ligand binding nor ligand release had been shown directly for any other compartment within the endomembrane system (Watanabe et al., 2004; Niemes et al., 2010a). Second, the results of the studies, which had successfully characterized the pH and Ca<sup>2+</sup> dependencies of VSR-cargo interaction *in vitro*, did not allow for predicting the whereabouts of receptor-ligand interaction *in vivo*, since the physicochemical conditions within plant cells had not yet been explored in sufficient detail (Kirsch et al., 1994; Watanabe et al., 2002). In order to provide the missing *in vivo* interaction data, we intended to implement an approach, capable of directly and individually probing all compartments *en-route* to the vacuole for the presence or absence of VSR-cargo interaction. Furthermore, to allow also for a profound interpretation of the *in-vitro* binding studies, we sought to determine the intra-compartmental pH values within the endomembrane system.

As VSRs have to be transported within the endomembrane system to fulfill their sorting function, receptor sub-populations are expected to be present at different compartments at the same point in time. Since we intended to test VSR-cargo interaction for each organelle type individually, we had to design an experimental approach enabling us to pinpoint and retain the VSR-derivative, which would be employed for the binding studies, at only one specific compartment of choice. For the manipulation of VSR-(derivative) localization within the endomembrane system, three different approaches have been applied in the past: First, analysis of trafficking mutants. Second, trapping VSRs by blocking individual steps in intracellular transport via the application of pharmaceutical treatments or the expression of dominant effector mutants. Third, fusing the cargo-interacting Luminal Binding Domain (LBD) of VSRs to compartment-specific markers. Even though all three of them had been proven very

valuable during the prior characterization of VSRs, none of them was applicable for all compartments of the endomembrane system while still providing the high targeting-specificity needed for the given task. So was the application of the trafficking mutants, which were initially employed to study the importance of the VSR C-terminus for efficient transport of the whole receptor, hampered by all mutant VSRs being partially localized at endosomal compartments (daSilva et al., 2006; Saint-Jean et al., 2010). The introduction a transport block, which was for example elegantly used to monitor the effect of sorting nexins 1 and 2 mutants on the trafficking of VSR-derivatives, was also not a perfect solution, because VSRs would not only accumulate in the organelle directly upstream to the block but were also expected to backlog further, possibly up to the ER (Niemes et al., 2010b). Blocking transport might additionally cause serious alteration of the physicochemical conditions of the affected compartments. Those alterations in turn might then interfere with receptor-ligand interaction. Finally, there was the possibility of employing LBD-marker fusions, which had already been used to show receptor-ligand interaction in the ER (Niemes et al., 2010a). This was, however, only applicable for the ER and MVB, since the N-termini of the respective marker proteins faced the compartmental lumen (type-I transmembrane proteins). This allowed the LBD to be fused via its C-terminus and thus to be maintained in a functional conformation. The markers for the Golgi and the TGN exhibit their C-terminus to the compartmental lumen (type-II transmembrane proteins). To overcome the limitations imposed by the topology of the type-II transmembrane marker proteins, we planned to link the LBD and the markers proteins in a post-translational instead of a translational manner. This would allow for the assembly of precisely targetable sensors for VSR-ligand interactions.

To implement such a link within the plant cell, we intended to make use of the highly specific interaction between so-called nanobodies and their respective antigens. Nanobodies are the variable domain of the heavy-chain-only antibodies found in camelids (Hamers-Casterman et al., 1993; Muyldermans, 2001). These small peptides with a size of only about 15 kDa are very stable, can be heterologously expressed and are fully capable of antigen-binding (Muyldermans, 2001). Moreover, their coding sequences can be directly fused to the ones of other proteins to generate nanobody-fusion proteins that still possess antigen-binding capabilities (Rothbauer et al., 2006). This allowed us to fuse an Anti-GFP Nanobody (Nb<sub>G</sub>) to the C-terminus of the LBD,

which could in turn bind to any marker protein exhibiting GFP in the lumen of a given compartment within the endomembrane system. The resulting protein complex would then be efficiently targeted by the sorting signals present in the marker protein and contain the LBD in the same functional orientation as it is present in an a full-length VSR. With this setup, the nanobody-epitope interaction that leads to sensor-assembly already occurs in the ER lumen, since all marker proteins, we intended to use as anchor constructs for the LBD, are inserted into the membrane in this very organelle. This was particularly important for the MVB/LE marker GFP-BP80, which is a truncated VSR having its LBD replaced by a GFP (Li et al., 2002; daSilva et al., 2005). This molecule localizes at the MVB and is thus no longer associated with a compartment that is passed by the otherwise non-anchored and thus secreted LBD-Nb<sub>G</sub> on its route to the PM.

For the characterization of the compartmental pH values within the endomembrane system, we intended to exploit the fact that the chromophore of GFP in its protonated state exhibits a shorter fluorescent lifetime than in its unprotonated state (Heikal et al., 2001). This allowed for the application Fluorescence Lifetime Imaging (FLIM) to measure the pH of individual compartments in a non-invasive manner. For this to be successful, I designed a system of highly localization-specific compartmental markers, which had to meet two further requirements to serve as pH-sensors. First, all markers had to contain the very same GFP-variety and second, the marker topology had to be chosen in a way that the fluorophore was exhibited towards the lumen of the compartment of interest. I opted for the use of enhanced GFP instead of wildtype GFP, since the dynamic range of pH-induced changes in average fluorescence lifetimes within a population of the former matches well with the pH values expected within an eukaryotic cell (Heikal et al., 2001).

For targeting of the GFP, I chose the following markers: Calnexin (CNX) for the ER,  $\alpha$ -Mannosidase1 (ManI) for the Golgi, Syntaxin Of Plants 41 (SYP41) and SYP 61 for the TGN and BP80 for the MVB (Nebenführ et al., 1999; Uemura et al., 2004; daSilva et al., 2005; Niemes et al., 2010a). To achieve the required topology, I fused the GFP with the N-terminus of the type-I transmembrane proteins and with the C-terminus of type-II transmembrane proteins and tail-anchored syntaxins, respectively. This resulted in GFP-CNX, GFP-BP80, ManI-GFP, SYP41-GFP and SYP61-GFP. To test whether N- and C-terminally fused GFP exhibited different lifetimes, I designed two

additional constructs. These constructs encode for GFP fused to either terminus of a peptide, which is expressed in the cytosol and post-translationally inserted in the PM via S-acetylation (GFP-Box and Box-GFP; Lavy and Yalovsky, 2006; Scheuring et al., 2012). Furthermore, those two proteins allowed for the assessment of the cytosolic pH. I had to establish FLIM for our laboratory, thus I chose transiently transformed protoplast as a model system, since single cells are way more suitable for this technique than thick tissues. The tightly controllable expression levels warranted by electro-transfected protoplast, allowed, furthermore, for high signal to noise ratios and for short imaging times. After verifying correct localization for all pH-sensors, I recorded their fluorescent lifetimes (Fig. 1).

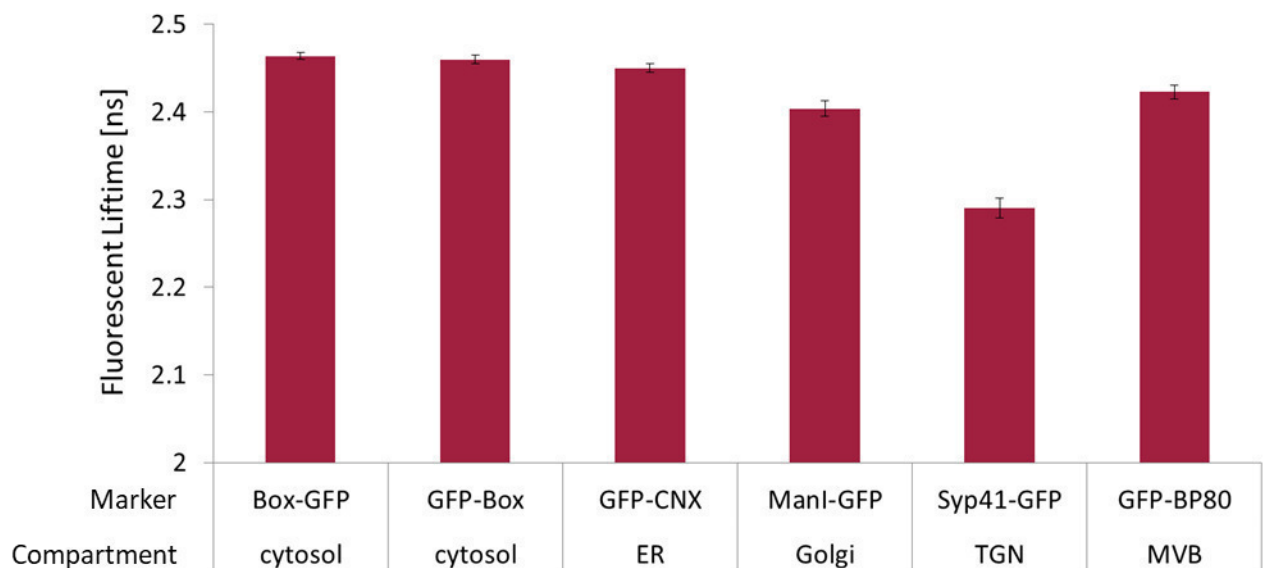


Figure 1: Average fluorescent lifetimes of N- and C-terminal GFP-fusion proteins located within intracellular compartments. Sample size  $n \geq 14$  for each GFP marker. Error bars indicate standard errors of the mean.

As the lifetime of Box-GFP and GFP-Box showed no significant differences ( $t(29)=1.08$ ;  $p=0.29$ ; Fäßler, unpublished), we concluded that any occurring shortening of lifetimes between the other samples had indeed been caused by reduced pH values compared to the cytosol. Since the cytosol is expected to be rather neutral and the lifetime values of the cytosolic and the ER-localized pH-sensors exhibit no significant differences (Tukey  $\alpha=0.05$ ), we assumed the ER to also exhibit a pH value of around 7, which would be suitable for the already reported VSR-ligand binding in this

compartment (Kirsch et al., 1994; Watanabe et al., 2004; Niemes et al., 2010a). In sharp contrast to the situation in the ER, my results clearly indicated that the TGN is more acidic than the Golgi and the MVB (Fig. 1). Considering the *in-vitro* evidence, which demonstrated the abolishment of VSR-cargo interaction at lower pH, we concluded already at this point that the TGN was the most likely acceptor-compartment for receptor-mediated vacuolar sorting (Kirsch et al., 1994). Thus, we predicted for the upcoming interaction-analysis that ligand binding would occur in all organelles upstream of the TGN, namely ER and Golgi, and would be abolished in downstream compartments like the MVB/LE or the previously reported late PVCs (Foresti et al., 2010).

Acquisition of calibration curves, which would have been needed for calculating absolute pH values, and inclusion of these findings in our manuscript was omitted, since similar studies concerning intracellular pH measurements had been published prior to our initial submission by Shen et al. (2013) and Martiniere et al. (2013).

### **7.1.1 *In vivo* interaction studies by measuring Förster resonance energy transfer through fluorescence lifetime imaging microscopy (FRET/FLIM)**

In order to characterize the interaction between VSRs and their cargo in the compartments of the endomembrane system, we had already devised a strategy to specifically target the LBD to specific compartments. Next, we had to decide on how to monitor the ligand binding status of those LBDs. Due to the reversibility and the pH- and  $\text{Ca}^{2+}$ -dependent nature of this interaction between VSRs and their cargo, it was crucial to dismiss any techniques that necessitated breaking up cells and extracting proteins, such as for example co-immune precipitation. While the application of those approaches is very valuable to determine whether proteins of interest can interact in general, they inevitably also include steps that separate cargo/LBD-Nb<sub>G</sub>/GFP-marker complexes from membranes and incubate them in buffer solutions for their recovery. At that point, the physicochemical conditions of the organelle, in which the complex had formerly localized, would be completely overridden by the conditions of the buffer, which would confer either ligand binding or ligand releasing conditions.

With those considerations in mind, we opted for performing an *in vivo* approach based on live cell imaging. In this regard, we had to decide between Förster Resonance Energy Transfer (FRET) monitoring techniques and Bi-Molecular Fluorescence

Complementation (BIFC) assays. We chose the former, as they allow for the direct monitoring of the interaction status of the proteins of interest and not for the general occurrence of interaction. This was of particular importance, since we were not only interested in where the interaction between VSRs and their cargo is initiated and maintained but also where it is abolished, as the reversible nature of the VSR-ligand interaction is a specific requirement for the concept of receptor-mediated sorting. BIFC could not have provided this information, since LBD and cargo molecules fused to the N- or C-terminal part of YFP would already bind each other in the ER, for which VSR-ligand interaction had initially been shown, and thereby cause complementation of the YFP (Watanabe et al., 2004; Niemes et al., 2010a). This interaction driven YFP complementation, however, would keep the initially interacting molecules glued together irrespective of the potentially ligand releasing conditions in downstream compartments. Thus, it would not allow for the identification of the endpoint of VSR-mediated transport at all. To enable the monitoring of the reversible VSR-ligand interaction, we opted for FRET-FLIM, as this specific variant of FRET detection is least prone to false positive results and is not dependent on bleaching, which could otherwise affect intra-organellar conditions due to photo toxicity (Bucherl et al., 2014; De Los Santos et al., 2015).

FRET studies demand a combination of two fluorophores, for which the emission spectrum of the first overlaps with the excitation spectrum of the other. Those fluorophores are referred to as donor and acceptor, respectively. As energy transfer from a donor- to an acceptor-population causes a decrease of average donor-fluorescence lifetime and efficient FRET occurs only within a distance of less than 10 nm, performing FLIM allows probing for interaction-inferring proximity of the proteins of interest with each other. A commonly used fluorophore combination in this regard consists of the donor GFP, for which lifetime reduction can easily be determined, and the acceptor RFP, which allows for a sufficient spectral overlap (Wang et al., 2014; Kriechbaumer et al., 2015).

Regardless of the choice of fluorophores, FRET-FLIM experiments require three types of controls. First, a donor-only sample, employed to assess the basic lifetime of the donor in the respective environment. Second, a negative control, which is used to exclude that a non-interacting but co-localizing acceptor-fusion protein at the chosen expression levels interferes with the donor's fluorescence lifetime. Third, a positive

control validating that the lifetime of the donor can, indeed, be reduced by an interacting acceptor-fusion protein under the conditions at hand. Donor-only controls are the easiest to set up, since they, most of the time, only involve single expression of the donor-fluorophore fused to a protein of interest. In most cases, negative controls are also not too difficult to implement, as the acceptor-fluorophore can be directed to the desired location by fusing it to small sorting signals, which are, in general, unlikely to interact with the donor-fusion protein. However, positive controls can, especially in case of an initial characterization of protein-protein interaction, be almost impossible to perform, if there are no known interactors of the donor-fusion protein. To overcome this problem, I set out to devise a universal acceptor, suitable for all GFP-based donors to come.

For this, I designed an interactor that binds directly to the GFP, which is the common denominator that produces the readout in all those experiments. I, therefore, fused the acceptor-fluorophore directly to the Nb<sub>G</sub>, as this nanobody has been shown to bind GFP (Schornack et al., 2009).

This Nb<sub>G</sub>-RFP construct reduced the fluorescent lifetime of cytosolic GFP in a highly significant manner in all performed FRET-FLIM analyses, while comparable amounts of cytosolic RFP had no effect on the donor.

As Nb<sub>G</sub>-RFP was able to bind free GFP in the cytosol, we anticipate it to be able to bind any cytosolic GFP-fusion protein. In addition, its application together with non-cytosolic donors should be viable, as sorting signals can be attached to Nb<sub>G</sub>-RFP in order to target it towards any other intracellular location.

### **7.1.2 Receptor-mediated sorting of soluble vacuolar proteins ends at the *trans*-Golgi network/early endosome**

For the FRET-FLIM measurements aiming at characterizing VSR-ligand interaction, we intended to use the GFP-tagged marker proteins, which I had already designed, characterized and applied for measuring the intracellular pH values, as donors. By doing so, we could apply the gathered knowledge regarding the required expression levels and the to-be-expected donor-only lifetimes (Fig. 1). Especially the second point was important, as the fluorescent lifetime of GFP is drastically reduced in the TGN due to the low compartmental pH values. This might have led to false positive interpretation of FRET-FLIM interaction data, if we had not included a donor-only control (Fäßler and



Pimpl, 2017). An RFP fused with the vacuolar sorting signal of Aleurain (aleuRFP) was used as acceptor-fluorophore (Humair et al., 2001). We chose this specific molecule, since my initial study revealed that aleuRFP, in comparison to other tested RFP-fusions, e.g. RFP-Chitinase and RFP-Sporamin, was more efficiently transported to the vacuole and was not prone to accumulation in the ER (Fäßler, unpublished).

This setup warrants that FRET effects can only occur if the LBD-Nb<sub>G</sub> linked to the GFP-tagged anchor interacts with the aleuRFP in the respective compartment and thus forces the two fluorophores into close proximity. Expression of Secreted RFP (secRFP) instead of aleuRFP was chosen to serve as a negative control, since the sorting signal of Aleurain, which actually interacts with the LBD, is not present in secRFP (Kirsch et al., 1994). Co-expression of an anchor with an LBD-Nb<sub>G</sub>, which is translationally fused to RFP, represented the perfect general positive control. As donor-only control, we opted not for single expression of the respective GFP-tagged marker but rather for co-expression of the whole LBD-cargo interaction sensor consisting of marker and the LBD-Nb<sub>G</sub>. This allowed to assess all possible effects the binding of the Nb<sub>G</sub> to the GFP might have on the measured fluorescent lifetime in the other samples.

The compartment-specific FRET-FLIM analysis revealed that VSR-ligand interaction occurs in the ER, the *cis*- and the *trans*-Golgi. In contrast, the TGN/EE and the MVB were identified as non-binding compartments. Thus, the TGN/EE is the first organelle *en-route* to the vacuole that allows for dissociation of ligands and the receptors. This suggests that the TGN/EE is the target of VSR-mediated sorting. Our results, furthermore, imply that soluble proteins, which have been transported into the TGN/EE, then follow the route to the vacuole without the involvement of a further receptor-mediated sorting step. In order to test our hypothesis regarding a putative default transport of soluble proteins from the TGN/EE towards the vacuole, we intended to deliver a fluorescent protein lacking any sorting signals directly into the TGN/EE and monitor for the possible accumulation of fluorescence signal in the vacuole. If indeed the bulk of fluorescent protein would arrive in this location, this very organelle had to be the final destination of default transport downstream of the TGN/EE.

For the practical application, we exploited the fact that the TGN in plants also has the function of the EE (Dettmer et al., 2006). This allowed us to incubate protoplasts

directly in a medium containing the fluorescent reporter protein, which was thereby funneled directly into the TGN/EE via endocytic uptake. We chose 3xRFP secreted from another protoplast population as a reporter, since proteins from this source could be attested to have passed intracellular quality control and to not contain vacuolar sorting signal as they had already been efficiently secreted by a plant cell. Furthermore, this 3xRFP reporter exhibited strong fluorescent signals even under acidic conditions, which should be favorable for detection in the lumen of a lytic vacuole, where GFP-derived tracers would be hard to detect (Tamura et al., 2003). A fusion protein consisting of 3xRFP and Nb<sub>G</sub> (3xRFP-Nb<sub>G</sub>) in combination with the anchor constructs SYP61-GFP and GFP-BP80 would additionally allow trapping the reporter 3xRFP-Nb<sub>G</sub> within the TGN/EE and MVB/LE, respectively. This would in turn enable us to prove that this molecule is transported along the same route as released VSR cargo. Imaging cells, which had taken up either of the two reporters, we revealed that endocytosed proteins, which did not contain any vacuolar sorting signals, are transported to the vacuole via the TGN/EE and the MVB/LE.

Our findings also allowed to bring *in vitro* VSR-ligand interaction data into agreement with the *in vivo* pH measurements of the compartments of the endomembrane system. Formerly, ligand release was supposed to take place at the MVB. Minding the pH dependency of receptor-ligand interaction, with binding at pH 6.5 to 7 and release at pH 5.5 and below, this inferred the MVB being more acidic than the TGN (Kirsch et al., 1994). This, however, has been shown to be a misconception, as two independent fluorescence-intensity-based and my FLIM-based measurements identified the TGN/EE as the most acidic compartment *en-route* to the vacuole (Fig. 1; Martiniere et al., 2013; Shen et al., 2013). Our FRET-FLIM results indicating dissociation of VSRs and their cargo in the TGN/EE fit well to the distinct acidification occurring between Golgi and TGN/EE, with the former possessing a binding-promoting pH of 6.8 and the latter a release-inducing pH of 5.7 (Fig. 1; Martiniere et al., 2013; Shen et al., 2013).

## **7.2. Nanobody-triggered lockdown of VSRs reveals ligand reloading in the Golgi**

We have shown, that VSRs bind their cargo in the ER and the Golgi at neutral pH and release it in the acidic TGN/EE (Künzli et al., 2016). While this is a one-way trip for the cargo proteins, VSRs might be recycled to an organelle, which again allows for ligand binding, to engage in further rounds of transport. Such a cycling of VSRs would enable a single receptor to sort a large amount of cargo molecules during its lifetime. This would also allow plant cells to thrive at very low VSR levels and to keep vacuolar sorting, regarding receptor turnover, highly efficient. Based on these considerations and the recycling of Cation-Independent Manose-6-Phosphate Receptors (ciMPPRs), which sort lysosomal cargo in mammalian cells, a similar mechanism has been implied for VSRs in plants (Duncan, 1988). Yet up to this point, no direct experimental evidence supporting this notion has been provided.

Therefore, we set out to determine whether and, if so, towards which compartment VSRs are recycled. To do so, we had to devise a strategy that allowed discriminating between newly synthesized VSRs and those receptors, which had putatively been transported back from a non-binding compartment to an organelle favoring VSR-ligand interaction. Furthermore, such an approach would have to provide the possibility to trap VSRs in putative recycling targets, namely the ER and the Golgi. This was necessary in order to show that putatively recycled receptors actually pass through those compartments, as they have in microscopy studies only been localized in non-binding compartments under steady state conditions (Li et al., 2002).

One of the first decisions we had to make while planning our experimental setups was which reporter to employ for the visualization of receptor-trafficking: derivatives of the full-length receptors or of GFP-BP80, which is a commonly used reporter for the transport of VSRs. GFP-BP80 essentially only consists of an intraluminal GFP, a transmembrane domain and the C-terminus of a VSR (daSilva et al., 2006). Except for ligand binding, this molecule had always been considered to behave like a wildtype VSR, especially since the immune-fluorescence signals, caused by  $\alpha$ VSR antibodies in GFP-BP80 lines, co-localized with the GFP signals (Li et al., 2002). In addition, GFP-BP80 fluorescence had not been detected in the vacuole, which was interpreted as indication for its capability to be retrogradely transported within the endomembrane system in the same fashion as it had been hypothesized for functional VSRs.

Considering this, we would have chosen a GFP-BP80 derivative as the reporter in our upcoming experiments, had I not made the subsequent discovery during characterization of the applicability of the Nb<sub>G</sub>-GFP-binding in the endomembrane system: The reason why GFP-BP80 had not been detected in the vacuole is not that it is recycled but that it is degraded upon arrival due to the conditions within the vacuole.

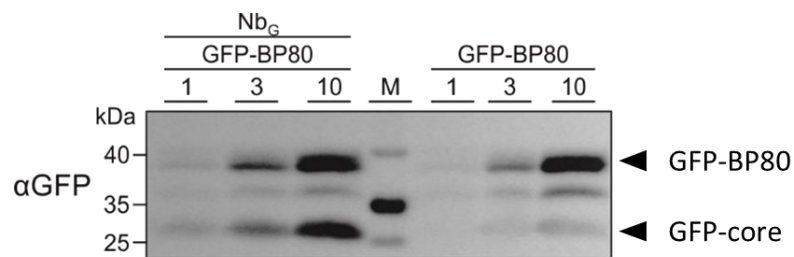


Figure 2: Western blot analysis of GFP-BP80 protein-levels in the presence (left) and absence (right) of Nb<sub>G</sub>. GFP-BP80 has an estimated size of 38 kDa. GFP-core has an estimated size of 28 kDa.

When I co-expressed GFP-BP80 and secreted Nb<sub>G</sub> and performed Western blotting to analyze expression levels (Fig. 2), I observed that specifically in the presence of secreted Nb<sub>G</sub> a GFP-derived vacuolar degradation product, the GFP-core, can be detected in GFP-BP80 expressing samples (daSilva et al., 2005). Since the signal, which corresponds to the full-length GFP-BP80, exhibits the same intensity irrespective of Nb<sub>G</sub>-expression, we concluded that the strong presence of GFP-core was caused by specific stabilization of this degradation product by the Nb<sub>G</sub> and not by increased degradation of GFP-BP80. The rapid break-down of GFP-BP80 and all its detectable degradation products had thus previously prevented the identification of the lytic vacuole as the final destination of this protein. As this meant that GFP-BP80 was most likely not recycling within the endomembrane system, a protein based on it was not to be considered a suitable reporter for the putative retrograde transport of VSRs. Instead, we opted for using a reporter derived from a full-length VSR.

In order to differentiate putative recycled reporters from newly synthesized ones, we intended to label those molecules, which had at least once been transported through the TGN/EE and had released their ligands there, with an endocytosed fluorescent protein. This led us to employ an Nb<sub>G</sub>-VSR fusion protein as a reporter for the transport of VSRs, since it enabled the use of endocytosed GFP-derivatives as labelling agents. The immediate advantage of this specific approach over an enzymatic labelling, which was performed to show the recycling of ciMPRs in mammals, was the compatibility

with confocal microscopy, allowing the intracellular tracking of the Nb<sub>G</sub>-VSR-bound GFP (Duncan, 1988). Another favorable aspect of this strategy was that excessive labelling agent, which was endocytosed but not linked to a VSR, would end up in the vacuole, where it was unable to produce confounding fluorescent signals due to the acidic and degradative conditions (Fig. 2; Tamura et al., 2003).

By applying this labelling technique, we showed, that Nb<sub>G</sub>-VSR, in contrast to the most likely recycling incompetent GFP-BP80, localizes in the TGN/EE. Thus, this very organelle might be the starting point of retrograde transport of receptors. In this case, accumulation could be explained by the transport back being the rate-limiting step of overall VSR-trafficking. Retrograde transport starting from the TGN/EE would be in agreement with the fact that receptor-ligand interaction is abolished in this compartment (Künzl et al., 2016). Further anterograde transport of VSRs would thus not just be unnecessary but might also pose unfavorable for an efficient receptor recycling: As ESCRTs become active during MVB biogenesis, VSRs could per chance be packed into nascent intra-luminal vesicles from where they cannot be returned to the cis-Golgi but are transported to the lumen of the vacuole.

In the next step, we needed to trap the labeled and recycled Nb<sub>G</sub>-VSR to compartmental markers within the organelles putatively targeted by retrograde VSR transport. To do so, we made use of another nanobody-epitope pair. Fusing the Anti- $\alpha$ -Synuclein Nanobody (Nbs) to the intraluminal domains of marker proteins and adding its antigen, which is a linear 23 amino acids long epitope found in the  $\alpha$ -Synuclein (SYN) protein, to a VSR reporter should enable the formation of a marker-VSR complex if all components are present within the same compartment (Guilliams et al., 2013). With this complex containing the sorting signal of the marker, the VSR reporter would be retained in the compartment of interest.

By incubating cells that expressed Nb<sub>G</sub>-VSR and an Nbs-marker fusion in medium, which contained the dual epitope linker GFP-SYN instead of the single epitope GFP, we aimed at combining both, the labelling and the trapping approach. Hereby, the GFP part of the molecule would specifically label VSRs in the TGN/EE and the SYN would trigger a lock-down should the reporter pass through an upstream compartment that contained a marker-Nbs fusion protein.

Employing this strategy, we were able to reveal that VSRs indeed recycle. Furthermore, we showed that recycled VSRs can be trapped in the *cis*- and *trans*-

cisternae of the Golgi but not in the ER. This implied that specifically the *cis*-side of the Golgi, as the most upstream location for which the presence of a recycled VSR has been shown, is the target of the retrograde VSR transport. Furthermore, co-accumulation of a vacuolar reporter with recycled Nb<sub>G</sub>-VSRs, which were locked in this compartment, demonstrated that VSRs are capable of interacting with their ligands, even after they have been retrieved from endosomal compartments. This specifically supported the concept that recycling of VSRs allows them to participate in several rounds of cargo-binding and release, before the receptors themselves are sorted for vacuolar delivery by the ESCRT machinery.

### **7.3. Dissection of the ESCRT-II assembly and recruitment by nanobody-based *in vivo* precipitation (iVIP)**

#### **7.3.1 Localization of Vacuolar Protein Sorting 22 (VPS22), VPS25 and VPS36**

In order to understand the molecular mechanism of ESCRT-mediated protein sorting in the context of endomembrane system, we aimed at characterizing the plant equivalent of the complex that resembles the heart of the ESCRT machinery in yeasts and mammals: ESCRT-II. In this regard, we aimed at characterizing the interactions between its putative subunits Vacuolar Protein Sorting 22 (VPS22), VPS25 and VPS36, as well as the respective localization of those three proteins.

For the localization studies *in planta*, we first generated *Arabidopsis* lines homozygous for a *pVPS36::VPS36-GFP* construct and the *vps36* knock-out causing SALK\_130246.49.85.x insertion. Expression of VPS36-GFP in these lines rescued the otherwise lethal phenotype of the *vps36* knock-out. Confocal analysis of rescued plants revealed a strong presence of VPS36-GFP at the PM. GFP signals were also observed less frequently at dot-like structures, There they partially co-localized with the styryl Fei-Mao (FM) dye 4-64. As this dye is an endocytic tracer, this indicated that plant VPS36, like its counterpart in yeast, partially localizes at endosomal structures (Babst et al., 2002b; Bolte et al., 2004). Even though VPS36-GFP was able to rescue the *vps36* knock-out phenotype and thus had to be at least partially functional, its PM localization was rather unexpected and might have been caused by the presence of the GFP-tag. To rule this out and to monitor for the intracellular distribution of ESCRT-II in general on an ultrastructural level, we aimed at localizing all three putative subunits, namely VPS22, VPS25 and VPS36, in wildtype plants by immune-electron

microscopy. For this, I raised specific antibodies against each of these three proteins and characterized them in respect to their ability to bind denatured and native VPS22, VPS25 or VPS36, respectively. Since all of them were proven to cross react with native antigens in immune precipitation assays, we employed them for *in-situ* studies on high-pressure frozen and freeze substituted *Arabidopsis* roots. To our great surprise, all three putative ESCRT-II subunits were found to be most prominently localized at the PM and only to a lesser extent at the TGN and the MVB. We interpreted the fact that all three proteins showed a similar distribution within the cell, including the intriguing and plant-specific accumulation at the PM, as a first indication that they actually form a complex. Likewise, transiently co-expressed VPS36-GFP, VPS22-RFP and VPS25-BFP2 exhibited perfect co-localization at the PM of tobacco mesophyll protoplasts. Furthermore, the protoplast system allowed for individual expression of fluorescently tagged VPS22, VPS25 or VPS36, to study their localization independently from each other. Under these circumstances, only VPS36 fusions were recruited to the plasma membrane. In contrast, VPS22-RFP and VPS25-RFP were completely cytosolic and showed no co-localization with a co-expressed PM marker. Since endogenous VPS22 and VPS25 had been detected at the PM in our ultrastructural analysis and VPS22- and VPS25-fusion proteins had been observed at the PM when co-expressed with VPS36-GFP, I hypothesized that their localization depends on the availability of VPS36. To test for this hypothesis, either VPS22-RFP or VPS25-RFP was co-expressed with VPS36-GFP. Now, both of them co-localized with VPS36-GFP at the PM indicating that VPS36 attaches to the PM independently of VPS22 and VPS25 and also mediates the recruitment of the latter two to this very site.

### **7.3.2 VPS22, VPS25 and VPS36 interact *in vivo***

Even though VPS22, VPS25 and VPS36 were found to co-localize and PM localization of all three seemed to depend on the same VPS36-mediated mechanism, it remained unclear, whether they form a complex in plant cells. Proofing the existence of such a complex required the demonstration of the interactions between its putative subunits. To perform interaction analyses *in vivo*, I opted for a FRET-FLIM approach. Here, VPS36-GFP was employed as energy donor, while either VPS25-RFP or VPS22-RFP was co-expressed as potential acceptors. Both RFP-fusion proteins, in sharp contrast to Cytosolic RFP (cytRFP), reduced the fluorescent lifetime of VPS36-GFP in a highly

significant fashion. This indicated a distance of less than 10 nm between the acceptor- and the donor-fluorophores implying an interaction between VPS36 and VPS22 as well as VPS25.

These findings hinted towards VPS36 being the central protein of plant ESCRT-II as it interacted with both other subunits and mediated their membrane attachment. To further characterize the ESCRT-II complex formation, we generated truncated mutants and tested for their ability to interact with VPS22 and VPS25. Already the deletion of 33 amino acids at the C-terminus of VPS36 (VPS36 $\Delta$ 33) abolished its capability of binding VPS25. However, VPS22-RFP was still able to bind to VPS36 $\Delta$ 33-GFP. This indicated that the VPS22-interaction site within VPS36 is located closer to the N-terminus than the VPS25-interaction site and showed that the loss of the ability to bind VPS25 was indeed caused by the truncation of an interaction motif and not due to general misfolding of VPS36 $\Delta$ 33-GFP. To also map the VPS22-interaction site, we further removed 33 amino acid stretches from the C-terminus of VPS36. While VPS36 $\Delta$ 66 and VPS36 $\Delta$ 99 still bound VPS22-RFP, VPS36 $\Delta$ 132-GFP was no longer able to do so. Because VPS36 $\Delta$ 132-GFP was still recruited to the PM, gross misfolding of this protein could again be excluded as a cause for non-interaction. The occurring FRET-effect in the presence of RFP-Nb<sub>G</sub> additionally demonstrated the functionality of this molecule as an energy donor. These results allowed the conclusion that the VPS22-interaction motif is situated between the 132th and 99th most C-terminal residues of VPS36.

After characterizing the interaction of VPS22 and VPS25 with VPS36, I intended to probe the putative VPS22-VPS25 interaction, which has been suggested based on yeast-2-hybrid screening results (Richardson et al., 2011; Shahriari et al., 2011). For this, VPS25-GFP was co-expressed with VPS22-RFP, VPS36-RFP as positive control and cytRFP as negative control. VPS22-RFP and VPS36-RFP but not cytRFP reduced the fluorescent lifetime of VPS25-GFP in FRET-FLIM studies significantly. This clearly indicated that VPS22 and VPS25 interact in plants but also raised the question whether VPS22 and VPS36 bind to the very same VPS25 molecule or to two different VPS25 moieties.



### 7.3.3 Establishing the indirect *in vivo* precipitation (iVIP) in plant cells

In order to assess whether one or two VPS25 moieties are present in a single ESCRT-II complex, I first had to find a suitable approach, which would enable me to discriminate between protein complexes containing one or two molecules of the same kind. Localization studies did not suffice in this case: A mixed population of complexes containing either one of two different fluorescent VPS25 derivatives would show the same fluorescence distribution as a mixed population of complexes containing any bivalent combination of those two VPS25 variants. Both would be observable as perfectly co-localizing fluorescent signals at the PM. Also, FRET and BiFC assays aimed at showing the presence of two different VPS25 variants within a single ESCRT-II complex suffered from a major drawback: Possible signals indicating the presence of VPS25-YFP-N-terminus and VPS25-YFP-C-terminus or VPS25-GFP and VPS25-RFP within one ESCRT-II complex would be confounded by ESCRT-II complexes containing two VPS25 moieties of the same kind. Those complexes would neither exhibit YFP-fluorescence in BiFC analysis nor any GFP-lifetime reduction in FRET-FLIM. For these reasons, those two approaches were not suitable to positively identify the presence of ESCRT-II complexes containing two VPS25 subunits.

However, fluorescence-3-hybrid (F3H) offered the possibility to produce a clear read-out (Herce et al., 2013). In F3H, which had not yet been applied in plants, a Nb<sub>G</sub>-fusion protein that resides at a morphologically distinct intracellular structure is used to precipitate a GFP-tagged protein of interest to the very same structure via a nanobody-epitope interaction. This alteration of intracellular distribution, which the protein of interest experiences, is also expected to apply to all interactors. Thus, if other co-expressed proteins exhibit the same shift in localization as the protein of interest, they are considered interactors. However, proteins maintaining their initial localization are considered non-interactors. In theory, this alters not only the localization of direct interactors but of whole complexes, if they contain at least a single GFP-labeled protein. Should we, in our case, alter the localization of VPS25-GFP via F3H, the distribution of another fluorescent VPS25 derivative would only be affected, if both proteins were situated within the very same ESCRT-II complex. Thus, if ESCRT-II harbored two VPS25 proteins, a localization shift of not only VPS25-GFP but also the other VPS25 variant would be expected. However, if ESCRT-II complexes incorporated only one VPS25 moiety, just the complexes containing VPS25-GFP and

not those containing the other VPS25 derivative would change their localization. Since this approach was aimed at monitoring indirect interactions and was essentially the *in vivo* variant of an immune precipitation, we dubbed it Indirect *In Vivo* Precipitation (iVIP).

Yet, before performing such a complex experiment, it was necessary to implement the concept of iVIP in plant cells. The first step in this process was to design the Nb<sub>G</sub>-fusion protein most suitable for later precipitation of VPS25-GFP *in vivo*. For the localization of this Nb<sub>G</sub>-fusion protein, the ER was chosen. A localization shift from the PM or the cytosol towards the reticulate and cisternal structures of this compartment was easily identifiable with the given resolution of confocal microscopy. To anchor the Nb<sub>G</sub> to the ER, a construct consisting of a signal peptide, a small intraluminal domain, the transmembrane domain as well as the cytosolic tail of Calnexin and the Nb<sub>G</sub> (CNX-Nb<sub>G</sub>) was designed. This protein positioned the Nb<sub>G</sub> at the surface of the ER and thus exposed it to the cytosol. This allowed for access of GFP-tagged proteins to the nanobody.

In order to assess the applicability of CNX-Nb<sub>G</sub> for the precipitation of cytosolic proteins in plant cells, its general ability to pull down Cytosolic GFP (cytGFP) onto the surface of the ER had to be demonstrated. For this, CNX-Nb<sub>G</sub> was co-expressed together with cytGFP, cytRFP, which served as negative control, and the ER marker BFP2-CNX. While cytRFP exhibited a characteristic cytosolic localization, cytGFP and BFP2-CNX co-localized at the ER indicating that the CNX-Nb<sub>G</sub>-induced pattern shift was specific for GFP. The same nanobody-epitope interaction-based recruitment also occurred, when VPS25-GFP and VPS25-RFP instead of cytGFP and cytRFP were co-expressed with CNX-Nb<sub>G</sub> and BFP2-CNX: Only VPS25-GFP but not VPS25-RFP, which served as negative control, was present at the ER-surface.

After the CNX-Nb<sub>G</sub>-mediated precipitation of GFP-tagged proteins had been successfully demonstrated, I analyzed the co-precipitation of interactors. For this, CNX-Nb<sub>G</sub>, VPS25-GFP and BFP2-CNX were co-expressed together with either VPS22-RFP or VPS36-RFP. Now, VPS25-GFP and the RFP-tagged molecules co-localized with BFP2-CNX at the ER illustrating the applicability of CNX-Nb<sub>G</sub> for the upcoming iVIP experiments.

Interestingly, in cells, in which VPS36-RFP was co-precipitated onto the ER, an altered ER phenotype, characterized by large and flat cisternae in close proximity to the PM,

was observable. We hypothesized that this phenotype was caused by VPS36-RFP binding directly to the PM while at the very same time being attached to the ER via VPS25-GFP and CNX-Nb<sub>G</sub>. Thus, the ER would be linked to the PM and the lamellar cisternae would represent the attachment sites. Aiming to verify this, Box-GFP, which is a PM-attached marker protein, was co-expressed with CNX-Nb<sub>G</sub> and RFP-HDEL, an ER marker accumulating less prominently in cisternae than BFP2-CNX (Scheuring et al., 2012). Indeed, cells expressing all of those constructs showed flat and PM proximal ER cisternae. This was also the case when VPS36-GFP was expressed instead of Box-GFP. The size of flattened cisternae was increased with increased levels of Box-GFP or VPS36-GFP, respectively. Together, this clearly indicated, that the interaction between these PM-localized proteins and CNX-Nb<sub>G</sub> induced ER-PM linkage. Interestingly, tubular ER, which was strongly labeled by RFP-HDEL, seemed unaffected and appeared wildtype-like. This selective recruitment of cisternal ER to PM might be explained by the mainly cisternal localization of CNX-fusion proteins, restricting CNX-Nb<sub>G</sub> and Box-GFP or VPS36-GFP from linking filamentous ER to the PM. Nevertheless, the total appearance of the ER was clearly altered. Thus, we wanted to confirm that its functionality was not affected. Therefore the ER export of soluble and membrane-bound proteins was monitored by confocal analysis of cells co-expressing either the vacuolar marker aleuRFP or the *cis*-Golgi marker Man1-RFP with VPS36-GFP in absence and presence of CNX-Nb<sub>G</sub> (Nebenführ et al., 1999; Humair et al., 2001). The RFP-tagged markers showed their characteristic distribution irrespective of the observed morphological ER-phenotype. Therefore, we concluded that the ER was still functional.

To determine the stoichiometry of the ESCRT-II complex, two differently tagged VPS25 variants, VPS22, VPS36 and CNX-Nb<sub>G</sub> had to be co-expressed. In this experiment, verifying the expression of five different constructs within a single cell posed a challenge. Only three fluorophores, which were unambiguously distinguishable by our confocal microscopy setup, were at our disposal. As I intended to use GFP and RFP as tags for VPS25, only BFP2 was left to fuse to either VPS22 or VPS36, while presence of CNX-Nb<sub>G</sub> could be monitored via its ER-recruiting effect on VPS25-GFP. Analyzing expression of VPS22 or VPS36 via Western blot was also not an option, as it would only allow for general detection of expression but would not allow for drawing any conclusions regarding co-expression within an individual cell.

Thus, we decided to employ a morphological read-out to assess the presence of either VPS22 or VPS36. As it had been already established that co-expression of CNX-Nb<sub>G</sub>, VPS25-GFP and VPS36 induced formation of large and flat ER cisternae, I aimed at utilizing this phenotype to verify VPS36 expression in a given protoplast. This allowed for employing a BFP2 fusion of VPS22 (VPS22-BFP2), which enabled the detection of this molecule directly by its fluorescence.

### **7.3.4 The plant ESCRT-II complex contains two VPS25 subunits**

In order to assess whether a single ESCRT-II complex contains one or two VPS25 moieties, the following constructs were co-expressed: VPS25-GFP, VPS25-RFP, VPS22-BFP2, CNX-Nb<sub>G</sub> and VPS36 fused to SYN (VPS36-SYN), which also allowed general verification of VPS36-SYN expression in Western blots via a custom-made Nbs-horseradish-peroxidase fusion. Protoplasts were analyzed for complete co-localization of fluorescent signals at the ER, which would imply the presence of two VPS25 moieties within a single ESCRT-II complex. Quintuple transformed cells indeed exhibited co-precipitation of VPS25-RFP onto the ER. Yet, without co-expressed VPS22-BFP2 or VPS36-SYN, VPS25-RFP remained cytosolic and was not detected at the ER. This indicated that ESCRT-II contains two VPS25 molecules and that VPS22 or VPS36, on their own, can only bind one VPS25 subunit each. These results are in agreement with the situation in yeast, as in this organism ESCRT-II possesses two VPS25 moieties, which are both needed for ESCRT-III recruitment to endosomal membranes (Teo et al., 2004; Teis et al., 2010).

Together, we showed that unlike the conventional F3H method, iVIP is not limited to test only direct protein-protein interaction. It is also suitable to analyze which proteins link those subunits of a complex together that do not make direct physical contact with each other. We, therefore, expect iVIP to become a staple technique for the analysis protein complex composition, especially in cases in which immune precipitation is not applicable, due to the effects cell lysis and extraction conditions might exhibit on protein-protein interactions and protein stability. While conducting iVIP experiments, I discovered a morphological ER phenotype, which is caused by forcing a PM attached protein onto the surface of the ER. Comparable flattening effects on the cisternae were observed upon co-expression of CNX-Nb<sub>G</sub> and either Box-GFP or VPS36-GFP, even though their modes of PM attachment are different, as the first depends on S-

acetylation and the second, most likely, on phospho-inositol-phosphate-binding (Lavy and Yalovsky, 2006; Im and Hurley, 2008). Extrapolating from this data, it should be possible to assess PM association of soluble GFP-fusion proteins by co-expressing them with the ER localized CNX-Nb<sub>G</sub>. In this scenario, PM association of the Nb<sub>G</sub>-trapped GFP-fusion protein would co-recruit the ER onto the PM resulting in a detectable morphological read-out. We consider this strategy especially useful, since in plant cells, which often harbor large vacuoles and only a thin layer of cytosol, it can be difficult to differentiate between a protein being cytosolic or PM-attached by simple localization studies.

The homology in complex composition between plant and yeast ESCRT-II might also indicate homologous molecular function, namely the recruitment of two ESCRT-III filaments in parallel (Teis et al., 2010). This is in line with the putative interaction between *Arabidopsis* VPS25 and the ESCRT-III subunit VPS20 (Richardson et al., 2011; Shahriari et al., 2011). As genetic evidence additionally points out that the absence of VPS36 greatly reduces the number of ESCRT-III-dependent ILVs within late endosomes, a similarity of endosomal ESCRT-II function in yeast and plants cannot be dismissed (Wang et al., 2017). The role of ESCRT-II at the PM of plant cells, however, remains elusive. In opisthokonta, ESCRT is not as prominent at the PM but is still engaged in a variety of processes at this site. It has been shown to be involved in the polar distribution of mRNA, to control the formation of microvesicles, to support membrane repair and to play a role during cytokinesis (Irion and St Johnston, 2007; Morita et al., 2007; Wehman et al., 2011; Nabhan et al., 2012; Jimenez et al., 2014). Since cytokinesis in plants follows a fundamentally different mechanism, a similar involvement of ESCRT seems to be rather unlikely (Balasubramanian et al., 2004; Jürgens, 2005). Nevertheless, participation of plant ESCRT-II in mRNA distribution, microvesicle formation and membrane repair cannot be ruled out and should be explored in the future.

Based on the *vps36-1* phenotype, there is also another role ESCRT-II might play at the PM: Macroscopically, the appearance of *vps36-1* mutants resembles the phenotype of *free1* and *amsh3* seedlings, which are defective in ubiquitin-dependent sorting of membrane proteins (Isono et al., 2010; Gao et al., 2014; Wang et al., 2017). The absence of other *vps36-1*-specific effects on plant development hints towards PM localized and EE/LE localized ESCRT-II being involved in the same pathway, namely

the transport of to-be-degraded PM proteins (Wang et al., 2017). At the PM, ESCRT-II might perform the initial recognition of poly-ubiquitinated proteins destined for vacuolar delivery. In this regard, ESCRT-II could either link cargo to adaptor proteins, thus taking actively part during endocytosis, or just be co-transported with ubiquitinated proteins promoting an efficient ESCRT-III recruitment upon arrival at endosomal compartments. VPS36 linking ubiquitinated proteins to adaptors could also explain why endocytosis specifically sequesters poly-ubiquitinated proteins from the PM (Scheuring et al., 2012): VPS36 harbors more than one ubiquitin-binding site, which is an attribute associated with proteins exhibiting high binding affinities for ubiquitin chains (Hawryluk et al., 2006; Scheuring et al., 2012; Wang et al., 2017). Speculations like this are especially tempting, since the identity of the plant poly-ubiquitin-receptor, mediating endocytosis of to-be-degraded PM proteins, has not yet been unambiguously determined. Even though proteins of the Tom1-Like (TOL) family and Src Homology-3 Domain-Containing Protein 2 (SH3P2) have been suggested as candidates, *in vivo* evidence supporting those claims is still scarce (Korbei et al., 2013; Nagel et al., 2017). Here, FRET- or F3H-based approaches might deliver further insights by demonstrating the direct interactions of ESCRT-II, the TOLs or SH3P2 with a poly-ubiquitinated cargo at the PM.

#### **7.4. Closing remarks**

My research focused on the biosynthetic and the endocytic pathways leading to the plant vacuole. Those transport routes merge at the TGN/EE. We have demonstrated that soluble molecules, which reached this organelle via endocytosis, are transported by default to the vacuole (Künzl et al., 2016). As we have furthermore shown, that VSRs do not interact with their cargo in this compartment, which we have additionally identified as the most likely starting point for retrograde VSR transport, we postulate that VSR-mediated transport is abolished in the TGN/EE (Künzl et al., 2016; Frühholz et al., 2018).

However, our conclusion stands at first glance in conflict with evidence hinting at the very same compartment being passed by secretory bulk flow, which would further infer default transport from the TGN to the PM (Viotti et al., 2010; Kang et al., 2011). The most robust pieces of evidence supporting this are immune electron micrographs of wildtype cells, which have not been treated with any type of transport inhibitors. Those

clearly show the presence of secreted cell-wall building blocks, namely xyloglycans, in the TGN (Kang et al., 2011). As there are no active sorting mechanisms known for this kind of molecules, they have to be assumed *bona-fide* markers for secretory bulk flow. An explanation to the ostensible contradictions regarding the two possible directions of default transport originating from the TGN/EE might be provided by considering the biogenesis and the fate of this organelle: According to structural and functional analysis, the *trans*-most cisternae of a Golgi can transform into a TGN, which will separate at some point from the stack (Viotti et al., 2010; Kang et al., 2011). It can give rise to SVs, which fuse with the PM, as well as CCVs, which have a yet unknown destination, and absorb endocytic vesicles thus becoming a TGN/EE before giving rise to MVBs/LEs via maturation (Dettmer et al., 2006; Kang et al., 2011; Scheuring et al., 2011). It is, furthermore, unknown whether TGN/EEs completely disassemble during MVB/LE biogenesis or whether parts of them might reassociate with *trans*-Golgi cisternae. This means that a TGN is not a static organelle and thus different studies might have led to varying but still accurate results depending on the state of monitored TGNs and the applied methodology.

Taking the time-component, which underlies a constant maturation, into account, a new model of TGN-related trafficking can be proposed. Yet, for that, the relevant steps have to be chronologically ordered. Evidence provided by us indicates that endocytosis and ligand release from the VSRs happens after secretion of soluble cargo has taken place (Künzli et al., 2016). The two processes bound to happen later are recycling of membrane proteins back to the PM, as this process is necessarily downstream of endocytosis, and MVB biogenesis, which is, as we have shown, also downstream of endocytosis (Künzli et al., 2016). The resulting order, in which trafficking events relevant for VSR-mediated transport take place at the TGN/EE, would thus be the following: VSRs retain their cargo within a not yet acidified TGN during the formation of huge SVs, which mediate default secretion. As apoplasmic content of arriving endocytic vesicles and the molecular activity of the V-ATPases then acidify the TGN/EE, the reduced pH induces dissociation of VSRs and their cargo (Dettmer et al., 2006; Martiniere et al., 2013; Shen et al., 2013; Künzli et al., 2016). Afterwards, recycling of membrane proteins back towards the PM takes place. This is mediated by CCVs, which possess a way smaller lumen than SVs and thus are not expected to have a relevant impact on the default transport of soluble cargo occurring

from here on towards the vacuole (Kang et al., 2011; Künzl et al., 2016). Finally, the remaining TGN/EE matures to MVB/LEs and VSRs are recycled for further rounds of transport (Scheuring et al., 2011; Frühholz et al., 2018).

ESCRT-mediated formation of ILVs is most probably occurring in parallel to those VSR-related transport events. Time-wise, its onset has to be downstream of the arrival of to-be-degraded PM proteins via endocytosis and the PI3P-dependent recruitment of FREE1/ESCRT-I (Scheuring et al., 2012; Gao et al., 2014). Recognition and pre-accumulation of ubiquitinated proteins by SH3P2, the TOLs and possibly ESCRT-II prior to endosomal delivery might increase efficiency of this process, which is likely to continue during endosomal maturation, as ESCRT components can also be found on MVBs (Scheuring et al., 2011; Korbei et al., 2013; Nagel et al., 2017; Fäßler et al., unpublished).

This model does not only explain, how two default transport events can originate from the TGN. Its proposed chronology is also in line with the presence of V-ATPases and CCV-budding being more closely associated with free and thus older TGN/EEs (Kang et al., 2011). Nevertheless, it still needs further validation and awaits the integration of other processes occurring during the maturation of a TGN, such as recycling of Golgi associated proteins back to the stack or the salvaging of V-ATPases.

For my studies to be successful, I had to design experiments, which allow for precise subcellular targeting of protein domains while maintaining their native topology, for post-transcriptional labelling and trapping of receptors and for the *in vivo* detection of indirect interactions between proteins. The strategies underlying these approaches had two things in common. They were based on the nanobody-epitope interactions and they employed transfected tobacco mesophyll protoplast as a model system. The usage of protoplasts was not necessitated by the employment of nanobodies but by experimental setups demanding tightly controlled co-expression of several effectors and reporters. Thus, the application of nanobodies is not restricted to this system. Implementing them in transgenic lines could open this new and exciting technology up to a wide variety of plant biologist. Especially iVIP could be easily implemented in other plant-based system. Transformation of an inducible CNX-Nb<sub>G</sub> construct into lines, which have already been created for co-immune precipitation experiments, would be the only major time investment. After induction, iVIP experiments should then produce the same read-out as in protoplasts allowing for *in vivo* assessment of direct and



indirect interactions via confocal microscopy. We anticipate this to support protein-protein interaction studies in many fields of research.

## 8. References

- Amerik, A.Y., Li, S.J., and Hochstrasser, M.** (2000). Analysis of the deubiquitinating enzymes of the yeast *Saccharomyces cerevisiae*. *Biol Chem* **381**.
- Babst, M., Sato, T.K., Banta, L.M., and Emr, S.D.** (1997). Endosomal transport function in yeast requires a novel AAA-type ATPase, Vps4p. *Embo j* **16**, 1820-1831.
- Babst, M., Wendland, B., Estepa, E.J., and Emr, S.D.** (1998). The Vps4p AAA ATPase regulates membrane association of a Vps protein complex required for normal endosome function. *The EMBO Journal* **17**, 2982-2993.
- Babst, M., Katzmann, D.J., Estepa-Sabal, E.J., Meerloo, T., and Emr, S.D.** (2002a). ESCRT-III: An endosome-associated heterooligomeric protein complex required for MVB sorting. *Developmental Cell* **3**, 271-282.
- Babst, M., Katzmann, D.J., Snyder, W.B., Wendland, B., and Emr, S.D.** (2002b). Endosome-associated complex, ESCRT-II, recruits transport machinery for protein sorting at the multivesicular body. *Developmental Cell* **3**, 283-289.
- Balasubramanian, M.K., Bi, E., and Glotzer, M.** (2004). Comparative Analysis of Cytokinesis in Budding Yeast, Fission Yeast and Animal Cells. *Current Biology* **14**, R806-R818.
- Barberon, M., Zelazny, E., Robert, S., Conejero, G., Curie, C., Friml, J., and Vert, G.** (2011). Monoubiquitin-dependent endocytosis of the iron-regulated transporter 1 (IRT1) transporter controls iron uptake in plants. *Proc Natl Acad Sci U S A* **108**, E450-458.
- Barbez, E., Dunser, K., Gaidora, A., Lendl, T., and Busch, W.** (2017). Auxin steers root cell expansion via apoplastic pH regulation in *Arabidopsis thaliana*. *Proceedings of the National Academy of Sciences of the United States of America* **114**, E4884-E4893.
- Barlowe, C., Orci, L., Yeung, T., Hosobuchi, M., Hamamoto, S., Salama, N., Rexach, M.F., Ravazzola, M., Amherdt, M., and Schekman, R.** (1994). COPII: A membrane coat formed by Sec proteins that drive vesicle budding from the endoplasmic reticulum. *Cell* **77**, 895-907.
- Bednarek, S.Y., Wilkins, T.A., Dombrowski, J.E., and Raikhel, N.V.** (1990). A carboxyl-terminal propeptide is necessary for proper sorting of barley lectin to vacuoles of tobacco. *The Plant cell* **2**, 1145-1155.
- Benghezal, M., Wasteneys, G.O., and Jones, D.A.** (2000). The C-Terminal Dilysine Motif Confers Endoplasmic Reticulum Localization to Type I Membrane Proteins in Plants. *The Plant cell* **12**, 1179-1201.
- Bethke, P.C., Swanson, S.J., Hillmer, S., and Jones, R.L.** (1998). From Storage Compartment to Lytic Organelle: The Metamorphosis of the Aleurone Protein Storage Vacuole. *Annals of Botany* **82**, 399-412.

- Bilodeau, P.S., Urbanowski, J.L., Winistorfer, S.C., and Piper, R.C.** (2002). The Vps27p Hse1p complex binds ubiquitin and mediates endosomal protein sorting. *Nat Cell Biol* **4**, 534-539.
- Blobel, G., and Dobberstein, B.** (1975). Transfer of proteins across membranes. I. Presence of proteolytically processed and unprocessed nascent immunoglobulin light chains on membrane-bound ribosomes of murine myeloma. *The Journal of cell biology* **67**, 835-851.
- Bolte, S., Talbot, C., Boute, Y., Catrice, O., Read, N.D., and Satiat-Jeunemaitre, B.** (2004). FM-dyes as experimental probes for dissecting vesicle trafficking in living plant cells. *J Microsc* **214**, 159-173.
- Bottanelli, F., Foresti, O., Hanton, S., and Denecke, J.** (2011). Vacuolar transport in tobacco leaf epidermis cells involves a single route for soluble cargo and multiple routes for membrane cargo. *The Plant cell* **23**, 3007-3025.
- Brown, W.J., Goodhouse, J., and Farquhar, M.G.** (1986). Mannose-6-phosphate receptors for lysosomal enzymes cycle between the Golgi complex and endosomes. *The Journal of cell biology* **103**, 1235-1247.
- Bucherl, C.A., Bader, A., Westphal, A.H., Laptanok, S.P., and Borst, J.W.** (2014). FRET-FLIM applications in plant systems. *Protoplasma* **251**, 383-394.
- Cai, Y., Zhuang, X., Gao, C., Wang, X., and Jiang, L.** (2014). The Arabidopsis Endosomal Sorting Complex Required for Transport III Regulates Internal Vesicle Formation of the Prevacuolar Compartment and Is Required for Plant Development. *Plant Physiology* **165**, 1328-1343.
- Cao, X., Rogers, S.W., Butler, J., Beevers, L., and Rogers, J.C.** (2000). Structural requirements for ligand binding by a probable plant vacuolar sorting receptor. *The Plant cell* **12**, 493-506.
- Carter, C., Pan, S., Zouhar, J., Avila, E.L., Girke, T., and Raikhel, N.V.** (2004). The vegetative vacuole proteome of *Arabidopsis thaliana* reveals predicted and unexpected proteins. *The Plant Cell Online* **16**, 3285-3303.
- Chaumont, F., Barrieu, F., Herman, E.M., and Chrispeels, M.J.** (1998). Characterization of a Maize Tonoplast Aquaporin Expressed in Zones of Cell Division and Elongation. *Plant Physiology* **117**, 1143-1152.
- Chidambaram, S., Zimmermann, J., and von Mollard, G.F.** (2008). ENTH domain proteins are cargo adaptors for multiple SNARE proteins at the TGN endosome. *Journal of Cell Science* **121**, 329-338.
- Contreras, I., Ortiz-Zapater, E., and Aniento, F.** (2004a). Sorting signals in the cytosolic tail of membrane proteins involved in the interaction with plant ARF1 and coatomer. *Plant J* **38**, 685-698.
- Contreras, I., Yang, Y., Robinson, D.G., and Aniento, F.** (2004b). Sorting signals in the cytosolic tail of plant p24 proteins involved in the interaction with the COPII coat. *Plant & cell physiology* **45**, 1779-1786.

- Crowell, E.F., Bischoff, V., Desprez, T., Rolland, A., Stierhof, Y.-D., Schumacher, K., Gonneau, M., Höfte, H., and Vernhettes, S.** (2009). Pausing of Golgi Bodies on Microtubules Regulates Secretion of Cellulose Synthase Complexes in *Arabidopsis*. *The Plant cell* **21**, 1141-1154.
- daSilva, L.L., Foresti, O., and Denecke, J.** (2006). Targeting of the plant vacuolar sorting receptor BP80 is dependent on multiple sorting signals in the cytosolic tail. *The Plant cell* **18**, 1477-1497.
- daSilva, L.L., Taylor, J.P., Hadlington, J.L., Hanton, S.L., Snowden, C.J., Fox, S.J., Foresti, O., Brandizzi, F., and Denecke, J.** (2005). Receptor salvage from the prevacuolar compartment is essential for efficient vacuolar protein targeting. *The Plant cell* **17**, 132-148.
- De Los Santos, C., Chang, C.-W., Mycek, M.-A., and Cardullo, R.A.** (2015). FRAP, FLIM, and FRET: Detection and analysis of cellular dynamics on a molecular scale using fluorescence microscopy. *Molecular reproduction and development* **82**, 587-604.
- Denecke, J., Botterman, J., and Deblaere, R.** (1990). Protein secretion in plant cells can occur via a default pathway. *The Plant cell* **2**, 51-59.
- Denecke, J., De Rycke, R., and Botterman, J.** (1992). Plant and mammalian sorting signals for protein retention in the endoplasmic reticulum contain a conserved epitope. *EMBO J* **11**, 2345-2355.
- Dettmer, J., Hong-Hermesdorf, A., Stierhof, Y.D., and Schumacher, K.** (2006). Vacuolar H<sup>+</sup>-ATPase activity is required for endocytic and secretory trafficking in *Arabidopsis*. *The Plant cell* **18**, 715-730.
- Dhonukshe, P., Aniento, F., Hwang, I., Robinson, D.G., Mravec, J., Stierhof, Y.-D., and Friml, J.** (2007). Clathrin-Mediated Constitutive Endocytosis of PIN Auxin Efflux Carriers in *Arabidopsis*. *Current Biology* **17**, 520-527.
- Dombrowski, J.E., Schroeder, M.R., Bednarek, S.Y., and Raikhel, N.V.** (1993). Determination of the functional elements within the vacuolar targeting signal of barley lectin. *The Plant cell* **5**, 587-596.
- Driouich, A., Faye, L., and Staehelin, A.** (1993). The plant Golgi apparatus: a factory for complex polysaccharides and glycoproteins. *Trends in Biochemical Sciences* **18**, 210-214.
- Duncan, J.R.K., S.** (1988). Intracellular movement of two mannose 6-phosphate receptors: return to the Golgi apparatus. *The Journal of cell biology* **106**, 617-628.
- Fan, L., Hao, H., Xue, Y., Zhang, L., Song, K., Ding, Z., Botella, M.A., Wang, H., and Lin, J.** (2013). Dynamic analysis of *Arabidopsis* AP2  $\sigma$  subunit reveals a key role in clathrin-mediated endocytosis and plant development. *Development* **140**, 3826-3837.

- Fäßler, F., and Pimpl, P.** (2017). In Vivo Interaction Studies by Measuring Förster Resonance Energy Transfer Through Fluorescence Lifetime Imaging Microscopy (FRET/FLIM). In *Plant Protein Secretion: Methods and Protocols*, L. Jiang, ed (New York, NY: Springer New York), pp. 159-170.
- Flynn, G.C., Pohl, J., Flocco, M.T., and Rothman, J.E.** (1991). Peptide-binding specificity of the molecular chaperone BiP. *Nature* **353**, 726-730.
- Ford, M.G.J., Mills, I.G., Peter, B.J., Vallis, Y., Praefcke, G.J.K., Evans, P.R., and McMahon, H.T.** (2002). Curvature of clathrin-coated pits driven by epsin. *Nature* **419**, 361-366.
- Foresti, O., and Denecke, J.** (2008). Intermediate Organelles of the Plant Secretory Pathway: Identity and Function. *Traffic* **9**, 1599-1612.
- Foresti, O., Gershlick, D.C., Bottanelli, F., Hummel, E., Hawes, C., and Denecke, J.** (2010). A Recycling-Defective Vacuolar Sorting Receptor Reveals an Intermediate Compartment Situated between Prevacuoles and Vacuoles in Tobacco. *The Plant cell* **22**, 3992-4008.
- Frand, A.R., Cuozzo, J.W., and Kaiser, C.A.** (2000). Pathways for protein disulphide bond formation. *Trends in Cell Biology* **10**, 203-210.
- Frühholz, S., Fäßler, F., Kolukisaoglu, Ü., and Pimpl, P.** (2018). Nanobody-triggered lockdown of VSRs reveals ligand reloading in the Golgi. *Nature Communications* **9**, 643.
- Fujimoto, M., Arimura, S., Ueda, T., Takanashi, H., Hayashi, Y., Nakano, A., and Tsutsumi, N.** (2010). Arabidopsis dynamin-related proteins DRP2B and DRP1A participate together in clathrin-coated vesicle formation during endocytosis. *Proceedings of the National Academy of Sciences of the United States of America* **107**, 6094-6099.
- Gadeyne, A., Sánchez-Rodríguez, C., Vanneste, S., Di Rubbo, S., Zauber, H., Vanneste, K., Van Leene, J., De Winne, N., Eeckhout, D., Persiau, G., Van De Slijke, E., Cannoot, B., Vercruysse, L., Mayers, Jonathan R., Adamowski, M., Kania, U., Ehrlich, M., Schweighofer, A., Ketelaar, T., Maere, S., Bednarek, Sebastian Y., Friml, J., Gevaert, K., Witters, E., Russinova, E., Persson, S., De Jaeger, G., and Van Damme, D.** (2014). The TPLATE Adaptor Complex Drives Clathrin-Mediated Endocytosis in Plants. *Cell* **156**, 691-704.
- Gao, C., Yu, C.K.Y., Qu, S., San, M.W.Y., Li, K.Y., Lo, S.W., and Jiang, L.** (2012). The Golgi-Localized *Arabidopsis* Endomembrane Protein12 Contains Both Endoplasmic Reticulum Export and Golgi Retention Signals at Its C Terminus. *The Plant cell* **24**, 2086-2104.
- Gao, C., Luo, M., Zhao, Q., Yang, R., Cui, Y., Zeng, Y., Xia, J., and Jiang, L.** (2014). A Unique Plant ESCRT Component, FREE1, Regulates Multivesicular Body Protein Sorting and Plant Growth. *Current Biology* **24**, 2556-2563.

- Geldner, N., Friml, J., Stierhof, Y.-D., Jurgens, G., and Palme, K.** (2001). Auxin transport inhibitors block PIN1 cycling and vesicle trafficking. *Nature* **413**, 425-428.
- Geldner, N., Anders, N., Wolters, H., Keicher, J., Kornberger, W., Muller, P., Delbarre, A., Ueda, T., Nakano, A., and Jürgens, G.** (2003). The Arabidopsis GNOM ARF-GEF Mediates Endosomal Recycling, Auxin Transport, and Auxin-Dependent Plant Growth. *Cell* **112**, 219-230.
- Geuze, H.J., Slot, J.W., Strous, G.J., Hasilik, A., and von Figura, K.** (1985). Possible pathways for lysosomal enzyme delivery. *The Journal of cell biology* **101**, 2253-2262.
- Gillooly, D.J., Raiborg, C., and Stenmark, H.** (2003). Phosphatidylinositol 3-phosphate is found in microdomains of early endosomes. *Histochemistry and Cell Biology* **120**, 445-453.
- Griffiths, G., and Simons, K.** (1986). The trans Golgi network: sorting at the exit site of the Golgi complex. *Science* **234**, 438-443.
- Gubler, F., Jacobsen, J.V., and Ashford, A.E.** (1986). Involvement of the Golgi apparatus in the secretion of  $\alpha$ -amylase from gibberellin-treated barley aleurone cells. *Planta* **168**, 447-452.
- Guilliams, T., El-Turk, F., Buell, A.K., O'Day, E.M., Aprile, F.A., Esbjorner, E.K., Vendruscolo, M., Cremades, N., Pardon, E., Wyns, L., Welland, M.E., Steyaert, J., Christodoulou, J., Dobson, C.M., and De Genst, E.** (2013). Nanobodies Raised against Monomeric alpha-Synuclein Distinguish between Fibrils at Different Maturation Stages. *Journal of Molecular Biology* **425**, 2397-2411.
- Hamers-Casterman, C., Atarhouch, T., Muyldermans, S., Robinson, G., Hammers, C., Songa, E.B., Bendahman, N., and Hammers, R.** (1993). Naturally occurring antibodies devoid of light chains. *Nature* **363**, 446.
- Hammond, C., and Helenius, A.** (1994). Folding of VSV G protein: sequential interaction with BiP and calnexin. *Science* **266**, 456-458.
- Hammond, C., Braakman, I., and Helenius, A.** (1994). Role of N-linked oligosaccharide recognition, glucose trimming, and calnexin in glycoprotein folding and quality control. *Proceedings of the National Academy of Sciences of the United States of America* **91**, 913-917.
- Hanton, S.L., Renna, L., Bortolotti, L.E., Chatre, L., Stefano, G., and Brandizzi, F.** (2005). Diacidic Motifs Influence the Export of Transmembrane Proteins from the Endoplasmic Reticulum in Plant Cells. *The Plant cell* **17**, 3081-3093.
- Happel, N., Honing, S., Neuhaus, J.M., Paris, N., Robinson, D.G., and Holstein, S.E.** (2004). Arabidopsis micro A-adaptin interacts with the tyrosine motif of the vacuolar sorting receptor VSR-PS1. *Plant J* **37**, 678-693.

- Harris, P.J., and Northcote, D.H.** (1971). Polysaccharide formation in plant Golgi bodies. *Biochimica et Biophysica Acta (BBA) - General Subjects* **237**, 56-64.
- Hawryluk, M.J., Keyel, P.A., Mishra, S.K., Watkins, S.C., Heuser, J.E., and Traub, L.M.** (2006). Epsin 1 is a Polyubiquitin-Selective Clathrin-Associated Sorting Protein. *Traffic* **7**, 262-281.
- Heikal, A.A., Hess, S.T., and Webb, W.W.** (2001). Multiphoton molecular spectroscopy and excited-state dynamics of enhanced green fluorescent protein (EGFP): acid–base specificity. *Chemical Physics* **274**, 37-55.
- Henne, William M., Buchkovich, Nicholas J., and Emr, Scott D.** (2011). The ESCRT Pathway. *Developmental Cell* **21**, 77-91.
- Henne, W.M., Boucrot, E., Meinecke, M., Evergren, E., Vallis, Y., Mittal, R., and McMahon, H.T.** (2010). FCHo Proteins Are Nucleators of Clathrin-Mediated Endocytosis. *Science* **328**, 1281-1284.
- Herce, H.D., Deng, W., Helma, J., Leonhardt, H., and Cardoso, M.C.** (2013). Visualization and targeted disruption of protein interactions in living cells. *Nat Commun* **4**, 2660.
- Hiatt, A., Cafferkey, R., and Bowdish, K.** (1989). Production of antibodies in transgenic plants. *Nature* **342**, 76-78.
- Hinrichsen, L., Meyerholz, A., Groos, S., and Ungewickell, E.J.** (2006). Bending a membrane: How clathrin affects budding. *Proceedings of the National Academy of Sciences* **103**, 8715-8720.
- Hinz, G., Colanesi, S., Hillmer, S., Rogers, J.C., and Robinson, D.G.** (2007). Localization of Vacuolar Transport Receptors and Cargo Proteins in the Golgi Apparatus of Developing Arabidopsis Embryos. *Traffic* **8**, 1452-1464.
- Hoflack, B., and Kornfeld, S.** (1985). Purification and characterization of a cation-dependent mannose 6-phosphate receptor from murine P388D1 macrophages and bovine liver. *J Biol Chem* **260**, 12008-12014.
- Holwerda, B.C., Padgett, H.S., and Rogers, J.C.** (1992). Proaleurain vacuolar targeting is mediated by short contiguous peptide interactions. *The Plant cell* **4**, 307-318.
- Horner, H.T., and Arnott, H.J.** (1965). A HISTOCHEMICAL AND ULTRASTRUCTURAL STUDY OF YUCCA SEED PROTEINS. *American Journal of Botany* **52**, 1027-1038.
- Humair, D., Hernandez Felipe, D., Neuhaus, J.M., and Paris, N.** (2001). Demonstration in yeast of the function of BP-80, a putative plant vacuolar sorting receptor. *The Plant cell* **13**, 781-792.
- Hunziker, W., and Fumey, C.** (1994). A di-leucine motif mediates endocytosis and basolateral sorting of macrophage IgG Fc receptors in MDCK cells. *The EMBO Journal* **13**, 2963-2969.

- Huotari, J., and Helenius, A.** (2011). Endosome maturation. *The EMBO Journal* **30**, 3481-3500.
- Huttner, S., Veit, C., Vavra, U., Schoberer, J., Liebminger, E., Maresch, D., Grass, J., Altmann, F., Mach, L., and Strasser, R.** (2014). Arabidopsis Class I alpha-Mannosidases MNS4 and MNS5 Are Involved in Endoplasmic Reticulum-Associated Degradation of Misfolded Glycoproteins. *The Plant cell* **26**, 1712-1728.
- Hwang, C., Sinskey, A.J., and Lodish, H.F.** (1992). Oxidized redox state of glutathione in the endoplasmic reticulum. *Science* **257**, 1496-1502.
- Iijima, M., and Kono, Y.** (1992). Development of Golgi Apparatus in the Root Cap Cells of Maize (*Zea mays* L.) as Affected by Compacted Soil. *Annals of Botany* **70**, 207-212.
- Im, Y.J., and Hurley, J.H.** (2008). Integrated Structural Model and Membrane Targeting Mechanism of the Human ESCRT-II Complex. *Developmental Cell* **14**, 902-913.
- Im, Y.J., Wollert, T., Boura, E., and Hurley, J.H.** (2009). Structure and Function of the ESCRT-II-III Interface in Multivesicular Body Biogenesis. *Developmental Cell* **17**, 234-243.
- Irion, U., and St Johnston, D.** (2007). bicoid RNA localization requires specific binding of an endosomal sorting complex. *Nature* **445**, 554-558.
- Isono, E., Katsiarimpa, A., Muller, I.K., Anzenberger, F., Stierhof, Y.D., Geldner, N., Chory, J., and Schwechheimer, C.** (2010). The deubiquitinating enzyme AMSH3 is required for intracellular trafficking and vacuole biogenesis in *Arabidopsis thaliana*. *The Plant cell* **22**.
- Jahn, R., and Scheller, R.H.** (2006). SNAREs — engines for membrane fusion. *Nature Reviews Molecular Cell Biology* **7**, 631.
- Jensen, W.A.** (1965). The composition and ultrastructure of the nucellus in cotton. *Journal of Ultrastructure Research* **13**, 112-128.
- Jimenez, A.J., Maiuri, P., Lafaurie-Janvore, J., Divoux, S., Piel, M., and Perez, F.** (2014). ESCRT machinery is required for plasma membrane repair. *Science* **343**, 1247136.
- Jin, H., Yan, Z., Nam, K.H., and Li, J.** (2007). Allele-Specific Suppression of a Defective Brassinosteroid Receptor Reveals a Physiological Role of UGGT in ER Quality Control. *Molecular Cell* **26**, 821-830.
- Jochem, P., Rona, J.-P., Smith, J.A.C., and Lüttge, U.** (1984). Anion-sensitive ATPase activity and proton transport in isolated vacuoles of species of the CAM genus *Kalanchoë*. *Physiologia Plantarum* **62**, 410-415.
- Jürgens, G.** (2005). Plant cytokinesis: fission by fusion. *Trends in Cell Biology* **15**, 277-283.



- Kang, B.H., Nielsen, E., Preuss, M.L., Mastronarde, D., and Staehelin, L.A.** (2011). Electron tomography of RabA4b- and PI-4Kbeta1-labeled trans Golgi network compartments in Arabidopsis. *Traffic* **12**, 313-329.
- Kang, H., Kim, S.Y., Song, K., Sohn, E.J., Lee, Y., Lee, D.W., Hara-Nishimura, I., and Hwang, I.** (2012). Trafficking of Vacuolar Proteins: The Crucial Role of *Arabidopsis* Vacuolar Protein Sorting 29 in Recycling Vacuolar Sorting Receptor. *The Plant cell* **24**, 5058-5073.
- Kasai, K., Takano, J., Miwa, K., Toyoda, A., and Fujiwara, T.** (2011). High boron-induced ubiquitination regulates vacuolar sorting of the BOR1 borate transporter in *Arabidopsis thaliana*. *J Biol Chem* **286**, 6175-6183.
- Katzmann, D.J., Babst, M., and Emr, S.D.** (2001). Ubiquitin-dependent sorting into the multivesicular body pathway requires the function of a conserved endosomal protein sorting complex, ESCRT-I. *Cell* **106**, 145-155.
- Katzmann, D.J., Stefan, C.J., Babst, M., and Emr, S.D.** (2003). Vps27 recruits ESCRT machinery to endosomes during MVB sorting. *The Journal of cell biology* **162**, 413-423.
- Kelly, B.T., McCoy, A.J., Späte, K., Miller, S.E., Evans, P.R., Höning, S., and Owen, D.J.** (2008). A structural explanation for the binding of endocytic dileucine motifs by the AP2 complex. *Nature* **456**, 976-979.
- Kirchhausen, T., and Harrison, S.C.** (1981). Protein organization in clathrin trimers. *Cell* **23**, 755-761.
- Kirsch, T., Paris, N., Butler, J.M., Beevers, L., and Rogers, J.C.** (1994). Purification and initial characterization of a potential plant vacuolar targeting receptor. *Proc. Natl. Acad. Sci. USA* **91**, 3403-3407.
- Korbei, B., Moulinier-Anzola, J., De-Araujo, L., Lucyshyn, D., Retzer, K., Khan, M.A., and Luschig, C.** (2013). Arabidopsis TOL Proteins Act as Gatekeepers for Vacuolar Sorting of PIN2 Plasma Membrane Protein. *Current Biology* **23**, 2500-2505.
- Kostelansky, M.S., Schluter, C., Tam, Y.Y.C., Lee, S., Ghirlando, R., Beach, B., Conibear, E., and Hurley, J.H.** (2007). Molecular architecture and functional model of the complete yeast ESCRT-I heterotetramer. *Cell* **129**, 485-498.
- Kriechbaumer, V., Botchway, S.W., Slade, S.E., Knox, K., Frigerio, L., Oparka, K.J., and Hawes, C.** (2015). Reticulomics: Protein-protein interaction studies with two plasmodesmata-localised reticulon family proteins identify binding partners enriched at plasmodesmata, ER and the plasma membrane. *Plant Physiology*.
- Künzl, F., Frühholz, S., Fäßler, F., Li, B., and Pimpl, P.** (2016). Receptor-mediated sorting of soluble vacuolar proteins ends at the trans-Golgi network/early endosome. *Nature Plants* **2**, 16017.

- Kutschera, U., and Köhler, K.** (1994). Cell elongation, turgor and osmotic pressure in developing sunflower hypocotyls. *Journal of Experimental Botany* **45**, 591-595.
- Langhans, M., Marcote, M.J., Pimpl, P., Virgili-López, G., Robinson, D.G., and Aniento, F.** (2008). In vivo Trafficking and Localization of p24 Proteins in Plant Cells. *Traffic* **9**, 770-785.
- Lavy, M., and Yalovsky, S.** (2006). Association of Arabidopsis type-II ROPs with the plasma membrane requires a conserved C-terminal sequence motif and a proximal polybasic domain. *Plant J* **46**.
- Lee, H.-i., Gal, S., Newman, T.C., and Raikhel, N.V.** (1993). The Arabidopsis endoplasmic reticulum retention receptor functions in yeast. *Proceedings of the National Academy of Sciences* **90**, 11433-11437.
- Leitner, J., Petrášek, J., Tomanov, K., Retzer, K., Pařezová, M., Korbei, B., Bachmair, A., Zažímalová, E., and Luschig, C.** (2012). Lysine63-linked ubiquitylation of PIN2 auxin carrier protein governs hormonally controlled adaptation of Arabidopsis root growth. *Proceedings of the National Academy of Sciences* **109**, 8322-8327.
- Letourneur, F., Gaynor, E.C., Hennecke, S., Démollière, C., Duden, R., Emr, S.D., Riezman, H., and Cosson, P.** (1994). Coatamer is essential for retrieval of dilysine-tagged proteins to the endoplasmic reticulum. *Cell* **79**, 1199-1207.
- Li, R., Liu, P., Wan, Y., Chen, T., Wang, Q., Mettbach, U., Baluška, F., Šamaj, J., Fang, X., Lucas, W.J., and Lin, J.** (2012). A Membrane Microdomain-Associated Protein, *Arabidopsis* Flot1, Is Involved in a Clathrin-Independent Endocytic Pathway and Is Required for Seedling Development. *The Plant cell* **24**, 2105-2122.
- Li, X., Ed, E., and Wim, d.E.** (2013). Vacuolar protein sorting mechanisms in plants. *The FEBS journal* **280**, 979-993.
- Li, Y.B., Rogers, S.W., Tse, Y.C., Lo, S.W., Sun, S.S., Jauh, G.Y., and Jiang, L.** (2002). BP-80 and homologs are concentrated on post-Golgi, probable lytic prevacuolar compartments. *Plant & cell physiology* **43**, 726-742.
- Liu, J.-X., and Howell, S.H.** (2016). Managing the protein folding demands in the endoplasmic reticulum of plants. *New Phytologist* **211**, 418-428.
- Lousa, C.D., Gershlick, D.C., and Denecke, J.** (2012). Mechanisms and Concepts Paving the Way towards a Complete Transport Cycle of Plant Vacuolar Sorting Receptors. *The Plant cell* **24**, 1714-1732.
- Lu, D., Lin, W., Gao, X., Wu, S., Cheng, C., Avila, J., Heese, A., Devarenne, T.P., He, P., and Shan, L.** (2011). Direct ubiquitination of pattern recognition receptor FLS2 attenuates plant innate immunity. *Science* **332**, 1439-1442.
- Lu, Q., Hope, L.W., Brasch, M., Reinhard, C., and Cohen, S.N.** (2003). TSG101 interaction with HRS mediates endosomal trafficking and receptor down-

regulation. Proceedings of the National Academy of Sciences **100**, 7626-7631.

**Luo, F., Fong, Y.H., Zeng, Y., Shen, J., Jiang, L., and Wong, K.-B.** (2014). How Vacuolar Sorting Receptor Proteins Interact with Their Cargo Proteins: Crystal Structures of Apo and Cargo-Bound Forms of the Protease-Associated Domain from an *Arabidopsis* Vacuolar Sorting Receptor. The Plant cell **26**, 3693-3708.

**Luo, Y., Scholl, S., Doering, A., Zhang, Y., Irani, N.G., Rubbo, S.D., Neumetzler, L., Krishnamoorthy, P., Van Houtte, I., Mylle, E., Bischoff, V., Vernhettes, S., Winne, J., Friml, J., Stierhof, Y.-D., Schumacher, K., Persson, S., and Russinova, E.** (2015). V-ATPase-activity in the TGN/EE is required for exocytosis and recycling in *Arabidopsis*. Nature plants **1**, 15094-15094.

**Lynch, M.A., and Staehelin, L.A.** (1992). Domain-specific and cell type-specific localization of two types of cell wall matrix polysaccharides in the clover root tip. The Journal of cell biology **118**, 467-479.

**Martiniere, A., Bassil, E., Jublanc, E., Alcon, C., Reguera, M., Sentenac, H., Blumwald, E., and Paris, N.** (2013). In vivo intracellular pH measurements in tobacco and *Arabidopsis* reveal an unexpected pH gradient in the endomembrane system. The Plant cell **25**, 4028-4043.

**Martins, S., Dohmann, E.M., Cayrel, A., Johnson, A., Fischer, W., Pojer, F., Satiat-Jeunemaitre, B., Jaillais, Y., Chory, J., Geldner, N., and Vert, G.** (2015). Internalization and vacuolar targeting of the brassinosteroid hormone receptor BRI1 are regulated by ubiquitination. Nat Commun **6**, 6151.

**Matsuoka, K., and Neuhaus, J.-M.** (1999). Cis-elements of protein transport to the plant vacuoles. Journal of Experimental Botany **50**, 165-174.

**McMahon, H.T., and Boucrot, E.** (2011). Molecular mechanism and physiological functions of clathrin-mediated endocytosis. Nat Rev Mol Cell Biol **12**, 517-533.

**Meyer, D.I., Krause, E., and Dobberstein, B.** (1982). Secretory protein translocation across membranes-the role of the "docking protein". Nature **297**, 647-650.

**Miao, Y., Yan, P.K., Kim, H., Hwang, I., and Jiang, L.** (2006). Localization of Green Fluorescent Protein Fusions with the Seven *Arabidopsis* Vacuolar Sorting Receptors to Prevacuolar Compartments in Tobacco BY-2 Cells. Plant Physiology **142**, 945-962.

**Montesinos, J.C., Pastor-Cantizano, N., Robinson, D.G., Marcote, M.J., and Aniento, F.** (2014). *Arabidopsis* p24 $\delta$ 5 and p24 $\delta$ 9 facilitate Coat Protein I-dependent transport of the K/HDEL receptor ERD2 from the Golgi to the endoplasmic reticulum. The Plant Journal **80**, 1014-1030.

**Moore, P.J., and Staehelin, L.A.** (1988). Immunogold localization of the cell-wall-matrix polysaccharides rhamnogalacturonan I and xyloglucan during cell

expansion and cytokinesis in *Trifolium pratense* L.; implication for secretory pathways. *Planta* **174**, 433-445.

**Morita, E., Sandrin, V., Chung, H.Y., Morham, S.G., Gygi, S.P., Rodesch, C.K., and Sundquist, W.I.** (2007). Human ESCRT and ALIX proteins interact with proteins of the midbody and function in cytokinesis. *The EMBO Journal* **26**, 4215-4227.

**Muller, J., Piffanelli, P., Devoto, A., Miklis, M., Elliott, C., Ortmann, B., Schulze-Lefert, P., and Panstruga, R.** (2005). Conserved ERAD-like quality control of a plant polytopic membrane protein. *The Plant cell* **17**, 149-163.

**Munro, S., and Pelham, H.R.B.** (1987). A C-terminal signal prevents secretion of luminal ER proteins. *Cell* **48**, 899-907.

**Murphy, R.F., Powers, S., and Cantor, C.R.** (1984). Endosome pH measured in single cells by dual fluorescence flow cytometry: rapid acidification of insulin to pH 6. *The Journal of cell biology* **98**, 1757-1762.

**Muyldermans, S.** (2001). Single domain camel antibodies: current status. *Reviews in Molecular Biotechnology* **74**, 277-302.

**Nabhan, J.F., Hu, R., Oh, R.S., Cohen, S.N., and Lu, Q.** (2012). Formation and release of arrestin domain-containing protein 1-mediated microvesicles (ARMMs) at plasma membrane by recruitment of TSG101 protein. *Proceedings of the National Academy of Sciences* **109**, 4146-4151.

**Nagel, M.-K., Kalinowska, K., Vogel, K., Reynolds, G.D., Wu, Z., Anzenberger, F., Ichikawa, M., Tsutsumi, C., Sato, M.H., Kuster, B., Bednarek, S.Y., and Isono, E.** (2017). Arabidopsis SH3P2 is an ubiquitin-binding protein that functions together with ESCRT-I and the deubiquitylating enzyme AMSH3. *Proceedings of the National Academy of Sciences* **114**, E7197-E7204.

**Nakano, A., and Luini, A.** (2010). Passage through the Golgi. *Current Opinion in Cell Biology* **22**, 471-478.

**Nebenführ, A., Gallagher, L.A., Dunahay, T.G., Frohlick, J.A., Mazurkiewicz, A.M., Meehl, J.B., and Staehelin, L.A.** (1999). Stop-and-Go Movements of Plant Golgi Stacks Are Mediated by the Acto-Myosin System. *Plant Physiology* **121**, 1127-1141.

**Niemes, S., Labs, M., Scheuring, D., Krueger, F., Langhans, M., Jesenofsky, B., Robinson, D.G., and Pimpl, P.** (2010a). Sorting of plant vacuolar proteins is initiated in the ER. *Plant J* **62**, 601-614.

**Niemes, S., Langhans, M., Viotti, C., Scheuring, D., San Wan Yan, M., Jiang, L., Hillmer, S., Robinson, D.G., and Pimpl, P.** (2010b). Retromer recycles vacuolar sorting receptors from the trans-Golgi network. *Plant J* **61**.

**Nishimura, N., and Balch, W.E.** (1997). A Di-Acidic Signal Required for Selective Export from the Endoplasmic Reticulum. *Science* **277**, 556-558.

- Noguchi, K., Yasumori, M., Imai, T., Naito, S., Matsunaga, T., Oda, H., Hayashi, H., Chino, M., and Fujiwara, T.** (1997). bor1-1, an Arabidopsis thaliana mutant that requires a high level of boron. *Plant Physiol* **115**, 901-906.
- Occhialini, A., Gouzerh, G., Di Sansebastiano, G.-P., and Neuhaus, J.-M.** (2016). Dimerization of the Vacuolar Receptors AtRMR1 and -2 from Arabidopsis thaliana Contributes to Their Localization in the trans-Golgi Network. *International Journal of Molecular Sciences* **17**, 1661.
- Oh, I.S., Park, A.R., Bae, M.S., Kwon, S.J., Kim, Y.S., Lee, J.E., Kang, N.Y., Lee, S., Cheong, H., and Park, O.K.** (2005). Secretome Analysis Reveals an Arabidopsis Lipase Involved in Defense against Alternaria brassicicola. *The Plant cell* **17**, 2832-2847.
- Ohno, H., Stewart, J., Fournier, M., Bosshart, H., Rhee, I., Miyatake, S., Saito, T., Gallusser, A., Kirchhausen, T., and Bonifacino, J.** (1995). Interaction of tyrosine-based sorting signals with clathrin-associated proteins. *Science* **269**, 1872-1875.
- Oliviusson, P., Heinzerling, O., Hillmer, S., Hinz, G., Tse, Y.C., Jiang, L., and Robinson, D.G.** (2006). Plant retromer, localized to the prevacuolar compartment and microvesicles in Arabidopsis, may interact with vacuolar sorting receptors. *The Plant cell* **18**, 1239-1252.
- Ordenes, V.R., Reyes, F.C., Wolff, D., and Orellana, A.** (2002). A Thapsigargin-Sensitive Ca<sup>2+</sup> Pump Is Present in the Pea Golgi Apparatus Membrane. *Plant Physiology* **129**, 1820-1828.
- Ordenes, V.R., Moreno, I., Maturana, D., Norambuena, L., Trewavas, A.J., and Orellana, A.** (2012). In vivo analysis of the calcium signature in the plant Golgi apparatus reveals unique dynamics. *Cell Calcium* **52**, 397-404.
- Ortiz-Zapater, E., Soriano-Ortega, E., Marcote, M.J., Ortiz-Masiá, D., and Aniento, F.** (2006). Trafficking of the human transferrin receptor in plant cells: effects of tyrphostin A23 and brefeldin A. *The Plant Journal* **48**, 757-770.
- Owens, T., and Poole, R.J.** (1979). Regulation of Cytoplasmic and Vacuolar Volumes by Plant Cells in Suspension Culture. *Plant Physiology* **64**, 900-904.
- Paez Valencia, J., Goodman, K., and Otegui, M.S.** (2016). Endocytosis and Endosomal Trafficking in Plants. *Annu Rev Plant Biol* **67**, 309-335.
- Paris, N., Stanley, C.M., Jones, R.L., and Rogers, J.C.** (1996). Plant Cells Contain Two Functionally Distinct Vacuolar Compartments. *Cell* **85**, 563-572.
- Paris, N., Rogers, S.W., Jiang, L., Kirsch, T., Beevers, L., Phillips, T.E., and Rogers, J.C.** (1997). Molecular Cloning and Further Characterization of a Probable Plant Vacuolar Sorting Receptor. *Plant Physiology* **115**, 29-39.
- Park, M., Lee, D., Lee, G.-J., and Hwang, I.** (2005). AtRMR1 functions as a cargo receptor for protein trafficking to the protein storage vacuole. *The Journal of cell biology* **170**, 757-767.

- Park, S.-Y., Yang, J.-S., Schmider, A.B., Soberman, R.J., and Hsu, V.W.** (2015). Coordinated regulation of bidirectional COPI transport at the Golgi by CDC42. *Nature* **521**, 529-532.
- Pastor-Cantizano, N., Bernat-Silvestre, C., Marcote, M.J., and Aniento, F.** (2018). Loss of Arabidopsis p24 function affects ERD2 trafficking and Golgi structure, and activates the unfolded protein response. *J Cell Sci* **131**.
- Petiot, A., Fauré, J., Stenmark, H., and Gruenberg, J.** (2003). PI3P signaling regulates receptor sorting but not transport in the endosomal pathway. *The Journal of cell biology* **162**, 971-979.
- Phillipson, B.A., Pimpl, P., da Silva, L.L., Crofts, A.J., Taylor, J.P., Movafeghi, A., Robinson, D.G., and Denecke, J.** (2001). Secretory bulk flow of soluble proteins is efficient and COPII dependent. *The Plant cell* **13**.
- Pickart, C.M., and Eddins, M.J.** (2004). Ubiquitin: structures, functions, mechanisms. *Biochimica et Biophysica Acta (BBA) - Molecular Cell Research* **1695**, 55-72.
- Pimpl, P., Movafeghi, A., Coughlan, S., Denecke, J., Hillmer, S., and Robinson, D.G.** (2000). In Situ Localization and in Vitro Induction of Plant COPI-Coated Vesicles. *The Plant cell* **12**, 2219-2235.
- Pond, L., Kuhn, L.A., Teyton, L., Schutze, M.P., Tainer, J.A., Jackson, M.R., and Peterson, P.A.** (1995). A role for acidic residues in di-leucine motif-based targeting to the endocytic pathway. *J Biol Chem* **270**, 19989-19997.
- Quan, E.M., Kamiya, Y., Kamiya, D., Denic, V., Weibezahn, J., Kato, K., and Weissman, J.S.** (2008). Defining the glycan destruction signal for endoplasmic reticulum-associated degradation. *Mol Cell* **32**, 870-877.
- Raiborg, C., Bremnes, B., Mehlum, A., Gillooly, D.J., D'Arrigo, A., Stang, E., and Stenmark, H.** (2001). FYVE and coiled-coil domains determine the specific localisation of Hrs to early endosomes. *Journal of Cell Science* **114**, 2255-2263.
- Ren, X., and Hurley, J.H.** (2010). VHS domains of ESCRT-0 cooperate in high-avidity binding to polyubiquitinated cargo. *The EMBO Journal* **29**, 1045-1054.
- Richardson, L.G.L., Howard, A.S.M., Khuu, N., Gidda, S.K., McCartney, A., Morphy, B.J., and Mullen, R.T.** (2011). Protein-Protein Interaction Network and Subcellular Localization of the Arabidopsis Thaliana ESCRT Machinery. *Frontiers in plant science* **2**, 20.
- Rohrer, J., and Kornfeld, R.** (2001). Lysosomal hydrolase mannose 6-phosphate uncovering enzyme resides in the trans-Golgi network. *Mol Biol Cell* **12**, 1623-1631.
- Roth, T.F., and Porter, K.R.** (1964). YOLK PROTEIN UPTAKE IN THE OOCYTE OF THE MOSQUITO *Aedes Aegypti*. *The Journal of cell biology* **20**, 313-332.

- Rothbauer, U., Zolghadr, K., Tillib, S., Nowak, D., Schermelleh, L., Gahl, A., Backmann, N., Conrath, K., Muyldermans, S., Cardoso, M.C., and Leonhardt, H.** (2006). Targeting and tracing antigens in live cells with fluorescent nanobodies. *Nat Meth* **3**, 887-889.
- Saalbach, G., Jung, R., Kunze, G., Saalbach, I., Adler, K., and Müntz, K.** (1991). Different legumin protein domains act as vacuolar targeting signals. *The Plant cell* **3**, 695-708.
- Sahagian, G.G., Distler, J., and Jourdian, G.W.** (1981). Characterization of a membrane-associated receptor from bovine liver that binds phosphomannosyl residues of bovine testicular beta-galactosidase. *Proceedings of the National Academy of Sciences of the United States of America* **78**, 4289-4293.
- Saint-Jean, B., Seveno-Carpentier, E., Alcon, C., Neuhaus, J.M., and Paris, N.** (2010). The cytosolic tail dipeptide Ile-Met of the pea receptor BP80 is required for recycling from the prevacuole and for endocytosis. *The Plant cell* **22**, 2825-2837.
- Saito, Y., Kimura, K., Oka, T., and Nakano, A.** (1998). Activities of Mutant Sar1 Proteins in Guanine Nucleotide Binding, GTP Hydrolysis, and Cell-Free Transport from the Endoplasmic Reticulum to the Golgi Apparatus. *The Journal of Biochemistry* **124**, 816-823.
- Saksena, S., Wahlman, J., Teis, D., Johnson, A.E., and Emr, S.D.** (2009). Functional Reconstitution of ESCRT-III Assembly and Disassembly. *Cell* **136**, 97-109.
- Samuels, A.L., Giddings, T.H., and Staehelin, L.A.** (1995). Cytokinesis in tobacco BY-2 and root tip cells: a new model of cell plate formation in higher plants. *The Journal of cell biology* **130**, 1345-1357.
- Scheuring, D., Kunzl, F., Viotti, C., San Wan Yan, M., Jiang, L., Schellmann, S., Robinson, D.G., and Pimpl, P.** (2012). Ubiquitin initiates sorting of Golgi and plasma membrane proteins into the vacuolar degradation pathway. *BMC plant biology* **12**, 164-180.
- Scheuring, D., Viotti, C., Kruger, F., Kunzl, F., Sturm, S., Bubeck, J., Hillmer, S., Frigerio, L., Robinson, D.G., Pimpl, P., and Schumacher, K.** (2011). Multivesicular bodies mature from the trans-Golgi network/early endosome in *Arabidopsis*. *The Plant cell* **23**.
- Schoberer, J., and Strasser, R.** (2011). Sub-Compartmental Organization of Golgi-Resident N-Glycan Processing Enzymes in Plants. *Molecular Plant* **4**, 220-228.
- Schornack, S., Fuchs, R., Huitema, E., Rothbauer, U., Lipka, V., and Kamoun, S.** (2009). Protein mislocalization in plant cells using a GFP-binding chromobody. *The Plant Journal* **60**, 744-754.
- Seaman, M.N.J.** (2004). Cargo-selective endosomal sorting for retrieval to the Golgi requires retromer. *The Journal of cell biology* **165**, 111-122.

- Semenza, J.C., Hardwick, K.G., Dean, N., and Pelham, H.R.B.** (1990). ERD2, a yeast gene required for the receptor-mediated retrieval of luminal ER proteins from the secretory pathway. *Cell* **61**, 1349-1357.
- Sergeeva, L.I., Keurentjes, J.J.B., Bentsink, L., Vonk, J., van der Plas, L.H.W., Koornneef, M., and Vreugdenhil, D.** (2006). Vacuolar invertase regulates elongation of *Arabidopsis thaliana* roots as revealed by QTL and mutant analysis. *Proceedings of the National Academy of Sciences of the United States of America* **103**, 2994-2999.
- Shahriari, M., Richter, K., Keshavaiah, C., Sabovljevic, A., Huelskamp, M., and Schellmann, S.** (2011). The *Arabidopsis* ESCRT protein-protein interaction network. *Plant Molecular Biology* **76**, 85.
- Shen, J., Zeng, Y., Zhuang, X., Sun, L., Yao, X., Pimpl, P., and Jiang, L.** (2013). Organelle pH in the *Arabidopsis* endomembrane system. *Mol Plant* **6**, 1419-1437.
- Shen, Y., Wang, J., Ding, Y.u., Lo, S.W., Gouzerh, G., Neuhaus, J.-M., and Jiang, L.** (2011). The Rice RMR1 Associates with a Distinct Prevacuolar Compartment for the Protein Storage Vacuole Pathway. *Molecular Plant* **4**, 854-868.
- Shewry, P.R., Napier, J.A., and Tatham, A.S.** (1995). Seed storage proteins: structures and biosynthesis. *The Plant Cell Online* **7**, 945-956.
- Shields, S.B., Oestreich, A.J., Winistorfer, S., Nguyen, D., Payne, J.A., Katzmann, D.J., and Piper, R.** (2009). ESCRT ubiquitin-binding domains function cooperatively during MVB cargo sorting. *The Journal of cell biology* **185**, 213-224.
- Shimada, T., Fuji, K., Tamura, K., Kondo, M., Nishimura, M., and Hara-Nishimura, I.** (2003). Vacuolar sorting receptor for seed storage proteins in *Arabidopsis thaliana*. *Proc Natl Acad Sci U S A* **100**, 16095-16100.
- Slagsvold, T., Aasland, R., Hirano, S., Bache, K.G., Raiborg, C., Trambaiolo, D., Wakatsuki, S., and Stenmark, H.** (2005). Eap45 in mammalian ESCRT-II binds ubiquitin via a phosphoinositide-interacting GLUE domain. *Journal of Biological Chemistry* **280**, 19600-19606.
- Spitzer, C., Reyes, F.C., Buono, R., Sliwinski, M.K., Haas, T.J., and Otegui, M.S.** (2009). The ESCRT-Related CHMP1A and B Proteins Mediate Multivesicular Body Sorting of Auxin Carriers in *Arabidopsis* and Are Required for Plant Development. *The Plant cell* **21**, 749-766.
- Spitzer, C., Schellmann, S., Sabovljevic, A., Shahriari, M., Keshavaiah, C., Bechtold, N., Herzog, M., Müller, S., Hanisch, F.-G., and Hülkamp, M.** (2006). The *Arabidopsis elch* mutant reveals functions of an ESCRT component in cytokinesis. *Development* **133**, 4679-4689.
- Staehelein, L.A.** (1997). The plant ER: a dynamic organelle composed of a large number of discrete functional domains. *Plant J* **11**, 1151-1165.



- Staehein, L.A., and Moore, I.** (1995). The plant Golgi apparatus: structure, functional organization and trafficking mechanisms. *Annual review of plant biology* **46**, 261-288.
- Staehein, L.A., Giddings, T.H., Kiss, J.Z., and Sack, F.D.** (1990). Macromolecular Differentiation of Golgi Stacks in Root-Tips of Arabidopsis and Nicotiana Seedlings as Visualized in High-Pressure Frozen and Freeze-Substituted Samples. *Protoplasma* **157**, 75-91.
- Stael, S., Wurzinger, B., Mair, A., Mehlmer, N., Vothknecht, U.C., and Teige, M.** (2012). Plant organellar calcium signalling: an emerging field. *Journal of Experimental Botany* **63**, 1525-1542.
- Stevenson, J., Huang, E.Y., and Olzmann, J.A.** (2016). Endoplasmic Reticulum-Associated Degradation and Lipid Homeostasis. *Annu Rev Nutr* **36**, 511-542.
- Stimpson, H.E., Toret, C.P., Cheng, A.T., Pauly, B.S., and Drubin, D.G.** (2009). Early-arriving Syp1p and Ede1p function in endocytic site placement and formation in budding yeast. *Mol Biol Cell* **20**, 4640-4651.
- Subbarao, K.V., Datta, R., and Sharma, R.** (1998). Amylases synthesis in scutellum and aleurone layer of maize seeds. *Phytochemistry* **49**, 657-666.
- Swaminathan, S., Amerik, A.Y., and Hochstrasser, M.** (1999). The Doa4 deubiquitinating enzyme is required for ubiquitin homeostasis in yeast. *Molecular Biology of the Cell* **10**, 2583-2594.
- Sweitzer, S.M., and Hinshaw, J.E.** (1998). Dynamin Undergoes a GTP-Dependent Conformational Change Causing Vesiculation. *Cell* **93**, 1021-1029.
- Takeuchi, M., Ueda, T., Sato, K., Abe, H., Nagata, T., and Nakano, A.** (2000). A dominant negative mutant of Sar1 GTPase inhibits protein transport from the endoplasmic reticulum to the Golgi apparatus in tobacco and Arabidopsis cultured cells. *The Plant Journal* **23**, 517-525.
- Tamura, K., Shimada, T., Ono, E., Tanaka, Y., Nagatani, A., Higashi, S.-i., Watanabe, M., Nishimura, M., and Hara-Nishimura, I.** (2003). Why green fluorescent fusion proteins have not been observed in the vacuoles of higher plants. *The Plant Journal* **35**, 545-555.
- Tanchak, M.A., and Fowke, L.C.** (1987). The morphology of multivesicular bodies in soybean protoplasts and their role in endocytosis. *Protoplasma* **138**, 173-182.
- Teis, D., Saksena, S., and Emr, S.D.** (2008). Ordered Assembly of the ESCRT-III Complex on Endosomes Is Required to Sequester Cargo during MVB Formation. *Developmental Cell* **15**, 578-589.
- Teis, D., Saksena, S., Judson, B.L., and Emr, S.D.** (2010). ESCRT-II coordinates the assembly of ESCRT-III filaments for cargo sorting and multivesicular body vesicle formation. *The EMBO Journal* **29**, 871-883.

- Teo, H., Perisic, O., Gonzalez, B., and Williams, R.L.** (2004). ESCRT-II, an endosome-associated complex required for protein sorting: Crystal structure and interactions with ESCRT-III and membranes. *Developmental Cell* **7**, 559-569.
- Teo, H., Gill, D.J., Sun, J., Perisic, O., Veprintsev, D.B., Vallis, Y., Emr, S.D., and Williams, R.L.** (2006). ESCRT-I core and ESCRT-II GLUE domain structures reveal role for GLUE in linking to ESCRT-I and membranes. *Cell* **125**, 99-111.
- Thayer, S.S., and Huffaker, R.C.** (1984). Vacuolar Localization of Endoproteases EP<sub>1</sub> and EP<sub>2</sub> in Barley Mesophyll Cells. *Plant Physiology* **75**, 70-73.
- Tse, Y.C., Mo, B., Hillmer, S., Zhao, M., Lo, S.W., Robinson, D.G., and Jiang, L.** (2004). Identification of Multivesicular Bodies as Prevacuolar Compartments in *Nicotiana tabacum* BY-2 Cells. *The Plant cell* **16**, 672-693.
- Uemura, T.** (2016). Physiological Roles of Plant Post-Golgi Transport Pathways in Membrane Trafficking. *Plant and Cell Physiology* **57**, 2013-2019.
- Uemura, T., Suda, Y., Ueda, T., and Nakano, A.** (2014). Dynamic Behavior of the trans-Golgi Network in Root Tissues of Arabidopsis Revealed by Super-Resolution Live Imaging. *Plant and Cell Physiology* **55**, 694-703.
- Uemura, T., Ueda, T., Ohniwa, R.L., Nakano, A., Takeyasu, K., and Sato, M.H.** (2004). Systematic Analysis of SNARE Molecules in *Arabidopsis*: Dissection of the post-Golgi Network in Plant Cells. *Cell Structure and Function* **29**, 49-65.
- Viotti, C., Bubeck, J., Stierhof, Y.D., Krebs, M., Langhans, M., van den Berg, W., van Dongen, W., Richter, S., Geldner, N., Takano, J., Jurgens, G., de Vries, S.C., Robinson, D.G., and Schumacher, K.** (2010). Endocytic and secretory traffic in Arabidopsis merge in the trans-Golgi network/early endosome, an independent and highly dynamic organelle. *The Plant cell* **22**, 1344-1357.
- Vitale, A., Bielli, A., and Ceriotti, A.** (1995). The Binding Protein Associates with Monomeric Phaseolin. *Plant Physiol* **107**, 1411-1418.
- Vögeli-Lange, R., and Wagner, G.J.** (1990). Subcellular Localization of Cadmium and Cadmium-Binding Peptides in Tobacco Leaves. Implication of a Transport Function for Cadmium-Binding Peptides **92**, 1086-1093.
- Von Schaewen, A., and Chrispeels, M.J.** (1993). Identification of Vacuolar Sorting Information in Phytohemagglutinin, An Unprocessed Vacuolar Protein. *Journal of Experimental Botany* **44**, 339-342.
- Wakuta, S., Mineta, K., Amano, T., Toyoda, A., Fujiwara, T., Naito, S., and Takano, J.** (2015). Evolutionary Divergence of Plant Borate Exporters and Critical Amino Acid Residues for the Polar Localization and Boron-Dependent Vacuolar Sorting of AtBOR1. *Plant and Cell Physiology* **56**, 852-862.

- Walter, P., and Blobel, G.** (1981a). Translocation of proteins across the endoplasmic reticulum III. Signal recognition protein (SRP) causes signal sequence-dependent and site-specific arrest of chain elongation that is released by microsomal membranes. *The Journal of cell biology* **91**, 557-561.
- Walter, P., and Blobel, G.** (1981b). Translocation of proteins across the endoplasmic reticulum. II. Signal recognition protein (SRP) mediates the selective binding to microsomal membranes of in-vitro-assembled polysomes synthesizing secretory protein. *The Journal of cell biology* **91**, 551-556.
- Walter, P., Ibrahimi, I., and Blobel, G.** (1981). Translocation of proteins across the endoplasmic reticulum. I. Signal recognition protein (SRP) binds to in-vitro-assembled polysomes synthesizing secretory protein. *The Journal of cell biology* **91**, 545-550.
- Wang, H.J., Hsu, Y.W., Guo, C.L., Jane, W.N., Wang, H., Jiang, L., and Jauh, G.Y.** (2017). VPS36-Dependent Multivesicular Bodies Are Critical for Plasmamembrane Protein Turnover and Vacuolar Biogenesis. *Plant Physiol* **173**, 566-581.
- Wang, P., Hawkins, Timothy J., Richardson, C., Cummins, I., Deeks, Michael J., Sparkes, I., Hawes, C., and Hussey, Patrick J.** (2014). The Plant Cytoskeleton, NET3C, and VAP27 Mediate the Link between the Plasma Membrane and Endoplasmic Reticulum. *Current Biology* **24**, 1397-1405.
- Watanabe, E., Shimada, T., Kuroyanagi, M., Nishimura, M., and Hara-Nishimura, I.** (2002). Calcium-mediated association of a putative vacuolar sorting receptor PV72 with a propeptide of 2S albumin. *J Biol Chem* **277**, 8708-8715.
- Watanabe, E., Shimada, T., Tamura, K., Matsushima, R., Koumoto, Y., Nishimura, M., and Hara-Nishimura, I.** (2004). An ER-localized form of PV72, a seed-specific vacuolar sorting receptor, interferes the transport of an NPIR-containing proteinase in Arabidopsis leaves. *Plant & cell physiology* **45**, 9-17.
- Wehman, Ann M., Poggioli, C., Schweinsberg, P., Grant, Barth D., and Nance, J.** (2011). The P4-ATPase TAT-5 Inhibits the Budding of Extracellular Vesicles in *C. elegans* Embryos. *Current Biology* **21**, 1951-1959.
- Wiedmann, M., Kurzchalia, T.V., Bielka, H., and Rapoport, T.A.** (1987). Direct probing of the interaction between the signal sequence of nascent preprolactin and the signal recognition particle by specific cross-linking. *The Journal of cell biology* **104**, 201-208.
- Wollert, T., and Hurley, J.H.** (2010). Molecular Mechanism of Multivesicular Body Biogenesis by ESCRT Complexes. *Nature* **464**, 864-869.
- Wollert, T., Wunder, C., Lippincott-Schwartz, J., and Hurley, J.H.** (2009). Membrane scission by the ESCRT-III complex. *Nature* **458**, 172-177.
- Yu, Q., Tang, C., and Kuo, J.** (2000). A critical review on methods to measure apoplastic pH in plants. *Plant Soil* **219**, 29-40.

- Yu, Z., Gonciarz, M.D., Sundquist, W.I., Hill, C.P., and Jensen, G.J.** (2008). Cryo-EM Structure of Dodecameric Vps4p and Its 2:1 Complex with Vta1p. *Journal of Molecular Biology* **377**, 364-377.
- Zhang, G.F., and Staehelin, L.A.** (1992). Functional Compartmentation of the Golgi Apparatus of Plant Cells. Immunocytochemical Analysis of High-Pressure Frozen- and Freeze-Substituted Sycamore Maple Suspension Culture Cells **99**, 1070-1083.
- Zhu, Y., Doray, B., Poussu, A., Lehto, V.-P., and Kornfeld, S.** (2001). Binding of GGA2 to the Lysosomal Enzyme Sorting Motif of the Mannose 6-Phosphate Receptor. *Science* **292**, 1716-1718.
- Zipfel, C., Robatzek, S., Navarro, L., Oakeley, E.J., Jones, J.D., Felix, G., and Boller, T.** (2004). Bacterial disease resistance in Arabidopsis through flagellin perception. *Nature* **428**, 764-767.

## 9. Appendix

### **Receptor-mediated sorting of soluble vacuolar proteins ends at the *trans*-Golgi network/early endosome**

Fabian Künzli, Simone Frühholz, **Florian Fäßler**, Beibei Li and Peter Pimpl

*Nature Plants* 2, Article number: 16017 (2016), doi:10.1038/nplants.2016.17

<https://www.nature.com/articles/nplants201617>

# **Vacuolar sorting receptors transport ligands from the ER and the Golgi to the TGN/EE**

**Fabian Künzl, Simone Frühholz, Florian Fäßler, Beibei Li and Peter Pimpl\***

Center for Plant Molecular Biology (ZMBP), University of Tübingen, Germany

**\* Corresponding author:**

Peter Pimpl, ZMBP, University of Tübingen, Auf der Morgenstelle 32, D-72076 Tübingen

Tel: +49-7071-2978889

Fax: +49-7071-295797

e-mail: [peter.pimpl@zmbp.uni-tuebingen.de](mailto:peter.pimpl@zmbp.uni-tuebingen.de)

**Running title:** Compartment-specific analysis of VSR-ligand interaction

## **Abstract**

Sorting of soluble vacuolar proteins is of vital importance for plant cells and requires that vacuolar sorting receptors (VSRs) bind and release their cargo ligands. However, it is controversial, where in the endomembrane system these interactions occur. Here, we present an *in vivo* analysis of VSR-ligand interactions for all compartments of the vacuolar transport route. For this, we have developed compartment-specific VSR sensors and performed FRET-FLIM analysis to monitor for ligand binding. We show that VSRs bind ligands in the ER and in the Golgi, but not in the *trans*-Golgi network/early endosome (TGN/EE) nor in multivesicular late endosomes (MVBs/LEs). This implies that *post*-TGN/EE trafficking of ligands towards the vacuole is VSR-independent. We verify this by demonstrating that also non-VSR-ligands are delivered to the vacuole from the TGN/EE after endocytic uptake. Thus, we postulate that vacuolar sorting receptors transport ligands from the ER and the Golgi to the TGN/EE, followed by a VSR-independent default flow onwards to the vacuole.

## Introduction

Soluble vacuolar proteins and their corresponding vacuolar sorting receptors (VSRs) were identified in plants more than twenty years ago<sup>1,2</sup>. However, the mechanism of VSR-mediated sorting as implemented in the plant endomembrane system<sup>3</sup> is still not yet understood. Vacuolar sorting signals of soluble plant proteins are encoded by short peptide motifs within the amino acid sequence<sup>1</sup>. The first VSR was isolated from detergent-solubilised Golgi and clathrin-coated vesicle (CCV) fractions at neutral pH using synthetic peptides containing sorting signals<sup>5</sup>. VSRs are type I transmembrane proteins encoded by a gene family unique to plants<sup>4-6</sup>. They bind ligands via a structured N-terminal luminal binding domain (LBD) consisting of a protease associated domain, a central domain and three epidermal growth factor repeats<sup>7,8</sup>. VSRs also carry sorting signals for their own transport in the cytosolic C-terminus<sup>9-11</sup>. Based on assumed similarities to the lysosomal sorting machinery in mammals concerning receptor localisation and pH dependency of ligand binding, it was proposed almost twenty years ago that VSR-mediated sorting in plants occurs via CCV-facilitated transport from the *trans*-Golgi to a prevacuolar compartment, where ligands dissociate due to the lower pH. In the intervening years, major discoveries have challenged this model: the *trans*-Golgi network (TGN) in plants was identified as the early endosome (EE)<sup>12,13</sup> that is distinct from the Golgi stack<sup>14</sup>. This hybrid structure (TGN/EE) has now been shown to be the most acidic compartment *en route* to the vacuole<sup>15-17</sup>. The TGN/EE harbours the retromer complex necessary for recycling of the VSRs<sup>18,19</sup>. Most important, however, was the demonstration that the TGN/EE is the source for the biogenesis of the prevacuolar compartment, the multivesicular late endosome (MVB/LE), which confers transport by fusion with the vacuole<sup>20</sup>. These recent findings still await integration into the proposed concept of VSR-mediated sorting. In order to determine the compartments that constitute the framework for the bi-directional receptor transport, it is of paramount importance to firstly identify the locations at which VSRs bind or release their ligands. To this end, we have developed genetically encoded VSR sensors that allow for non-invasive compartment-specific detection of VSR-ligand interactions *in vivo*. We assembled VSR sensors from a soluble LBD of a VSR and a compartment-specific green fluorescent protein (GFP)-containing membrane markers via antibody-epitope interaction.



For this, we utilised the antigen-binding capability of the V<sub>H</sub>H domain of a heavy-chain antibody<sup>21</sup>, termed nanobody (Nb), that was recently raised against GFP in alpacas (*Lama pacu*)<sup>22,23</sup>. Based on the amino acid sequence of this anti-GFP Nb, we have generated a coding sequence for the expression of a soluble GFP-binding LBD fusion protein (LBD-Nb). VSR sensor assembly occurs upon coexpression of this LBD-Nb with a compartment-specific membrane marker protein that exposes GFP in the compartmental lumen, thereby reconstituting a GFP-tagged membrane protein.

We monitored for VSR-ligand interaction by coexpression of the self-assembling sensors with red fluorescent protein (RFP) ligands in a comprehensive approach, combining localisation analysis with Förster-resonance energy transfer-fluorescence lifetime imaging microscopy (FRET-FLIM). We firstly analysed the localisation of assembled sensors and the soluble ligands to test whether the presence of the sensor results in coaccumulation of ligands, as a preliminary indication for VSR-ligand interaction. In the second step, we applied FRET-FLIM to either verify or negate VSR-ligand interactions<sup>24,25</sup>. This is possible since FRET occurs only across short distances between 1 and 10 nm, thus allowing to differentiate between interaction-dependent and -independent colocalisation of proteins<sup>24</sup>.

With this novel strategy, we were able to show that VSRs bind ligands only in the ER and in the Golgi stack, but not in *post*-Golgi compartments such as the TGN/EE or the MVB/LE. This suggests that *post*-TGN/EE trafficking of soluble proteins towards the vacuole is independent of VSR-ligand interactions.

Confirmation of this conclusion was provided by identifying the vacuole as being the default location for soluble proteins of the endocytic route that merges with the biosynthetic vacuolar route at the TGN/EE. Consequently, we postulate a two-stage process for vacuolar transport of soluble proteins. Firstly, VSRs confer the transport of ligands to the TGN/EE, followed by a VSR-independent default flow onwards to the vacuole via budding of MVBs/LEs and their fusion with the vacuole.

## RESULTS

### Compartment-specific targeting via nanobody-mediated protein assembly

The challenge in using genetically encoded reporters for non-invasive compartment-specific analysis *in vivo* is to achieve their precise targeting<sup>26</sup>. This is particularly true for the analysis of the Golgi stack, the TGN/EE and the MVB/LE, since sorting signals specific for these compartments are largely unknown. A common targeting strategy is the use of translational fusions between reporter domains and membrane marker proteins. This is however subject to topology restrictions of the fusion partners and it has to be mentioned that the N-terminal LBD of the type I VSRs can only be fused to type I membrane marker proteins<sup>27</sup>. Type I membrane markers, however, are only known for the ER and the MVB/LE but neither for the Golgi stack nor the TGN/EE. To overcome these constraints, we developed a targeting strategy based on nanobody-mediated protein assembly. To demonstrate successful targeting, we have generated a construct consisting of a fluorescent LBD fused to an anti-GFP nanobody<sup>23</sup> as a soluble VSR (LBD-RFP-Nb) that can be used in combination with epitope (GFP)-tagged membrane marker proteins to assemble compartment-specific VSR sensors *in vivo* (Fig. 1a). To rule out that the soluble VSR bears intrinsic sorting signals that compromise targeting, we first analysed its transport properties (Fig. 1b-d). Fluorescence signals of LBD-RFP-Nb are largely absent in cells but appear when ER export is prevented by Sec12 overproduction<sup>28</sup>. To test for nanobody-mediated protein assembly in all compartments *en route* to the vacuole, we have expressed the soluble VSR with membrane anchors for ER (GFP-CNX), Golgi (Man1-GFP), TGN/EE (SYP61-GFP) and MVBs/LEs (GFP-BP80; Fig. 1e-i, Supplementary Table 1). In all cases, strong red-fluorescence signals from LBD-RFP-Nb become detectable and colocalise precisely with the respective anchor due to nanobody-epitope interaction at the inner leaflet of the compartmental membrane. This is most evident for the colocalising signals at the ring-shaped periphery of the Golgi (Fig. 1f) and at ring-like MVB/LE structures after treatment with wortmannin (WM)<sup>29</sup> (Fig. 1i). Together, these data show that nanobody-epitope interactions persist in the lumen of all compartments along the vacuolar route, irrespective of their individual biochemical properties.

### **Assembled VSR sensors possess ligand-binding competence**

We have generated a soluble LBD-Nb fusion protein for coexpression with the GFP-based membrane anchors. Due to the nanobody-epitope interaction, both molecules constitute a green-fluorescent membrane protein, employed as compartment-specific VSR sensors. Usage of these sensors together with a red-fluorescent ligand allows testing for receptor-ligand interactions via sensor-ligand colocalisation analysis and via FRET-FLIM as an intensity-independent approach to detect FRET<sup>24</sup>. For this, we used the established model ligand Aleu-RFP. This soluble vacuolar reporter carries 24 amino acids from the *Petunia* thiol protease aleurain that contains the sequence-specific vacuolar sorting motif NPIR<sup>30</sup>.

Upon coexpression, binding of Aleu-RFP to the anchored LBD of the sensor triggers close proximity of the RFP from the ligand and the GFP upstream of the LBD within the sensor and thus allows for FRET to occur. In this situation, excited-stage energy from the donor GFP is transferred to the acceptor RFP of the ligand, thereby reducing the fluorescence lifetime of GFP<sup>24</sup>. Consequently, lack of ligand binding does not alter the fluorescence lifetime, even if both fluorophores colocalise interaction-independently in the same compartment (Fig. 2a).

During the course of VSR-mediated sorting, ligand binding is reversible. Therefore, we expected to identify compartments *en route* to the vacuole that either support or restrict ligand binding. To rule out that the experiments were compromised by differences in the ligand-binding competence of the LBD-Nb in the context of different membrane anchors, we first confirmed the ligand-binding capability of all VSR sensors *in vitro* (Fig 2b, Supplementary Fig. 1). For this, we assembled sensors in the ER, Golgi, TGN/EE and MVB/LE (Supplementary Fig. 2) and immunoprecipitated them by using GFP antibodies in bead-binding assays. For direct comparison of their ligand-binding capabilities, we incubated the bead-bound VSR sensors with the ligand Aleu-RFP<sup>30</sup> at binding conditions<sup>2</sup>. In all cases, Aleu-RFP was coprecipitated while secretory Sec-RFP in control experiments was not. This demonstrates that all assembled VSR sensors possess ligand-binding competence.

### **VSR-ligand interaction occurs in the ER but not in the MVB/LE**

We have recently shown that placement of LBDs in the lumen of the ER triggers accumulation of ligands, suggesting VSR-ligand binding<sup>27</sup>. Consistently, assembly

of VSR sensors in the ER also retains the ligand Aleu-RFP, preventing vacuolar delivery (Fig. 3a,b). To test whether this accumulation is indeed due to VSR-ligand interaction, we performed FRET-FLIM. We took advantage of the fact that the ER marker GFP-Calnexin (CNX) induces sheet-like ER cisternae without affecting ER function<sup>31</sup>, resulting in an enlarged signal surface facilitating FLIM recording. The analysis revealed a highly significant reduction of the GFP lifetime in the presence of the ligand, with values well within the range of recently reported protein-protein interactions using this pair of fluorophores for FRET-FLIM in plants<sup>25</sup>.

In sharp contrast, fluorescence lifetime was not influenced by the ER-localising non-ligand RFP-HDEL and the secretory marker Sec-RFP, even if present in the ER at high levels upon inhibition of ER export by brefeldin A (BFA), or in the absence of the LBD-Nb as binding partner (Fig. 3c, Supplementary Fig. 3a). This direct comparison between the model ligand Aleu-RFP with the non-ligands RFP-HDEL and Sec-RFP ( $\pm$ BFA) reveals that the recorded reduction of fluorescence lifetime is specific for VSR-ligand interaction, thus identifying the ER as a compartment that promotes VSR-ligand binding.

Receptor-mediated transport of ligands is completed by their release. With the MVB/LE being the last morphologically characterised compartment *en route* to the vacuole, ligands should be released from receptors here at the latest. At steady-state conditions, Aleu-RFP localises to the MVB/LE in addition to the vacuole, which is not altered by the LBD-Nb after sensor assembly (Fig. 3d,e). Therefore, it is difficult to judge VSR-ligand interactions in this compartment solely by the assessment of localisation. FRET-FLIM analysis however revealed that these colocalising ligands do not influence the fluorescence lifetime of the VSR sensor (Fig. 3f, Supplementary Fig. 3b). Reduction of fluorescence lifetime of the GFP in the sensor can only be triggered in controls by direct attachment of RFP to the sensor via nanobody-epitope interaction (LBD-RFP-Nb, compare to Fig. 1h). This demonstrates that the VSR sensors do not bind ligands in this compartment. To extend the analysis, we applied the drug WM which induces enlargement of MVBs/LEs by homotypic fusion<sup>29</sup>. The resulting ring-like structures now reveal a differential distribution, with signals from the VSR sensor being present at the limiting membrane while signals from Aleu-RFP locate to the compartmental lumen (Fig 3g). This also suggests that ligands do not bind to VSRs in this transit compartment towards the vacuole, since this would indeed result in close proximity

of the fluorophores (compare to Fig. 1i). Together, these data demonstrate that ligands do interact with the VSR sensors in the ER and that they do not interact in the MVB/LE. These findings furthermore reveal that only a combination of localisation analysis and FRET-FLIM allows for a reliable assessment of whether a given compartment supports or restricts VSR-ligand binding.

### **VSR-ligand interaction occurs in the Golgi stack but not in the TGN/EE**

Having identified the ER as compartment that supports ligand binding and MVBs/LEs as compartments that do not, we next tested Golgi and TGN/EE for possible VSR-ligand interactions. The *cis*-Golgi marker  $\alpha$ -mannosidase 1 (Man1)-GFP does not colocalise with Aleu-RFP, whose punctate signals represent MVBs/LEs (Fig. 4a, compare to Fig. 3d,g). Assembly of VSR sensors in the Golgi however causes colocalisation of Aleu-RFP with all GFP-labelled VSR sensors (Fig. 4b). These colocalising signals appear in addition to the RFP signals from punctate MVBs/LEs and the vacuole. The redistribution of Aleu-RFP to the Golgi can be emphasised by the employment of transport competitors for the endogenous VSRs<sup>32</sup>, which reduce vacuolar delivery. The competitor HA-BP80, a HA-epitope-tagged LBD-deletion mutant of BP80, reduces RFP signals in MVBs/LEs and in the vacuole, but does not alter Golgi-colocalisation of the VSR sensors with Aleu-RFP (Fig. 4c). The colocalising signals at the inner leaflet of the Golgi membrane are similar to the signals previously seen for the LBD-RFP-Nb targeted to this compartment (compare to Fig. 1f). This suggests an interaction between the sensors and ligands.

FRET-FLIM analysis revealed a highly significant reduction of the fluorescence lifetime of the donor GFP in the VSR sensor (Fig. 4d, Supplementary Fig. 4a). This reduction depends on the presence of the LBD, demonstrating that the Golgi-localisation of Aleu-RFP is caused by interaction with the VSR sensor. We have also assessed VSR-ligand interaction in the *trans*-face of the stack by using the *trans*-Golgi marker sialyltransferase (ST)-GFP for VSR sensor assembly (Fig. 4e). Aleu-RFP does also not colocalise with the membrane marker ST-GFP (Fig. 4f). In the presence of the LBD-Nb, the distribution pattern of Aleu-RFP shifts, resulting in colocalisation of the ligand and sensor (Fig.4g, Supplementary Fig. 4b), suggesting an interaction to occur. This was verified by FRET-FLIM analysis (Fig.

4h), revealing that Aleu-RFP causes a highly significant decrease of the fluorescence lifetime, which does not occur in the absence of the LBD-Nb. The situation in the TGN/EE yields another picture. Here, assembly of VSR sensors does not cause colocalisation of the ligand Aleu-RFP (Fig. 5a-c), questioning the occurrence of VSR-ligand interactions. FRET-FLIM analysis of the TGN/EE-localising VSR sensor revealed that Aleu-RFP does not influence the fluorescence lifetime of the sensor, a situation identical to control experiments where the non-ligand Sec-RFP was used instead (Fig. 5d, Supplementary Fig. 5). To demonstrate that protein-protein interactions can shorten the lifetime in the TGN, we attached the red-fluorescent LBD (LBD-RFP-Nb) via nanobody-epitope interaction to the membrane anchor SYP61-GFP. This control confirmed the assembly of VSR sensors in the TGN/EE as illustrated in Fig. 1g and proves that the principle of FRET-FLIM interaction analysis is also applicable to this compartment (Fig. 5d).

Together, these data favour the idea that VSRs and ligands do not interact in the TGN/EE. Consequently, it is tempting to speculate that the VSRs in this compartment have already released their ligands. This however would imply that these VSRs bind ligands upstream of the TGN/EE. To verify this hypothesis, we blocked the arrival of the TGN/EE-targeted VSR sensor with the drug BFA, causing retention of sensors and ligands in the ER (Fig. 5e). BFA-induced ER localisation causes a drastic increase of the fluorescence lifetime of SYP61-GFP-based sensors, with values being identical to those of ER-targeted GFP-CNX-based sensors (compare to Fig. 3c). Under these conditions, coexpressed Aleu-RFP strongly reduces fluorescence lifetime of the SYP61-GFP-based sensor, demonstrating ligand binding. This does not occur in the presence of Sec-RFP (Fig. 5f, Supplementary Fig. 5). The capability of the TGN/EE-targeted VSR sensor to bind ligands in the ER was furthermore confirmed by coimmunoprecipitation (Fig. 5g). Here, only BFA-triggered ER-localisation of the VSR sensor resulted in coimmunoprecipitation of the ligand Aleu-RFP, which does not occur if the sensor localises to the TGN/EE. (Fig. 5g, compare to Fig. 3a-c). Altogether, our data demonstrate that VSRs bind their ligands very early in the secretory pathway and release ligands upon arrival in the TGN/EE.

## **VSRs do not mediate *post*-TGN/EE transport of soluble proteins to the vacuole**

The compartment-specific analysis identified the ER and the Golgi as compartments that promote VSR-ligand binding while the TGN/EE and the MVB/LE restrict this interaction. This suggests that VSRs do not contribute to the *post*-TGN/EE transport of soluble vacuolar proteins towards the vacuole.

Receptor-independent transport from the TGN/EE to the vacuole furthermore implies that this route does not require sorting signals and is thus the default route for soluble proteins.

To test for this hypothesis, we have developed a strategy to analyse *post*-TGN/EE transport of soluble proteins lacking vacuolar sorting signals. Since these signals are required for the VSR-mediated sorting to the TGN/EE via the biosynthetic pathway, we took advantage of the early endosomal properties of the TGN/EE and targeted soluble proteins to the TGN/EE via the endocytic route. For these experiments, we used triple (3x) RFP from the culture medium of 3xRFP-secreting protoplasts as a fluorescent reporter protein for endocytic uptake. The use of a reporter that was secreted by protoplasts ensures that this reporter does neither carry cryptic intrinsic vacuolar sorting signals nor signs of damage that could possibly trigger vacuolar degradation via mechanisms of quality control later on<sup>33,34</sup>.

Incubation of cells expressing cytosolic GFP (Cyt-GFP) with 3xRFP results in vacuolar delivery of this reporter (Fig. 6a). Consequently, the endocytosed reporter is recovered as soluble protein from cellular extracts and does not cofractionate with membranes (Fig 6b). To prove that the reporter reaches the vacuole via the TGN/EE and the MVB/LE, we used the protoplast-secreted anti-GFP nanobody fusion 3xRFP-Nb, which is also delivered to the vacuole in endocytic uptake assays (Fig. 6c). This time however, we used cells expressing GFP-membrane anchors either at the cell surface (SYP132-GFP), the TGN/EE (SYP61-GFP) or the MVB/LE (GFP-BP80). In all cases, the reporter 3xRFP-Nb colocalised with the respective membrane anchor due to nanobody-mediated assembly (Fig. 6d-f), demonstrating its transport via the endocytic route. Together, this shows that soluble proteins reach the vacuole from the TGN/EE independent of sorting receptors, defining the vacuole as being the default location of *post*-TGN/EE transport of soluble proteins.

## Discussion

V<sub>H</sub>H domains of heavy-chain antibodies from camelids, termed nanobodies, are the smallest polypeptides capable of epitope-binding<sup>35</sup>. The specificity of this interaction together with their size of only 13 kDa turns an ever increasing number of engineered nanobodies into powerful tools for research, diagnostics and therapeutics<sup>35</sup>. Amongst first applications for nanobodies was their use as chromobodies<sup>22</sup>. These fusion proteins between a nanobody and a fluorescent protein have been expressed in the cytosol of plant cells, allowing for specific detection of proteins by the nanobody-mediated attachment of a fluorescent reporter<sup>36,37</sup> but also for manipulation of protein function, possibly by masking of functional domains of the target protein by reporter-attachment<sup>37</sup>.

Here, we have employed an anti-GFP nanobody to develop novel VSR sensors for the analysis of VSR-ligand interactions in the lumen of the compartments of the endomembrane system. These sensors assemble via nanobody-triggered interaction from a soluble LBD-nanobody fusion protein with an epitope-tagged compartment-specific membrane anchor. We see this strategy as an approach to overcome current limitations with respect to compartment-specific targeting of functional protein domains, allowing for the analysis of protein-protein interactions *in vivo* that does not redundantise the analysis of the intricate interaction between unmodified full-length VSR and endogenous ligands in the future.

The use of this system allows now for the first time the direct linkage of the type I LBD with type II membrane anchors for the Golgi and the TGN/EE, thus enabling the use of the very same sensing protein at different locations, rather than employing VSR trafficking mutants that exhibit altered distributions<sup>11,16</sup>.

We demonstrate that VSR-ligand interactions occur in the ER and Golgi, but don't occur in the TGN/EE or MVBs/LEs (Fig. 6g). These data are in agreement with previous observations, showing that LBDs, when fused to the ER retrieval signal HDEL<sup>32,38</sup> or to the transmembrane domain of an ER-marker<sup>27</sup>, cause accumulation of soluble vacuolar proteins. Moreover, VSRs have been initially isolated from solubilised Golgi fractions with immobilised sorting signals at neutral pH<sup>2</sup>, which is also found in these compartments<sup>15,16</sup>. Release of ligands was suggested to occur at low pH<sup>2</sup> and in combination with the initial localisation of VSRs at the Golgi and at prevacuoles, it was suggested that VSRs transport their



ligands between these compartments<sup>5</sup>. Since then, localisation analysis was refined and VSRs were also found in *trans*-Golgi cisternae<sup>39</sup>, TGN/EE<sup>18,40</sup>, MVBs/LEs<sup>18,29,41</sup> and even at the PM<sup>11,42</sup>, implying that the sole use of localisation data of receptors is insufficient to judge the ligand-binding status of VSRs<sup>3</sup>. Our data show ligand binding of the SYP61-GFP-based sensor *in vitro* and *in vivo*. However, this depends strictly on its intracellular localisation, with demonstrated binding in the ER but the complete lack thereof in the TGN/EE, suggesting that ligands have been released in the TGN/EE.

We employed FRET-FLIM analysis to monitor for VSR-ligand interactions. The fluorescence lifetime is an intrinsic property of a fluorophore and depends on the environmental pH<sup>43</sup>, with decreasing pH lowering lifetime. The FLIM data obtained for the VSR sensor reveals compartment-specific fluorescence lifetimes, thus reflecting on relative compartmental pH. Recorded fluorescence lifetimes were longest in the ER, falling off in *cis*- to *trans*-Golgi and were shortest in the TGN/EE, suggesting that the TGN/EE exhibits a low pH that could have triggered the release of the ligand. This is also supported by recently reported pH values for intracellular compartments<sup>15-17</sup>, identifying the TGN/EE with pH values ranging from 6.3-5.5 as being the most acidic compartment of the vacuolar route and MVBs/LEs possessing either similar<sup>15</sup> or an even slightly more alkaline pH<sup>16</sup>, whilst the pH was highest in the ER (pH 7.1-7.5)<sup>15-17</sup>. Together, our data are in full agreement with the originally proposed concept of pH-dependent binding and release of ligands<sup>2</sup>.

Another key factor modulating VSR-ligand interaction is calcium<sup>44</sup>, possibly due to conformational changes induced by Ca<sup>2+</sup>-binding to an EGF repeat within the LBD<sup>7,44</sup>. Ca<sup>2+</sup> facilitates ligand binding and prevents release, even at a pH of 4<sup>44</sup>, showing that Ca<sup>2+</sup> supports ligand binding at unfavourable pH<sup>3</sup>. Experimental data on compartmental Ca<sup>2+</sup> concentrations are scarce. The presence of Ca<sup>2+</sup> pumps in the ER and the tonoplast suggests that concentrations are the highest there, with an estimate from 50  $\mu$ M to 5 mM<sup>45</sup>, falling off to the nanomolar range in compartments *en route* to the vacuole like the Golgi<sup>46</sup>. Together, this suggests that VSR-mediated sorting depends on an intricate interplay between pH, Ca<sup>2+</sup> and possibly other factors that differ between the compartments in order to trigger ligand binding and release.

Release of ligands in the TGN implies that further anterograde transport of soluble proteins to the vacuole is independent of VSRs. This is in full agreement with the TGN-localisation of the VSR-recycling retromer complex<sup>18,19</sup> and the observation that MVBs/LEs originate at the TGN/EE<sup>20</sup> and fuse with the vacuole. This scenario does not necessitate VSRs for the ligands to be exported from the TGN/EE. Consequently, all soluble proteins would share the fate of the very same passive vacuolar delivery via the MVB/LE. Indeed, our endocytic uptake assays with secreted non-ligand proteins revealed vacuolar delivery after fluid phase endocytosis. We have traced the endocytosed reporter in the TGN/EE and the MVB/LE, thus confirming the operation of such a passive vacuolar delivery via the endocytic pathway. Alternatively, it could be speculated that secreted soluble proteins might possess positive sorting information for yet unidentified receptors that mediate endocytosis and TGN/EE export. A prerequisite for such a scenario however would be that these receptors do not bind the secretory proteins already in the TGN/EE to prevent vacuolar delivery prior to reaching the PM. However, together with previously reported findings that even endocytosed polystyrene beads reach the vacuole via the endocytic route<sup>47</sup>, it seems justified to postulate that the vacuole is the default location for soluble proteins of the endocytic route, which consequently does not require a receptor-mediated transport step between the TGN/EE and the MVB/LE for vacuolar delivery.

## METHODS

**Plant materials.** *Nicotiana tabacum* L. SR1 was grown on Murashige and Skoog medium supplemented with 2% sucrose, 0.5 g/L MES and 0.8 % Agar at pH 5.7 in 16/8 h light–dark cycles at 22 °C.

**Plasmid constructs.** All constructs are given in Supplemental Table 1. DNA manipulations were performed according to established procedures, using pUC<sup>48</sup>-/pGreenII<sup>34</sup>-based vectors and *Escherichia coli* MC1061. A anti-GFP nanobody (Nb) sequence was generated by reverse-translation of the aa sequence<sup>23</sup>, optimised for *Arabidopsis*-specific codon-usage (EMBOSS Backtranseq), modified with N-/C-terminal HA-/6x-His-tags and chemically-synthesised (GeneArt Gene

Synthesis). LBD-RFP-Nb was assembled from AtVSR4 (GenBank accession NM\_127036)-LBD, RFP<sup>34</sup> and Nb. Compartment-specific anchors uniformly carried EGFP (GenBank accession BAQ19368), warranting comparable spectroscopical properties. All red-fluorescent reporters are based on monomeric-RFP<sup>34</sup>. 3xRFP/3xRFP-Nb carry the N-terminal signal peptide of Sec-RFP. Correct localisation of all generated marker/reporter-fluorophore fusions was verified.

**Protoplast isolation and gene expression.** Protoplasts were isolated and electro-transfected as described<sup>49</sup>, using the square-wave pulse generator EPI-2500 (Fischer, Heidelberg). 10-50 ng/ $\mu$ L<sup>transformation</sup> plasmid DNA were transfected; expression occurred for 18-24 h at 25 °C in the dark.

**Biosynthesis of fluorescent reporters.** Protoplast-secreted reporters (3xRFP/3xRFP-Nb) for endocytic uptake experiments were obtained from cell-free culture medium after expression, harvesting, sonication and clearance, ruling out contaminations with reporter-synthesising cells during uptake-experiments. For endocytic uptake, populations of protoplasts expressing GFP markers were supplemented with cleared reporter-containing medium for 24 h.

**Confocal microscopy and statistical analysis.** Imaging was performed using a Leica TCS-SP8 CLSM, with a x63 (1.2 NA) water immersion objective. Fluorophores were excited (ex) and emission (em) was detected by line switching in sequential mode using HyD detectors: CFP (ex/em: 458 nm/464-525 nm), GFP (ex/em: 488 nm/496-525 nm), and RFP (ex/em: 561 nm/569-636 nm). Pinholes were adjusted to 1 Airy unit for each wavelength. *Post*-acquisition image-processing was performed using Adobe Photoshop CS3 (v10.0.1) and CorelDraw X6 (v16.0.0.707). Calculation of the linear Pearson's correlation coefficient ( $r_p$ ) and nonlinear Spearman's rank correlation coefficient ( $r_s$ ) of red and green fluorescent signals and ROI selection was performed as previously described, with threshold levels set to 10. For statistics, correlation coefficients of 10 individually analysed cells per experiment were considered and are given as mean values with standard errors of the mean. Statistical significance was calculated using ANOVA, followed by Tukey's HSD test.

**Fluorescence lifetime imaging microscopy.** Data acquisition was performed with a Leica TCS-SP8 equipped with a PicoHarp-300-TCSPC-module, a PDL-808

Sepia multichannel-picosecond pulsed-diode-laser-driver and was analysed using SymPhoTime v5.3.2.2 (PicoQuant). GFP was excited with a 470 nm laser (LDH-P-C-470B) at 40 MHz pulse-frequency. Emission was recorded at 496-525 nm by time-correlated single-photon-counting (TCSPC) until reaching a count of 500 photons per pixel. To calculate fluorescence lifetimes, TCSPC histograms were reconvoluted with an instrumental-response-function (IRF) and fitted against a bi-exponential decay function. Only fittings giving  $\chi^2$  values between 0.9 and 1.4 were considered. All fluorescence signals of organellar markers were specifically selected with the software's 'region of interest' selection tools to avoid potential miscalculations caused by background noise. In case of GFP-BP80, vacuolar background fluorescence, as seen in addition to punctate endosomal signals, was excluded from lifetime calculations. All selected signals of a cell were recorded and calculated as mean lifetime. Per experimental condition, 12-20 cells were independently analysed, thus representing a total of more than 200 individual Golgi stacks, TGNs/EEs or MVBs/LEs. For statistics, calculated lifetimes of all cells were averaged. Error bars indicate standard errors of the mean. Statistical significance was calculated as above.

**Harvesting, protein extraction and immunoblotting.** Cell-free medium was harvested after flotation of cells for 5 min at 80 g, using syringes and sealed pre-punctured tubes. Proteins from medium-samples were precipitated as described<sup>50</sup>. After resealing, cells were diluted 5-fold with 250 mM NaCl and sedimented by centrifugation as above. Cells were extracted by sonication in extraction buffer (100 mM Tris, pH 7.8, 200 mM NaCl, 1 mM EDTA, 2 %  $\beta$ -mercaptoethanol and 0.2 % Triton X-100) for PAGE/WB analysis or in 2x binding buffer (40 mM HEPES, 300 mM NaCl, 2 mM  $\text{CaCl}_2$ , 2 mM  $\text{MgCl}_2$ , pH 7.1) for (Co-)IP/ligand binding analysis. Extracts were cleared by centrifugation at 20,000 g for 15 min at 4 °C. For SDS-PAGE/WB, all processed samples/beads were finally mixed 1:1 with 2x Xtreme loading dye<sup>33</sup> and denatured for 5 min at 95 °C. SDS-PAGE/WB was performed as described<sup>33</sup>. Antibodies used: mouse monoclonal anti-GFP (Roche 11814460001, 1:1,000), rat monoclonal anti-RFP (ChromoTek, 1:1,000) and rat monoclonal anti-HA-Peroxidase (Roche 12013819001, 1:2,500).

**Immunoprecipitation and ligand binding.** For IP/Co-IP and binding assays, sensors were assembled *in vivo* (+/- ligands/BFA) and extracted 1:1 in 2x binding buffer. Immunoprecipitation was performed overnight with rabbit polyclonal GFP antibodies (Life Technologies A6455)-coupled Protein A beads (10001D, Life Technologies) at 4 °C. Beads were 3x washed with binding buffer and either immediately processed for SDS-PAGE/WB or incubated with Aleu-RFP/Sec-RFP (controls), which were in parallel samples transiently expressed and recovered from cell extracts/medium as described above, prior to processing for SDS-PAGE/WB. For cellular fractionation by osmotic shock, cells were resuspended in a 4-fold volume of Tris buffer (50 mM Tris, pH 8.0, 1 mM EDTA) and cleared. Supernatant (S) was recovered, the membrane pellet (P) was resuspended in the initial volume of extraction buffer, and S-/P-samples were processed for SDS-PAGE/WB.

## References

- 1 Holwerda, B. C., Padgett, H. S. & Rogers, J. C. Proaleurain vacuolar targeting is mediated by short contiguous peptide interactions. *Plant Cell* **4**, 307-318 (1992).
- 2 Kirsch, T., Paris, N., Butler, J. M., Beevers, L. & Rogers, J. C. Purification and initial characterization of a potential plant vacuolar targeting receptor. *Proc. Natl. Acad. Sci. USA* **91**, 3403-3407 (1994).
- 3 Robinson, D. G. & Pimpl, P. Receptor-mediated transport of vacuolar proteins: a critical analysis and a new model. *Protoplasma* **251**, 247-264, doi:10.1007/s00709-013-0542-7 (2014).
- 4 Ahmed, S. U., Bar-Peled, M. & Raikhel, N. V. Cloning and subcellular location of an Arabidopsis receptor-like protein that shares common features with protein-sorting receptors of eukaryotic cells. *Plant Physiol.* **114**, 325-336 (1997).
- 5 Paris, N. *et al.* Molecular cloning and further characterization of a probable plant vacuolar sorting receptor. *Plant Physiol.* **115**, 29-39 (1997).
- 6 De Marcos Lousa, C., Gershlick, D. C. & Denecke, J. Mechanisms and concepts paving the way towards a complete transport cycle of plant vacuolar sorting receptors. *Plant Cell* **24**, 1714-1732, doi:10.1105/tpc.112.095679 (2012).
- 7 Cao, X., Rogers, S. W., Butler, J., Beevers, L. & Rogers, J. C. Structural requirements for ligand binding by a probable plant vacuolar sorting receptor. *Plant Cell* **12**, 493-506 (2000).
- 8 Luo, F. *et al.* How vacuolar sorting receptor proteins interact with their cargo proteins: crystal structures of apo and cargo-bound forms of the protease-associated domain from an Arabidopsis vacuolar sorting receptor. *Plant Cell* **26**, 3693-3708, doi:10.1105/tpc.114.129940 (2014).

- 9 daSilva, L. L., Foresti, O. & Denecke, J. Targeting of the plant vacuolar sorting receptor BP80 is dependent on multiple sorting signals in the cytosolic tail. *Plant Cell* **18**, 1477-1497 (2006).
- 10 Kim, H. *et al.* Homomeric interaction of AtVSR1 is essential for its function as a vacuolar sorting receptor. *Plant Physiol.* **154**, 134-148 (2010).
- 11 Saint-Jean, B., Seveno-Carpentier, E., Alcon, C., Neuhaus, J. M. & Paris, N. The cytosolic tail dipeptide Ile-Met of the pea receptor BP80 is required for recycling from the prevacuole and for endocytosis. *Plant Cell* **22**, 2825-2837 (2010).
- 12 Dettmer, J., Hong-Hermesdorf, A., Stierhof, Y. D. & Schumacher, K. Vacuolar H<sup>+</sup>-ATPase activity is required for endocytic and secretory trafficking in Arabidopsis. *Plant Cell* **18**, 715-730 (2006).
- 13 Lam, S. K. *et al.* BFA-induced compartments from the Golgi apparatus and trans-Golgi network/early endosome are distinct in plant cells. *Plant J.* **60**, 865-881 (2009).
- 14 Foresti, O. & Denecke, J. Intermediate organelles of the plant secretory pathway: identity and function. *Traffic* **9**, 1599-1612 (2008).
- 15 Shen, J. *et al.* Organelle pH in the Arabidopsis Endomembrane System. *Mol Plant* **6**, 1419-1437, doi:10.1093/mp/sst079 (2013).
- 16 Martiniere, A. *et al.* In Vivo Intracellular pH Measurements in Tobacco and Arabidopsis Reveal an Unexpected pH Gradient in the Endomembrane System. *Plant Cell* **25**, 4028-4043, doi:10.1105/tpc.113.116897 (2013).
- 17 Luo, Y. *et al.* V-ATPase activity in the TGN/EE is required for exocytosis and recycling in Arabidopsis. *Nature Plants* **1**, 15094, doi:10.1038/nplants.2015.94 (2015).
- 18 Niemes, S. *et al.* Retromer recycles vacuolar sorting receptors from the trans-Golgi network. *Plant J.* **61**, 107-121 (2010).
- 19 Stierhof, Y. D., Viotti, C., Scheuring, D., Sturm, S. & Robinson, D. G. Sorting nexins 1 and 2a locate mainly to the TGN. *Protoplasma* **250**, 235-240, doi:10.1007/s00709-012-0399-1 (2013).
- 20 Scheuring, D. *et al.* Multivesicular bodies mature from the trans-Golgi network/early endosome in Arabidopsis. *Plant Cell* **23**, 3463-3481, doi:10.1105/tpc.111.086918 (2011).
- 21 Hamers-Casterman, C. *et al.* Naturally occurring antibodies devoid of light chains. *Nature* **363**, 446-448, doi:10.1038/363446a0 (1993).
- 22 Rothbauer, U. *et al.* Targeting and tracing antigens in live cells with fluorescent nanobodies. *Nature methods* **3**, 887-889, doi:10.1038/nmeth953 (2006).
- 23 Kubala, M. H., Kovtun, O., Alexandrov, K. & Collins, B. M. Structural and thermodynamic analysis of the GFP:GFP-nanobody complex. *Protein Sci.* **19**, 2389-2401, doi:10.1002/pro.519 (2010).
- 24 Bucherl, C. A., Bader, A., Westphal, A. H., Liptenok, S. P. & Borst, J. W. FRET-FLIM applications in plant systems. *Protoplasma* **251**, 383-394, doi:10.1007/s00709-013-0595-7 (2014).
- 25 Kriechbaumer, V. *et al.* Reticulomics: Protein-protein interaction studies with two plasmodesmata-localised reticulon family proteins identify binding partners enriched at plasmodesmata, ER and the plasma membrane. *Plant Physiol.*, doi:10.1104/pp.15.01153 (2015).
- 26 Martiniere, A., Desbrosses, G., Sentenac, H. & Paris, N. Development and properties of genetically encoded pH sensors in plants. *Frontiers in plant science* **4**, 523, doi:10.3389/fpls.2013.00523 (2013).

- 27 Niemes, S. *et al.* Sorting of plant vacuolar proteins is initiated in the ER. *Plant J.* **62**, 601-614 (2010).
- 28 Nishikawa, S., Hirata, A. & Nakano, A. Inhibition of endoplasmic reticulum (ER)-to-Golgi transport induces relocalization of binding protein (BiP) within the ER to form the BiP bodies. *Mol. Biol. Cell* **5**, 1129-1143 (1994).
- 29 Tse, Y. C. *et al.* Identification of multivesicular bodies as prevacuolar compartments in *Nicotiana tabacum* BY-2 cells. *Plant Cell* **16**, 672-693 (2004).
- 30 Humair, D., Hernandez Felipe, D., Neuhaus, J. M. & Paris, N. Demonstration in yeast of the function of BP-80, a putative plant vacuolar sorting receptor. *Plant Cell* **13**, 781-792 (2001).
- 31 Runions, J., Brach, T., Kuhner, S. & Hawes, C. Photoactivation of GFP reveals protein dynamics within the endoplasmic reticulum membrane. *J Exp Bot* **57**, 43-50 (2006).
- 32 daSilva, L. L. *et al.* Receptor salvage from the prevacuolar compartment is essential for efficient vacuolar protein targeting. *Plant Cell* **17**, 132-148 (2005).
- 33 Pimpl, P. *et al.* Golgi-mediated vacuolar sorting of the endoplasmic reticulum chaperone BiP may play an active role in quality control within the secretory pathway. *Plant Cell* **18**, 198-211 (2006).
- 34 Scheuring, D. *et al.* Ubiquitin initiates sorting of Golgi and plasma membrane proteins into the vacuolar degradation pathway. *BMC plant biology* **12**, 164-180, doi:10.1186/1471-2229-12-164 (2012).
- 35 Muyldermans, S. Nanobodies: natural single-domain antibodies. *Annu. Rev. Biochem.* **82**, 775-797, doi:10.1146/annurev-biochem-063011-092449 (2013).
- 36 Rocchetti, A., Hawes, C. & Kriechbaumer, V. Fluorescent labelling of the actin cytoskeleton in plants using a cameloid antibody. *Plant methods* **10**, 12, doi:10.1186/1746-4811-10-12 (2014).
- 37 Schornack, S. *et al.* Protein mislocalization in plant cells using a GFP-binding chromobody. *Plant J.* **60**, 744-754, doi:10.1111/j.1365-313X.2009.03982.x (2009).
- 38 Watanabe, E. *et al.* An ER-Localized Form of PV72, a Seed-Specific Vacuolar Sorting Receptor, Interferes the Transport of an NPIR-Containing Proteinase in *Arabidopsis* Leaves. *Plant Cell Physiol.* **45**, 9-17 (2004).
- 39 Hillmer, S., Movafeghi, A., Robinson, D. G. & Hinz, G. Vacuolar storage proteins are sorted in the cis-cisternae of the pea cotyledon Golgi apparatus. *J. Cell Biol.* **152**, 41-50 (2001).
- 40 Hinz, G., Colanesi, S., Hillmer, S., Rogers, J. C. & Robinson, D. G. Localization of vacuolar transport receptors and cargo proteins in the Golgi apparatus of developing *Arabidopsis* embryos. *Traffic* **8**, 1452-1464 (2007).
- 41 Viotti, C. *et al.* Endocytic and Secretory Traffic in *Arabidopsis* Merge in the Trans-Golgi Network/Early Endosome, an Independent and Highly Dynamic Organelle. *Plant Cell* **22**, 1344-1357 (2010).
- 42 Wang, H., Zhuang, X., Hillmer, S., Robinson, D. G. & Jiang, L. Vacuolar Sorting Receptor (VSR) Proteins Reach the Plasma Membrane in Germinating Pollen Tubes. *Mol Plant* **4**, 845-853 (2011).
- 43 Schmitt, F. J. *et al.* eGFP-pHsens as a highly sensitive fluorophore for cellular pH determination by fluorescence lifetime imaging microscopy (FLIM). *Biochim. Biophys. Acta* **1837**, 1581-1593, doi:10.1016/j.bbabi.2014.04.003 (2014).

- 44 Watanabe, E., Shimada, T., Kuroyanagi, M., Nishimura, M. & Hara-Nishimura, I. Calcium-mediated association of a putative vacuolar sorting receptor PV72 with a propeptide of 2S albumin. *J. Biol. Chem.* **277**, 8708-8715 (2002).
- 45 Stael, S. *et al.* Plant organellar calcium signalling: an emerging field. *J Exp Bot* **63**, 1525-1542, doi:10.1093/jxb/err394 (2012).
- 46 Ordenes, V. R. *et al.* In vivo analysis of the calcium signature in the plant Golgi apparatus reveals unique dynamics. *Cell Calcium* **52**, 397-404, doi:10.1016/j.ceca.2012.06.008 (2012).
- 47 Etxeberria, E., Gonzalez, P., Baroja-Fernandez, E. & Romero, J. P. Fluid phase endocytic uptake of artificial nano-spheres and fluorescent quantum dots by sycamore cultured cells: evidence for the distribution of solutes to different intracellular compartments. *Plant Signal Behav* **1**, 196-200 (2006).
- 48 Phillipson, B. A. *et al.* Secretory bulk flow of soluble proteins is efficient and COPII dependent. *Plant Cell* **13**, 2005-2020 (2001).
- 49 Bubeck, J. *et al.* The syntaxins SYP31 and SYP81 control ER-Golgi trafficking in the plant secretory pathway. *Traffic* **9**, 1629-1652 (2008).
- 50 Pimpl, P., Hanton, S. L., Taylor, J. P., Pinto-DaSilva, L. L. & Denecke, J. The GTPase ARF1p Controls the Sequence-Specific Vacuolar Sorting Route to the Lytic Vacuole. *Plant Cell* **15**, 1242-1256 (2003).

### **Acknowledgments**

We thank Sébastien Peter (Institute of Physical and Theoretical Chemistry, University of Tübingen) for technical support and helpful discussions on FRET-FLIM. We would like to thank Diana Vranjkovic and Natalie Gerling for technical help. The financial support of the Deutsche Forschungsgemeinschaft (PI 769/1-2 and the Collaborative Research Centre SFB 1101 “Molecular Encoding of Specificity in Plant Processes” and TPA03) and the Deutscher Akademischer Austauschdienst (Project 57057314) is gratefully acknowledged.

### **Author contributions**

F.K., F.F., S.F and P.P. designed and analysed the experiments. F.K., S.F., F.F. and B.L. performed experiments. F.K. and P.P. wrote the manuscript.

### **Additional information**

Correspondence and requests for materials should be addressed to P.P.

### **Competing interests**

The authors declare no competing financial interests.



## Figure Legends and Tables

### Figure 1. Compartment-specific targeting of luminal ligand-binding domains (LBDs) in the plant endomembrane system via nanobody-epitope interactions.

(a) Nanobody (Nb)-mediated sensor assembly by coexpression of soluble LBD-RFP-Nb with luminal GFP-epitope-exposing type I/II membrane proteins. (b) Immunodetection of LBD-RFP-NB ± Sec12 overproduction in cells/medium (C)/(M) using α-HA. Loading control: coexpressed Golgi marker ERD2-CFP (α-GFP), mock-transfection (co). (c,d) CLSM analysis of cells from (b). Soluble/secreted LBD-RFP-Nb accumulates with ERD2-CFP in the ER upon Sec12 overproduction (+Sec12). (e-i) Sensor assembly by coexpression of LBD-RFP-Nb with the epitope-tagged anchors (e) GFP-CNX (type I) in the ER, (f) Man1-GFP (type II) in the Golgi, (g) SYP61-GFP (type II) in the TGN/EE, (h,i) GFP-BP80 (type I) in the MVB/LE, and (i) in wortmannin-induced (+WM, 30 μM, 1 h) ring-like MVB/LE structures (arrowheads). Inlays: c,f-i magnifications; d,e cortical sections. Scale bars (μm): 5/2.5 (inlays).

### Figure 2. All assembled VSR sensors are ligand-binding competent.

(a) Principle of compartment-specific VSR-ligand interaction-analysis via FRET-FLIM. Expression of GFP-tagged membrane anchors with soluble LBD-Nbs reconstitutes fluorescent VSR sensors. Binding of red-fluorescent ligands (Aleu-RFP) leads to close proximity and thus FRET, thereby shortening the fluorescence lifetime of GFP. (b) Immunoblot revealing ligand-binding capability of all VSR sensors *in vitro*. Sensors were assembled by coexpression of LBD-Nb with either GFP-CNX, Man1-GFP, SYP61-GFP, or GFP-BP80 in tobacco protoplasts, immunoprecipitated (anti-GFP antibody-coated beads, IP: α-GFP), and incubated with Aleu-RFP. Immunoblots (IB) were probed with antibodies to detect anchors (α-GFP), LBD-Nb (α-HA) and Aleu-RFP/Sec-RFP (α-RFP).

### Figure 3. Analysis of VSR-ligand interaction identifies the ER as compartment that favours ligand binding whilst the MVB/LE restricts ligand binding.

(a,b) Assembly of ER-localising VSR sensors from GFP-CNX+LBD-Nb retains coexpressed vacuolar Aleu-RFP in the ER. (c) FRET-FLIM reveals Aleu-RFP-

triggered FRET/reduced fluorescence lifetime compared to controls expressing RFP-HDEL, Sec-RFP, or  $\Delta$ LBD-Nb. **(d,e)** Coexpressed Aleu-RFP and GFP-BP80 colocalise in MVBs/LEs also upon sensor assembly (GFP-BP80+LBD-Nb). **(f)** FRET-FLIM revealing that Aleu-RFP doesn't trigger FRET/reduce fluorescence lifetime of MVB/LE-localising sensors compared to controls with Nb-mediated attachment of RFP (LBD-RFP-Nb, see Fig. 1). **(g)** Differential distribution of GFP-BP80 and Aleu-RFP in wortmannin-induced ring-like MVB/LE-structures (30  $\mu$ M, 1 h) is not altered by sensor assembly (+LBD-Nb). FLIM data are presented as mean  $\pm$  s.e.m. fluorescence lifetime of  $n=12/17$  **(c/f)** measurements. Significance was calculated using ANOVA, followed by Tukey's HSD test (\*\*\*)  $P<0.001$  compared to every other group; NS, not significant). Images (right) showing fluorescence intensity/lifetime of sensors. Scale bars ( $\mu$ m): 5/2.5 (inlays). Inlays: **a,b**, cortical section; **d,e**: magnifications.

**Figure 4. The Golgi provides ligand-binding conditions for VSRs. (a)**

Coexpressed *cis*-Golgi marker Man1-GFP and the soluble vacuolar reporter Aleu-RFP don't colocalise. **(b)** Assembly of Golgi-localised VSR sensors from Man1-GFP+LBD-Nb retains Aleu-RFP in the Golgi (arrowheads). **(c)** Golgi retention is highlighted by reduction of Aleu-RFP signals in MVBs/LEs and vacuoles by coexpression of the VSR-transport competitor HA-BP80. **(d)** FRET-FLIM analysis identifies the Golgi as compartment favouring ligand binding. Coexpression of Aleu-RFP causes FRET-triggered decrease of fluorescence lifetime of the sensor, which doesn't occur in the absence of the LBD ( $\Delta$ LBD-Nb). **(e)** VSR sensor assembly in the *trans*-Golgi by coexpression of LBD-RFP-Nb with the marker ST-GFP. **(f,g)** Golgi retention of Aleu-RFP caused by assembly of VSR sensors from ST-GFP+LBD-Nb. **(h)** FRET-FLIM analysis demonstrates ligand binding in the *trans*-Golgi. Golgi movement was reduced by application of 4  $\mu$ m LatB 1 h prior to FLIM. Data are presented/calculated as in Fig. 3,  $n=12$  measurements. Scale bars ( $\mu$ m): 5/2.5 (inlays). Inlays: magnifications.

**Figure 5. The TGN/EE does not provide ligand-binding conditions for VSRs.**

**(a,b)** Aleu-RFP doesn't colocalise with the TGN/EE marker SYP61-GFP and is not retained upon sensor assembly (SYP61-GFP+LBD-Nb). Inlays: magnification. **(c)** Pearson's ( $r_p$ ) and Spearman's ( $r_s$ ) correlation (PSC) coefficients of SYP61-

GFP/Aleu-RFP signals from **a,b**, with colocalising SYP61-GFP/LBD-RFP-Nb (see Fig. 1g) for comparison. Statistical analysis/annotations as in Fig. 3,  $n=10$  cells,  $*** P<0.001$ . **(d)** Aleu-RFP doesn't trigger FRET/reduce fluorescence lifetime of TGN/EE-localising sensors (identical to Sec-RFP in negative controls). FRET is triggered in positive controls by attachment of RFP (LBD-RFP-Nb, see Fig. 1). **(e)** BFA-induced ER coaccumulation of sensors (SYP61-GFP+LBD-Nb) and Aleu-RFP (+BFA). Inlay: cortical section. **(f)** Coexpression of SYP61-GFP-based sensors with Aleu-RFP or Sec-RFP  $\pm$ BFA. Aleu-RFP triggers FRET/reduces fluorescence lifetime only in the presence of BFA due to redistribution of sensors/ligands to the binding-favouring ER. Data in **d,f** are presented/calculated as in Fig. 3,  $n=17/20$  (**d/f**) measurements. TGN/EE movement was reduced by application of 4  $\mu$ m LatB 1 h prior to FLIM. **(g)** Proteins were expressed as indicated ( $\pm$  BFA), sensors were immunoprecipitated (anti-GFP antibody-coated beads, IP:  $\alpha$ -GFP), and immunoblotted (IB). Total extracts (T) and immunoprecipitates (IP) were probed with  $\alpha$ -GFP (Anchor),  $\alpha$ -HA (LBD-Nb), and  $\alpha$ -RFP (Aleo-RFP/Sec-RFP), revealing ligand binding of SYP61-GFP-based sensors in the ER (+BFA, black arrowhead) but not in the TGN/EE (-BFA, white arrowhead). For **e-g**, BFA (36  $\mu$ M) was applied after transfection. Scale bars ( $\mu$ m): 5/2.5 (inlays).

**Figure 6. Vacuolar delivery of endocytosed soluble proteins does not depend on sorting signals.** **(a)** Endocytic uptake and vacuolar delivery of 3xRFP by Cyt-GFP-expressing protoplasts. **(b)** Immunoblot of cellular extracts after uptake of 3xRFP, osmotic shock (total proteins, T), and fractionation into membrane (M) and soluble (S) fractions identify endocytosed 3xRFP as soluble protein (left). Cells expressing the plasma membrane marker RFP-TMD23 served as fractionation control (right). **(c)** Endocytic uptake and vacuolar delivery of nanobody-tagged reporter 3xRFP-Nb (compare to **a**). **(d-f)** Mapping of the transport route to the vacuole by nanobody-mediated anchoring of endocytosed 3xRFP-Nb in the TGN/EE and MVB/LE. Incubation of cells exposing GFP at **(d)** the surface (SYP132-GFP), **(e)** the TGN/EE (SYP61-GFP) or **(f)** the MVB/LE (GFP-BP80) with 3xRFP-Nb leads to accumulation of the reporter at the corresponding locations, demonstrating that endocytosed non-VSR-ligand 3xRFP-Nb transits the TGN/EE and MVB/LE *en route* to the vacuole. Inlays:

magnifications. Scale bars ( $\mu\text{m}$ ): 5/2.5 (inlays). **(g)** Concept of sorting and transport of soluble vacuolar proteins. The ER and the Golgi provide binding conditions (green) for VSR-ligand interaction, while the *post*-Golgi compartments TGN/EE and MVB/LE do not (red).

**Supplementary Figure 1. Uncropped immunoblot.** Detection of the immunoprecipitated compartmental markers GFP-CNX, Man1-GFP, SYP61-GFP, and GFP-BP80 as illustrated in Figure 2b. Concentration series (c1-c3) were loaded in SDS-PAGE to equalise the amounts of markers for the detection of the coexpressed/coimmunoprecipitated LBD-Nb. Sections cut for Figure 2b are highlighted by black rectangles. The Immunoblot (IB) was probed with  $\alpha$ -GFP.

**Supplementary Figure 2. The assembly of VSR sensors does not influence the localisation of the membrane anchors.** Protoplasts were transfected with plasmids encoding for the indicated proteins and incubated 24 h before CLSM analysis. **(a-d)** Sensors were assembled from LBD-Nb and the GFP-tagged membrane anchors and localisation was compared to RFP-tagged derivatives of the respective compartmental marker. **(a)** Colocalisation with RFP-CNX in the ER, **(b)** colocalisation with Man1-RFP in the Golgi, **(c)** colocalisation with RFP-SYP61 in the TGN/EE, and **(d)** colocalisation with RFP-BP80 in the MVB/LE. Inlays in **a-d**: magnifications. Scale bars ( $\mu\text{m}$ ): 5/2.5  $\mu\text{m}$  (inlays). **(e)** Pearson's ( $r_P$ ) and Spearman's ( $r_S$ ) correlation (PSC) coefficients calculated for green and red signals as shown in **a-d** demonstrating colocalisation. PSC coefficients are presented as mean  $\pm$  s.e.m ( $n = 10$  individual cells). Statistical significance was calculated using ANOVA, followed by Tukey's HSD test (\*\*\*)  $P < 0.001$ .

**Supplementary Figure 3. Representative CLSM images of cells analysed by FRET-FLIM to assess VSR-ligand binding in the ER and the MVB/LE.** **(a)** FLIM data for the ER. The diagram shows the fluorescence lifetimes from Figure 3c plus additional controls analysed 6 h after application of 36  $\mu\text{M}$  BFA. The different experimental groups are represented by Latin numbers (I-VI). A representative image is given for each group ensuring expression of tested fluorescent pairs. **(b)** FLIM data for the MVB/LE. The diagram shows the fluorescence lifetimes from Figure 3f. The different experimental groups are represented by Latin numbers (I-

IV). A representative image is given for each group ensuring expression of tested fluorescent pairs. Scale bars: 5  $\mu\text{m}$ . Statistics: \*\*\*  $P < 0.001$ ; NS, not significant.

**Supplementary Figure 4. Representative CLSM images of cells analysed by FRET-FLIM to assess VSR-ligand binding in the Golgi.** (a) FLIM data for the *cis*-Golgi. The diagram shows the fluorescence lifetimes from Figure 4d. The different experimental groups are represented by Latin numbers (I-IV). A representative image is given for each group ensuring expression of tested fluorescent pairs. (b) FLIM data for the *trans*-Golgi. The diagram shows the fluorescence lifetimes from Figure 4h. The different experimental groups are represented by Latin numbers (I-IV). A representative image is given for each group ensuring expression of tested fluorescent pairs. Scale bars: 5  $\mu\text{m}$ . Statistics: \*\*\*  $P < 0.001$ ; NS, not significant.

**Supplementary Figure 5. Representative CLSM images of cells analysed by FRET-FLIM to assess VSR-ligand binding in the TGN/EE.** (a) The diagram shows the fluorescence lifetimes from Figure 5d,f ( $\pm$  BFA) in direct comparison. The different experimental groups are represented by Latin numbers (I-IV). A representative image is given for each group ensuring expression of tested fluorescent pairs. Scale bars: 5  $\mu\text{m}$ . Statistics: \*\*\*  $P < 0.001$ ; NS, not significant.

**Figure 1**

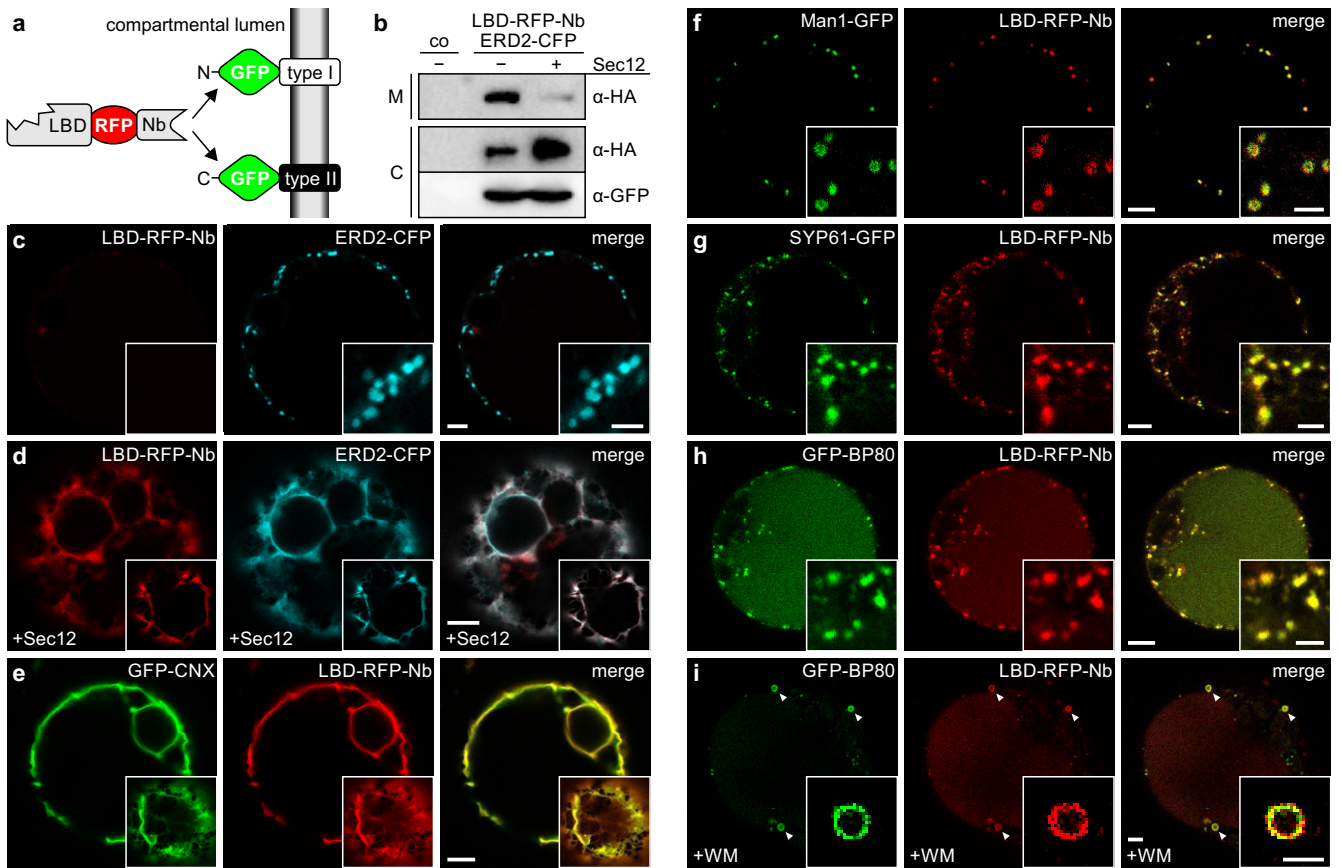


**Figure 1. Compartment-specific targeting of luminal ligand-binding domains (LBDs) in the plant endomembrane system via nanobody-epitope interactions.** (a) Nanobody (Nb)-mediated sensor assembly by coexpression of soluble LBD-RFP-Nb with luminal GFP-epitope-exposing type I/II membrane proteins. (b) Immunodetection of LBD-RFP-NB ± Sec12 overproduction in cells/medium (C)/(M) using α-HA. Loading control: coexpressed Golgi marker ERD2-CFP (α-GFP), mock-transfection (co). (c,d) CLSM analysis of cells from (b). Soluble/secreted LBD-RFP-Nb accumulates with ERD2-CFP in the ER upon Sec12 overproduction (+Sec12). (e-i) Sensor assembly by coexpression of LBD-RFP-Nb with the epitope-tagged anchors (e) GFP-CNX (type I) in the ER, (f) Man1-GFP (type II) in the Golgi, (g) SYP61-GFP (type II) in the TGN/EE, (h,i) GFP-BP80 (type I) in the MVB/LE, and (i) in wortmannin-induced (+WM, 30 μM, 1 h) ring-like MVB/LE structures (arrowheads). Inlays: c,f-i magnifications; d,e cortical sections. Scale bars (μm): 5/2.5 (inlays).

## Figure 2

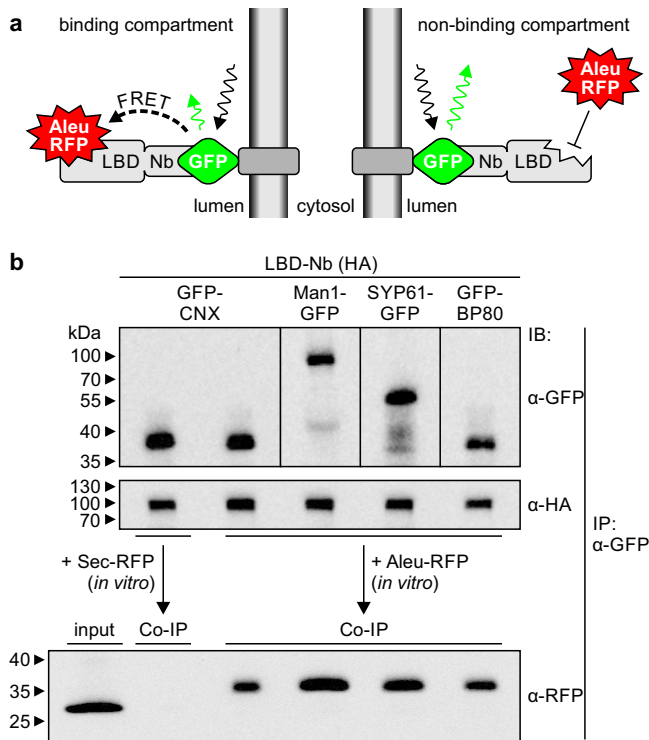


**Figure 2. All assembled VSR sensors are ligand-binding competent.** (a) Principle of compartment-specific VSR-ligand interaction-analysis via FRET-FLIM. Expression of GFP-tagged membrane anchors with soluble LBD-Nbs reconstitutes fluorescent VSR sensors. Binding of red-fluorescent ligands (Aleu-RFP) leads to close proximity and thus FRET, thereby shortening the fluorescence lifetime of GFP. (b) Immunoblot revealing ligand-binding capability of all VSR sensors *in vitro*. Sensors were assembled by coexpression of LBD-Nb with either GFP-CNX, Man1-GFP, SYP61-GFP, or GFP-BP80 in tobacco protoplasts, immunoprecipitated (anti-GFP antibody-coated beads, IP: α-GFP), and incubated with Aleu-RFP. Immunoblots (IB) were probed with antibodies to detect anchors (α-GFP), LBD-Nb (α-HA) and Aleu-RFP/Sec-RFP (α-RFP).

**Figure 3**

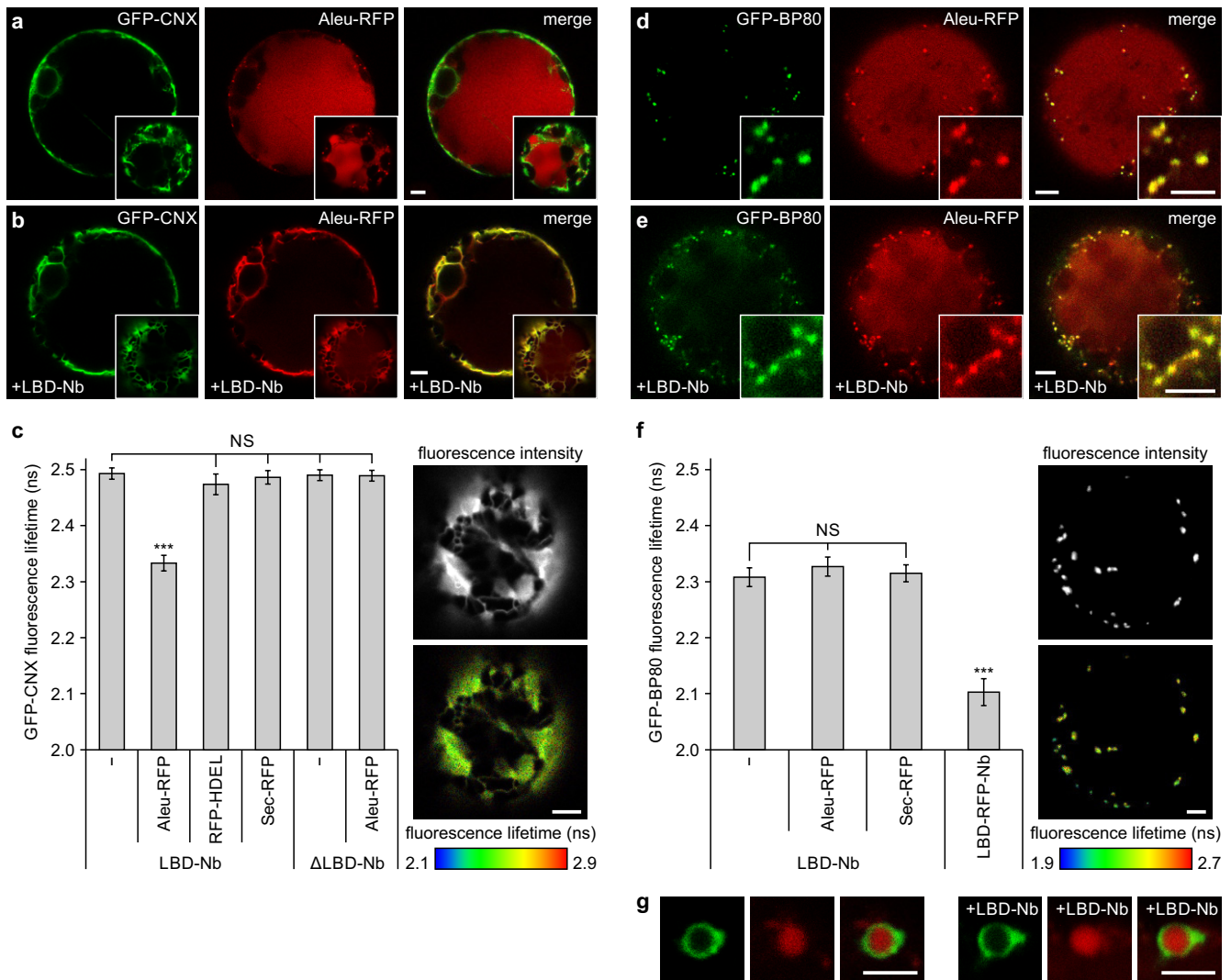


**Figure 3. Analysis of VSR-ligand interaction identifies the ER as compartment that favours ligand binding whilst the MVB/LE restricts ligand binding.** (a,b) Assembly of ER-localising VSR sensors from GFP-CNX+LBD-Nb retains coexpressed vacuolar Aleu-RFP in the ER. (c) FRET-FLIM reveals Aleu-RFP-triggered FRET/reduced fluorescence lifetime compared to controls expressing RFP-HDEL, Sec-RFP, or ΔLBD-Nb. (d,e) Coexpressed Aleu-RFP and GFP-BP80 colocalise in MVBs/LEs also upon sensor assembly (GFP-BP80+LBD-Nb). (f) FRET-FLIM revealing that Aleu-RFP doesn't trigger FRET/reduce fluorescence lifetime of MVB/LE-localising sensors compared to controls with Nb-mediated attachment of RFP (LBD-RFP-Nb, see Fig. 1). (g) Differential distribution of GFP-BP80 and Aleu-RFP in wortmannin-induced ring-like MVB/LE-structures (30 μM, 1 h) is not altered by sensor assembly (+LBD-Nb). FLIM data are presented as mean ± s.e.m. fluorescence lifetime of  $n=12/17$  (c/f) measurements. Significance was calculated using ANOVA, followed by Tukey's HSD test (\*\*\*)  $P < 0.001$  compared to every other group; NS, not significant). Images (right) showing fluorescence intensity/lifetime of sensors. Scale bars (μm): 5/2.5 (inlays). Inlays: a,b, cortical section; d,e: magnifications.



**Figure 4**

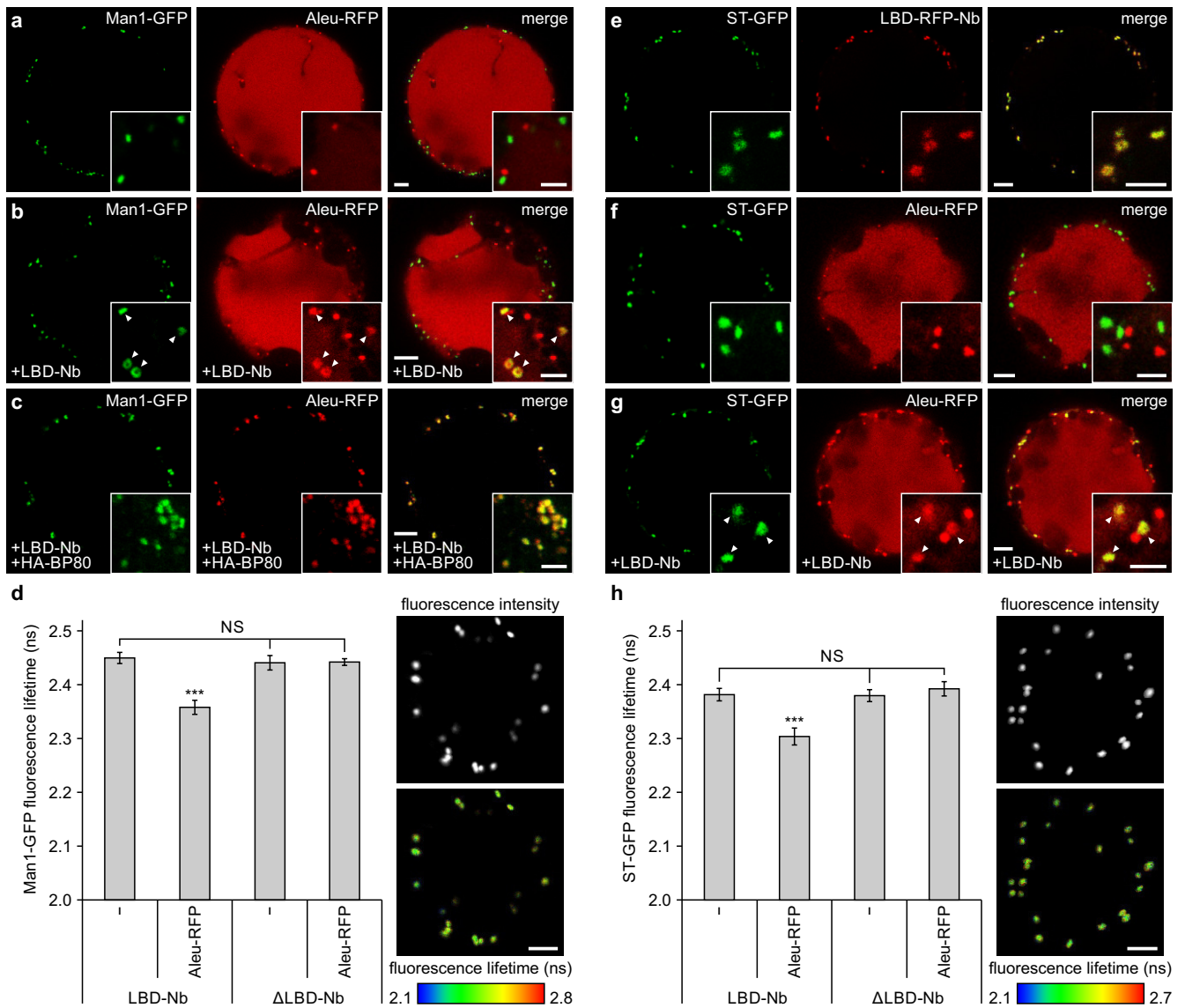


**Figure 4. The Golgi provides ligand-binding conditions for VSRs.** (a) Coexpressed *cis*-Golgi marker Man1-GFP and the soluble vacuolar reporter Aleu-RFP don't colocalise. (b) Assembly of Golgi-localised VSR sensors from Man1-GFP+LBD-Nb retains Aleu-RFP in the Golgi (arrowheads). (c) Golgi retention is highlighted by reduction of Aleu-RFP signals in MVBs/LEs and vacuoles by coexpression of the VSR-transport competitor HA-BP80. (d) FRET-FLIM analysis identifies the Golgi as compartment favouring ligand binding. Coexpression of Aleu-RFP causes FRET-triggered decrease of fluorescence lifetime of the sensor, which doesn't occur in the absence of the LBD ( $\Delta$ LBD-Nb). (e) VSR sensor assembly in the *trans*-Golgi by coexpression of LBD-RFP-Nb with the marker ST-GFP. (f,g) Golgi retention of Aleu-RFP caused by assembly of VSR sensors from ST-GFP+LBD-Nb. (h) FRET-FLIM analysis demonstrates ligand binding in the *trans*-Golgi. Golgi movement was reduced by application of 4  $\mu$ m latrunculin B 1 h prior to FLIM. Data are presented/calculated as in Fig. 3,  $n=12$  measurements. Scale bars ( $\mu$ m): 5/2.5 (inlays). Inlays: magnifications.

**Figure 5**

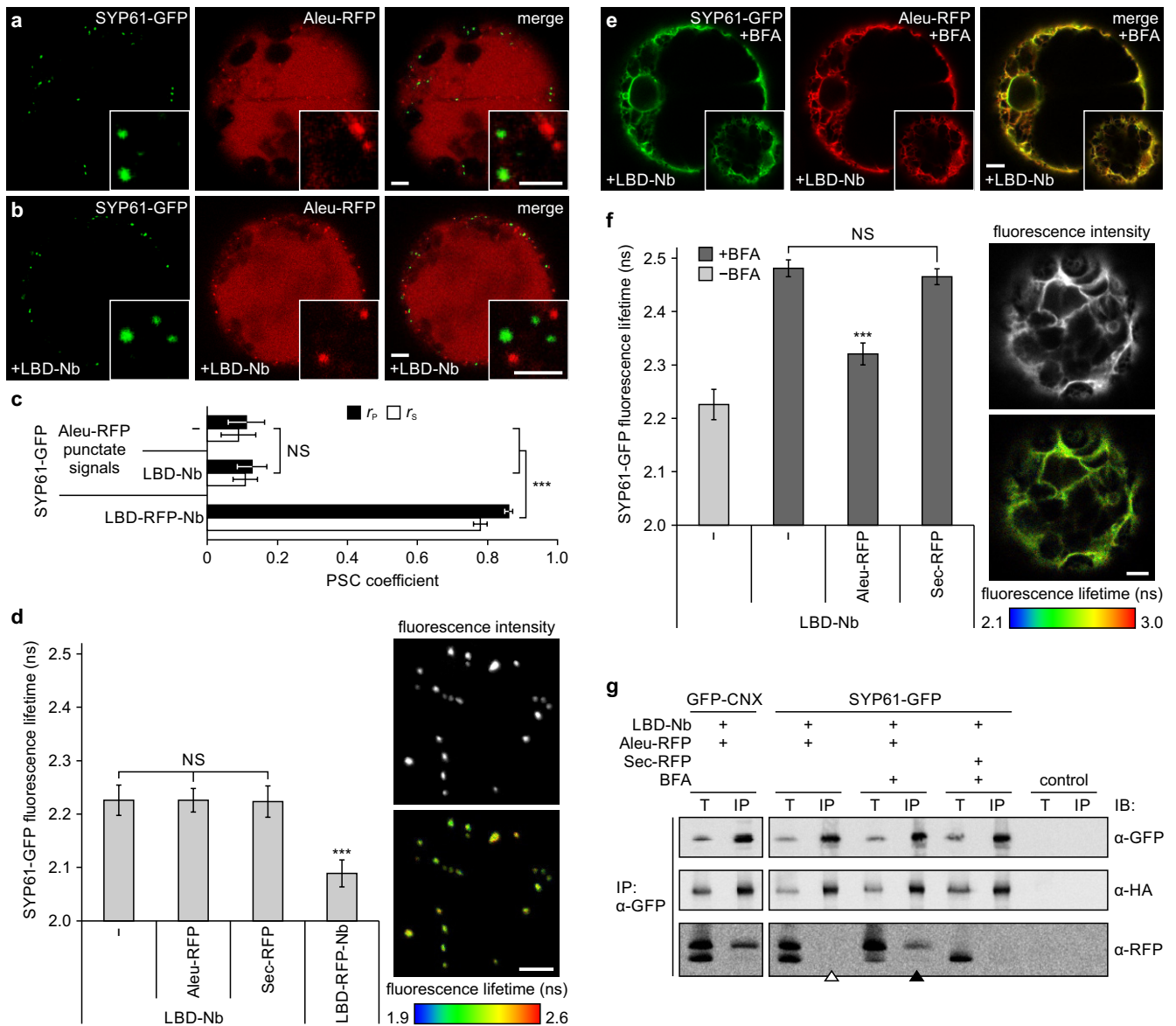


**Figure 5. The TGN/EE does not provide ligand-binding conditions for VSRs.** (a,b) Aleu-RFP doesn't colocalise with the TGN/EE marker SYP61-GFP and is not retained upon sensor assembly (SYP61-GFP+LBD-Nb). Inlays: magnification. (c) Pearson's ( $r_p$ ) and Spearman's ( $r_s$ ) correlation (PSC) coefficients of SYP61-GFP/Aleu-RFP signals from a,b, with colocalising SYP61-GFP/LBD-RFP-Nb (see Fig. 1g) for comparison. Statistical analysis/annotations as in Fig. 3,  $n=10$  cells, \*\*\*  $P<0.001$ . (d) Aleu-RFP doesn't trigger FRET/reduce fluorescence lifetime of TGN/EE-localising sensors (identical to Sec-RFP in negative controls). FRET is triggered in positive controls by attachment of RFP (LBD-RFP-Nb, see Fig. 1). (e) BFA-induced ER coaccumulation of sensors (SYP61-GFP+LBD-Nb) and Aleu-RFP (+BFA). Inlay: cortical section. (f) Coexpression of SYP61-GFP-based sensors with Aleu-RFP or Sec-RFP  $\pm$ BFA. Aleu-RFP triggers FRET/reduces fluorescence lifetime only in the presence of BFA due to redistribution of sensors/ligands to the binding-favouring ER. Data in d,f are presented/calculated as in Fig. 3,  $n=17/20$  (d/f) measurements. TGN/EE movement was reduced by application of 4  $\mu$ m latrunculin B 1 h prior to FLIM. (g) Proteins were expressed as indicated ( $\pm$  BFA), sensors were immunoprecipitated (anti-GFP antibody-coated beads, IP:  $\alpha$ -GFP), and immunoblotted (IB). Total extracts (T) and immunoprecipitates (IP) were probed with  $\alpha$ -GFP (Anchor),  $\alpha$ -HA (LBD-Nb), and  $\alpha$ -RFP (Aleu-RFP/Sec-RFP), revealing ligand binding of SYP61-GFP-based sensors in the ER (+BFA, black arrowhead) but not in the TGN/EE (-BFA, white arrowhead). For e-g, BFA (36  $\mu$ M) was applied after transfection. Scale bars

**Figure 6**

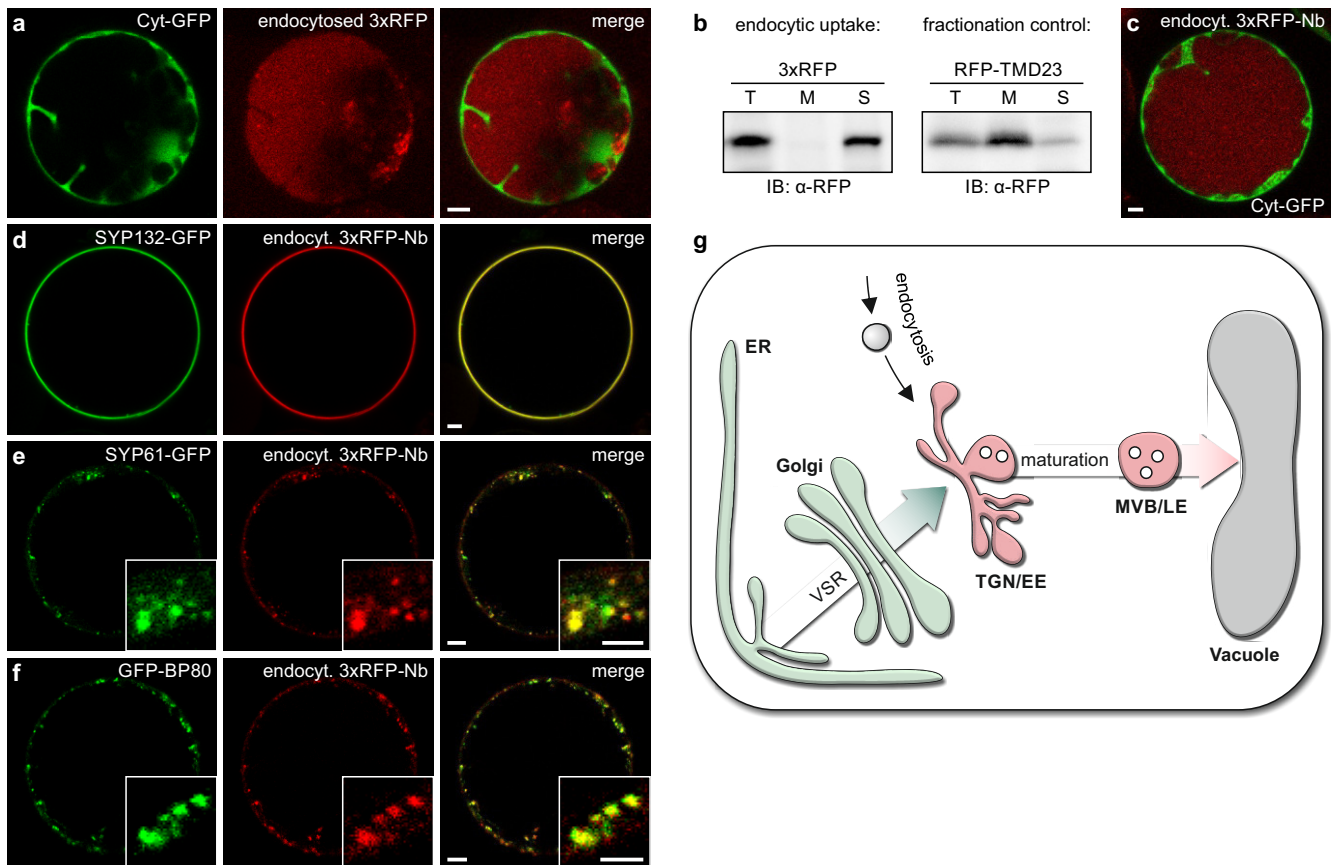
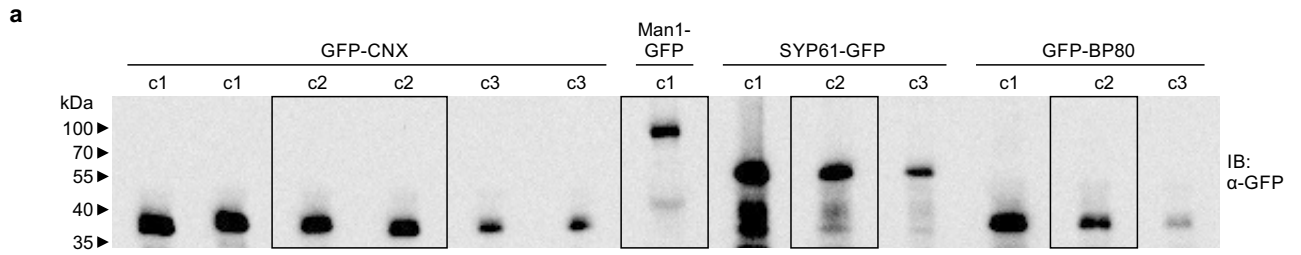


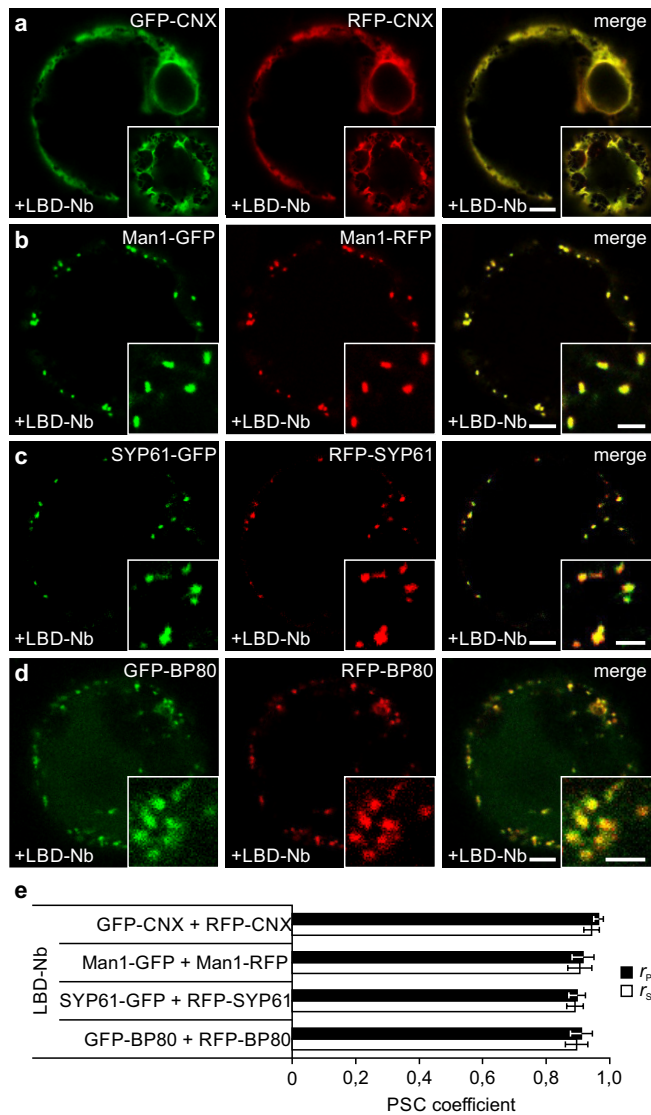
**Figure 6. Vacuolar delivery of endocytosed soluble proteins does not depend on sorting signals.** (a) Endocytic uptake and vacuolar delivery of 3xRFP by Cyt-GFP-expressing protoplasts. (b) Immunoblot of cellular extracts after uptake of 3xRFP, osmotic shock (total proteins, T), and fractionation into membrane (M) and soluble (S) fractions identify endocytosed 3xRFP as soluble protein (left). Cells expressing the plasma membrane marker RFP-TMD23 served as fractionation control (right). (c) Endocytic uptake and vacuolar delivery of nanobody-tagged reporter 3xRFP-Nb (compare to a). (d-f) Mapping of the transport route to the vacuole by nanobody-mediated anchoring of endocytosed 3xRFP-Nb in the TGN/EE and MVB/LE. Incubation of cells exposing GFP at (d) the surface (SYP132-GFP), (e) the TGN/EE (SYP61-GFP) or (f) the MVB/LE (GFP-BP80) with 3xRFP-Nb leads to accumulation of the reporter at the corresponding locations, demonstrating that endocytosed non-VSR-ligand 3xRFP-Nb transits the TGN/EE and MVB/LE *en route* to the vacuole. Inlays: magnifications. Scale bars ( $\mu\text{m}$ ): 5/2.5 (inlays). (g) Concept of sorting and transport of soluble vacuolar proteins. The ER and the Golgi provide binding conditions (green) for VSR-ligand interaction, while the *post*-Golgi compartments TGN/EE and MVB/LE do not (red).

## Supplementary Figure 1



**Supplementary Figure 1. Uncropped immunoblot.** Detection of the immunoprecipitated compartmental markers GFP-CNX, Man1-GFP, SYP61-GFP, and GFP-BP80 as illustrated in Figure 2b. Concentration series (c1-c3) were loaded in SDS-PAGE to equalise the amounts of markers for the detection of the coexpressed/coimmunoprecipitated LBD-Nb. Sections cut for Figure 2b are highlighted by black rectangles. The Immunoblot (IB) was probed with  $\alpha$ -GFP.

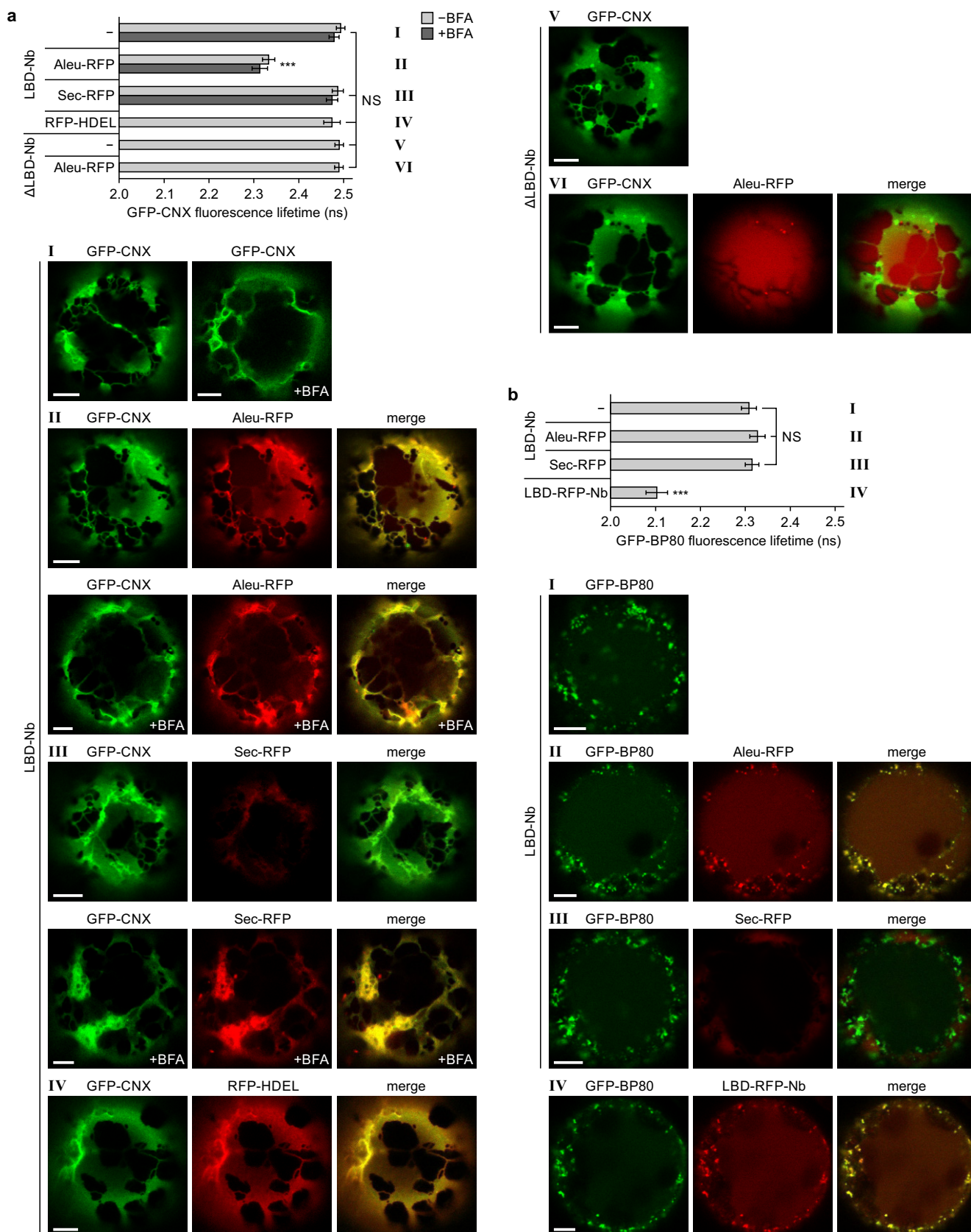
## Supplementary Figure 2



**Supplementary Figure 2. The assembly of VSR sensors does not influence the localisation of the membrane anchors.** Protoplasts were transfected with plasmids encoding for the indicated proteins and incubated 24 h before CLSM analysis. **(a-d)** Sensors were assembled from LBD-Nb and the GFP-tagged membrane anchors and localisation was compared to RFP-tagged derivatives of the respective compartmental marker. **(a)** Colocalisation with RFP-CNX in the ER, **(b)** colocalisation with Man1-RFP in the Golgi, **(c)** colocalisation with RFP-SYP61 in the TGN/EE, and **(d)** colocalisation with RFP-BP80 in the MVB/LE. Inlays in **a-d**: magnifications. Scale bars ( $\mu\text{m}$ ): 5/2.5  $\mu\text{m}$  (inlays). **(e)** Pearson's ( $r_p$ ) and Spearman's ( $r_s$ ) correlation (PSC) coefficients calculated for green and red signals as shown in **a-d** demonstrating colocalisation. PSC coefficients are presented as mean  $\pm$  s.e.m ( $n = 10$  individual cells). Statistical significance was calculated using ANOVA, followed by Tukey's HSD test (\*\*\*)

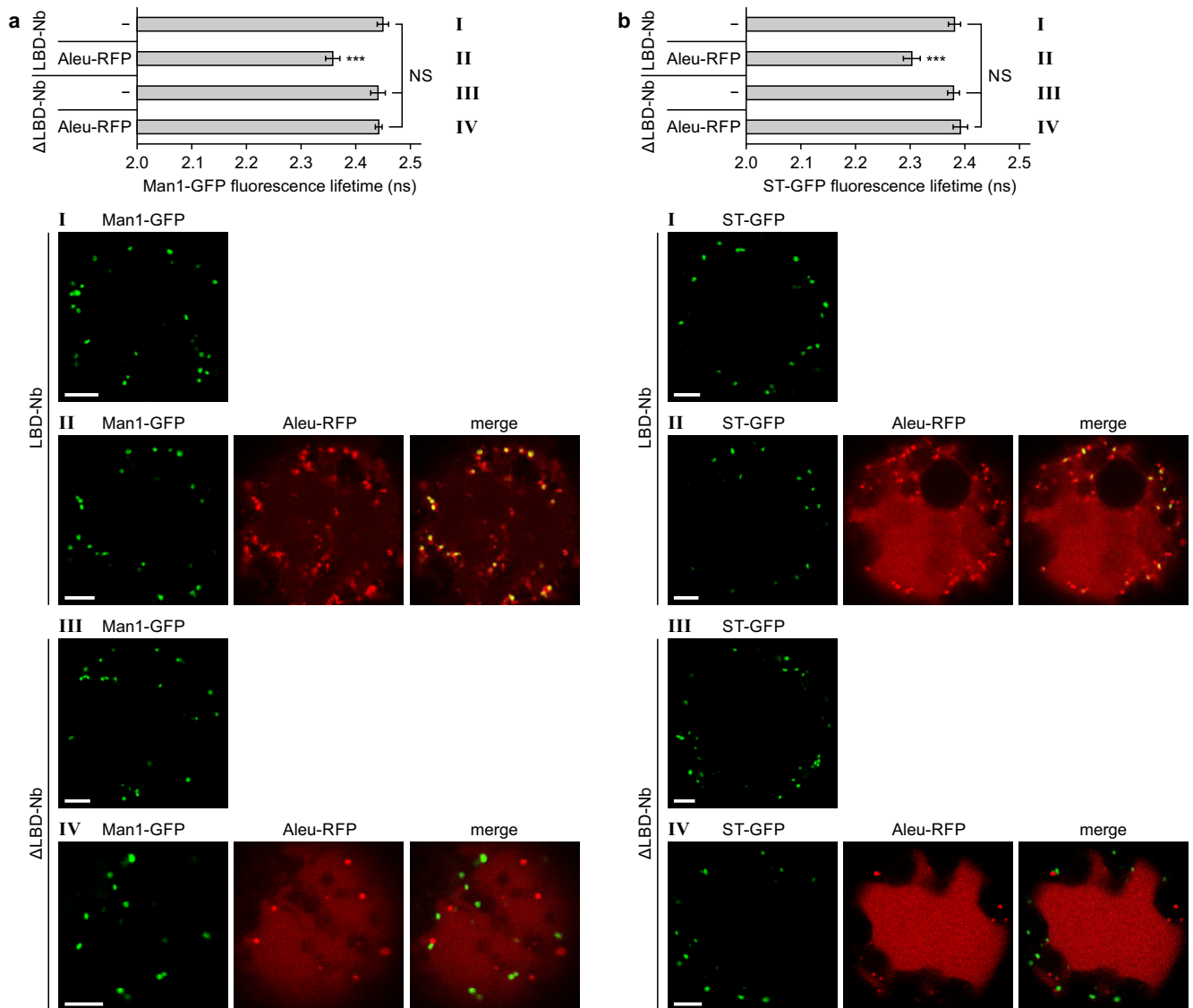


### Supplementary Figure 3



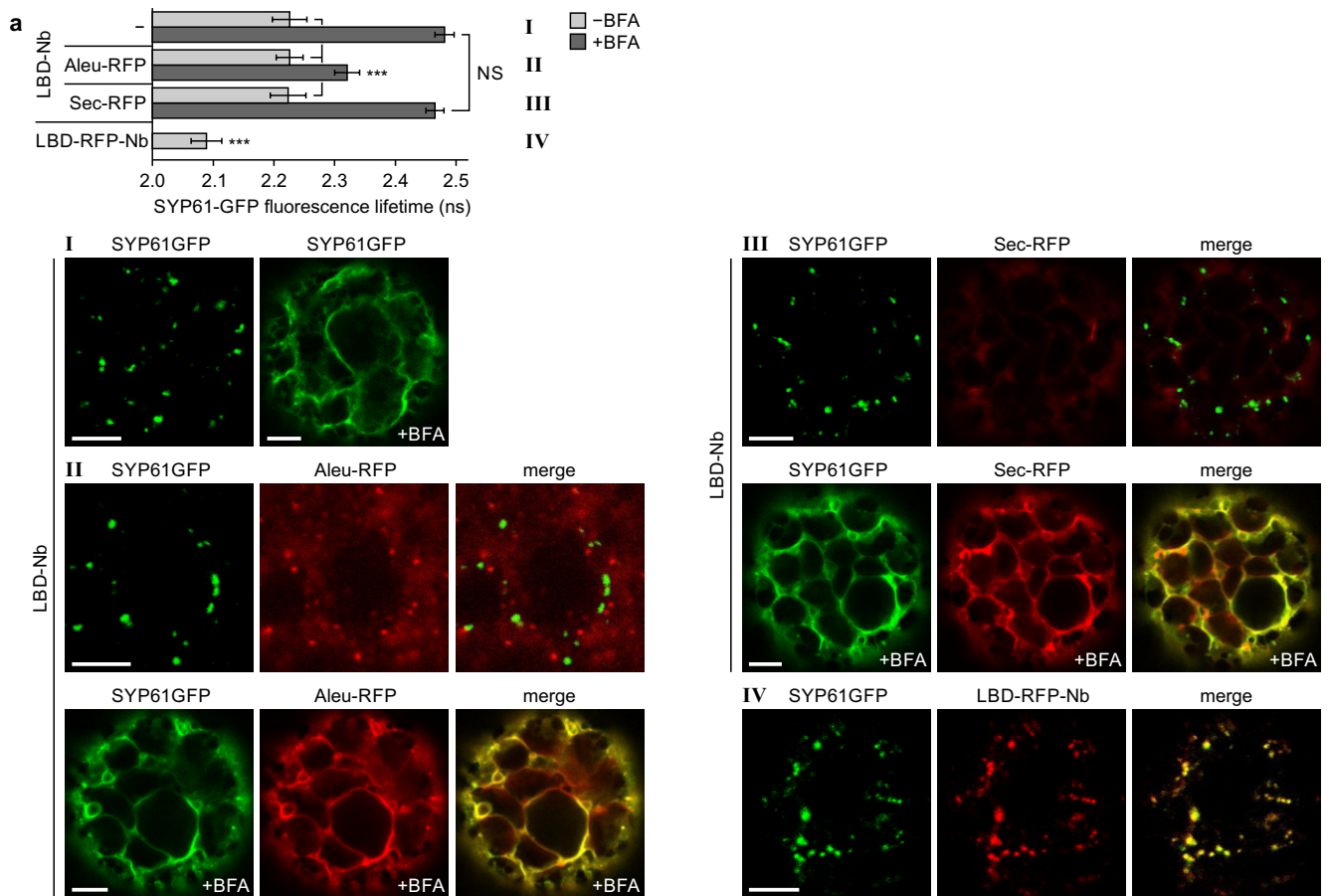
**Supplementary Figure 3. Representative CLSM images of cells analysed by FRET-FLIM to assess VSR-ligand binding in the ER and the MVB/LE. (a)** FLIM data for the ER. The diagram shows the fluorescence lifetimes from Figure 3c plus additional controls analysed 6 h after application of 36  $\mu$ M BFA. The different experimental groups are represented by Latin numbers (I-VI). A representative image is given for each group ensuring expression of tested fluorescent pairs. **(b)** FLIM data for the MVB/LE. The diagram shows the fluorescence lifetimes from Figure 3f. The different experimental groups are represented by Latin numbers (I-IV). A representative image is given for each group ensuring expression of tested fluorescent pairs. Scale bars: 5  $\mu$ m. Statistics: \*\*\*  $P < 0.001$ ; NS, not significant.

## Supplementary Figure 4



**Supplementary Figure 4. Representative CLSM images of cells analysed by FRET-FLIM to assess VSR-ligand binding in the Golgi.** (a) FLIM data for the *cis*-Golgi. The diagram shows the fluorescence lifetimes from Figure 4d. The different experimental groups are represented by Latin numbers (I-IV). A representative image is given for each group ensuring expression of tested fluorescent pairs. (b) FLIM data for the *trans*-Golgi. The diagram shows the fluorescence lifetimes from Figure 4h. The different experimental groups are represented by Latin numbers (I-IV). A representative image is given for each group ensuring expression of tested fluorescent pairs. Scale bars: 5  $\mu$ m. Statistics: \*\*\*  $P < 0.001$ ; NS, not significant.

## Supplementary Figure 5



**Supplementary Figure 5. Representative CLSM images of cells analysed by FRET-FLIM to assess VSR-ligand binding in the TGN/EE.** (a) The diagram shows the fluorescence lifetimes from Figure 5d,f ( $\pm$  BFA) in direct comparison. The different experimental groups are represented by Latin numbers (I-IV). A representative image is given for each group ensuring expression of tested fluorescent pairs. Scale bars: 5  $\mu$ m. Statistics: \*\*\*  $P < 0.001$ ; NS, not significant.



**Supplementary Table 1**

	Primers	Sequence (5'-3' direction)	Template	Recipient Vector
<b>LBD-RFP-Nb (pBL14)</b>	LBD_ <i>NheI</i> _S	AGCTGAGCTAGCATGAA GCAGCTTCTATGTTA	first strand cDNA from 3-day-old <i>A. thaliana</i> seedlings	pCN1 <sup>1</sup> ; modified to contain following strategic restriction sites: P35S- <i>NheI</i> -CDS- <i>Bam</i> HI-T3nos
	LBD_ <i>SalI</i> _AS	GCTGATGTCGACGCAAG TGTCATGGTCTCTCA		
	mRFP_ <i>SalI</i> _S	TGCCGGGTCGACATGGC CTCCTCCGAGGACGT	pFK12 <sup>1</sup>	
	mRFP_ <i>KpnI</i> _AS	TCCTTAGGTACCTGCTCC AGTGCTGTGGCGGC		
	PLUS: anti-GFP nanobody ( <i>KpnI</i> / <i>Bam</i> HI); chemically synthesised			
<b>LBD-Nb (pFF29)</b>	LBD_ <i>NheI</i> _S	AGCTGAGCTAGCATGAA GCAGCTTCTATGTTA	first strand cDNA from 3-day-old <i>A. thaliana</i> seedlings	pBL14 (see above); cut <i>KpnI</i> / <i>NheI</i>
	LBD_ <i>KpnI</i> _AS	CGTATTGGTACCGCAAGT GTCATGGTCTCTCA		
<b>ΔLBD-Nb (pFK120)</b>	Nb_ <i>NheI</i> _S	AGTCTAGCTAGCGCCATG TATCCTTATGATGTTCC	pBL14 (see above)	RFP-TMD23 in pCN1 <sup>1</sup> ; cut <i>Bam</i> HI/ <i>NheI</i> to keep the N- terminal signal peptide of RFP- TMD23
	Nb_ <i>Bam</i> HI_AS	TGCTTCGGATCCCTAATG AT		
<b>Cyt-RFP-Nb (pFF31)</b>	mRFP_ <i>ClaI</i> _S	AGTCTAATCGATGGCCTC CTCCGAGGACGT	pBL14 (see above)	RFP-TMD23 in pCN1 <sup>1</sup> ; cut <i>Bam</i> HI/ <i>ClaI</i>
	Nb_ <i>Bam</i> HI_AS	TGCTTCGGATCCCTAATG AT		
<b>GFP-CN<sub>X</sub> (pFF4)</b>	EGFP_ <i>NheI</i> _S	GCATGAGCTAGCGCCAT GGTGAGCAAGGGCGAGG	pJB13 <sup>2</sup>	pFK120 (see above); cut <i>Bam</i> HI/ <i>NheI</i>
	EGFP_ <i>NotI</i> _AS	AGTCTAGCGCGCCGCCCT TGACAGCTCGTCCATGC		
	CN <sub>X</sub> -TMD_ <i>NotI</i> _S	GATCCGGCGCGCGCGAA CTGATTGAGAAAGCCGA	pSLH6 <sup>3</sup>	
	CN <sub>X</sub> -CT_ <i>Bam</i> HI_AS	TGCTTCGGATCCTCTAGA GC		
<b>GFP-BP80 (pFF3)</b>	BP80a-TMD_ <i>NotI</i> _S	AGTCTAGCGCGCCGCATC AGTAAGACGGTTTCA	pLL38 <sup>3</sup>	pFF4 (see above); cut <i>Bam</i> HI/ <i>NotI</i>
	BP80a- CT_ <i>Bam</i> HI_AS	TGCTTCGGATCCCTTAGG CA		
<b>Man1-GFP (pFF6)</b>	Man1_ <i>NheI</i> _S	GCATGAGCTAGCATGGC GAGAGGGAGCAGATC	pBP30 <sup>4</sup>	pBL14 (see above); cut <i>Bam</i> HI/ <i>NheI</i>
	Man1_ <i>NotI</i> _AS	AGTCTAGCGCGCCGCCAC TAGTTCTAGAAAAGGT		
	EGFP_ <i>NotI</i> _S	AGTCTAGCGCGCCGCATG GTGAGCAAGGGCGAGGA	pJB13 <sup>2</sup>	
	EGFP_ <i>Bam</i> HI_AS	AGCTGAGGATCCTTACTT GTACAGCTCGTCCA		
<b>SYP61-GFP (pFF25)</b>	SYP61_ <i>NheI</i> _S	AGTCTAGCTAGCATGTCT TCAGCTCAAGATCC	pDS13 <sup>5</sup>	pFF6 (see above); cut <i>NotI</i> / <i>NheI</i>
	SYP61_ <i>NotI</i> _AS	GCTGTAGCGCGCCGCCGG TCAAGAAGACAAGAACGA		
<b>SYP132-GFP (FF13)</b>	SYP132_ <i>NheI</i> _S	AGTCTAGCTAGCATGAAC GATCTTCTGAAGGG	RFP-SYP132 <sup>5</sup>	pFF6 (see above); cut <i>NotI</i> / <i>NheI</i>
	SYP132_ <i>NotI</i> _AS	GATCCGGCGCGCCGCCAG CACTCTTGTTCCTCAAG		
<b>Cyt-RFP (pFK98)</b>	mRFP_ <i>NheI</i> _S	AGTCTAGCTAGCATGGCC TCCTCCGAGGACG	pFK12 <sup>1</sup>	pGD5 <sup>5</sup> ; cut <i>Bam</i> HI/ <i>NheI</i>
	mRFP_ <i>Bam</i> HI_AS	AGTCTAGGATCCTTATGC TCCAGTACTGTGGCGGC		

<b>Sec-RFP (pFF14)</b>	SP_XhoI_SalI_S	TCGAGATGAAAGCCTTCA CACTCGCTCTCTTCTTAG CTCTTTCCCTCTATCTCC TGCCAATCCAGCCATGA CG	Complementary oligonucleotides to assemble the coding sequence of the GFP- spo N-terminal signal peptide <sup>3</sup>	pCN1 <sup>1</sup> ; modified to contain following strategic restriction sites: P35S-XhoI-CDS-SpeI-T3nos
	SP_SalI_XhoI_AS	TCGACGTCATGGCTGGAT TGGCAGGAGATAGAGG GAAAGAGCTAAGAAGAG AGCGAGTGTGAAGGCTTT CATC		
	mRFP_SalI_S	CTCTATGTCGACTATGGC CTCTCCGAGGACGT	pFK12 <sup>1</sup>	
	mRFP_SpeI_AS	AGTCTAACTAGITTATGC TCCAGTACTGTGGCGGC		
<b>Aleu-RFP (pFF15)</b>	Aleu_XhoI_S	AGTCTACTCGAGATGTCT CGTCTGTCACTCCT	aleu-GFP <sup>7</sup>	pFF14 (see above); cut <u>SpeI/XhoI</u>
	Aleu_NheI_AS	CATTGCGCTAGCGCTTTC CA		
	mRFP_NheI_S	CTTTCTGCTAGCGCCATG GC	pFK12 <sup>1</sup>	
	mRFP_SpeI_AS	AGTCTAACTAGITTATGC TCCAGTACTGTGGCGGC		
<b>3xRFP (pSF70)</b>	mRFP_SalI_S	TGCCGGGTCGACGATGG CCTCTCCGAGGACGT	pFK12 <sup>1</sup>	pFF14 (see above); cut <u>SpeI/SalI</u> to keep the N- terminal signal peptide of pFF14
	mRFP_NdeI_AS	TTCGGACATATGTGCTCC AGTACTGTGGCGGC		
	mRFP_NdeI_S	AGTCTACATATGGCTCC TCCGAGGACG	pFK12 <sup>8</sup>	
	mRFP_NheI_AS	AGTCTAGCTAGCTGCTCC AGTACTGTGGC		
	mRFP_NheI_S	GTTGACTGCTAGCGCCAT GGCCTCCTC	pFK12 <sup>1</sup>	
	mRFP_SpeI_AS	CTGCAACTAGTTTATGCT CCAGTACTGTGGCGGC		
<b>3xRFP-Nb (pSF71)</b>	mRFP_NheI_S	AGTCTAGCTAGCATGGCC TCCTCCGAGGACG	pFK12 <sup>1</sup>	pSF70 (see above); cut <u>HindIII/NheI</u>
	mRFP_KpnI_AS	TCCTTAGGTACCTGCTCC AGTGCTGTGGCGGC		
	PLUS: anti-GFP nanobody-T3nos ( <u>KpnI/HindIII</u> ), subcloned from pBL14 (see above)			
<b>RFP-CNX (pLBY13)</b>	CNX-TMD_SalI_S	AGTCTAGTCGACGGAAC GATTGAGAAAGCCGAG	pSLH6 <sup>3</sup>	RFP-TMD23 in pCN1 <sup>1</sup> ; cut <u>BamHI/SalI</u>
	CNX-CT_BamHI_AS	AGTCTAGGATCCCTAATT ATCACGTCTCGGTT		
<b>GFP-SYP61 (pFK94)</b>	EGFP_NcoI_S	AGTCTACCATGGTGAGCA AGGGCGAGG	pJB13 <sup>2</sup>	pDS13 <sup>5</sup> ; cut <u>Clal/NcoI</u>
	EGFP_Clal_AS	AGTCTAATCGATGCTCCA CCCTTGACAGCTCGTCC ATGC		
<b>RFP-SYP61 (pML4)</b>	mRFP_NheI_S	AGTCTAGCTAGCATGGCC TCCTCCGAGGACG	pBP30 <sup>4</sup>	pGD5 <sup>5</sup> ; cut <u>BamHI/NheI</u>
	mRFP_Clal_AS	GCTGTAATCGATGCGGC GCCGGTGGAGTGGCGGC		
	PLUS: SYP61 ( <u>Clal/BamHI</u> ), subcloned from pDS13 <sup>5</sup>			

<b>RFP-BP80 (pFK121)</b>	BP80a-SP_NheI_S	TCCTTAGCTAGCATGAAG CAGCTTCTGTGTTA	pJLH21 <sup>3</sup>	pGD5 <sup>5</sup> ; cut <u>BamHI/NheI</u>
	BP80a-SP_NotI_AS	AGTCTAGCGGCCGCGAG CCTCGCTAAAAGGGGAA		
	mRFP_NotI_S	AGTCTAGCGGCCGCATG GCCTCTCCGAGGACGT	pBP30 <sup>4</sup>	
	mRFP_SalI_AS	AGTCTAGTCGACCGGCG CCGGTGGAGTGGCGGC		
	BP80a-TMD_SalI_S	GCTGATGTCGACTTTCAC AAGTGAATCAGCG	pLL38 <sup>3</sup>	
	BP80a- CT_BamHI_AS	TGCTTCGGATCCCTTAGG CA		
<b>HA-BP80 (pFK119)</b>	SP_ClaI_S	CTCTATATCGATGAGGCT TT	pFK120 (see above)	pFF3 (see above); cut <u>NotI/ClaI</u>
	HA_NotI_AS	AGTCTAGCGGCCGCGCAG CATAATCAGGAACATCA		
<b>ST-GFP (pSF83)</b>	ST_NheI_S	ACTGCAGCTAGCATGATT CATACCAACTTGAA	ST-YFP <sup>9</sup>	pFF03 (see above); cut <u>NotI/NheI</u>
	ST_NotI_AS	CTAGCAGCGCGCGCGGG CCACTTCTCCTGGCTCT		
<b>RFP-HDEL (pFK 123)</b>	sp_ClaI_S	CTCTATATCGATGAGGCT TTGTAAATTCACAG	pFK12 <sup>1</sup>	RFP-TMD23 in pCN1 <sup>1</sup> ; cut <u>BamHI/ClaI</u>
	RFP- HDEL_BamHI_AS	AGTCTAGGATCCCTAAAG CTCATCATGTGCTCCAGT ACTGTGGCG		

#### Established plasmids used in this study

<b>Cyt-GFP<sup>10</sup></b>	Cytosolic GFP
<b>ERD2-CFP<sup>9</sup></b>	<i>cis</i> -Golgi marker
<b>Man1-RFP<sup>4</sup></b>	<i>cis</i> -Golgi marker
<b>Sec12<sup>11</sup></b>	Guanine nucleotide exchange factor (GEF) for the GTPase Sar1p

#### References

- 1 Scheuring, D. *et al.* Ubiquitin initiates sorting of Golgi and plasma membrane proteins into the vacuolar degradation pathway. *BMC plant biology* **12**, 164-180, (2012).
- 2 Bubeck, J. *et al.* The syntaxins SYP31 and SYP81 control ER-Golgi trafficking in the plant secretory pathway. *Traffic* **9**, 1629-1652, (2008).
- 3 daSilva, L. L. *et al.* Receptor salvage from the prevacuolar compartment is essential for efficient vacuolar protein targeting. *Plant Cell* **17**, 132-148, (2005).
- 4 Nebenfuhr, A. *et al.* Stop-and-go movements of plant Golgi stacks are mediated by the acto-myosin system. *Plant Physiol.* **121**, 1127-1142, (1999).
- 5 Niemes, S. *et al.* Retromer recycles vacuolar sorting receptors from the trans-Golgi network. *Plant J.* **61**, 107-121, (2010).
- 6 Reichardt, I. *et al.* Mechanisms of functional specificity among plasma-membrane syntaxins in Arabidopsis. *Traffic* **12**, 1269-1280, (2011).
- 7 Humair, D., Hernandez Felipe, D., Neuhaus, J. M. & Paris, N. Demonstration in yeast of the function of BP-80, a putative plant vacuolar sorting receptor. *Plant Cell* **13**, 781-792, (2001).
- 8 Robinson, D. G. *et al.* Trying to make sense of retromer. *Trends Plant Sci.* **17**, 431-439, (2012).
- 9 Brandizzi, F. *et al.* The destination for single-pass membrane proteins is influenced markedly by the length of the hydrophobic domain. *Plant Cell* **14**, 1077-1092, (2002).
- 10 Scheuring, D. *et al.* Multivesicular bodies mature from the trans-Golgi network/early endosome in Arabidopsis. *Plant Cell* **23**, 3463-3481, (2011).
- 11 Phillipson, B. A. *et al.* Secretory bulk flow of soluble proteins is COPII dependent. *Plant Cell* **13**, 2005-2020, (2001).

## **Nanobody-triggered lockdown of VSRs reveals ligand reloading in the Golgi**

Simone Frühholz, **Florian Fäßler**, Üner Kolukisaoglu and Peter Pimpl

*Nature Communications* 9, Article number: 643 (2018), doi:10.1038/s41467-018-02909-6

<https://www.nature.com/articles/s41467-018-02909-6>

# **Nanobody triggered lockdown of VSRs reveals ligand reloading in the Golgi**

**Simone Frühholz<sup>2</sup>, Florian Fäßler<sup>2</sup>, Üner Kolukisaoglu<sup>2</sup> and Peter Pimpl<sup>1,2</sup>**

<sup>1</sup>SUSTech-PKU Institute of Plant and Food Science (IPFS), Department of Biology, Southern University of Science and Technology (SUSTech), Shenzhen, Guangdong 518055, China.

<sup>2</sup>Center for Plant Molecular Biology (ZMBP), University of Tübingen, Auf der Morgenstelle 32, 72076 Tübingen, Germany.

Correspondence and requests for materials should be addressed to P.P. (email: [pimpl@sustc.edu.cn](mailto:pimpl@sustc.edu.cn))

## **Abstract**

Protein degradation in lytic compartments is crucial for eukaryotic cells. At the heart of this process, vacuolar sorting receptors (VSRs) bind soluble hydrolases in the secretory pathway and release them into the vacuolar route. Sorting efficiency is suggested to result from receptor recycling. However, how and to where plant VSRs recycle remains controversial. Here we present a nanobody-epitope interaction-based protein labeling and tracking approach to dissect their anterograde and retrograde transport routes *in vivo*. We employ simultaneously two different nanobody-epitope pairs: one for the location-specific post-translational fluorescence labeling of receptors and the other pair to trigger their compartment-specific lockdown via an endocytosed dual epitope linker protein. We demonstrate VSR-recycling from the TGN/EE, thereby identifying the *cis*-Golgi as the recycling target and show that recycled VSRs reload ligands. This is evidence that bidirectional VSR-mediated sorting of vacuolar proteins exists and occurs between the Golgi and the TGN/EE.

## Introduction

Degradation in lytic compartments is a hallmark of eukaryotic cells. It allows for rapid modulations of compartmental protein and lipid compositions as responses to cellular communication or environmental cues<sup>1,2,3,4</sup>. This necessitates constant supply of vacuoles/lysosomes with acid hydrolyses by the action of sorting receptors<sup>5</sup>. Despite its significance for viability and development, the core mechanism of vacuolar sorting receptor (VSR)-mediated protein transport and its implementation in the plant endomembrane system is still controversial<sup>5,6</sup>.

The concept of receptor-mediated protein transport dates back to the discovery of the low-density lipoprotein receptor and the cation independent (CI)-mannose 6-phosphate receptor (MPR) for lysosomal sorting in mammals<sup>7,8,9</sup>. They bind ligands either at the cell surface or the TGN and transport them to endosomes, where ligands are released due to low compartmental pH<sup>8,10</sup>. The key to the efficiency of this transport however, is the continuous recycling of receptors after ligand release, allowing receptors to go through hundreds of transport-cycles during their life span<sup>7,8,11,12,13</sup>.

The recycling route of MPRs was most elegantly mapped biochemically, by assaying for Golgi cisternae-specific glycan processing after receptor labeling with [<sup>3</sup>H]galactose at the cell surface by using exogenous galactosyltransferases<sup>14</sup>. However, endogenous VSRs do not localize to the cell surface and are thus not amendable to exogenously applied modifying enzymes to decipher their function or to trace their transport route *in vivo*.

VSRs are type I transmembrane proteins and bind ligands via a luminal ligand-binding domain (LBD), whereas their cytosolic tail carries the sorting information for their own transportation<sup>15,16,17,18,19,20,21,22,23</sup>. They were originally proposed to transport ligands into prevacuoles, nowadays referred to as multivesicular bodies/late endosomes (MVBs/LEs)<sup>16,19,21,24,25,26</sup>. However, we have recently demonstrated that VSRs bind ligands in the early secretory pathway and instead release them in the *trans*-Golgi network (TGN)<sup>27</sup>, the early endosome (EE) of plants (TGN/EE)<sup>28,29</sup>. This raised the fundamental questions as to how to where VSRs recycle after ligand release. To address this, we have devised a strategy that utilizes the *in vivo* interaction of two different antibody-epitope pairs. This allows (a) for the location-specific green fluorescent protein (GFP)-labeling of VSRs in the TGN/EE and (b) for the tracking and lockdown of such labeled VSRs in upstream compartments, upon retrograde recycling. For this, we have translationally fused a variable domain of a lama (*Lama pacu*)

heavy chain antibody ( $V_{HH}$ )<sup>27, 30</sup>, termed nanobody (Nb), that was raised against GFP ( $Nb_G$ )<sup>27, 31</sup> to a VSR ( $Nb_G$ -VSR). The other Nb, which was raised against  $\alpha$ -synuclein ( $Nb_S$ )<sup>32</sup>, was fused to compartment-specific membrane marker proteins. Finally, we have designed a dual epitope linker protein, which contains the epitopes of both nanobodies and therefore allows for both, specific GFP-labeling of the  $Nb_G$ -tagged VSR via the GFP domain and attachment to  $Nb_S$ -tagged compartmental marker proteins via the  $\alpha$ -synuclein (SYN) epitope. Labeling of  $Nb_G$ -VSR in the lumen of the TGN/EE is achieved by incubation of  $Nb_G$  and  $Nb_S$  fusion protein-expressing cells with the dual epitope linker protein GFP-SYN, which is endocytosed and delivered to the TGN/EE. Using this approach, we have traced GFP-labeled VSRs from the TGN/EE back to the *cis*-Golgi, where we demonstrate their ligand binding capability. Together, these data demonstrate the cycling of VSRs between the Golgi stack and the TGN/EE.

## RESULTS

### Post-translational GFP-labeling via endocytosed GFP

The challenge when analyzing bidirectional protein transport of sorting receptors in live-cell imaging studies is to differentiate between anterograde and retrograde transported receptors under steady state conditions. This is particularly true when translational fusions between receptors and fluorescent proteins are used. Here, fluorescent signals become detectable immediately after synthesis and protein folding in the ER and they persist throughout the lifespan of the molecule. Consequently, the localization of the receptor does not provide any information on its transport direction or ligand status (**Fig. 1a**). An analysis of receptor recycling therefore demands strategies that allow for the specific tracing of those VSRs that have released their ligands in the TGN/EE<sup>27</sup> and are about to be recycled. This requirement is fulfilled if a post-translational labeling strategy is used where signals of the labeled VSRs become first detectable in the TGN/EE (**Fig. 1b**). To achieve this, we have devised an approach that accounts for both, the target-specificity of the labeling and the intracellular location where the labeling occurs. For this, we have employed a GFP-binding nanobody ( $Nb_G$ )<sup>27, 31</sup> that is translationally fused to the VSR and we deliver its epitope GFP as the fluorescent labeling agent to the TGN/EE via endocytosis. We produced the labeling GFP as a



secretory protein in another population of tobacco mesophyll protoplasts. The resulting GFP-containing culture medium is then used for labeling of the cell population that expresses the Nb<sub>G</sub>-tagged VSRs. This strict separation between cells that produce the labeling agent GFP and cells that are used for the labeling ensures that no newly synthesized VSR on its anterograde route is labeled prior to reaching the TGN/EE.

To develop a compartment-specific post-translational GFP-labeling strategy, we firstly decided to employ the established marker proteins  $\alpha$ -mannosidase 1 (Man1) for the *cis*-Golgi, sialyltransferase (ST) for the *trans*-Golgi, SYNTAXIN OF PLANTS (SYP) 61 for the TGN/EE, and the luminal ligand binding domain-deprived ( $\Delta$ LBD) binding protein 80 kDa (BP80) from *Pisum sativum* for MVB/LE in coexpression experiments to discriminate between the various punctate signals (**Supplementary Fig. 1**). Next, we generated and tested red fluorescent protein (RFP)-tagged Nb<sub>G</sub> fusion proteins of these markers in tobacco mesophyll protoplasts for post-translational labeling in the TGN/EE (SYP61-RFP-Nb<sub>G</sub>), the MVB/LE (Nb<sub>G</sub>-RFP-BP80 $\Delta$ LBD), the *trans*-Golgi (ST-RFP-Nb<sub>G</sub>), the *cis*-Golgi (Man1-RFP-Nb<sub>G</sub>) and the ER (Nb<sub>G</sub>-RFP-Calnexin (CNX)). After transfection with the respective marker construct, we incubated the cells in GFP-containing culture medium for the endocytic uptake of GFP (endocyt GFP) (**Fig. 1c-g**). Confocal laser-scanning microscopy (CLSM) demonstrated that the endocytosed GFP was trapped by the Nb<sub>G</sub>-tagged markers SYP61-RFP-Nb<sub>G</sub> and Nb<sub>G</sub>-RFP-BP80 $\Delta$ LBD in the TGN/EE and downstream in the MVB/LE, respectively (**Fig. 1c,d**). In sharp contrast, labeling of the markers in compartments upstream of the TGN/EE like the *trans/cis*-Golgi (ST-RFP-Nb<sub>G</sub>, Man1-RFP-Nb<sub>G</sub>) or the ER (Nb<sub>G</sub>-RFP-CNX) with endocytosed GFP was never observed (**Fig. 1e-g**). However, post-translational GFP-labeling based on Nb<sub>G</sub>-epitope interaction is also possible in these compartments, if the labeling agent GFP is coexpressed as a secretory protein (Sec-GFP) with the respective Nb<sub>G</sub>-fusion proteins (**Fig. 1h-j**). This shows that post-translational GFP-labeling via Nb<sub>G</sub>-epitope interaction is applicable to Nb<sub>G</sub>-tagged proteins in all compartments and furthermore demonstrates that endocytosed GFP alone does not reach locations upstream of the TGN/EE like the *cis/trans*-Golgi and the ER. Consequently, this also demonstrates that none of the Nb<sub>G</sub>-tagged markers that reside in the ER or the Golgi apparatus, ever reach or cycle through the TGN/EE in order to reach their respective steady state distribution.

## Post-translationally labeled VSRs localize to the TGN/EE

In the next step, we applied this post-translational GFP-labeling protocol to VSRs (**Fig. 2a,b**). To better judge the labeling efficiency, we tagged a fluorescent VSR<sup>33</sup> with the Nb<sub>G</sub> (Nb<sub>G</sub>-RFP-VSR) and performed post-translational GFP-labeling (**Fig. 2b**). CLSM-based colocalization reveals almost perfectly matching punctate signals of the red Nb<sub>G</sub>-RFP-VSR and the green signals from the endocytosed GFP (**Fig. 2c,d**), demonstrating a high degree of labeling efficiency. However, since Nb<sub>G</sub>-RFP-VSR can acquire the labeling GFP only in the TGN/EE, this high degree of colocalization furthermore suggests that under steady state conditions almost all of the Nb<sub>G</sub>-RFP-VSR molecules had already reached the TGN/EE, at least once.

We have recently demonstrated that VSRs bind their ligands in the ER, in the *cis*- and *trans*-Golgi, but release their ligands in the TGN/EE<sup>27</sup>. Therefore, we hypothesized that the ligand-free receptors that were post-translationally labeled with endocytosed GFP in the TGN/EE would recycle to an upstream compartment for ligand reloading. In such a scenario, we would then expect to detect a population of labeled VSRs in a compartment upstream of the TGN/EE. To precisely define the VSR localizations we next post-translationally labeled non-fluorescent Nb<sub>G</sub>-tagged VSRs (Nb<sub>G</sub>-VSR) with endocytosed GFP and tested for colocalization with established red fluorescent compartmental markers (**Fig. 2e,f**) for the TGN/EE (RFP-SYP61), the MVB/LE and vacuole (Aleu-RFP), *trans*- and *cis*-Golgi (ST-RFP and Man1-RFP, respectively) and for the ER (RFP-CNX) in coexpression experiments (**Fig. 2g-m**). The post-translationally labeled Nb<sub>G</sub>-VSRs colocalized with the TGN/EE marker (**Fig. 2g**).

Surprisingly, the post-translationally labeled Nb<sub>G</sub>-VSRs neither colocalized with the MVB/LE and vacuole marker Aleu-RFP (**Fig. 2h,i**) nor with markers for upstream compartments like the *trans*- and *cis*-Golgi or the ER (**Fig. 2j-m**). This steady state localization of Nb<sub>G</sub>-VSR at the TGN/EE rather than at the MVB/LE, as is commonly assumed, is not restricted to post-translationally labeled Nb<sub>G</sub>-VSRs, it is also seen in control experiments using the fluorescent full-length receptor fusion protein Nb<sub>G</sub>-RFP-VSR (**Supplementary Fig. 2**). The differential localization of these full-length VSRs and LBD-lacking MVB/LE markers of the RFP/GFP-BP80ΔLBD type, therefore suggests that the presence of the LBD is required for both, the ligand binding capability and for the correct transport of the receptor.

## Nanobody triggered lockdown of recycled VSRs

One possible explanation for the TGN/EE-localization of VSRs under steady state conditions is that VSRs do not recycle to reload ligands. Such a one-way transport mode was suggested for members of the receptor homology region-transmembrane domain-RING-H2 (RMR) receptor family, which sort proteins to the protein storage vacuole<sup>34</sup>. However, considering that the TGN/EE is expected to be the recycling point of a bidirectional transport system<sup>27, 35</sup>, the TGN/EE-localization of cycling VSRs may indicate that anterograde transport is faster than the subsequent recycling step. To test for his hypothesis, we have devised a strategy that allows for the specific detection of recycled receptors in compartments upstream of the TGN/EE by blocking their further export and onward forwarding upon completion of recycling. For this, we have combined the nanobody-mediated post-translational labeling of recycling VSRs in the TGN/EE with an approach for compartment-specific lockdown of these labeled VSRs via an antibody-epitope interaction that is triggered by a second nanobody-epitope pair (**Fig. 3a-c**).

Hereto, we translationally fused a nanobody that is directed against the mammalian  $\alpha$ -synuclein (Nbs) to red fluorescent compartment-specific membrane markers (CM-RFP-Nbs) and we fused its corresponding epitope termed SYN, which is a sequence of 23 amino acids, to GFP (GFP-SYN). Endocytic uptake of this dual epitope linker as the labeling agent by cells coexpressing Nb<sub>G</sub>-VSRs and Nbs-tagged compartmental markers was then expected to firstly label Nb<sub>G</sub>-VSRs in the TGN/EE and then to trigger an *in vivo* crosslink between the SYN-epitope of the GFP-SYN-labeled VSR and the Nbs-tagged compartmental marker in the compartmental lumen.

This complex strategy required that we first test whether Nbs interacts with the SYN-epitope in the lumen of secretory pathway compartments. To this end, we developed an assay for analyzing protein-protein interaction *in vivo*. This assay is based on the simultaneous use of a quantifiable soluble secretory reporter with a soluble vacuolar protein, each of which carries either the nanobody or the epitope, respectively. In this approach, the interaction occurring between the Nbs and the epitope triggers the attachment of the vacuolar sorting signal to the secretory reporter and consequently, its transport to the lytic vacuole via the vacuolar sorting machinery (**Fig. 3d,e**).

We therefore tagged the secretory reporter  $\alpha$ -amylase from barley (*Hordeum vulgare*)<sup>36</sup> with the SYN-epitope (amylase-SYN) and employed the vacuolar reporter Aleu-RFP as a Nbs-

fusion protein (Aleu-RFP-Nb<sub>S</sub>). Quantitative transport analysis of the secretory amylase-SYN in tobacco mesophyll protoplasts shows that its secretion is drastically reduced by the coexpressed vacuolar Aleu-RFP-Nb<sub>S</sub> (**Fig. 3f**), suggesting an interaction between the Nb<sub>S</sub> and the SYN-epitope. In the next step, we tested the functionality of Nb<sub>S</sub> in the context of the compartment-specific membrane anchors for the ER, *cis*- and *trans*-Golgi and the TGN/EE. For this, we fused the Nb<sub>S</sub> to RFP-CNX (Nb<sub>S</sub>-RFP-CNX), Man1-RFP (Man1-RFP-Nb<sub>S</sub>), ST-RFP (ST-RFP-Nb<sub>S</sub>) and SYP61-RFP (SYP61-RFP-Nb<sub>S</sub>) and verified firstly their correct location in colocalization experiments with their respective GFP-tagged counterpart (**Supplementary Fig. 3**). Second, we tested their ability to bind the dual epitope linker GFP-SYN (**Fig. 3g-j**). To do this, we immunoprecipitated the above-mentioned marker proteins and their Nb<sub>S</sub>-tagged pendants, the anchors, with RFP antibodies in bead-binding assays and subjected all of them to the GFP-SYN-containing culture medium from GFP-SYN-secreting protoplasts. The immunoblot analysis of the precipitates revealed that all of the Nb<sub>S</sub>-tagged anchors coprecipitated the SYN-epitope-tagged GFP, whilst this molecule was absent in precipitates from markers lacking the Nb<sub>S</sub>. To rule out that on the other side the SYN-epitope from GFP-SYN perturbs the interaction between the GFP-epitope and Nb<sub>G</sub>, we performed comparative coimmunoprecipitation experiments using bead-bound Nb<sub>G</sub>-VSR with either secreted GFP or secreted GFP-SYN, to show that the Nb<sub>G</sub>-VSR binds GFP and GFP-SYN to comparable levels (**Fig. 3k**).

Finally, we performed colocalization experiments of GFP-SYN-labeled Nb<sub>G</sub>-VSRs with the markers for the TGN/EE, *trans*- and *cis*-Golgi and the ER, showing that the labeling of Nb<sub>G</sub>-VSR with GFP-SYN does not alter the localization of the labeled VSR (**Supplementary Fig. 4**, compare to **Fig. 2**).

Together, these results show that this second Nb<sub>S</sub>-SYN nanobody-epitope pair is suitable for triggering a stable linkage between proteins, both *in vitro* and *in vivo*. The results also demonstrate that each epitope of GFP-SYN is accessible for Nb<sub>G</sub> or Nb<sub>S</sub> interaction.

### **The *cis*-Golgi is the target of the VSR-recycling route**

To apply the strategy for nanobody triggered lockdown to the analysis of VSR recycling, we have subjected cells that coexpress Nb<sub>G</sub>-tagged VSRs with the above-mentioned Nb<sub>S</sub>-tagged anchors to post-translational VSR-labeling using the endocytosed dual epitope linker GFP-SYN (**Fig. 4**). First labeling of Nb<sub>G</sub>-VSRs in cells coexpressing the TGN/EE anchor SYP61-

RFP-Nb<sub>S</sub> resulted in almost perfect colocalization of both signals (**Fig. 4a**), as was seen before when the non-tagged TGN/EE marker was used (**Fig. 4b**). This suggested that the endocytosed Nb<sub>G</sub>-VSR-labeling agent GFP-SYN does not generally perturb membrane trafficking events in the presence of the Nb<sub>S</sub>-tagged membrane anchor. In the next step, we subjected cells that coexpressed the anchors for the upstream compartments to this procedure. Here, the localization of the GFP-SYN-labeled Nb<sub>G</sub>-VSRs shifted drastically and now colocalized with the *trans*-Golgi anchor ST-RFP-Nb<sub>S</sub> (**Fig. 4c,d**, compare to **4b**). Likewise, localization of GFP-SYN-labeled Nb<sub>G</sub>-VSRs shifted strongly towards the *cis*-Golgi when the anchor Man1-RFP-Nb<sub>S</sub> was used for the lockdown of the labeled Nb<sub>G</sub>-VSR (**Fig. 4e,f**, compare to **4b**). The colocalization of GFP-SYN-labeled VSRs and the Nb<sub>S</sub>-tagged anchors for the *trans*- and *cis*-Golgi strictly depends on the presence of the second nanobody-epitope pair and was never observed when marker pendants without the Nb<sub>S</sub>-tag were used (**Fig. 4d,f**, compare to **Supplementary Figs 4 and 5**). This suggests, that the VSRs did indeed recycle from the TGN/EE to the Golgi stack. To rule out that the GFP-SYN triggered crosslink between Nb<sub>G</sub>-VSR and ST-RFP-Nb<sub>S</sub> or Man1-RFP-Nb<sub>S</sub> altered the Golgi-localization of the anchors in these experiments, we used the fungal toxin brefeldin A (BFA) as a diagnostic tool to confirm the Golgi localization of both anchors. In tobacco, BFA causes a fusion between Golgi stacks and the ER<sup>37</sup> thereby triggering a shift of signals from Golgi anchors to the ER. After BFA-treatment, the punctate signals from crosslinked GFP-SYN-labeled VSR-*cis*- and *trans*-Golgi cisternal anchors became detectable in the nuclear envelope (**Fig. 4g,h**). This demonstrated that the lockdown did not alter the localization of the Golgi anchors. In sharp contrast, a colocalization between GFP-SYN-labeled Nb<sub>G</sub>-VSRs and the ER anchor Nb<sub>S</sub>-RFP-CNX was never observed (**Fig. 4i**). This, however, indicates that the VSRs do not recycle to upstream compartments further than the *cis*-Golgi.

### **Recycled VSRs reload ligands in the *cis*-Golgi**

We have previously used the soluble model ligand Aleu-RFP together with a soluble Nb<sub>G</sub>-tagged LBD of a VSR that was anchored to a GFP-tagged membrane marker by nanobody-epitope interaction. There, ligand binding to the anchored LBD in a given compartment was visualized through coaccumulation/colocalization of the otherwise passing ligands<sup>27</sup>. We have now extended this visualization concept to the analysis of the ligand-binding capabilities of recycled full-length VSRs in the Golgi (**Fig. 5a-d**).

Hereto, we performed a *cis*-Golgi-specific dual-epitope triggered VSR-lockdown in cells, coexpressing the vacuolar reporter Aleu-RFP, Nb<sub>G</sub>-VSR, Man1-Nb<sub>S</sub>, which is used for the lockdown and Man1-blue fluorescent protein (BFP)<sub>2</sub>, which serves as neutral marker to verify the localization (**Fig. 5e**). The analysis clearly shows the triple-overlap of the fluorescence signals from the vacuolar reporter Aleu-RFP with the recycled GFP-SYN-labeled Nb<sub>G</sub>-tagged VSR and the *cis*-Golgi marker Man1-BFP<sub>2</sub>, demonstrating the interaction between the recycled VSRs and the ligand in the *cis*-Golgi. The same was also seen when the VSR lockdown was performed in the *trans*-Golgi by using ST-Nb<sub>S</sub> (**Supplementary Fig. 6a**). In sharp contrast, no colocalization between VSRs and ligands are seen in controls without the Nb<sub>S</sub>-SYN triggered VSR lockdown: neither in the absence of the Nb<sub>S</sub>-tagged anchor (**Fig. 5f**, **Supplementary Fig. 6b**) nor in the absence of the SYN-epitope, when GFP is used for the labeling instead of GFP-SYN (**Fig. 5g**, **Supplementary Fig. 6c**). This was to be expected, since “free” labeled VSRs localize to the TGN/EE in these controls (compare to **Fig. 2g,i** and **Supplementary Fig. 4a**), a compartment that does not provide ligand-binding conditions<sup>27</sup>.

## Discussion

Being only about 125 amino acids long, nanobodies are the smallest entities, capable of specific antigen recognition and binding<sup>38</sup>. Nanobodies are therefore ideally suited for the generation of genetically encoded molecular tools for the identification, localization and manipulation of protein function in living cells for basic research and applied sciences<sup>39, 40</sup>. We have previously generated VSR-sensors for a compartment-specific analysis of VSR-ligand interactions<sup>27</sup>. They self-assemble from soluble VSR\_LBD-Nb<sub>G</sub> fusion proteins and GFP-tagged compartment-specific membrane anchors. Using this approach, we have demonstrated that VSRs bind ligands in the ER, the *cis*- and the *trans*-Golgi and ultimately release ligands in the TGN/EE<sup>27</sup>, thereby opening the question about the fate of VSRs after this step. The analysis of bidirectional receptor transport and receptor recycling in particular, however, is technically most challenging in living cells. It requires molecular tools that permit the strict differentiation between VSRs from the anterograde and the retrograde trafficking route.

To overcome these constraints, we have taken advantage of the TGN as also being the EE by incubating Nb<sub>G</sub>-VSR-expressing cells with exogenously applied protoplast-secreted GFP to

trigger compartment-specific labeling of VSRs in the TGN/EE by its endocytic uptake. This ensures labeling of only those VSRs that have reached the recycling point, whereas newly synthesized VSRs from the anterograde route remain invisible. Most interesting for future application however is, the simultaneous use of two different Nb-epitope pairs *in vivo*. This allows for triggering a protein-specific lockdown of recycled Nb<sub>G</sub>-VSRs at Nbs-tagged membrane proteins by the exogenously applied dual epitope linker peptide GFP-SYN. Using this strategy, we demonstrated retrograde VSR recycling to the *cis*-Golgi as being the most distant compartment upstream of the TGN/EE. Together with the fact that VSRs reload ligands after recycling, this supports the concept of bidirectional VSR transport.

Based on our investigations we now present the following concept for the operation of VSR-mediated vacuolar sorting in the plant endomembrane system (**Fig. 6**). Newly synthesized VSRs bind ligands in the early secretory pathway<sup>23, 27, 41, 42</sup> at neutral pH<sup>21, 26, 43</sup> and transport them to the TGN/EE, where they ultimately release their ligands<sup>27</sup>, due to a shift in compartmental pH. The TGN/EE is the most acidic compartment en route to the vacuole<sup>26, 43, 44</sup>, since it harbors characteristic V-ATPases<sup>28</sup> that are absent from the MVBs/LEs<sup>45</sup>, thus preventing further acidification. Therefore, the locations for binding and release of ligands are in agreement with the initially recorded pH dependency for VSR-ligand interactions *in vitro*<sup>21</sup>. After release in the TGN/EE, ligands progress without further involvement of VSRs onwards to the lytic vacuole by default<sup>27</sup>. This occurs due to a maturation event of the TGN/EE that results in the biogenesis of a MVB/LE<sup>46, 47</sup>. While fusion of the MVB/LE with the vacuole represents the final step in the vacuolar delivery of ligands<sup>46</sup> it is unrelated to VSR function. VSRs, however, recycle from the TGN/EE back to the *cis*-Golgi, for ligand reloading and renewed rounds of ligand delivery to the TGN/EE. Considering the life span of VSRs greatly exceeding the time it takes for a round of transport, it is plausible to assume that cycling VSRs bear the brunt of the ligand transport from the Golgi to the TGN/EE with only a minor contribution of *de novo* synthesized VSRs, binding their ligands in the ER.

## Methods

### Plant materials

*Nicotiana tabacum* L. SR1 was grown on Murashige and Skoog medium supplemented with 2 % (w/v) sucrose, 0.5 g L<sup>-1</sup> MES and 0.8 % (w/v) Agar at pH 5.7 in 16/8 h light–dark cycles at 22 °C.

### Plasmid constructs

All constructs are given in Supplementary Table 1. DNA manipulations were performed according to established procedures, using pGreenII<sup>48</sup>-based vectors and *Escherichia coli* MC1061. An anti-SYN nanobody sequence was generated by reverse-translation of the amino acid sequence NbSyn87 without the C-terminal 6xHis tag<sup>32</sup>, optimized for *Arabidopsis*-specific codon usage (EMBOSS Backtranseq), modified with an N-terminal HA-tag and chemically synthesized (GeneArt Gene Synthesis). The blue fluorescent protein mTagBFP2 (GenBank AIQ82697.1) was also generated by reverse translation of the amino acid sequence, optimized for *Arabidopsis*-specific codon usage (EMBOSS Backtranseq) and chemically synthesized (GeneArt Gene Synthesis).

All VSR constructs were assembled from AtVSR4 (GenBank accession no. NM\_127036) and fused to the GFP nanobody<sup>27</sup>. The red fluorescent compartment specific anchors carry a monomeric RFP<sup>48</sup>. The correct localization of all generated VSR-/marker-fluorophore fusions was verified.

### Protoplast isolation and gene expression

Protoplasts were isolated from perforated leaflets by over-night incubation in incubation buffer (3,05 g L<sup>-1</sup> Gamborg B5 Medium, 500 mg L<sup>-1</sup> MES, 750 mg L<sup>-1</sup> CaCl<sub>2</sub>·2H<sub>2</sub>O, 250 mg L<sup>-1</sup> NH<sub>4</sub>NO<sub>3</sub> adjusted to pH 5.7 with KOH) supplemented with 0.2 % w/v macerozyme and 0.4 % w/v cellulase) at 25 °C in the dark. They were rebuffed by washing them three times in 50 mL electrotransfection-buffer (137 g L<sup>-1</sup> sucrose, 2.4 g L<sup>-1</sup> HEPES, 6 g L<sup>-1</sup> KCl, 600 mg L<sup>-1</sup> CaCl<sub>2</sub>·2H<sub>2</sub>O adjusted to pH 7.2 with KOH). 150 µL protoplasts in a total volume of 600 µL electrotransfection-buffer were electrotransfected with 1–10 µg plasmid DNA using the square-wave pulse generator EPI-2,500 (Fischer) applying a pulse at 130 V for 10 ms. After transfection, each sample was supplemented with 2 ml incubation buffer and incubated for 18–24 h at 25 °C in the dark.



### **Biosynthesis of fluorescent reporters**

Protoplast-secreted reporters (GFP/GFP-SYN) for endocytic uptake experiments were obtained from cell-free culture medium after expression, harvesting, sonication and clearance, ruling out contaminations with reporter-synthesizing cells during uptake experiments. For the endocytic uptake, populations of protoplasts expressing Nb<sub>G</sub>/Nb<sub>S</sub>-tagged constructs were supplemented with cleared reporter-containing medium for 20 h.

### **Confocal microscopy and statistical analysis**

Image acquisition was performed using a Leica TCS-SP8 confocal laser-scanning microscope, equipped with a ×63 (1.2 numerical aperture) water immersion objective. Fluorophores were excited (ex) and emission (em) was detected in sequential line scanning mode using HyD detectors: mTagBFP2 (ex/em, 405 nm/407–452 nm), GFP (ex/em, 488 nm/496–525 nm) and RFP (ex/em, 561 nm/569–636 nm). Pinholes were adjusted to 1 Airy unit for each wavelength. Post-acquisition image processing and assembly of figures was performed using Adobe Photoshop CS3 and CorelDraw X8.

The linear Pearson's correlation coefficient ( $r_p$ ) and the nonlinear Spearman's rank coefficient ( $r_s$ ) of green and red fluorescent signals was calculated with the PSC colocalization plug-in (<http://www.cpiib.ac.uk/~afrench/coloc.html>) for ImageJ<sup>48</sup>. The threshold levels were set to 10. For the statistics, 10 individual cells were analyzed and the correlation coefficients are shown as mean values with standard errors of the mean. Statistical significance was calculated with R using an unpaired, two tailed *t-test*<sup>49</sup>.

### **Analysis of the SYN-nanobody epitope interaction**

Cell-free culture medium was harvested after flotation of electrotransfected tobacco protoplasts for 5 min at 80 g in sealed pre-punctured tubes, using insulin syringes. Afterwards, cells were harvested by addition of 7.5 mL of 250 mM NaCl, sedimentation for 7 min at 80 g, followed by removal of the supernatant. The culture medium was cleared by centrifugation at 20,000 g for 15 min at 4 °C and diluted with  $\alpha$ -amylase extraction buffer (50 mM acid malic, 50 mM sodium chloride, 2 mM calcium chloride, 0.02% (w/v) sodium azide). Cell samples were extracted in a total volume of 250  $\mu$ g with  $\alpha$ -amylase extraction buffer, sonicated and

centrifuged at 20,000 g for 15 min at 4 °C. The supernatant was recovered and employed for the reporter assay and SDS-PAGE/Western blot (SDS-PAGE/WB).

The quantitative reporter transport analysis was performed in samples from the cell extracts and the culture medium, using the  $\alpha$ -amylase reagent kit (Megazyme R-CAAR4). Individual enzymatic assays were started by addition of 30  $\mu$ l of substrate solution to 30  $\mu$ l of extracted and diluted sample. After incubation at 40 °C, the reaction was stopped by the addition of 150  $\mu$ L of 1% w/v Trizma base. 200  $\mu$ L of the reaction was transferred into a well of a microtitre plate to measure absorbance at 405 nm<sup>50</sup>.

For SDS-PAGE/WB, samples were mixed 1:1 with freshly prepared 2 $\times$  Xtreme loading dye (900  $\mu$ L of sample buffer (0.1 % (w/v) bromophenol blue, 5 mM EDTA, 200 mM Tris-HCl, pH 8.8, 1 M sucrose) supplemented with 300  $\mu$ L 10 % w/v SDS and 20  $\mu$ L of 1 M DTT), incubated for 5 min at 95 °C and loaded onto 10 % (w/v) SDS-polyacrylamide gels. After electrophoretic separation at 40 mA, proteins were electroblotted onto nitrocellulose membranes at 200 mA. For immunodetection, membranes were incubated in blocking solution (TBS-T (6.06 g L<sup>-1</sup> Trizma base, 8.88 g L<sup>-1</sup> NaCl, 0.05 % (v/v) Tween-20), supplemented with 5 % (w/v) BSA) for 30 min and then probed with the following antibodies diluted in blocking solution: rabbit polyclonal anti-GFP (Life Technologies A6455, 1:10,000), rat monoclonal anti-RFP (ChromoTek 5F8, 1:1,000) and rat monoclonal anti-HA–Peroxidase (Roche 12013819001, 1:2,500). Uncropped immunoblots are given in Supplementary Fig.7.

### **Immunoprecipitation**

For anchor-epitope and VSR-epitope interaction anchors/VSRs were expressed *in vivo* and extracted 1:1 in 2 $\times$  binding buffer (40 mM HEPES, 300 mM NaCl, 2 mM CaCl<sub>2</sub>, 2 mM MgCl<sub>2</sub>, pH 7.1) with 2% (v/v) CHAPS<sup>27</sup>. Immunoprecipitation was performed for 1 h with RFP-Trap®\_MA (ChromoTek, rxns-20) for the anchors and with Pierce™ Anti-HA Magnetic Beads (Life Technologies, 88836) for the VSRs at 4°C. Beads were washed three times with binding buffer containing 0.4% (v/v) CHAPS and afterwards incubated with GFP-SYN/GFP, which were in parallel samples transiently expressed and recovered from the medium, overnight at 4 °C. SDS-PAGE/WB was performed as described above.

### **Data availability**

Data will be available to readers on request

## References

1. Paez Valencia J, Goodman K, Otegui MS. Endocytosis and Endosomal Trafficking in Plants. *Annual review of plant biology* **67**, 309-335 (2016).
2. Carmona-Gutierrez D, Hughes AL, Madeo F, Ruckenstuhl C. The crucial impact of lysosomes in aging and longevity. *Ageing Res Rev* **32**, 2-12 (2016).
3. Jackson MP, Hewitt EW. Cellular proteostasis: degradation of misfolded proteins by lysosomes. *Essays Biochem* **60**, 173-180 (2016).
4. Schroder B, Saftig P. Intramembrane proteolysis within lysosomes. *Ageing Res Rev* **32**, 51-64 (2016).
5. Robinson DG, Neuhaus JM. Receptor-mediated sorting of soluble vacuolar proteins: myths, facts, and a new model. *J Exp Bot* **67**, 4435-4449 (2016).
6. Robinson DG, Pimpl P. Receptor-mediated transport of vacuolar proteins: a critical analysis and a new model. *Protoplasma* **251**, 247-264 (2014).
7. Goldstein JL, Brown MS. Binding and degradation of low density lipoproteins by cultured human fibroblasts. Comparison of cells from a normal subject and from a patient with homozygous familial hypercholesterolemia. *J Biol Chem* **249**, 5153-5162 (1974).
8. Gonzalez-Noriega A, Grubb JH, Talkad V, Sly WS. Chloroquine inhibits lysosomal enzyme pinocytosis and enhances lysosomal enzyme secretion by impairing receptor recycling. *J Cell Biol* **85**, 839-852 (1980).
9. Hoflack B, Kornfeld S. Purification and characterization of a cation-dependent mannose 6-phosphate receptor from murine P388D1 macrophages and bovine liver. *J Biol Chem* **260**, 12008-12014 (1985).
10. Mellman I, Fuchs R, Helenius A. Acidification of the endocytic and exocytic pathways. *Annu Rev Biochem* **55**, 663-700 (1986).
11. Rome LH, Weissmann B, Neufeld EF. Direct demonstration of binding of a lysosomal enzyme, alpha-L-iduronidase, to receptors on cultured fibroblasts. *Proc Natl Acad Sci USA* **76**, 2331-2334 (1979).
12. Sahagian GG, Neufeld EF. Biosynthesis and turnover of the mannose 6-phosphate receptor in cultured Chinese hamster ovary cells. *J Biol Chem* **258**, 7121-7128 (1983).
13. Brown MS, Anderson RG, Basu SK, Goldstein JL. Recycling of cell-surface receptors: observations from the LDL receptor system. *Cold Spring Harb Symp Quant Biol* **46 Pt 2**, 713-721 (1982).

14. Duncan JR, Kornfeld S. Intracellular movement of two mannose 6-phosphate receptors: return to the Golgi apparatus. *J Cell Biol* **106**, 617-628 (1988).
15. Ahmed SU, Bar-Peled M, Raikhel NV. Cloning and subcellular location of an Arabidopsis receptor-like protein that shares common features with protein-sorting receptors of eukaryotic cells. *Plant Physiol* **114**, 325-336 (1997).
16. Paris N, *et al.* Molecular cloning and further characterization of a probable plant vacuolar sorting receptor. *Plant Physiol* **115**, 29-39 (1997).
17. Cao X, Rogers SW, Butler J, Beevers L, Rogers JC. Structural requirements for ligand binding by a probable plant vacuolar sorting receptor. *Plant Cell* **12**, 493-506 (2000).
18. Luo F, Fong YH, Zeng Y, Shen J, Jiang L, Wong KB. How vacuolar sorting receptor proteins interact with their cargo proteins: crystal structures of apo and cargo-bound forms of the protease-associated domain from an Arabidopsis vacuolar sorting receptor. *Plant Cell* **26**, 3693-3708 (2014).
19. daSilva LL, Foresti O, Denecke J. Targeting of the plant vacuolar sorting receptor BP80 is dependent on multiple sorting signals in the cytosolic tail. *Plant Cell* **18**, 1477-1497 (2006).
20. Happel N, Honing S, Neuhaus JM, Paris N, Robinson DG, Holstein SE. Arabidopsis micro A-adaptin interacts with the tyrosine motif of the vacuolar sorting receptor VSR-PS1. *Plant J* **37**, 678-693 (2004).
21. Kirsch T, Paris N, Butler JM, Beevers L, Rogers JC. Purification and initial characterization of a potential plant vacuolar targeting receptor. *Proc Natl Acad Sci USA* **91**, 3403-3407 (1994).
22. Shen J, Ding Y, Gao C, Rojo E, Jiang L. N-linked glycosylation of AtVSR1 is important for vacuolar protein sorting in Arabidopsis. *Plant J* **80**, 977-992 (2014).
23. Watanabe E, *et al.* An ER-Localized Form of PV72, a Seed-Specific Vacuolar Sorting Receptor, Interferes the Transport of an NPIR-Containing Proteinase in Arabidopsis Leaves. *Plant Cell Physiol* **45**, 9-17 (2004).
24. Li YB, *et al.* BP-80 and Homologs are Concentrated on Post-Golgi, Probable Lytic Prevacuolar Compartments. *Plant Cell Physiol* **43**, 726-742 (2002).
25. Tse YC, *et al.* Identification of multivesicular bodies as prevacuolar compartments in *Nicotiana tabacum* BY-2 cells. *Plant Cell* **16**, 672-693 (2004).
26. Martiniere A, *et al.* In Vivo Intracellular pH Measurements in Tobacco and Arabidopsis Reveal an Unexpected pH Gradient in the Endomembrane System. *Plant Cell* **25**, 4028-4043 (2013).

27. Künzl F, Frühholz S, Fäßler F, Li B, Pimpl P. Receptor-mediated sorting of soluble vacuolar proteins ends at the trans-Golgi network/early endosome. *Nature Plants* **2**, 16017 (2016).
28. Dettmer J, Hong-Hermesdorf A, Stierhof YD, Schumacher K. Vacuolar H<sup>+</sup>-ATPase activity is required for endocytic and secretory trafficking in Arabidopsis. *Plant Cell* **18**, 715-730 (2006).
29. Lam SK, *et al.* Rice SCAMP1 defines clathrin-coated, trans-golgi-located tubular-vesicular structures as an early endosome in tobacco BY-2 cells. *Plant Cell* **19**, 296-319 (2007).
30. Rothbauer U, *et al.* Targeting and tracing antigens in live cells with fluorescent nanobodies. *Nature methods* **3**, 887-889 (2006).
31. Kubala MH, Kovtun O, Alexandrov K, Collins BM. Structural and thermodynamic analysis of the GFP:GFP-nanobody complex. *Protein Sci* **19**, 2389-2401 (2010).
32. Guilliams T, *et al.* Nanobodies raised against monomeric alpha-synuclein distinguish between fibrils at different maturation stages. *J Mol Biol* **425**, 2397-2411 (2013).
33. Saint-Jean B, Seveno-Carpentier E, Alcon C, Neuhaus JM, Paris N. The cytosolic tail dipeptide Ile-Met of the pea receptor BP80 is required for recycling from the prevacuole and for endocytosis. *Plant Cell* **22**, 2825-2837 (2010).
34. Shen Y, *et al.* The Rice RMR1 Associates with a Distinct Prevacuolar Compartment for the Protein Storage Vacuole Pathway. *Mol Plant* **4**, 854-868 (2011).
35. Niemes S, *et al.* Retromer recycles vacuolar sorting receptors from the trans-Golgi network. *Plant J* **61**, 107-121 (2010).
36. Rogers JC. Two barley alpha-amylase gene families are regulated differently in aleurone cells. *J Biol Chem* **260**, 3731-3738 (1985).
37. Ritzenthaler C, *et al.* Reevaluation of the effects of brefeldin A on plant cells using tobacco Bright Yellow 2 cells expressing Golgi-targeted green fluorescent protein and COPI antisera. *Plant Cell* **14**, 237-261 (2002).
38. Hamers-Casterman C, *et al.* Naturally occurring antibodies devoid of light chains. *Nature* **363**, 446-448 (1993).
39. Steeland S, Vandenbroucke RE, Libert C. Nanobodies as therapeutics: big opportunities for small antibodies. *Drug Discov Today* **21**, 1076-1113 (2016).

40. Dmitriev OY, Lutsenko S, Muyldermans S. Nanobodies as Probes for Protein Dynamics in Vitro and in Cells. *J Biol Chem* **291**, 3767-3775 (2016).
41. Niemes S, *et al.* Sorting of plant vacuolar proteins is initiated in the ER. *Plant J* **62**, 601-614 (2010).
42. Gershlick DC, *et al.* Golgi-Dependent Transport of Vacuolar Sorting Receptors Is Regulated by COPII, AP1, and AP4 Protein Complexes in Tobacco. *Plant Cell* **26**, 1308-1329 (2014).
43. Shen J, *et al.* Organelle pH in the *Arabidopsis* Endomembrane System. *Mol Plant* **6**, 1419-1437 (2013).
44. Luo Y, *et al.* V-ATPase activity in the TGN/EE is required for exocytosis and recycling in *Arabidopsis*. *Nature Plants* **1**, 15094 (2015).
45. Viotti C, *et al.* The Endoplasmic Reticulum Is the Main Membrane Source for Biogenesis of the Lytic Vacuole in *Arabidopsis*. *Plant Cell* **25**, 3434-3449 (2013).
46. Scheuring D, *et al.* Multivesicular bodies mature from the trans-Golgi network/early endosome in *Arabidopsis*. *Plant Cell* **23**, 3463-3481 (2011).
47. Singh MK, *et al.* Protein delivery to vacuole requires SAND protein-dependent Rab GTPase conversion for MVB-vacuole fusion. *Curr Biol* **24**, 1383-1389 (2014).
48. Scheuring D, *et al.* Ubiquitin initiates sorting of Golgi and plasma membrane proteins into the vacuolar degradation pathway. *BMC plant biology* **12**, 164 (2012).
49. Team RDC. R: A Language and Environment for Statistical Computing. [http://wwwR-project.org](http://www.R-project.org), (2008).
50. Foresti O, daSilva LL, Denecke J. Overexpression of the *Arabidopsis* syntaxin PEP12/SYP21 inhibits transport from the prevacuolar compartment to the lytic vacuole in vivo. *Plant Cell* **18**, 2275-2293 (2006).

## Acknowledgments

We thank Diana Vranjkovic for technical help. The financial support of the Deutsche Forschungsgemeinschaft (PI 769/1-2 and the Collaborative Research Centre SFB 1101 “Molecular Encoding of Specificity in Plant Processes” and TP A03) and the Deutscher

Akademischer Austauschdienst (Project 57057314 & 57219822) and the Southern University of Science and Technology (SUSTech)/SUSTech-PKU Institute of Plant and Food Science (IPFS) Start-up fund is gratefully acknowledged. P.P. is indebted to L. Kilmister for inspirations and support ♠.

### Author contributions

S.F., F.F., Ü.K. and P.P. designed and analysed the experiments. S.F. performed experiments. S.F. and P.P. wrote the manuscript, P.P. conceived the study.

### Competing interests

The authors declare no competing financial interests.

### Figure Legends

#### Figure 1. Post-translational GFP-labeling via nanobody-epitope interaction. (a)

Translational GFP-labeling of VSRs. (b) Post-translational GFP-labeling of a Nb<sub>G</sub>-tagged VSR in the TGN/EE by endocytosed GFP. (c-g) Post-translational GFP-labeling of compartment-specific Nb<sub>G</sub>-tagged red fluorescent membrane anchors (red) by endocytosed GFP (green) in (c) the TGN/EE and (d) the MVB/LE. Endocytosed GFP does not reach (e) the *trans*-Golgi, (f) the *cis*-Golgi nor (g) the ER. (h-j) Post-translational GFP-labeling by coexpression of secreted (Sec)-GFP (green) and Nb<sub>G</sub>-tagged red fluorescent membrane anchors (red) for (h) the *trans*-Golgi, (i) the *cis*-Golgi and (j) the ER. Insets in (g,j) show cortical sections, others show magnifications. Scale bars 10µm, insets 5µm.

#### Figure 2. Localization of post-translationally labeled Nb<sub>G</sub>-tagged VSRs. (a) Cycling Nb<sub>G</sub>-

tagged red fluorescent VSRs are (b) post-translationally labeled by endocytosed GFP. (c) GFP-labeled red fluorescent Nb<sub>G</sub>-tagged VSRs. (d) Pearson's ( $r_P$ ) and Spearman's ( $r_S$ ) correlation (PSC) coefficients of Nb<sub>G</sub>-RFP-VSRs and labeling GFP. Data are presented as average  $\pm$  s.e.m. of 10 individual cells. The graph shows a representative sample of two independent experiments.

(e,f) Colocalization of post-translationally GFP-labeled non-fluorescent cycling Nb<sub>G</sub>-tagged VSRs (Nb<sub>G</sub>-VSR) with red fluorescent compartmental markers (CM) for (g,i) the TGN/EE, (h,i) MVBs/LEs and vacuole, (j,l) the *trans*-/ and (k,l) *cis*-Golgi and (m) the ER. (i,l) PSC coefficients of the labeled Nb<sub>G</sub>-VSR and coexpressed markers RFP-SYP61, Aleu-RFP, Man1-RFP and ST-RFP are calculated and presented as in (d). Graphs show a representative sample of two independent experiments. Labeled Nb<sub>G</sub>-VSRs colocalize with the TGN/EE marker but not with markers for MVB/LE and vacuole and the *cis*-/*trans*-Golgi. (i) Significance was calculated using unpaired, two tailed *t-test* (n=10, P<0.001, \*\*\*, highly significant). Scale bars 10µm, insets 5µm. Insets show magnifications.

**Figure 3. Nanobody triggered lockdown of recycled VSRs.** (a) Coexpression of Nb<sub>G</sub>-VSRs with red fluorescent Nb<sub>S</sub>-tagged compartmental markers (anchors) and (b) post-translational labeling with the dual-epitope GFP-SYN in the TGN/EE to (c) anchor VSRs upon recycling. (d,e) Nb<sub>S</sub>-SYN epitope interaction occurs in the endomembrane system. (d) SYN epitope-tagged secreted amylase (amy-SYN) is (e) rerouted to the lytic vacuole (LV) upon Aleu-RFP-Nbs triggers attachment of the vacuolar sorting signal (Aleu). (f) Coexpression of amy-SYN with different amounts of Aleu-RFP-Nbs. Upper panel: secretion index (SI); lower panel: corresponding immunoblot (α-RFP). (g-j) Co-immunoprecipitations revealing Nb<sub>S</sub>-SYN epitope interaction. RFP-tagged markers and anchors for (g) ER, (h) *cis*-Golgi, (i) *trans*-Golgi and (j) TGN/EE were immunoprecipitated (IP, α-RFP), incubated with GFP-SYN and immunoblotted (IB). Total extracts (T) and immunoprecipitates (IP) were probed to detect markers, anchors (α-RFP) and co-precipitated GFP-SYN (α-GFP). (k) Co-immunoprecipitation revealing Nb<sub>G</sub>-GFP epitope interaction. Expressed Nb<sub>G</sub>-VSRs or samples from mock-transfected cells were immunoprecipitated (IP, α-HA), incubated with GFP or GFP-SYN and immunoblotted (IB). Total extracts (T) and immunoprecipitates (IP) were probed to detect VSRs (α-HA) and co-precipitated GFP (white arrowhead) or GFP-SYN (black arrowhead) (α-GFP), respectively.

**Figure 4 The *cis*-Golgi stack is the target of VSR recycling.** GFP-SYN labeled Nb<sub>G</sub>-VSR is locked to the anchors in (a) the TGN/EE (SYP61-RFP-Nbs), and after recycling to (c) *trans*-Golgi (ST-RFP-Nbs) and (e) *cis*-Golgi (Man1-RFP-Nbs) anchors but does not reach (i) the ER anchor Nb<sub>S</sub>-GFP-CNX. PSC coefficients of the labeled Nb<sub>G</sub>-VSR with (b) the marker Syp61-



RFP or the anchor Syp61-RFP-Nbs, presented/calculated as in (2g) with  $n=10$ ,  $P \geq 0.05$ , n.s., not significant, (d) the marker ST-RFP or the anchor ST-RFP-Nbs, presented/calculated as above with  $n=10$ ,  $P < 0.001$ , \*\*\*, highly significant and (f) the marker Man1-RFP or the anchor Man1-RFP-Nbs, presented/calculated as in (d). Graphs show a representative sample of two independent experiments. (g,h) BFA-treatment of samples from (c,e) for 1 h at 20  $\mu\text{M}$  triggers fusion of Golgi with ER, verifying Golgi-localization of locked VSRs from (c,e). Scale bars 10 $\mu\text{m}$ , insets 5 $\mu\text{m}$ , showing magnifications.

**Figure 5. VSRs bind ligands after recycling.** (a) Targeted VSR sensors (Nb<sub>G</sub>-LDB) were shown to bind Aleu-RFP ligands in the Golgi<sup>27</sup> (b) GFP-SYN labeled Nb<sub>G</sub>-VSRs are locked to the anchor Man1-Nbs in the *cis*-Golgi, positively identified by the marker Man1-BFP2. Ligand-binding of recycled full-length VSRs is assessed by colocalization with ligands (Aleo-RFP). Controls with cycling VSRs that lack (c) the anchor or (d) the SYN epitope at the labeling GFP for the VSR lockdown, result in VSR localization at the TGN/EE, which does not promote ligand binding. (e) GFP-SYN labeled Nb<sub>G</sub>-VSRs are locked after recycling in the *cis*-Golgi and colocalize with the Golgi marker Man1-BFP2 and bind the ligand Aleu-RFP, as shown by the overlapping signal peaks in the line intensity plot (see b). (f,g) Not locked VSRs (see c and d) do not localize to the Golgi and thus do not bind the ligand Aleu-RFP as judged by the separated peaks in the line intensity plots. Scale bars 10 $\mu\text{m}$ , insets 5 $\mu\text{m}$ , showing magnifications.

**Figure 6. Model for receptor mediated vacuolar sorting in plants.** VSRs bind ligands in the early secretory pathway and transport them to the TGN/EE. There, the ligands are released from the VSR. Next, VSRs are recycled back to the *cis*-Golgi stack for further rounds of ligand transport. Post-TGN/EE transport of released vacuolar cargo ligands but also endocytosed proteins occurs independent of VSRs and travel to the lytic vacuole per default. Transport in this route is mediated by multivesicular bodies, the late endosomes (MVBs/LEs). They bud off the TGN/EE in a maturation-based step and confer cargo delivery by their ultimate fusion with the lytic vacuole (LV).

**Figure 1**

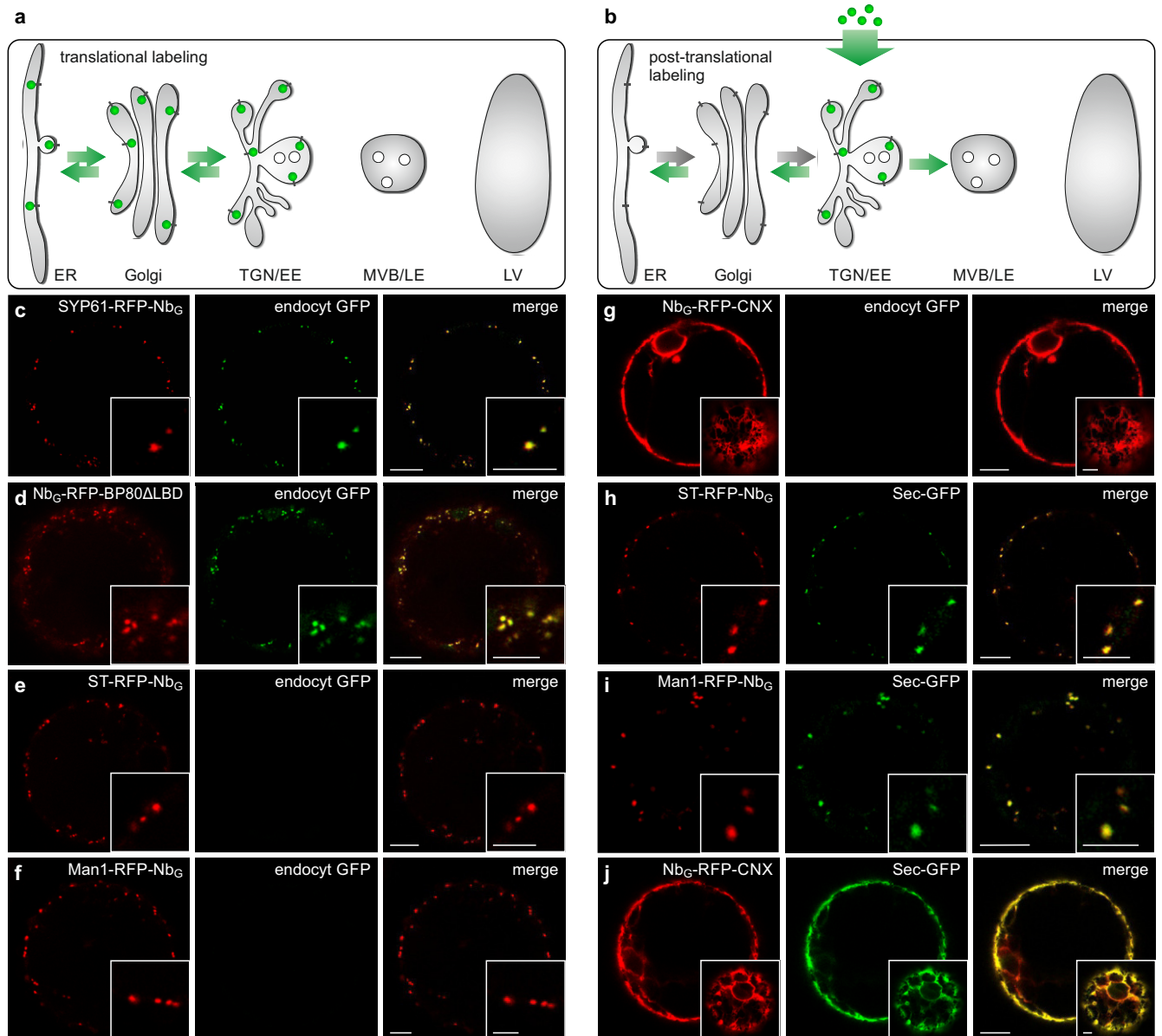


**Figure 1. Post-translational GFP-labeling via nanobody-epitope interaction.** (a) Translational GFP-labeling of VSRs. (b) Post-translational GFP-labeling of a Nb<sub>G</sub>-tagged VSR in the TGN/EE by endocytosed GFP. (c-g) Post-translational GFP-labeling of compartment-specific Nb<sub>G</sub>-tagged red fluorescent membrane anchors (red) by endocytosed GFP (green) in (c) the TGN/EE and (d) the MVB/LE. Endocytosed GFP does not reach (e) the *trans*-Golgi, (f) the *cis*-Golgi nor (g) the ER. (h-j) Post-translational GFP-labeling by coexpression of secreted (Sec)-GFP (green) and Nb<sub>G</sub>-tagged red fluorescent membrane anchors (red) for (h) the *trans*-Golgi, (i) the *cis*-Golgi and (j) the ER. Insets in (g,j) show cortical sections, others show magnifications. Scale bars 10µm, insets 5µm.

**Figure 2**

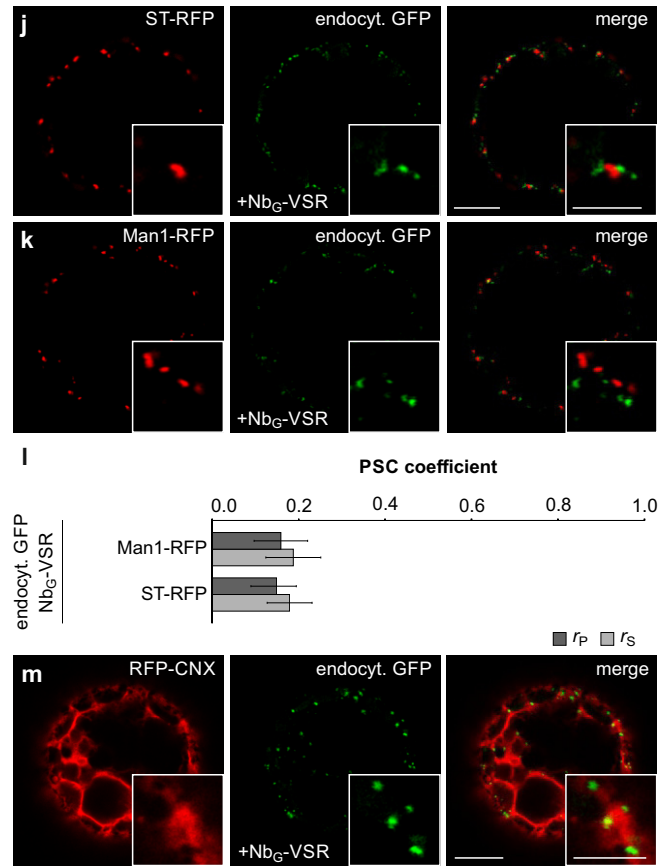
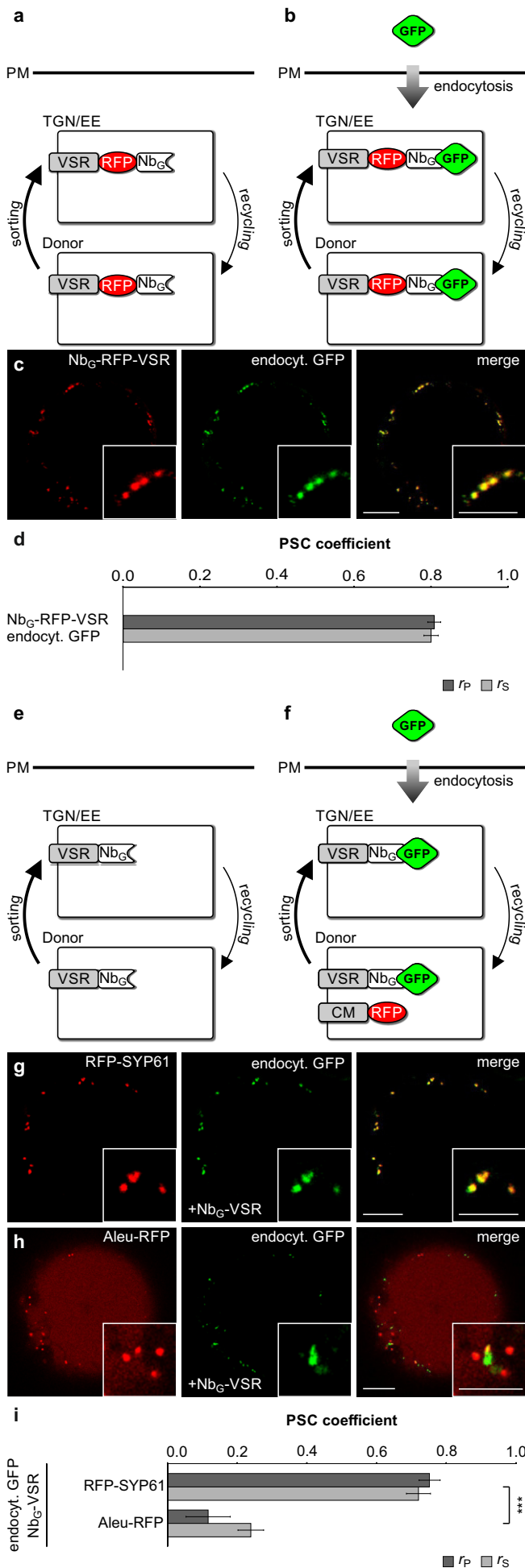


**Figure 2. Localization of post-translationally labeled Nb<sub>G</sub>-tagged VSRs.** (a) Cycling Nb<sub>G</sub>-tagged red fluorescent VSRs are (b) post-translationally labeled by endocytosed GFP. (c) GFP-labeled red fluorescent Nb<sub>G</sub>-tagged VSRs. (d) Pearson's ( $r_P$ ) and Spearman's ( $r_S$ ) correlation (PSC) coefficients of Nb<sub>G</sub>-RFP-VSRs and labeling GFP. Data are presented as average  $\pm$  s.e.m. of 10 individual cells. The graph shows a representative sample of two independent experiments. (e,f) Colocalization of post-translationally GFP-labeled non-fluorescent cycling Nb<sub>G</sub>-tagged VSRs (Nb<sub>G</sub>-VSR) with red fluorescent compartmental markers (CM) for (g,i) the TGN/EE, (h,i) MVBs/LEs and vacuole, (j,l) the *trans*-/ and (k,l) *cis*-Golgi and (m) the ER. (i,l) PSC coefficients of the labeled Nb<sub>G</sub>-VSR and coexpressed markers RFP-SYP61, Aleu-RFP, Man1-RFP and ST-RFP are calculated and presented as in (d). Graphs show a representative sample of two independent experiments. Labeled Nb<sub>G</sub>-VSRs colocalize with the TGN/EE marker but not with markers for MVB/LE and vacuole and the *cis*-/*trans*-Golgi. (i) Significance was calculated using unpaired, two tailed *t*-test ( $n=10$ ,  $P<0.001$ , \*\*\*, extremely significant). Scale bars 10 $\mu$ m, insets 5 $\mu$ m. Insets show magnifications.

**Figure 3**

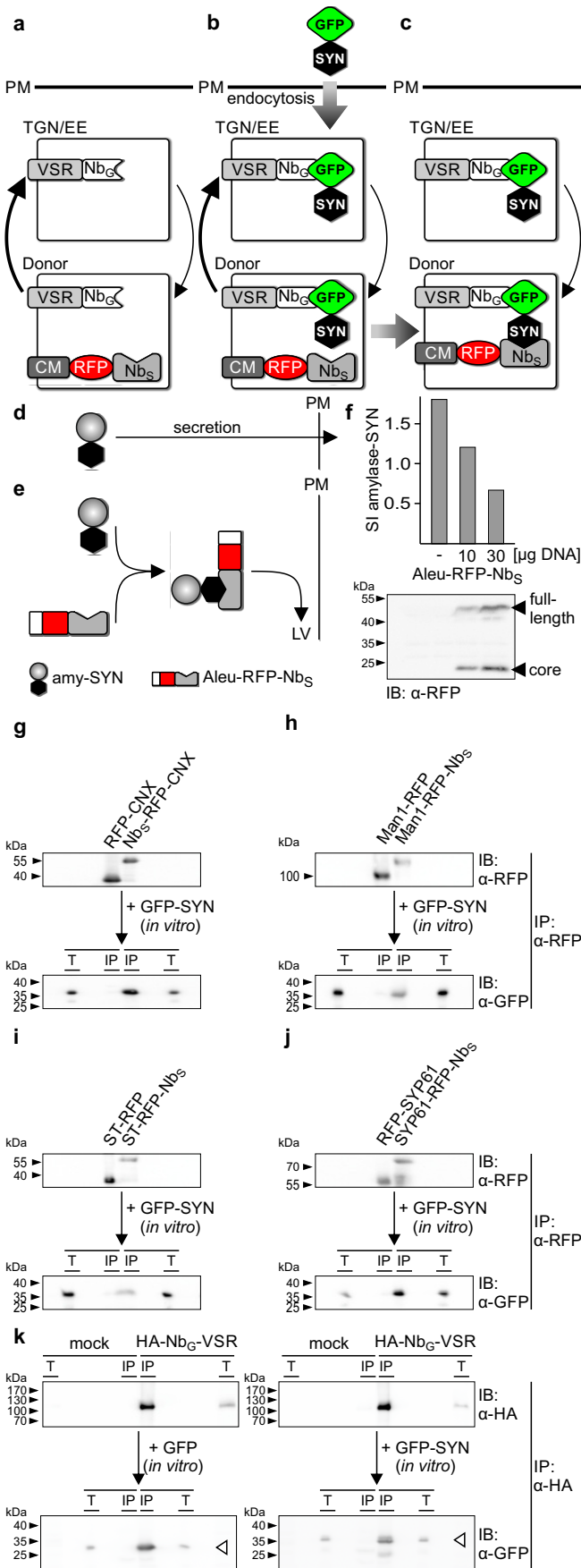


**Figure 3. Nanobody-triggered lockdown of recycled VSRs.** (a) Coexpression of Nb<sub>G</sub>-VSRs with red fluorescent Nb<sub>S</sub>-tagged compartmental markers (anchor) and (b) post-translational labeling with the dual-epitope GFP-SYN in the TGN/EE to (c) anchor VSRs upon recycling. (d,e) Nb<sub>S</sub>-SYN epitope interaction occurs in the endomembrane system. (d) SYN epitope-tagged secreted amylase (amy-SYN) is (e) rerouted to the LV upon Aleu-RFP-Nb<sub>S</sub> triggers attachment of the vacuolar sorting signal (Aleu). (f) Coexpression of amy-SYN with different amounts of Aleu-RFP-Nb<sub>S</sub>. Upper panel: secretion index (SI); lower panel: corresponding immunoblot (α-RFP). (g-j) Co-immunoprecipitations revealing Nb<sub>S</sub>-SYN epitope interaction. RFP-tagged markers and anchors for (g) ER, (h) *cis*-Golgi, (i) *trans*-Golgi and (j) TGN/EE were immunoprecipitated (IP, α-RFP), incubated with GFP-SYN and immunoblotted (IB). Total extracts (T) and immunoprecipitates (IP) were probed to detect markers, anchors (α-RFP) and co-precipitated GFP-SYN (α-GFP). (k) Co-immunoprecipitation revealing Nb<sub>G</sub>-GFP epitope interaction. Expressed Nb<sub>G</sub>-VSRs or samples from mock-transfected cells were immunoprecipitated (IP, α-HA), incubated with GFP or GFP-SYN and immunoblotted (IB). Total extracts (T) and immunoprecipitates (IP) were probed to detect VSRs (α-HA) and co-precipitated GFP (white arrowhead) or GFP-SYN (black arrowhead) (α-GFP), respectively.

**Figure 4**

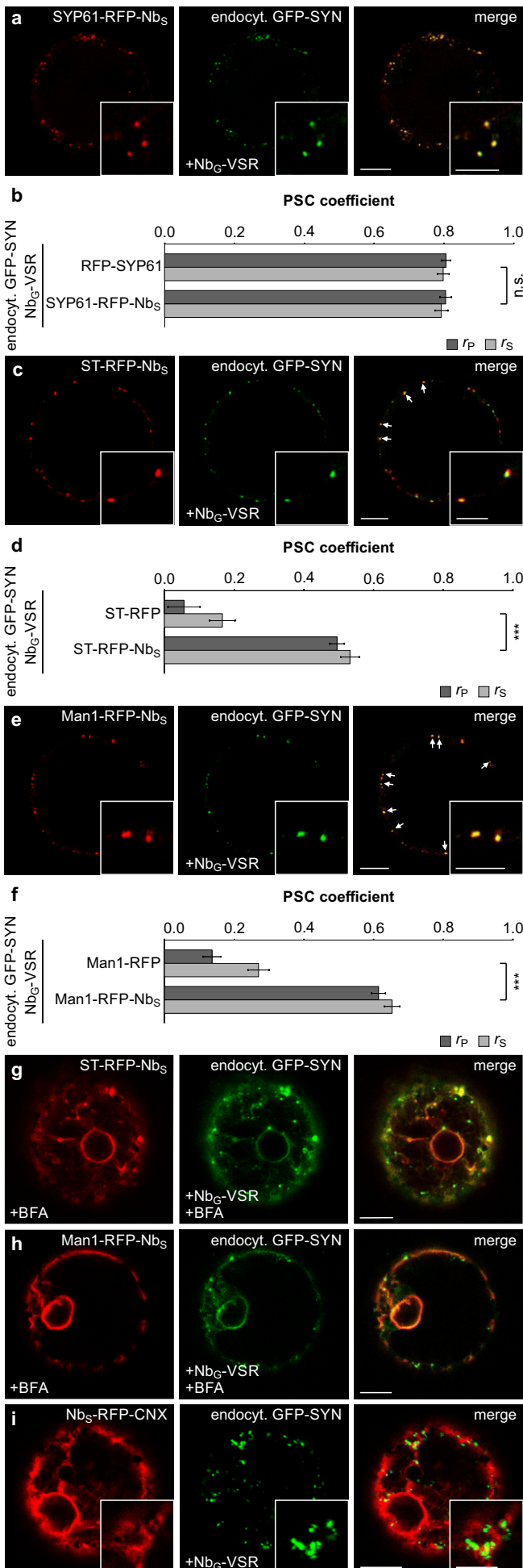


**Figure 4 The *cis*-Golgi stack is the target of VSR recycling.** GFP-SYN labeled Nb<sub>e</sub>-VSR is locked to the anchors in (a) the TGN/EE (SYP61-RFP-Nb<sub>s</sub>), and after recycling to (c) *trans*-Golgi (ST-RFP-Nb<sub>s</sub>) and (e) *cis*-Golgi (Man1-RFP-Nb<sub>s</sub>) but does not reach (i) the ER anchor Nb<sub>s</sub>-GFP-CNX. PSC coefficients of the labeled Nb<sub>e</sub>-VSR with (b) the marker Syp61-RFP or the anchor Syp61-RFP-Nb<sub>s</sub>, presented/calculated as in (2i) with n=10, P≥0.05, n.s., not significant, (d) the marker ST-RFP or the anchor ST-RFP-Nb<sub>s</sub>, presented/calculated as above with n=10, P<0.001, \*\*\*, extremely significant and (f) the marker Man1-RFP or the anchor Man1-RFP-Nb<sub>s</sub>, presented/calculated as in (d). Graphs show a representative sample of two independent experiments. (g,h) BFA-treatment of samples from (c,e) for 1 h at 20 μM triggers fusion of Golgi with ER, verifying Golgi-localization of locked VSRs from (c,e). Scale bars 10μm, insets 5μm, showing magnifications.

**Figure 5**

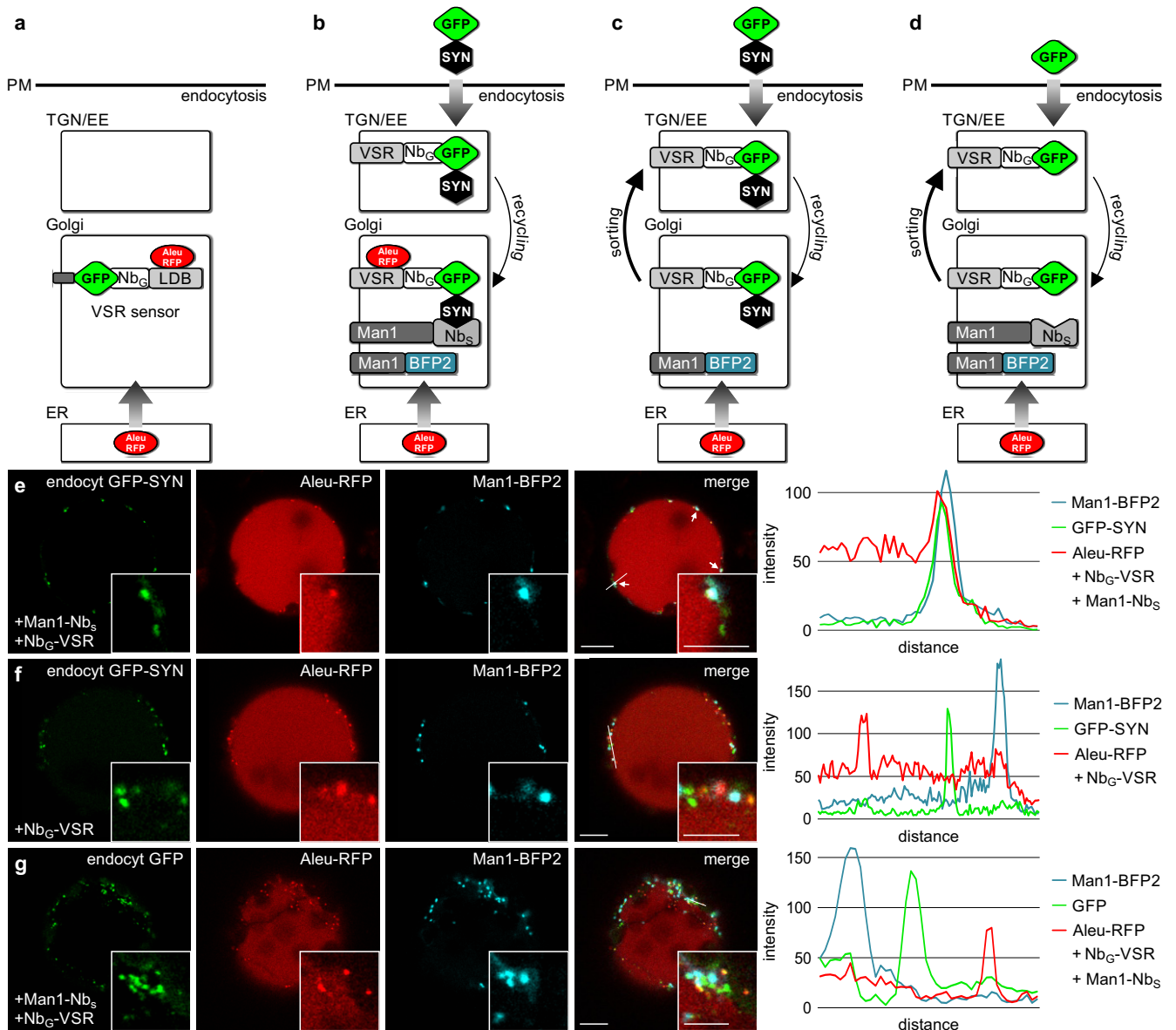


**Figure 5. VSRs bind ligands after recycling.** (a) Targeted VSR sensors (Nb<sub>G</sub>-LDB) were shown to bind Aleu-RFP ligands in the Golgi (b) GFP-SYN labeled Nb<sub>G</sub>-VSRs are locked to the anchor Man1-Nb<sub>S</sub> in the *cis*-Golgi, positively identified by the marker Man1-BFP2. Ligand-binding of recycled full-length VSRs is assessed by colocalization with ligands (Aleu-RFP). Controls with cycling VSRs that lack (c) the anchor or (d) the SYN epitope at the labeling GFP for the VSR lockdown, result in VSR localization at the TGN/EE, which does not promote ligand binding. (e) GFP-SYN labeled Nb<sub>G</sub>-VSRs are locked after recycling in the *cis*-Golgi and colocalize with the Golgi marker Man1-BFP2 and bind the ligand Aleu-RFP, as shown by the overlapping signal peaks in the line intensity plot (see b). (f,g) Not locked VSRs (see c and d) do not localize to the Golgi and thus do not bind the ligand Aleu-RFP as judged by the separated peaks in the line intensity plots. Scale bars 10μm, insets 5μm, showing magnifications.



**Figure 6**

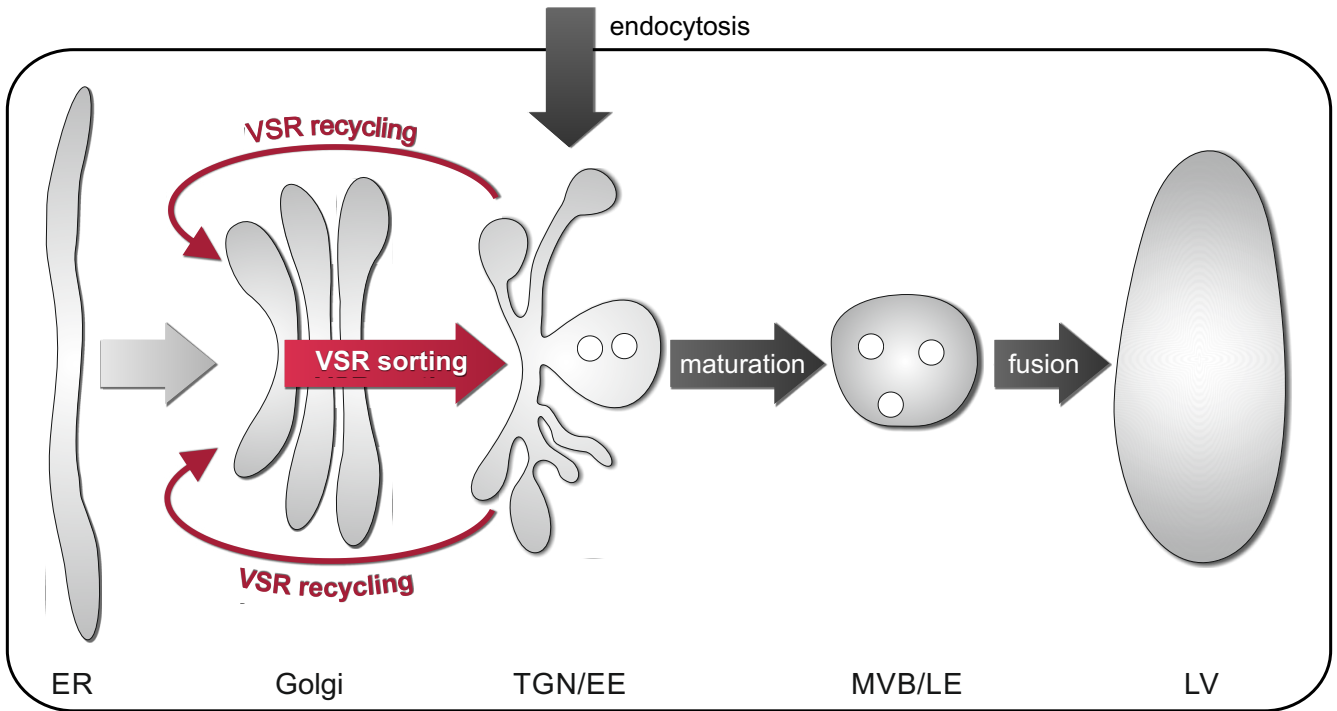
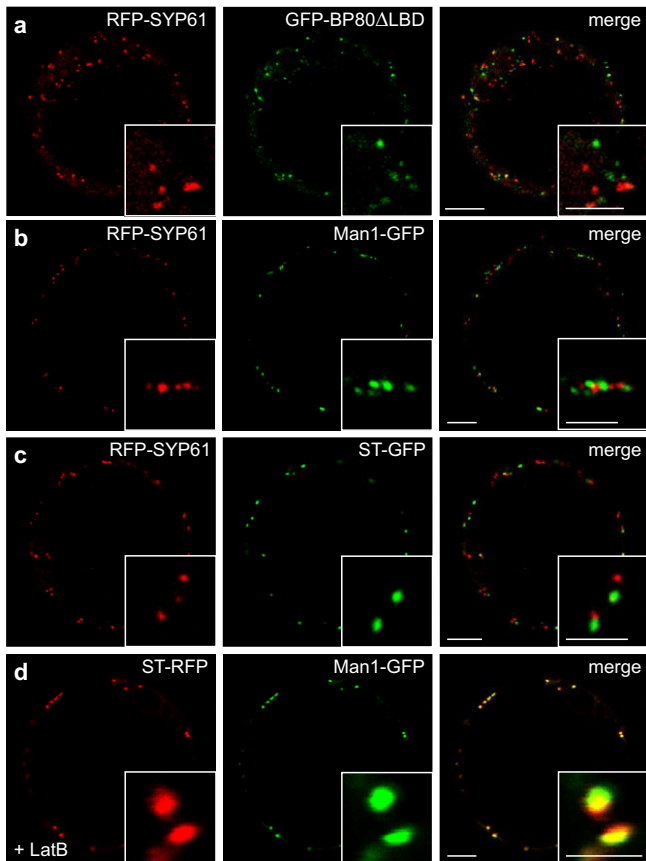


**Figure 6. Model for receptor mediated vacuolar sorting in plants.** VSRs bind ligands in the early secretory pathway and transport them to the TGN/EE. There, the ligands are released from the VSR. Next, VSRs are recycled back to the *cis*-Golgi stack for further rounds of ligand transport. Post-TGN/EE transport of released vacuolar cargo ligands but also endocytosed proteins occurs independent of VSRs and travel to the lytic vacuole per default. Transport in this route is mediated by multivesicular bodies, the late endosomes (MVBs/LEs). They bud off the TGN/EE in a maturation-based step and confer cargo delivery by their ultimate fusion with the lytic vacuole (LV).

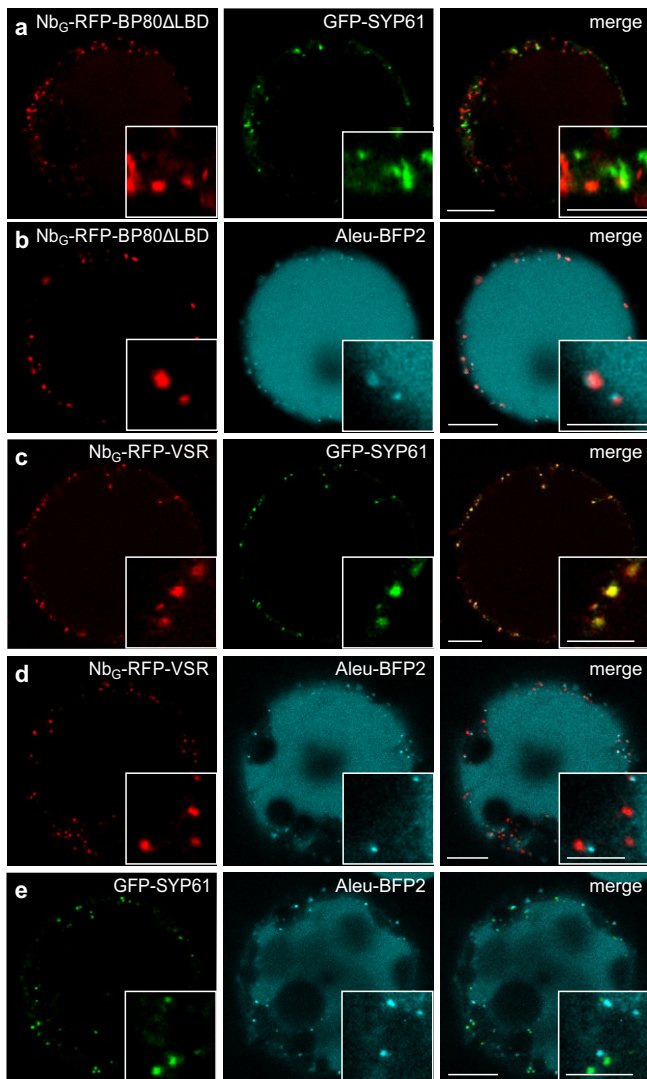
## Supplementary Figure 1



**Supplementary Figure 1. Membrane marker proteins to discriminate punctate signals in the MVB/LE, the TGN/EE and the *cis-trans*-Golgi in colocalization experiments.** Comparison of signals for TGN/EE, MVB/LE and *cis-trans*-Golgi in coexpression experiments. Coexpression of: (a) RFP-SYP61 with GFP-BP80ΔLBD to discriminate TGN/EE from MVB/LE, (b) RFP-SYP61 with Man1-GFP to discriminate TGN/EE from the *trans*-Golgi, (c) RFP-SYP61 with ST-GFP to discriminate TGN/EE from the *trans*-Golgi and (d) ST-RFP with Man1-GFP to discriminate between *cis*- and *trans*-Golgi. Performed in the presence of 4  $\mu$ M latrunculin B (LatB) to avoid Golgi movement during image acquisition. Scale bars 10 $\mu$ m, insets 5 $\mu$ m, showing magnifications.

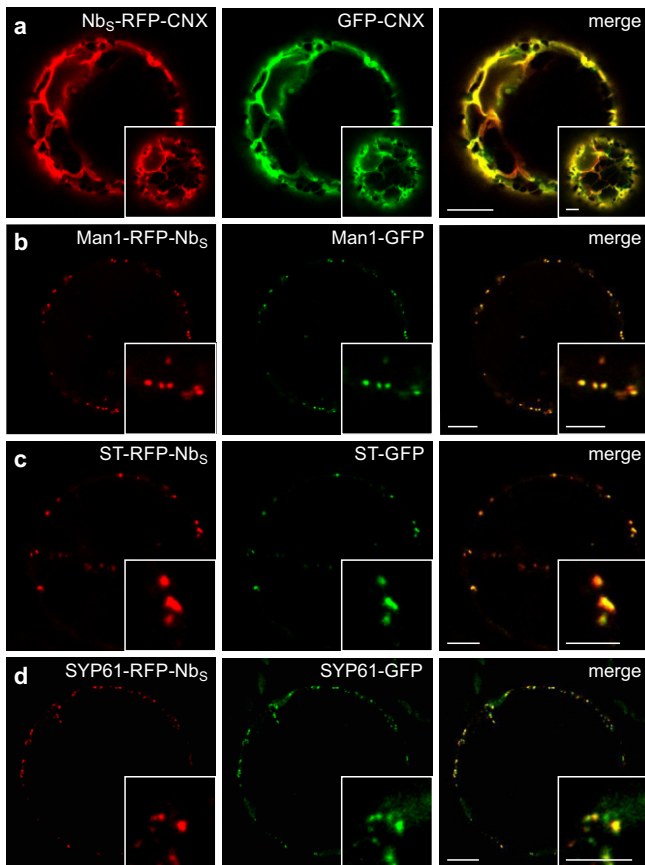


## Supplementary Figure 2



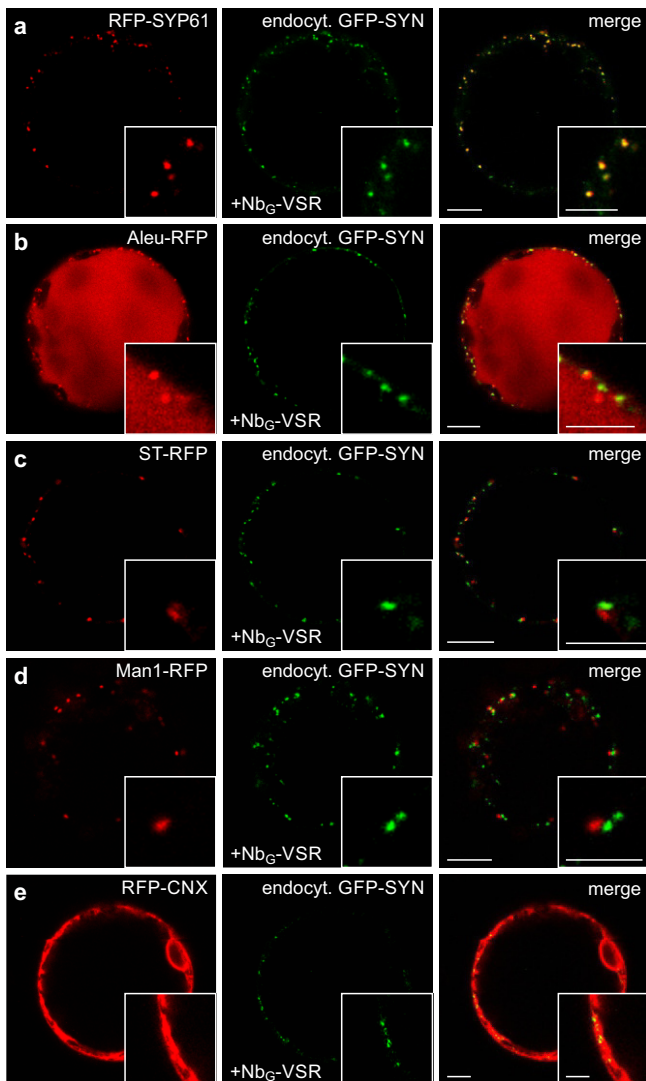
**Supplementary Figure 2. Differential localization of the fluorescent full-length VSR Nb<sub>g</sub>-RFP-VSR and the LBD-lacking MVB/LE marker Nb<sub>g</sub>-RFP-BP80ΔLBD.** (a) Coexpression of Nb<sub>g</sub>-RFP-BP80ΔLBD with the N-terminal GFP fusion of SYP61, GFP-SYP61, as marker for the TGN/EE, and (b) with the MVB/LE and vacuolar marker Aleu- blue fluorescent (BFP)2 confirms the unaltered MVB/LE localization of the marker Nb<sub>g</sub>-RFP-BP80ΔLBD. (c) In sharp contrast, coexpression of Nb<sub>g</sub>-RFP-VSR with GFP-SYP61, and with (d) Aleu-BFP2 confirms the unaltered TGN/EE localization of the receptor Nb<sub>g</sub>-RFP-VSR. (e) GFP-SYP61-labeled TGN/EE are clearly distinguishable from Aleu-BFP2-labeled MVB/LE in co-expression experiments (compare to Suppl. Fig. 1a).

### Supplementary Figure 3



**Supplementary Figure 3. Fusion of the Nb<sub>s</sub> to compartment-specific marker proteins does not alter their compartment-specific localization.** The localization of red fluorescent Nb<sub>s</sub>-tagged marker proteins is compared to their GFP-tagged counterparts. Colocalization of (a) Nb<sub>s</sub>-RFP-CNX with GFP-CNX in the ER, (b) Man1-RFP-Nb<sub>s</sub> with Man1-GFP in the *cis*-Golgi stack, (c) ST-RFP-Nb<sub>s</sub> with ST-GFP in the *trans*-Golgi stack and (d) SYP61-RFP-Nb<sub>s</sub> with Syp61-GFP in the TGN/EE. Scale bars 10 μm, insets 5 μm, showing magnifications.

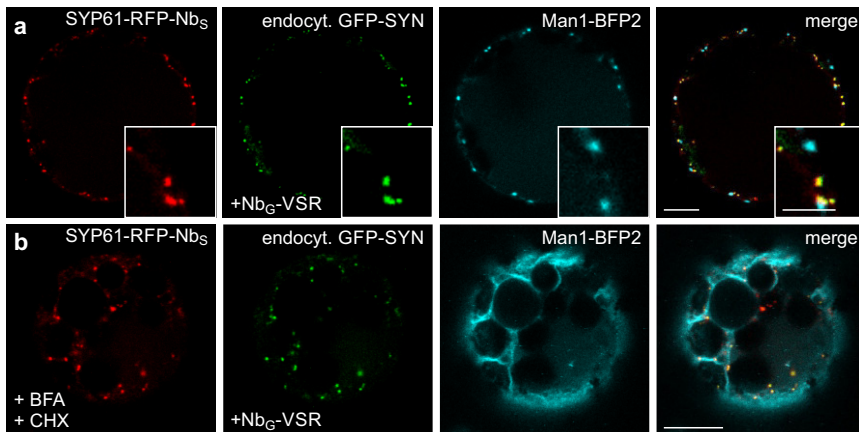
## Supplementary Figure 4



**Supplementary Figure 4. The GFP-SYN labeled Nb<sub>e</sub>-VSR localizes to the TGN/EE under steady state conditions.**

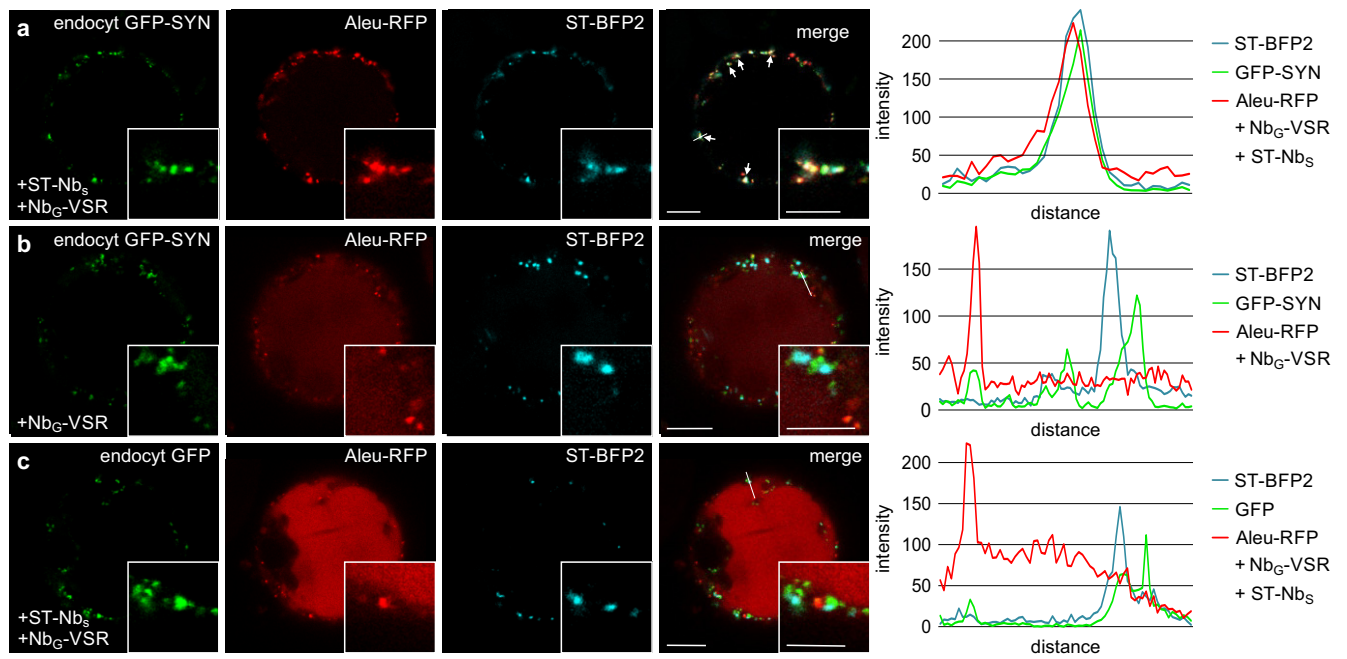
Colocalization of post-translationally GFP-SYN labeled non fluorescent Nb<sub>e</sub>-tagged VSRs with red fluorescent compartmental markers for (a) the TGN/EE, (b) the MVB/LE and the vacuole, (c) the *trans*-Golgi, (d) the *cis*-Golgi and (e) the ER. Scale bars 10 μm, insets 5 μm, showing magnifications.

## Supplementary Figure 5



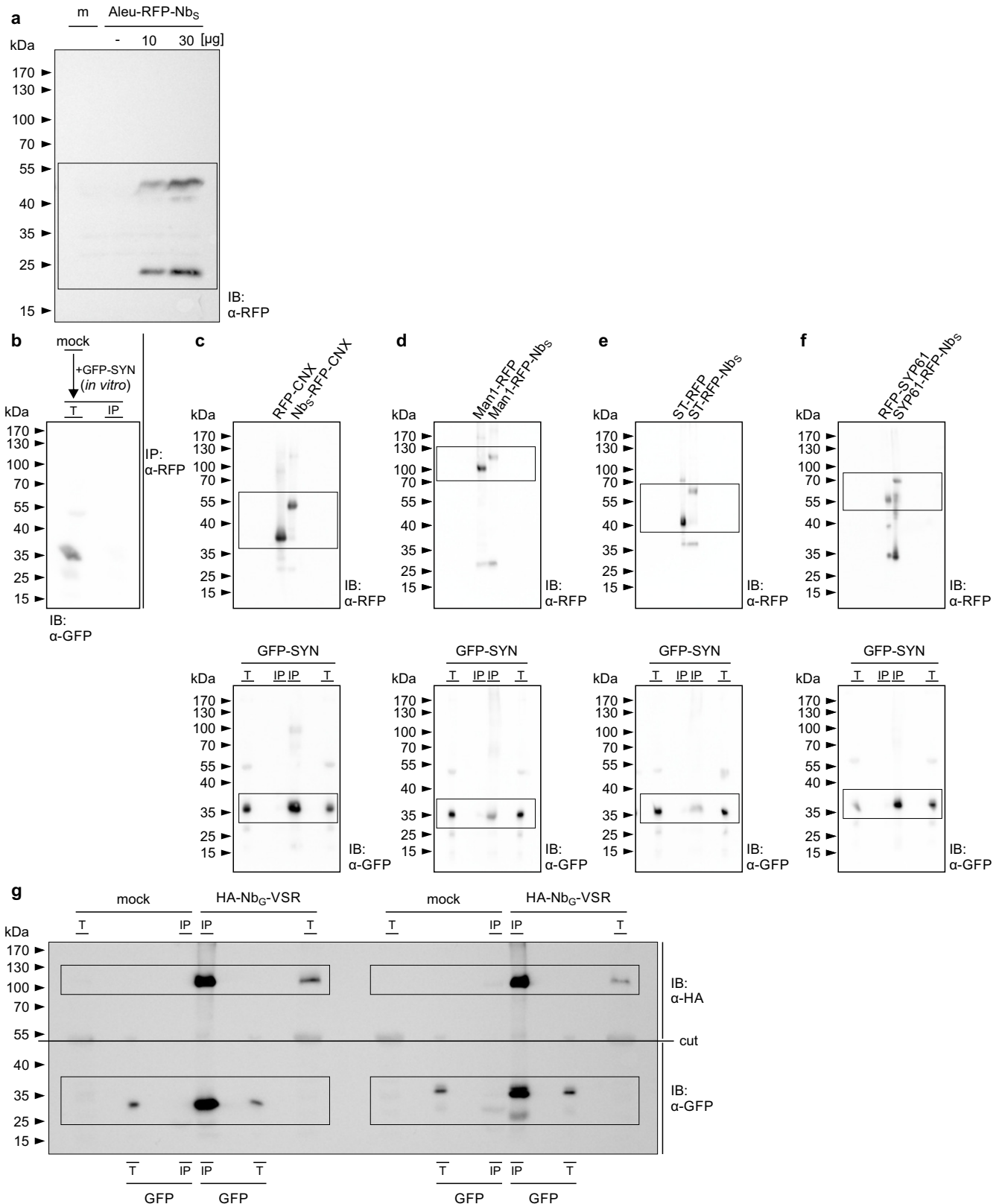
**Supplementary Figure 5. The TGN/EE-locked VSR does not colocalize with the coexpressed marker for the *cis*-Golgi.** (a,b) Colocalization of post-translationally GFP-SYN labeled non fluorescent Nb<sub>s</sub>-tagged VSRs with the TGN/EE membrane anchor SYP61-RFP-Nb<sub>s</sub> and the marker for the *cis*-Golgi Man1-BFP2 upon GFP-SYN-triggered lockdown. (a) The overlapping signals of the labeled VSR and the TGN/EE membrane anchor (yellow) do not colocalize with the signals of the Golgi marker (cyan). (b) The colocalizing signals of TGN/EE anchored and the locked VSR persist after BFA treatment, whilst the Golgi signal redistributes to the ER, due to the BFA-triggered fusion of these compartments. Cells were treated with 20 µM BFA and 50 µM cycloheximide (CHX) for 1 h prior to imaging analysis. Scale bars 10µm, insets 5µm, showing magnifications.

## Supplementary Figure 6



**Supplementary Figure 6. VSRs bind ligands in the *trans*-Golgi after recycling.** (a) GFP-SYN labeled Nb<sub>G</sub>-VSRs are locked after recycling in the *trans*-Golgi and colocalize with the *trans*-Golgi marker ST-BFP2 and bind the ligand Aleu-RFP, as shown by the overlapping signal peaks in the line intensity plot (compare to Figure 5b). (b,c) Not locked VSRs (compare to Figure 5c,d) do not localize to the Golgi and thus do not bind the ligand Aleu-RFP as judged by the separated peaks in the line intensity plots. Scale bars 10µm, insets 5µm, showing magnifications.

## Supplementary Figure 7



**Supplementary Figure 7. Uncropped immunoblots.** (a) Detection of Aleu-RFP-Nb<sub>s</sub> as illustrated in Figure 3f. Section shown in Figure 3f is highlighted with a black rectangle. The immunoblot (IB) was probed with α-RFP. (b-f) Detection of the markers/anchors and the dual epitope GFP-SYN as shown in Figure 3g-j. (b) Control using mock transfected protoplasts for the immunoprecipitation (IP, α-RFP). Beads were incubated with GFP-SYN and immunoblotted (IB). The total extract (T) and the immunoprecipitate (IP) was probed with α-GFP to detect GFP-SYN. (c-f) Sections shown in Figure 3g-j are highlighted with black rectangles. The immunoblots (IB) were probed to detect markers/anchors (α-RFP) and GFP-SYN (α-GFP). (g) Detection of VSRs and epitopes (GFP/GFP-SYN) as shown in Figure 3k. Sections shown in Figure 3k are highlighted with black rectangles. The immunoblots (IB) are probed to detect VSRs (α-HA) and GFP/GFP-SYN (α-GFP).

Supplementary Table 1

	Primers	Sequence (5'-3' direction)	Template	Recipient Vector
<b>Nb<sub>6</sub>-RFP-CN<sub>6</sub> (pDV01)</b>	Nb <sub>6</sub> _NheI_S	GCTCAGGCTAGCGCTAT GGACTATAAAGACGACGA CGACAAAATGGGATCTG GAGGAATGGCTCA	pBL14 <sup>1</sup>	pFF04 <sup>1</sup> ; cut <i>NotI</i> / <i>NheI</i> to keep the N-terminal signal peptide of pFF04
	Nb <sub>6</sub> _NcoI_AS	GGCCATCCATGGATGAT GATGATGATGATGAG	pFK12 <sup>2</sup>	
	RFP_NcoI_S	CATCATCCATGGATGGCC TCCTCCGAGGACGT		
	RFP_NotI_AS	GTCACTCCGCGCCGCTG CTCCAGTACTGTGGCGG C		
<b>Man1-RFP-Nb<sub>6</sub> (pSF65)</b>	RFP_NotI_S	GAGGATCCGCGCCGATG GCCTCCTCCGAGGACGT	pFK12 <sup>2</sup>	pFF06 <sup>1</sup> ; cut <i>BamHI</i> / <i>NotI</i>
	RFP_ClaI_AS	CATCATATCGATTGCTCC AGTACTGTGGCGGC	pDV01 (see above)	
	FLAG_ClaI_S	GAGGACATCGATATGGA CTATAAAGACGACGA		
	Nb <sub>6</sub> _BamHI_AS	GCATGAGGATCCCTAATG ATGATGATGATGATGAG		
<b>ST-RFP-Nb<sub>6</sub> (pSF128)</b>	PLUS: ST ( <i>NheI</i> / <i>NotI</i> ), subcloned from pSF83 <sup>1</sup>			pSF65 (see above); cut <i>NotI</i> / <i>NheI</i>
<b>Syp61-RFP-Nb<sub>6</sub> (pSF129)</b>	PLUS: Syp61 ( <i>NheI</i> / <i>NotI</i> ), subcloned from pFF25 <sup>1</sup>			pSF65 (see above); cut <i>NotI</i> / <i>NheI</i>
<b>Nb<sub>6</sub>-RFP-BP80ΔLBD (pSF130)</b>	PLUS: BP80 ( <i>NotI</i> / <i>BamHI</i> ), subcloned from pFF03 <sup>1</sup>			pDV01 (see above); cut <i>BamHI</i> / <i>NotI</i>
<b>Sec-GFP (pFK68)</b>	GFP_SalI_S	CATGACGTCGACTATGAG TAAAGGAGAAGAAC	GFP-spo <sup>3</sup>	pFF14 <sup>1</sup> ; cut <i>SpeI</i> / <i>SalI</i> to keep the N-terminal signal peptide of pFF14
	GFP-GGGG_SpeI_AS	TGCTTCACTAGICTATCC TCCTCCTCCTTTGTATAG TTCATCCATGC		
<b>Nb<sub>6</sub>-RFP-VSR (pSF75)</b>	Nb <sub>6</sub> _NheI_S	GCTCAGGCTAGCGCTAT GGACTATAAAGACGACGA CGACAAAATGGGATCTG GAGGAATGGCTCA	pBL14 <sup>1</sup>	pFF04 <sup>1</sup> ; cut <i>BamHI</i> / <i>NheI</i> to keep the N-terminal signal peptide of pFF04
	Nb <sub>6</sub> _NcoI_AS	GGCCATCCATGGATGAT GATGATGATGATGAG	pFK12 <sup>2</sup>	
	RFP_NcoI_S	CATCATCCATGGATGGCC TCCTCCGAGGACGT		
	RFP_NdeI_AS	TTCGGCCATATGTGCTCC AGTACTGTGGCGGC		
	VSR_NdeI_S	GTGGTTCATATGTTTAAC GAGGCTCGATTCTG	first strand cDNA from 3-day-old <i>A. thaliana</i> seedlings	
	VSR_BamHI_AS	CTAGTCGGATCCCTAGG CACGTTTCATCATTCTG		
<b>Nb<sub>6</sub>-VSR (pSF76)</b>	Nb <sub>6</sub> _NheI_S	GCTCAGGCTAGCGCTAT GGACTATAAAGACGACGA CGACAAAATGGGATCTG GAGGAATGGCTCA	pBL14 <sup>1</sup>	pSF75 (see above); cut <i>NdeI</i> / <i>NheI</i> to keep the N-terminal signal peptide of pSF75
	Nb <sub>6</sub> _NdeI_AS	GTCCTCCATATGATGATG ATGATGATGATGAG		
<b>ST-RFP (pSF84)</b>	RFP_NotI_S	TGGCCCGCGCCGCGATG GCCTCCTCCGAGGACGT	pFK44 <sup>2</sup>	pSF83 <sup>1</sup> ; cut <i>BamHI</i> / <i>NotI</i>
	RFP_BamHI_AS	TGCTTCGGATCCTTATGC TCCAGTACTGTGGC		
<b>Amy-SYN (pSF57)</b>	Amy_NcoI_S	CTATAACCATGGCGAACA AACACTTGTCCTC	pCN1 <sup>2</sup>	pCN1 <sup>2</sup> ; cut <i>BamHI</i> / <i>NcoI</i>
	Amy_NotI_AS	ATCAACGCGCCGCCGGA TCTTCTCCCATACGGCAT		
	SYN_NotI/ <i>BamHI</i> _S	GGCCGCGTTGATCCTGA TAATGAAGCATACGAAAT GCCTTCTGAAGAAGGCTA TCAAGATTGAACCGGA GGCTTAGG	Complementary oligonucleotides to assemble the coding sequence of the SYN-tag <sup>4</sup>	
	SYN_NotI/ <i>BamHI</i> _AS	GATCCCTAAGCCTCCGGT TCATAATCTTGATAGCCT TCTTCAGAAGGCATTTTCG TATGCTTCATTATCAGGA TCAACG		
<b>Aleu-RFP-Nbs (pDV02)</b>	PLUS: P35S-Aleu ( <i>EcoRI</i> / <i>NheI</i> ), subcloned from pFF15 <sup>1</sup>			pCN1 <sup>2</sup> ; cut <i>BamHI</i> / <i>EcoRI</i>
	RFP_NcoI_S	CTAGCGCCATGGCCTCC TCCGAGGAC	pFK12 <sup>2</sup>	
	RFP_KpnI_AS	ATACATGGTACCTGTCC AGTACTGTGGCGGC		
	PLUS: Nbs ( <i>KpnI</i> / <i>BamHI</i> ); chemically synthesized			

<b>GFP-SYN (pSF74)</b>	GFP_ <i>NheI</i> _S	GCATGAGCTAGCGCCAT GGTGAGCAAGGGCGAGG	pFF04 <sup>1</sup>	pFF04 <sup>1</sup> ; cut <i>Bam</i> HI/ <i>NheI</i> to keep the N-terminal signal peptide of pFF04
	mEGFP_ <i>Hind</i> III_AS	GTTGGGGTCTTTGCTAAG CTGGACTGGGTGCTCA G		
	mEGFP_ <i>Hind</i> III_S	CTGAGCACCAGTCCAA GCTTAGCAAAGACCCCAA C	pFF04 <sup>1</sup>	
	GFP_ <i>NotI</i> _AS	ATCAACGC GGCCGCCT TGACAGCTCGTCCATGC		
	PLUS: SYN ( <i>NotI/Bam</i> HI), subcloned from pSF57 (see above)			
<b>HA-Nbc-VSR (pSF88)</b>	HA_ <i>Nbc_NheI</i> _S	CTTTCTGCTAGCGCTATG TATCCGTATGATGTTCCA GATTATGCTATGGGATCT GGAGGAATGGCT	pBL14 <sup>1</sup>	pFK120 <sup>1</sup> ; cut <i>Bam</i> HI/ <i>NheI</i> to keep the N-terminal signal peptide of pFK120
	<i>Nbc_NdeI</i> _AS	GTCCTCCATATGATGATG ATGATGATGATGAG		
	PLUS: VSR4 ( <i>NdeI/Bam</i> HI), subcloned from pSF56 (see above)			
<b>Nbs-RFP-CNX (pDV03)</b>	<i>Nbs_NheI</i> _S	CGATACGCTAGCGCTATG GACTATAAAGACGACGAC GACAAAATGCAGGTGCA GCTGCAGGA	pDV02, see above	pFF04 <sup>1</sup> ; cut <i>NotI/NheI</i> to keep the N-terminal signal peptide of pFF04
	<i>Nbs_NcoI</i> _AS	CGATGACCATGGGCTGC TCACGGTCACCTGGG		
	RFP_ <i>NcoI</i> _S	AGTCTACCATGGATGGCC TCCTCCGAGGACGT	pFK12 <sup>2</sup>	
	RFP_ <i>NotI</i> _AS	AGTCTAGCGGCCCGCGG GTGCTCCAGTACTGTG		
<b>Man1-RFP-Nbs (pSF78)</b>	RFP_ <i>NotI</i> _S	GAGGATCGGGCCGCATG GCCTCCTCCGAGGACGT	pFK12 <sup>2</sup>	pFF06 <sup>1</sup> ; cut <i>Bam</i> HI/ <i>NotI</i>
	RFP_ <i>KpnI</i> _AS	TCCTTAGGTACCTGCTCC AGTGCTGTGGCGGC		
	PLUS: Nbs ( <i>KpnI/Bam</i> HI), subcloned from pDV02 (see above)			
<b>ST-RFP-Nbs (pSF82)</b>	PLUS: ST ( <i>NheI/NotI</i> ), subcloned from pSF83 <sup>1</sup>			pSF78 (see above); <i>NotI/NheI</i>
<b>Syp61-RFP-Nbs (pSF80)</b>	PLUS: RFP-Nbs ( <i>NotI/Bam</i> HI), subcloned from pSF78 (see above)			pFF25 <sup>1</sup> ; cut <i>Bam</i> HI/ <i>NotI</i>
<b>Man1-Nbs (pSF85)</b>	HA_ <i>NotI</i> _S	CATGTAGCGGCCGCTAT CCTTATGATGTTCTCTGA	pDV02, see above	pSF78 (see above); cut <i>Bam</i> HI/ <i>NotI</i>
	<i>Nbs_Bam</i> HI_AS	TGCTTCGGATCCCTAGCT GCTCAGGTCACCTGGG		
<b>Man1-mTagBFP2 (pSF143)</b>	PLUS: mTagBFP2 ( <i>NotI/Bam</i> HI); chemically synthesized			pFF06 <sup>1</sup> ; cut <i>Bam</i> HI/ <i>NotI</i>
<b>Aleu-mTagBFP2 (pFK106)</b>	PLUS: P35S-Aleu ( <i>EcoRI/NheI</i> ), subcloned from pFF15 <sup>1</sup>		pSF143, see above	pDS13 <sup>5</sup> ; cut <i>Bam</i> HI/ <i>EcoRI</i>
	mTagBFP2_ <i>NheI</i> _S	GAAAGCGCTAGCATGTCT GAACTATTAAGGA		
	mTagBFP2_ <i>Bam</i> HI_AS	TGCTTCGGATCCCTAATT CAACTATGTCCCA		
<b>ST-Nbs (pSF86)</b>	HA_ <i>NotI</i> _S	CATGTAGCGGCCGCTAT CCTTATGATGTTCTCTGA	pDV02, see above	pSF82 (see above); cut <i>Bam</i> HI/ <i>NotI</i>
	<i>Nbs_Bam</i> HI_AS	TGCTTCGGATCCCTAGCT GCTCAGGTCACCTGGG		
<b>ST-mTagBFP2 (pSF142)</b>	PLUS: mTagBFP2 ( <i>NotI/Bam</i> HI); chemically synthesized			pSF83 <sup>1</sup> ; cut <i>Bam</i> HI/ <i>NotI</i>
<b>Established plasmids used in this study</b>				
RFP-Syp61 <sup>1</sup>	TGN marker			
Aleu-RFP <sup>1</sup>	MBV/LE and vacuolar marker, VSR ligand			
Man1-RFP <sup>6</sup>	<i>cis</i> -Golgi marker			
RFP-CNX <sup>1</sup>	ER marker			
GFP-CNX <sup>1</sup>	ER marker			
Man1-GFP <sup>1</sup>	<i>cis</i> -Golgi marker			
ST-GFP <sup>1</sup>	<i>trans</i> -Golgi marker			
GFP-Syp61 <sup>1</sup>	TGN marker			
GFP-BP80ΔLBD <sup>1</sup>	MBV/LE marker			

## References

1. Künzl F, Frühholz S, Fäßler F, Li B, Pimpl P. Receptor-mediated sorting of soluble vacuolar proteins ends at the trans-Golgi network/early endosome. *Nat Plants*, 16017 (2016).
2. Scheuring D, *et al.* Ubiquitin initiates sorting of Golgi and plasma membrane proteins into the vacuolar degradation pathway. *BMC plant biology* **12**, 164 (2012).
3. daSilva LL, *et al.* Receptor salvage from the prevacuolar compartment is essential for efficient vacuolar protein targeting. *The Plant cell* **17**, 132-148 (2005).



4. Guilliams T, *et al.* Nanobodies raised against monomeric alpha-synuclein distinguish between fibrils at different maturation stages. *Journal of molecular biology* **425**, 2397-2411 (2013).
5. Niemes S, *et al.* Retromer recycles vacuolar sorting receptors from the trans-Golgi network. *The Plant journal : for cell and molecular biology* **61**, 107-121 (2010).
6. Nebenfuhr A, *et al.* Stop-and-go movements of plant Golgi stacks are mediated by the acto-myosin system. *Plant physiology* **121**, 1127-1142 (1999).

***In vivo* interaction studies by measuring Förster resonance energy transfer through fluorescence lifetime imaging microscopy (FRET/FLIM)**

**Florian Fäßler** and Peter Pimpl

In: Jiang L. (eds) Plant Protein Secretion. Methods in Molecular Biology, vol 1662. Humana Press, New York, NY, doi: 10.1007/978-1-4939-7262-3\_14

[https://link.springer.com/protocol/10.1007%2F978-1-4939-7262-3\\_14](https://link.springer.com/protocol/10.1007%2F978-1-4939-7262-3_14)

**In *vivo* interaction studies by measuring Förster resonance energy transfer through fluorescence lifetime imaging microscopy (FRET/FLIM)**

Florian Fäßler and Peter Pimpl\*

Center for Plant Molecular Biology, University of Tübingen, Auf der Morgenstelle 32,  
72076 Tübingen, Germany

\*e-mail: [peter.pimpl@zmbp.uni-tuebingen.de](mailto:peter.pimpl@zmbp.uni-tuebingen.de)

Running head: Protein-protein interaction analysis by FRET/FLIM

## **Abstract**

Combinations of multiple fluorescent fusion proteins are commonly generated and used for co-localization studies in live cell imaging but also biochemical analysis of protein-protein interactions by co-immunoprecipitation *in vitro*. Advanced microscopy techniques like Förster resonance energy transfer through fluorescence lifetime imaging microscopy (FRET/FLIM) nowadays enables the combination of both approaches. This opens up the possibility to perform a location-specific protein-protein interaction analysis *in vivo*. To this end, the non-radiant energy transfer from a donor to an acceptor fluorophore (FRET) is harnessed to test for close-proximity as an indicator for interaction, whilst the spectromicroscopical measurement of the fluorescence lifetime by FLIM serves as a readout.

Here, we describe FRET/FLIM measurements performed with a Leica TCS SP8/PicoHarp 300 combination to demonstrate the interaction between a RFP-tagged GFP-nanobody and its epitope, GFP, in the cytoplasm of tobacco mesophyll protoplasts.

**Key words** Protein-protein interaction, nanobody-epitope interaction, GFP nanobody, epitope-tagging localization specificity, *in vivo*, confocal microscopy, FRET, FLIM,

## 1 Introduction

The cloning, heterologous expression and observation of green fluorescent fusion proteins in living cells is a milestone in cell biology that opened up new opportunities for further experimental strategies<sup>1-3</sup>. Fusion proteins and their use for *in vivo* gene-expression and protein-localization studies have been continuously improved ever since, allowing nowadays for coexpression of multiple spectral variants for complex colocalization studies<sup>4-6</sup>. In parallel, microscopes have evolved to complex systems that fulfill the demand for advanced spectromicroscopical analyses<sup>7</sup>. This exceeds by far the detection of two fluorescently tagged proteins in colocalization studies but also allows for testing whether those proteins might interact with one another. Here, the interaction of two fluorescently tagged proteins results in close proximity of the respective fluorophores, thereby allowing for Förster resonance energy transfer (FRET) to occur. This non-radiant energy transfer between molecules happens only if both fluorophores lie within a 10 nm distance to each other whilst the emission spectrum of one fluorophore (donor) overlaps with the excitation spectrum of the other (acceptor)<sup>8-10</sup>. Two different aspects of FRET can be used to generate the read-out for protein-protein interactions: either the occurrence of acceptor fluorescence upon the excitation of the donor fluorophore or the quenching of the donor fluorophore. A donor fluorophore can relax either via FRET or by emitting fluorescence. However, the longer an individual donor remains in an excited state the more likely it is that the donor is quenched during this period by FRET, thereby reducing the average lifetime of all donor fluorophores. This change in average lifetime can be observed by fluorescence lifetime imaging microscopy (FLIM)<sup>11</sup>. These lifetime-based readouts for FRET are less influenced by variations in fluorophore concentrations, less prone to signal cross-contamination and less

affected by bleaching than intensity-based readouts<sup>12</sup>. FLIM, can be performed by different approaches: frequency-domain FLIM or time-domain FLIM. In frequency-domain FLIM, the lifetime of a given fluorophore is calculated based on the phase delay and the modulation depth of the fluorescence compared to the excitation intensity, which is modulated at a high frequency<sup>13</sup>. This strategy is usually performed by using a wide-field microscopy setup with simultaneous data acquisition of the whole sample via a CCD detector. Time domain FLIM on the other hand, uses a pulsed laser for excitation and is commonly performed using laser scanning microscopy setups. Here, a histogram of the fluorescence events that follow an excitation pulse is generated by either applying time-gated detection<sup>14</sup> or time-correlated single photon counting (TCSPC)<sup>15</sup>.

Here we describe the experimental strategy of an *in vivo* protein-protein interaction study by FRET/FLIM. We describe all steps for the recording of an instrumental response function for reconvolution (**Fig. 1**), data acquisition via TCSPC FLIM, fitting of the acquired histograms, the statistical analysis of the results and the generation of false color images as supportive data. For this demonstration, we employ a known protein-protein interaction between a red fluorescent GFP-binding V<sub>HH</sub> domain of a heavy-chain antibody, termed GFP nanobody (Nb<sub>G</sub>) and its epitope, GFP, in the cytosol. This interaction triggers a highly significant decrease of GFP fluorescence lifetime (**Fig. 2**). Such an effect does not occur, if cytosolic RFP is co-expressed instead of the red fluorescent Nb<sub>G</sub>. This demonstrates that the change in donor fluorescence lifetime is not simply caused by co-localization with an acceptor fluorophore without an occurring interaction.

## 2 Material

1. *Nicotiana Tabacum* L. SR1 is grown on solid Murashige and Skoog (MS) medium at sterile conditions in 16/8 h light-dark cycles at 22 °C.  
Mesophyll protoplasts were isolated, transfected and incubated for the transient expression of the respective proteins as described by Frühholz and Pimpl in the chapter “Analysis of Nanobody–Epitope Interactions in Living Cells via Quantitative Protein Transport Assays in this issue”. Here, we use enhanced green fluorescent protein (GFP) as donor fluorophore together with the monomeric red fluorescent protein (RFP) as acceptor fluorophore.
2. Confocal laser scanning microscope: TCS SP8, equipped with:
  - Lasers for reference imaging (Argon 488nm, DPSS 561 nm)
  - Detectors for reference imaging (Leica HyD)
  - Pulsed diode laser (LDH-P-C-470B)
  - Pulsed laser driver (PDL-808 Sepia)
  - Laser combining unit
  - FLIM Detector (SMD Emission SPFLIM PMT)
  - TCSPC Module (PicoHarp 300)
  - ×63 (1.2 numerical aperture) water immersion objective (Leica, Wetzlar, Germany).
3. Imaging software: Leica Application Suite (LAS) X (Leica Wetzlar, Germany).
4. FLIM Software: SymPhoTime 64 v2.1 (PicoQuant, Berlin, Germany).
5. Microscope slides 76x26 mm (Roth, Karlsruhe, Germany)

6. Cover glasses 22x22x0.13-0.16 mm (Menzel-Gläser, Braunschweig, Germany).
7. Laboratory labelling tape
8. Nail polish
9. Cut 1ml pipette tips

### **3 Methods**

#### **3.1 Experimental strategy**

FRET-FLIM experiments should contain at least three different types of samples:

1. “Donor-only” sample: This sample contains only the donor fluorophore fused to the protein of interest (POI), but not an acceptor fluorophore. This sample is required to measure the lifetime of the donor in the given environment as the baseline.
2. “Non-interactor” sample: This sample contains the donor fluorophore fused to the POI together with a colocalizing acceptor fluorophore (see **Note 1**), which is fused to a protein that co-localizes with the donor but doesn’t interact with the POI. The lifetime measured for this sample should not be statistically significantly different from to the “donor-only” sample. This “Non-interactor” sample can either be a specifically designed negative control (see note 1) or simply a sample from the experiment that turned out to contain a non-interacting acceptor fusion protein.
3. “Interactor” sample: This sample contains the donor fluorophore fused to the POI and an acceptor fluorophore fused to a protein that interacts with



the POI. The “interactor” sample can be a sample from the experiment that turned out to contain an interacting acceptor fusion protein. If this is however not the case, one must design a specific positive control to demonstrate that a shift in fluorescent lifetime is possible in the given micro-environment of the POI. When GFP is used as donor, a GFP-binding VHH domain of a heavy chain antibody, termed nanobody (NbG), fused to the acceptor fluorophore can serve as ideal positive control. Such a construct will attach the acceptor directly to the donor, thereby triggering close enough proximity between the fluorophores for FRET to occur (see **Note 2**). The lifetime measured for this sample should be statistically significantly different to the one of the “donor-only” control as well as to samples expressing the acceptor fused to a non-interactor.

### **3.2 Recording of an instrumental response function**

Reconvolution of fluorescence lifetime measurements requires recording of an instrumental response function (IRF).

1. Start the LAS X program and choose “FLIM-mode” in the “mode” drop-down menu.
2. Start the SymPhoTime 64 program and create a new Workspace by choosing the corresponding command in the “File” drop-down menu.
3. Within the “Setup FLIM” tab adjust one non-pulsed laser to 5 % power for the detection using PMTs or substantially less for the detection using

more sensitive detectors e.g. HyDs, activate the respective detector and adjust its detection range according to the laser's emission spectrum.

4. In LAS X within the "Setup Imaging" tab open the "Acquisition" sub-tab and change the "Acquisition Mode" mode from xyz to xzy. In the "Show AOBs Settings" menu set the mark for the laser you chose in step 5 to "Reflection". In the "Fluorifier Disc Setting" menu deselect "Auto select" and choose an empty filter position instead (see **Note 3**).
5. To setup the conditions for a FLIM test (see step 16 below), go to the "Setup FLIM" tab, open the "Acquisition" sub-tab and change the "Acquisition Mode" mode from xyz to xzy. Set the resolution to 256x256 and modify the scanning speed to adjust the pixel dwell time to  $\sim 20 \mu\text{s}$  (see **Note 4**). In the "Fluorifier Disc Setting" menu deselect "Auto select" choose an empty filter position instead.

This step will alter the parameters in the "Measurements" tab automatically.

6. Switch back to the "Setup Imaging" tab and click one time on the "Quick LUT" button, this puts up a false color image for the intensity measured by the PMT. This allows for easier focusing on the total reflection at the inner surface of the coverslip (see step 10 below).
7. Prepare the test slide for the IRF by applying two slices of the tape in parallel with a distance of 0.75 cm to each other onto a microscope slide. Use nail polish to glue the coverslip to the tape slices thereby bridging the gap between them (see **Note 5**).
8. Put the prepared slide on the microscope stage, use the stage clips for fixation (see **Note 1**) and focus onto the edge of the tape in between the

microscope slide and the cover slip. Shift the stage in x-direction away from the tape, that served as help for focusing.

9. Switch to “Live” mode and adjust the z-position of the stage to find the reflection of the inner surface of the cover slip, which faces the microscope slide (see **Note 6, Fig. 2**)
10. Stop “Live” mode.
11. Go to the “Setup FLIM” tab. Activate the pulsed laser and the SPFLIM PMT. Adjust the detection range of the SPFLIM PMT according to the pulsed laser’s emission spectrum. This step will alter the parameters in the “Measurements” tab automatically.
12. In the “Acquisition” subtab within the “Measurements” tab set the “Definition of FLIM acquisition time” to “Acquire until max: X photons/pixel” are reached and set the value X to 1000, to ensure sufficient photon counts for the calculation of the IRF.
13. Save these “FLIM Settings”. This allows you to skip steps 3-5, 11 and 12 for recording future IRFs.
14. Apply the strongest grey filter setting of the laser combining unit (see **Note 7**).
15. Go to the “Setup FLIM” tab and click “Run FLIM Test”. Change to the SymPhoTime 64 program and check the max. count rate. Next, adjust the filter settings of the laser combining unit that the measured kilo-counts per second equal 2% of the laser pulse rate (e.g. 800 kilo-counts per second for a pulse rate of 40 MHz) and stop the “FLIM Test”

16. Go to the “Measurements” tab. Click “Run FLIM”. The Measurement will automatically stop once 1000 photons have been counted for a single pixel (see **Note 8**). Now, you can proceed to 3.3 “data acquisition”.

### 3.3 Data acquisition

Acquisition of data has to be performed with the same intensity settings for the pulsed laser as was used for recording the IRF (see **Note 9**).

1. Reset all settings used for the acquisition of the IRF in the LAS X program but stay in “FLIM-mode” and keep the SymPhoTime 64 program running in the same workspace.
2. In the “Setup imaging” tab, activate and adjust the lasers and detectors used for detection of the donor and acceptor fluorophores - similar to your standard confocal imaging setups.
3. Within the “Setup FLIM” tab, open the “Acquisition” sub-tab and set the resolution to 256x256 and modify the scanning speed to adjust the pixel dwell time to  $\sim 20 \mu\text{s}$  (see **Note 4**).
4. Activate next the pulsed laser and the SPFLIM PMT. Adjust the detection range of the SPFLIM PMT to the emission spectrum of the donor fluorophore.
5. In the “Acquisition” subtab within the “Measurements” tab set the “Definition of FLIM acquisition time” to “Acquire until max: X photons/pixel” are reached and set the value X between 500 and 1000, dependent on strength and distribution of the signal (see **Note 10**).
6. Save these settings. This allows for skipping steps 2-5 in future experiments.

7. In the “Setup” subtab, enter the name of your sample in the “Base Name” field.
8. Prepare your sample by applying two slices of the tape in parallel, with a distance of 0.75 cm to each other onto a microscope slide. Use a 1 ml pipette with a cut tip to reduce shearing forces and add ~100  $\mu$ l of protoplast suspension onto the microscope slide in between the tapes and carefully mount a coverslip (see **Note 11**).
9. In the “Setup FLIM” tab switch to “Live” mode, search for a suitable protoplast, zoom in and take a reference image by clicking “Capture Image”.
10. Apply the strongest grey filter setting of the laser combining unit.
11. Go to the “Setup FLIM” tab and click “Run FLIM Test”. Change to the SymPhoTime 64 program. Next, adjust the filter settings of the laser combining unit that the measured kilo-counts per second are as high as possible but are still below 10% of the pulse rate of the laser (e.g. 4000 kilo-counts per second for a pulse rate of 40MHz).
12. Stop the “FLIM Test” and go to the “Measurements” tab. Click “Run FLIM” to start the measurement. The Measurement will automatically stop once 500 photons have been detected for a single pixel.
13. Repeat steps 9, 11 and 12 for at least 10 cells per sample.

### **3.4 Analysis**

The analysis of the acquired data can either be performed after each measurement directly within the session or at any time after.

1. Reload your workspace in the SymPhoTime 64 software that contains the acquired data set
2. Open the folder that contains the RAW data from the measurement for the analysis and select the corresponding ".ptu" file.
3. Enter the FLIM analysis environment by opening the "Analysis" tab, select the "Imaging" drop down menu and click "Start" within the "FLIM" box.
4. Choose "n-Exponential Reconvolution" in the "Fitting Model" drop-down menu and "Imported IRF" in the "IRF" drop-down menu.
5. Use the "Import" button next to the "IRF" drop-down menu to import the respective IRF.ptu file. Next, select the imported IRF in the "IRF" drop-down menu.
6. Set the "Model Parameter" according to your donor fluorophore (e.g. n=2 for cytosolic GFP, see **Note 12**).
7. Regions of interest (ROIs) within the image can be selected for the analysis (see **Note 13**).
8. Choose a ROI in the "Decay" drop-down menu for the analysis. If you want to analyze the whole image, choose "Overall decay".
9. Start the actual analysis by pressing firstly "Initial Fit" and then "Fit".
11. Find the " $\tau$  Av int [ns]" value for the calculated fluorescence lifetime in the "Parameters/Value/Fit" table. Note/copy this value for statistical analysis.
12. Check the  $\chi^2$ -value. It describes the quality of the fit and should be close to 1 (see **Note 14**).

13. To illustrate the results, false color images indicating the calculated fluorescence lifetimes can be produced. For this, chose the “Min” (blue) and “Max” (red) values for the “Fast Lifetime[ns]” color scale, accordingly. E.g. for mEGFP a lifetime difference of 100 ps can be visualized by setting “Min” to 2.0 ns and “Max” to 2.4 ns. Next, choose “3 Points” in the “Binning” menu and fix the parameters "Shift IRF" and "Bkgr IRF" by unchecking the corresponding boxes in the “Fit” lane of “Parameters/Value/Fit” table. Then press “FLIM Fit” to start the calculation (see **Note 15**).
14. False color images can be exported by right-clicking on the image to open the drop-down menu. Select “Export” and choose the file format. Here you can also choose to omit the scale bar from the image.
15. If the sample groups of lifetimes show equal variances and normal distribution, the statistical analysis can be performed by applying a one-way ANOVA, otherwise a non-parametric alternative must be chosen. Comparison of the sample groups can be achieved by following up the ANOVA with different post hoc tests: For comparison of all groups with a specific control group (e.g. the “donor-only” group) apply Dunnett’s test. For comparison of all sample groups with each other apply Tukey’s HSD test (see **Note 16**).

#### 4 Notes

1. Achievement of intracellular colocalization of donor and acceptor fluorophores might require the fusion of specific sorting signals to the acceptor fluorophore. E. g. a signal peptide for targeting the lumen of the

endomembrane system or the apoplast, or sorting signals for compartment-specific targeting.

2. The nanobody-epitope interaction between the NbG and GFP was recently shown to also occur in the lumen of all compartments of the secretory pathway (Künzl et al., 2016). However, if the donor fluorophore is fused to membrane proteins, it has to be considered that the NbG-acceptor fusion protein is also targeted to the location of the donor fluorophore (see **Note 1**).
3. These steps are mandatory for the reflected light to reach the detector.
4. This rather high pixel dwell time is of an advantage, since it allows the scan head to collect data for a single pixel over the course of several laser pulses, thereby reducing artifacts caused by the position change of the scan head.
5. It is mandatory that the coverslip used for recording the IRF stays in fixed position during acquisition. Otherwise, the reflection from the coverslip will move out of focus long before 1000 photons have been counted for an individual pixel.
6. While searching for the reflecting surface, adjust the z-position slowly.
7. This is important, since here reflected light is detected and its intensity will be much higher compared to the intensities of fluorescence signals and might therefore damage the detector.
8. If your TCSPC histogram shows multiple pulses or does show one incomplete pulse, it might hint to the fact that your detection window and the pulse rate of the laser do not match. This can be adjusted by an in-



or decrease of the temporal resolution in the SymPhoTime 64 software, respectively.

9. Since the laser intensity is set by an analog rotary controller, that might be changed by other users, recording of the IRF should be performed prior to each data acquisition session.
10. Acquisition of 500 photons/pixel was sufficient for the experiment shown, since the signal was homogeneously distributed over a large area of the specimen and the model used for fitting the fluorescence decay was bi-exponential. However, if signal strengths vary greatly within the specimen or if higher order models are required for fitting the fluorescence decay, more photons have to be counted. This in turn prolongs the acquisition time and might thus compromise the measurement due to the bleaching of signals. Moreover, in case of small and migrating signals, photon counts of more than 500 can hardly be achieved.
11. Apply only the amount of liquid sample that fills the space between the and the microscope slide and the coverslip during mounting to minimize the movement of the protoplasts.
12. The "Model Parameter"  $n$  depends on the decay model of the donor fluorophore. More complex decay models might necessitate higher photon counts (see **Note 10**).
13. This is a very valuable option if you experience strong background fluorescence and allows to exclude "false" fluorescence signals (e.g. from chloroplasts) from the life-time calculations. For this, right-click onto the false color-image and select "free ROI" from the drop down menu. To

create a positive ROI, right click and choose “Invert ROI” to deselect the entire image. Then, hold down “Shift” and press the left mouse button whilst choosing the ROI. To create a negative ROI, hold down “Ctrl” and press the left mouse button whilst choosing the ROI

14. Large  $\chi^2$ -values might indicate that the chosen “Model Parameter” does not match the real fluorescence decay of the donor fluorophore in the micro environment of the sample. Consider this option, adjust the “Model Parameter” accordingly, and re-do your “Initial Fit”.
15. The “3 Points” binning was most suitable for the experiment shown but it decreased considerably the spatial resolution. If a higher resolution is desired, decrease the binning parameter. This however might cause the fit for an individual pixel to rely on only very few photons. This can be checked by clicking on a pixel with an intensity that is representative for your ROI. As a result, an updated graph with the decay for this pixel appears additionally in light grey for direct comparison. If the amounts of photons per pixel is too low for the model in combination with the desired resolution/binning, you will have to increase the amount of photons measured during acquisition (see 3.3 step 6 and **Note 7**).
16. Check if lifetimes of “interactor” samples are significantly lower compared to the “donor-only” sample. If this is not the case, consider that the reduction of the fluorescence lifetime that is caused by FRET effects can be partially masked in cases of a high donor to acceptor ratio, since only a minor portion of donor fluorophores is affected few acceptor fluorophores (**Fig. 2 d**).

## Figure legends

**Fig. 1** Recording of an instrumental response function. **(a)** Total reflection image of the inner surface of the cover slip (see 3.2 step 9 and **Note 6**). **(b)** Total reflection image of the inner surface of only the microscopy slide, which is unsuitable for recording of the IRF.

**Fig. 2** FRET/FLIM analysis in Tobacco mesophyll protoplasts. Panels **(a-c)** protoplasts transfected according to the experimental strategy as outlined in 3.1. **(a)** “donor-only” sample, **(b)** “non-interactor” sample and **(c)** “interactor” sample”. Panel **(d)** “interactor” sample with high donor to acceptor ratio that partially masks the interaction (see **Note 16**). In each panel, GFP channel is given in the first row, the RFP channel is given in the second row, the merge of both channels is given in the third row and the representative false color FLIM image is given together with the respective color scale in the fourth row. Scale bars equal 10  $\mu\text{m}$ . **(e)** Graphical illustration of the processed average fluorescence lifetime of the experiments shown in **a-d**. Values are presented as mean  $\pm$  s.d. ( $n = 10$  individual cells). Statistical significance was calculated using ANOVA, followed by Tukey’s HSD test (\*\* $P < 0.001$ ; NS, not significant).

## References

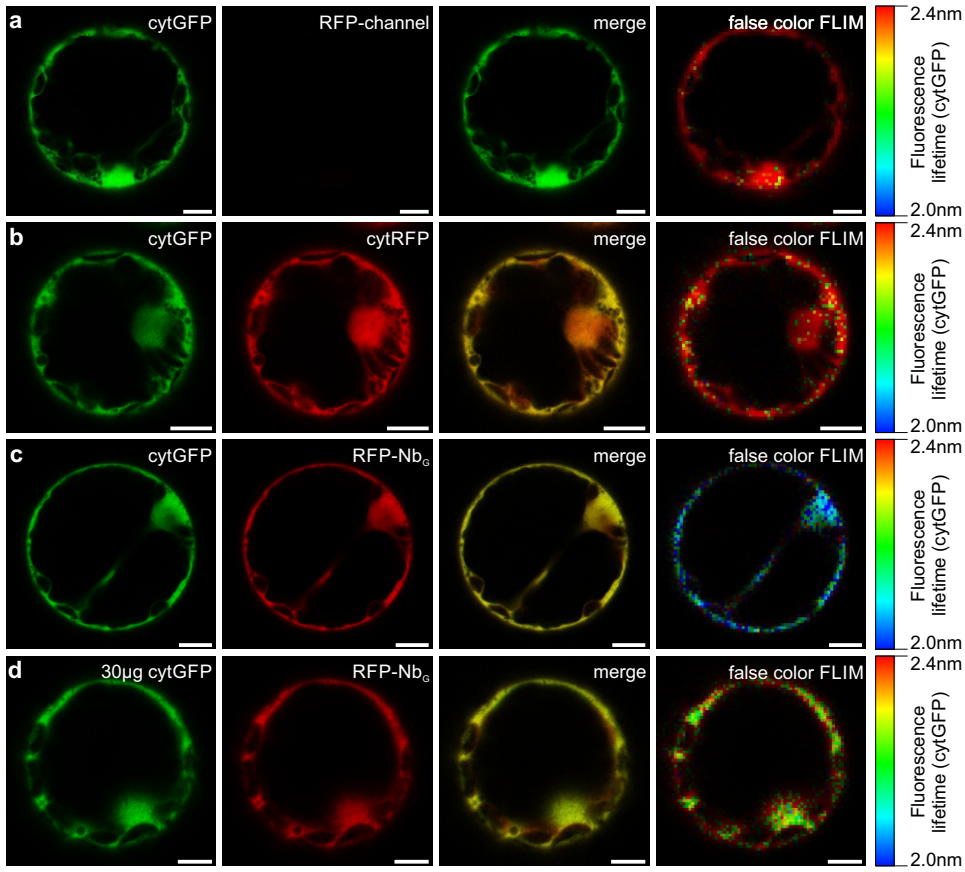
1. Prasher DC, Eckenrode VK, Ward WW, Prendergast FG, Cormier MJ (1992) Primary Structure of the Aequorea-Victoria Green-Fluorescent Protein. *Gene* 111(2):229-233.
2. Chalfie M, Tu Y, Euskirchen G, Ward WW, Prasher DC (1994) Green Fluorescent Protein as a Marker for Gene-Expression. *Science* 263(5148):802-805.

3. Haseloff J, Siemering KR, Prasher DC, Hodge S (1997) Removal of a cryptic intron and subcellular localization of green fluorescent protein are required to mark transgenic Arabidopsis plants brightly. *Proc. Natl. Acad. Sci. USA* 94(6):2122-2127.
4. Shaner NC, Patterson GH, Davidson MW (2007) Advances in fluorescent protein technology. *J. Cell Sci.* 120(Pt 24):4247-4260.
5. Künzl F, Frühholz S, Fäßler F, Li B, Pimpl P (2016) Receptor-mediated sorting of soluble vacuolar proteins ends at the trans-Golgi network/early endosome. *Nature Plants* 2:16017.
6. Niemes S, *et al.* (2010) Sorting of plant vacuolar proteins is initiated in the ER. *Plant J.* 62(4):601-614.
7. De Los Santos C, Chang CW, Mycek MA, Cardullo RA (2015) FRAP, FLIM, and FRET: Detection and analysis of cellular dynamics on a molecular scale using fluorescence microscopy. *Mol. Reprod. Dev.* 82(7-8):587-604.
8. Förster T (1948) Zwischenmolekulare Energiewanderung und Fluoreszenz. *Ann Phys* 437(1-2):55-75.
9. Förster T (1965) Delocalized excitation and excitation transfer. *Modern Quantum Chemistry Part III: Action of Light and Organic Crystals*: 93–137.
10. Edelhoch H, Brand L, Wilchek M (1967) Fluorescence studies with tryptophyl peptides. *Biochemistry* 6(2):547-559.
11. Gadella TWJ, van der Krogt GNM, Bisseling T (1999) GFP-based FRET microscopy in living plant cells. *Trends Plant Sci* 4(7):287-291.
12. Bucherl CA, Bader A, Westphal AH, Laptinok SP, Borst JW (2014) FRET-FLIM applications in plant systems. *Protoplasma* 251(2):383-394.
13. Gadella TWJ, Jovin TM, Clegg RM (1993) Fluorescence Lifetime Imaging Microscopy (Flim) - Spatial-Resolution of Microstructures on the Nanosecond Time-Scale. *Biophys Chem* 48(2):221-239.
14. Buurman EP, *et al.* (1992) Fluorescence Lifetime Imaging Using a Confocal Laser Scanning Microscope. *Scanning* 14(3):155-159.
15. Becker W, Bergmann A, König K, Tirlapur U (2001) Picosecond fluorescence lifetime microscopy by TCSPC imaging. *Proc Spie* 4262:414-419.

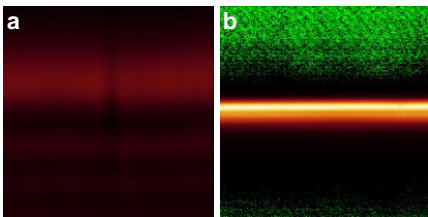
## **Acknowledgement**

We gratefully acknowledge the financial support of the Deutsche Forschungsgemeinschaft (PI 769/1-2 and the Collaborative Research Centre SFB 1101 “Molecular Encoding of Specificity in Plant Processes”) and of the German Academic Exchange Service (Project 57219822).

Fäßler and Pimpl, Figure 1



Fäßler and Pimpl, Figure 2



**Dissection of the ESCRT-II assembly and recruitment by nanobody-based *in vivo* precipitation (iVIP)**

**Florian Fäßler**, Yonglun Zeng, Jasmin S. Ehrismann, Simone Früholz, Carsten-Leo Greve, Liwen Jiang and Peter Pimpl (prepared manuscript)

# Dissection of plant ESCRT-II assembly and recruitment by nanobody-based *in vivo* precipitation (iVIP)

Florian Fäßler<sup>1</sup>, Yonglun Zeng<sup>2</sup>, Jasmin S. Ehrismann<sup>1</sup>, Carsten-Leo Greve<sup>1</sup>, Simone Frühholz<sup>1</sup>, Liwen Jiang<sup>2</sup> and Peter Pimpl<sup>1,3</sup> \*

<sup>1</sup> Center for Plant Molecular Biology (ZMBP), University of Tübingen, Germany

<sup>2</sup> School of Life Sciences, The Chinese University of Hong Kong, Shatin, New Territories, Hong Kong, China

<sup>3</sup> Department of Biology, Southern University of Science and Technology, Shenzhen, Guangdong, China

**\*corresponding author:**

Peter Pimpl, ZMBP, Southern University of Science and Technology, Shenzhen, Guangdong, China 518055

Tel: +86-0755-88018485

e-mail: pimpl@sustc.edu.cn

**Running title:** Assembly and recruitment of ESCRT-II

**Keywords:** nanobodies, ESCRT, protein degradation, FRET-FLIM, indirect *in vivo* precipitation (iVIP), fluorescent-3-hybrid



## Summary

Modulation of compartmental protein composition is crucial for eukaryotic cells. It enables rapid responses to intra-organismal and environmental cues. At the heart of this process, endosomal sorting complexes required for transport (ESCRTs) operate to target ubiquitinated membrane proteins for vacuolar degradation. For this, ESCRTs combine cargo recognition and sorting with intraluminal vesicle formation to sequester to-be-degraded proteins.

However, composition and function of plant ESCRT-II remains controversial.

Here, we present the novel nanobody-epitope interaction-based *in vivo* immune precipitation (iVIP): We employ Calnexin-anchored GFP-nanobodies, to precipitate GFP-tagged proteins onto the endoplasmic reticulum. This also shifts the fluorescence patterns of their direct and indirect interactors allowing for visualization of interactions by microscopy.

We demonstrate plasma membrane (PM) localization of all endogenous ESCRT-II subunits. Employing iVIP, we unravel the 1(VPS36):1(VPS22):2(VPS25) stoichiometry of ESCRT-II. Together, our data indicate that plant ESCRT-II, despite its evolutionary conserved composition, has to have a derived function at the PM.

## Introduction

The plasma membrane (PM) forms the interaction surface between a cell and its environment. There, translocators and receptors allow for the transport of nutrients and information<sup>1,2</sup>. Strict regulation of these proteins is thus necessary to avoid over-accumulation of micronutrients to toxic levels and to terminate signalling processes, respectively<sup>3,4</sup>. One regulatory mechanism controlling PM proteins is their degradation in the lumen of lytic compartments<sup>3-6</sup>. Even though the endosomal sorting complexes required for transport (ESCRTs) are known to be integral components of the underlying sorting process, their individual modes of action in plants remain controversial<sup>7,8</sup>.

In yeast, however, the ESCRT-machinery has been extensively studied and its function during the vacuolar sorting of PM proteins is well described: ESCRT-0, ESCRT-I and ESCRT-II bind and accumulate to be-degraded proteins, which have been marked by ubiquitination, at endosomal membranes<sup>9-11</sup>. ESCRT-III, which is able to deform membranes, induces formation of intraluminal vesicles that are necessary for delivery of membrane-bound proteins into the lumen of the vacuole<sup>12,13</sup>. Recruitment of ESCRT-III in this process is mediated by ESCRT-II and, as has very recently been shown, ESCRT-0<sup>13,14</sup>. This means localization after membrane recruitment and *locus operandi* of ESCRTs are essentially the same. For a possible plant ESCRT-II this, however, does not seem to be the case: Contrary to genetic evidence, which hints towards a conserved function of the putative subunit vacuolar protein sorting 36 (VPS36) at maturing endosomes, initial imaging studies performed with tagged VPS36 indicate almost exclusive PM localization<sup>8,15</sup>.

To resolve these contradictions, the localization of the endogenous VPS36 and of the other putative subunits as well as the actual composition of a plant ESCRT-II complex had to be analysed.

While performing localization studies and most *in vivo* protein-protein interaction analyses with established techniques as electron microscopy and FRET-FLIM, respectively, was feasible, the analysis of the ESCRT-II stoichiometry in living cells necessitated us to devise a novel approach: the indirect *in vivo* immune precipitation (iVIP). This technique is an advanced version of fluorescent-3-hybrid approach<sup>16</sup>. It employs an endoplasmic reticulum (ER)-surface anchored antibody, which recognizes GFP, to pull down GFP-tagged proteins and their fluorescently tagged direct and, most importantly, indirect interactors. The resulting shift of fluorescence pattern is observable, even in situation, in which molecule geometry, expressed numbers of

complex subunits or fluorophore ratios are unfavourable for other *in vivo* interaction analysis. To turn the ER into an affinity matrix for GFP, we translationally fused the V<sub>H</sub>H domain of a lama (*Lama pacu*) heavy-chain-only antibody, a so called nanobody (Nb), that was raised against GFP (Nb<sub>G</sub>) to the C-terminus of a derivative of the ER resident chaperon Calnexin (CNX)<sup>17,18</sup>. This cell autonomous expression of the antibody employed for the intracellular immune precipitation and the confocal based read out distinguish iVIP as a non-invasive protein-protein interaction assay. Using this technique and FRET FLIM we demonstrate, that VPS36, VPS22 and VPS25 assemble in a 1:1:2 ratio to form the plant ESCRT-II complex. We furthermore show the presence of all endogenous ESCRT-II subunits at the PM via immune electron microscopy. Together our data indicate that ESCRT-II is specifically recruited to the PM via its VPS36 subunit to fulfil a yet elusive function.

## RESULTS

### The ESCRT-II subunit VPS36 is essential for viability and localizes to the plasma membrane

The ESCRT-II subunit VPS36 was suggested to form the core of the ESCRT-II complex that links the cargo recognition function of ESCRT-I to the ESRT-III-triggered formation and release of ILVs, thereby fulfilling the sorting function that is essential to plant viability<sup>8</sup>. *Arabidopsis* seedlings, homozygous for a T-DNA insertion in the *VPS36* Gene (*vps36-1*) (**Fig. 1a**) exhibit strong delays in development during the first ten days after stratification (**Fig. 1b**) and die during or shortly after germination, respectively (**Fig. 1c,d**). *vps36-1* mutant plants have a similar appearance as *amsh3* and *free1* knock-out seedlings, which have to cope with impaired vacuolar transport of membrane proteins<sup>19,20</sup>. This lethal *vps36-1* phenotype is solely due to the lack of VPS36 function, since it is rescued by the expression of VPS36 fused to GFP (VPS36-GFP), under the control of the endogenous promotor (*pVP36*; **Fig. 1e,f**). Interestingly, VPS36-GFP mainly localizes to the PM in these rescue lines (*pVPS36::VPS36-GFP* in the *vps36-1* background) as judged by the co labeling of the PM with the styryl Fei-Mao dye 4-64 (FM4-64; **Fig. 1g,h**). FM4-64 serves also as marker for endosomal compartments<sup>21</sup>. However, in sharp contrast to the strong co-localization of signals at the PM, little co-localization is found between the VPS36-GFP signals and FM4-64 labeled endosomes (**Fig. 1h**).

Despite of its rescuing effect, the rather unexpected distribution of VPS36-GFP at the PM necessitated thorough localization analysis to exclude putative influences caused by the fluorescent tag<sup>22</sup>. Therefore, we aimed at localizing the endogenous VPS36 at the ultrastructural level<sup>22</sup>. For this, and to extend the analysis to all putative ESCRT-II subunits, we generated polyclonal antibodies against all three *Arabidopsis* ESCRT-II subunits. The antisera raised against VPS36, VPS22 and VPS25 exhibit specific cross-reaction with the respective antigens in protein gel blots, even when less than 10 ng of antigen were loaded per lane (**Fig. 1i**). However, since the envisaged *in situ* localization necessitated recognition of native epitopes, we also verified that all generated antisera exhibit cross-reactivity with their respective native antigens in immunoprecipitation experiments using HA-tagged ESCRT-II subunits (**Fig. 1j**).

Ultrastructural localization analysis of ESCRT-II subunits in high-pressure frozen *Arabidopsis* roots reveals immunogold decoration of the PM demonstrating the localization of the endogenous VPS36, the VPS22 and the VPS25 subunit at the PM (**Fig. 1k-m**). Together, these data show that the endogenous proteins are predominantly found at the PM, which is in complete agreement with the situation in the transgenic plants (**Fig. 1g,h**) and protoplasts co-expressing fluorescently tagged derivatives of all three putative ESCRT-II subunits (**Fig. 1q**).

### **VPS36 is necessary for the PM recruitment of VPS22 and VPS25**

It was suggested that membrane recruitment of the ESCRT-I complex in plants occurs via a subunit, FREE1<sup>19</sup>, while in the case of ESCRT-III subunits attach to the membranes individually<sup>7</sup>. To differentiate between these concepts of membrane binding in the case of ESCRT-II, we have analyzed the individual membrane binding capabilities of the putative subunits in tobacco mesophyll protoplasts.

VPS36-GFP perfectly co-localizes with a PM marker consisting of RFP and the GCCG Box of the ROP GTPase Rop10 (Box-RFP; **Fig. 2a**)<sup>6,23</sup>. Surprisingly, if VPS22-RFP or VPS25-RFP are individually co-expressed with the PM marker Box-GFP, both molecules do not co-localize with the marker but remain cytosolic, instead (**Fig. 2b,d**). However, co-expression of VPS36-GFP with either of them results in co-localization at the PM (**Fig. 2c,e**). This is most evident from the overlapping peaks of the corresponding fluorescence intensity plots of the enlargements of the merged images.

To rule out that the observed PM-localization of VPS36-GFP alters the membrane identity of the PM, thereby causing unspecific recruitment of VPS22 and VPS25, we have performed a location-

specific protein-protein interactions study at the PM via FRET-FLIM (**Fig. 2f-h**). The analysis showed, that co-expression of either of the potential energy acceptors, VPS22-RFP or VPS25-RFP, drastically reduces the fluorescence lifetime of the energy donor VPS36-GFP (**Fig. 2f**, see false-color images) This indicates the interaction of these proteins at the PM and implies the existence of a plant ESCRT-II complex consisting of VPS22, VPS25 and VPS36. A similar effect does not occur, if cytosolic RFP (cytRFP) is co-expressed as potential energy acceptor (**Fig. 2f,h**). Here, the measured fluorescence lifetime is comparable to the one of individually expressed VPS36-GFP (**Fig. 2f,g**).

To proof VPS36-triggered co-recruitment of the other ESCRT-II subunits and to narrow down putative regions necessary for the interaction, we have subjected C-terminal deletion mutants of VPS36-GFP lacking either 33 (VPS36 $\Delta$ 33-GFP) or 132 (VPS36 $\Delta$ 132-GFP) residues to co-expression analysis with VPS22-RFP or VPS25-RFP, respectively. VPS36 $\Delta$ 33-GFP is no longer able to bind VPS25-RFP, judged by the unaltered GFP fluorescence lifetime (**Fig. 3a,b**). This is also supported by the fact that unlike the full-length VPS36-GFP (**Fig. 2e,f**) this mutant fails to co-recruit VPS25-RFP to the PM (**Fig. 3c**). In contrast, VPS36 $\Delta$ 33-GFP is still able to bind VPS22-RFP and to co-recruit it to the PM (**Fig. 3a-c**). The ability to bind VPS22-RFP is only lost when 132 residues are deleted, since VPS22-RFP does neither trigger a reduction of the fluorescence lifetime of VPS36 $\Delta$ 132-GFP (**Fig. 3d,e**) nor is co-recruited to the PM by the mutant (**Fig. 3f**), as was shown for VPS36-GFP (**Fig. 2c,f**).

Interestingly, interaction of VPS25 is not restricted to VPS36 only (**Fig. 3g-i**), since the FRET-FLIM analysis reveals a reduction of the fluorescence lifetime of VPS25-GFP upon co-expression of either VPS36-RFP or VPS22-RFP (**Fig. 3g**). However, in the absence of the complex-recruiting VPS36 subunit, the VPS25-VPS22 complex remains cytosolic (**Fig. 3i, compare to Fig.1q**). With VPS25 interacting with both, VPS36 and VPS22, the question arose whether the very same VPS25 molecule binds to both of the other subunits or if VPS36 and VPS22 bind one separate VPS25 moiety each, as it is the case in yeast<sup>24</sup>. To approach this in an *in vivo* situation, a novel strategy to test for protein-protein interaction had to be deployed.

### **Indirect *in vivo* immune precipitation (iVIP)**

To determine whether one or two VPS25 moieties are integrated in an ESCRT-II complex, simple co-localization experiments, which employed co-expression of VPS25 molecules tagged with different fluorophores, were not sufficient. In the presence of VPS36 and VPS22 both

VPS25 fusion proteins are expected to be recruited to the PM resulting in co-localization independently of ESCRT-II conformation (**Fig. 4a,b**). In addition, the application of FRET-FLIM based on co-expressed VPS25-GFP and VPS25-RFP is impaired in this context: If ESCRT-II indeed contains only one VPS25 subunit no FRET and thus no lifetime reduction occurs. If two VPS25 moieties are present in each ESCRT-II the chance of one complex, which contains already one VPS25-GFP to attain another VPS25-GFP and not a VPS25-RFP, is 50%. In those complexes, which would then contain two donors instead of one donor and one acceptor, hetero FRET cannot occur. This would mask the FRET-effects occurring in complexes, which contain VPS25-GFP and VPS25-RFP, and thus compromise lifetime measurements (**Fig. 4b**). To overcome this, we aimed at employing nanobodies to apply a classical *in vitro* interaction method, namely the immune precipitation, in living cells. In this regard, we refined the fluorescent-3-hybrid technique, which has been used to assess direct interactions by precipitating fluorescently tagged proteins onto easily discernable intracellular structures, to be applicable for the analysis complex composition<sup>16</sup>: We planned to express an antiGFP nanobody (Nb<sub>G</sub>) fused to the C-terminus of the ER resident transmembrane protein Calnexin (CNX-Nb<sub>G</sub>), effectively turning the ER surface into an affinity matrix for GFP-tagged cytosolic proteins. Under these conditions, co-expression of VPS25-GFP, VPS25-RFP, VPS36 and a VPS22 fused to BFP2 (VPS22-BFP) was expected to produce differential outcomes depending on the conformation of the ESCRT-II complex. If one ESCRT-II only contains one VPS25 moiety, ER recruitment should only occur for complexes, which have integrated VPS25-GFP resulting in GFP and BFP fluorescence at the ER (**Fig. 4c**). If on the contrary ESCRT-II contains two VPS25 moieties, also VPS25-RFP should be co-recruited to ER resulting in GFP, BFP and RFP fluorescence at the ER (**Fig. 4d**). As our technique was based on the principles of immune precipitation, was intended to be performed in living cells and aimed at assessing the putative indirect interaction between two VPS25 moieties we dubbed it indirect *in vivo* precipitation (iVIP).

Still one problem had to be solved with this system: The expression of VPS36 had to be verified and the use of an additional fluorophore was technically not feasible. We combined two strategies to solve this problem. First, we fused a small tag to VPS36 to proof general expression in a population of protoplasts by Western blot analysis. Second, we made use of the fact, that VPS36 is recruited to the PM, to judge whether an individual cell is expressing the protein or not.

The tag of choice to allow for Western blot analysis was the  $\alpha$ -synuclein epitope (SYN), which was recognized by the SYN-nanobody (Nb<sub>SYN</sub>)<sup>25,26</sup>. As a detection reagent, we expressed a

secretory Nb<sub>SYN</sub>-horseradish-peroxidase fusion construct (Nb<sub>SYN</sub>-HRP) in protoplasts (**Fig. 4f**). The concentrated and rebuffed secreted protein can be used in Western blot applications to detect as little as 8 ng of purified antigen (**Fig. 4g**). To verify the applicability of this detection system we employed it on extracts from protoplast and, indeed, Nb<sub>SYN</sub>-HRP allowed for the detection of secreted, membrane-bound and cytosolic SYN-tagged proteins (**Fig. 4h**).

To verify expression of VPS36-SYN in individual cells, we wanted to exploit the combination of ESCRT-II being recruited to the ER via the VPS25-GFP-CNX-Nb<sub>G</sub> interaction as well as being simultaneously recruited to the PM via VPS36-SYN. This should attach the ER to PM resulting in a distinct morphological ER phenotype. To determine whether such an attachment of the ER to PM could be generally induced, we co-expressed CNX-Nb<sub>G</sub>, the ER marker RFP-HDEL and the PM marker Box-GFP. In this case, the nanobody-epitope interaction should bridge CNX-Nb<sub>G</sub> and Box-GFP thus forcing the ER into close proximity of the PM. The co-expression of these molecules, indeed, changed ER morphology. In comparison to wildtypic ER (**Sup.Fig. 1a**), cisternae increased in surface and formed laminar structures at which ER marker and PM marker co-localized (**Sup.Fig. 1b,c**). While laminar cisternae varied in size (**Sup.Fig. 1b,c**), reticular structures, however, remained unaltered (**Sup.Fig. 1a-c**). The same effects were achieved if VPS36-GFP was expressed instead of Box-GFP (**Sup.Fig. 1d-f**), again substantiating the specific recruitment of VPS36 to the PM. Furthermore, the co-localization of ER marker, VPS36-GFP and FM4-64 upon co-expression of CNX-Nb<sub>G</sub> at the PM in equatorial optical sections clearly showed that the ER is brought into very close proximity of the PM via the nanobody-epitope interaction (**Sup.Fig. 1g-j**). Thus, changes in ER morphology and localization could be exploited to detect the presence of non-fluorescently tagged VPS36 during upcoming iVIP experiments.

Since fluorescent-3-hybrid and thus iVIP was a completely novel experimental strategy in a plant system, we opted for an initial characterization prior to applying it to such complex problems as the stoichiometric analysis of ESCRT-II. As a first step, we showed that cytosolic GFP (cytGFP) but not cytRFP is recruited from the cytosol to a BFP-CNX-labeled ER when CNX-Nb<sub>G</sub> is co-expressed (**Fig. 5a,b**). The second step was to co-express VPS25-GFP and VPS25-RFP instead of cytGFP and cytRFP, respectively, with BFP-CNX. Again, only when additionally CNX-Nb<sub>G</sub> was present, the GFP signal did not co-localize with the RFP signal in the cytosol, but did match the signal distribution of the ER marker BFP-CNX (**Fig. 5c,d**). These changes, or the respective lack thereof, in the localization of small proteins like cytGFP, cytRFP, VPS25-GFP and VPS25-RFP is especially evident in the nucleus (**Fig. 6a-d**, inlays): Here the differences between localization

in the nuclear lumen and localization at the surrounding nuclear envelope can be unequivocally assessed via confocal microscopy (**Sup.Fig. 2a**). Since direct precipitation of GFP-tagged proteins proved to be feasible, we went on to intracellular co-immune precipitations. Therefore, we co-expressed either VPS22-RFP or VPS36-RFP with VPS25-GFP, CNX-Nb<sub>G</sub> and BFP-CNX. Consistent with the FRET-FLIM results (**Fig. 2f**) also fluorescent-3-hybrid indicated interaction between VPS25-GFP and each of the other two ESCRT-II subunits: Both, VPS22-RFP and VPS36-RFP could be co-precipitated upon the surface of the ER resulting in their co-localization with BFP-CNX (**Fig. 5e,f**). In the case of VPS36-RFP this led, as expected, also to the attachment of the ER to the PM (**Fig. 5f,g**) and to the formation of laminar cisternae (**Fig. 5g,h**). Notably one of the results of this characterization is also that VPS25 molecules do not interact with each other, since VPS25-RFP in opposition to VPS22-RFP and VPS36-RFP did not co-precipitate with VPS25-GFP (**Fig. 5d-f**). Now, with fluorescent-3-hybrid being able to show protein-protein interaction *in vivo* and VPS36-SYN expression being observable on a single cell level, the stage was set to probe the conformation of ESCRT-II for the presence of a second VPS25 moiety via iVIP.

### **One ESCRT-II complex contains two VPS25 molecules**

To assess whether ESCRT-II contains one or two VPS25 subunits, we co-expressed VPS25-GFP, VPS25-RFP, VPS22-BFP, VPS36-SYN and CNX-Nb<sub>G</sub>. With this iVIP setting CNX-Nb<sub>G</sub> should pull down VPS25-GFP resulting in co-precipitation of the whole ESCRT-II complex. If the individual complexes contained no additional VPS25 molecule, VPS25-RFP should not be co-precipitated (**Fig. 4b**). If ESCRT-II, however, includes a second VPS25 moiety, VPS25-RFP can be co-recruited to the ER (**Fig. 4c**). The latter was indeed the case. VPS25-RFP co-localizes with the remainder of the co-expressed ESCRT-II subunits on the surface of laminar ER cisternae and at the nuclear envelope (**Fig.6 a-c**). This finding was further reinforced by the results of line intensity analysis showing perfectly matching peaks for all fluorescently tagged ESCRT-II subunits (**Fig. 6c**).

These observations, however, can only be made if both, VPS36-SYN and VPS22-BFP, are co-expressed. When VPS36-SYN is absent, VPS25-RFP stays cytosolic and is not co-recruited to the ER (**Fig. 6d-f**). This is indicated by the RFP signal not highlighting the filamentous ER structures labelled by VPS25-GFP and VPS22-BFP (**Fig. 6e**), the absence of VPS25-RFP from the nuclear envelope (**Fig. 6f**, inlays) and the lack of a clear peak in the line intensity profile for



VPS25-RFP. The situation is similar, when VPS22-BFP is absent instead of VPS36-SYN. Again, VPS25-RFP is not present at laminar ER cisternae (**Fig. 6g,h**) and exhibits strong fluorescence signal in the nuclear lumen (**Fig. 6j**, inlays). Its corresponding line intensity profile does, furthermore, not match with the one of VPS25-GFP (**Fig. 6j**). The presence of laminar ER cisternae in this experiment (**Fig.6g,h,j**) and in the one mentioned above (**Fig. 6a-c**) indicated VPS36-SYN expression, which was also verified by Western blot analysis (**Fig. 6i**). Together this additionally showed, that while VPS22 and VPS36 can individually interact with one VPS25 molecule each, neither of them alone is capable of binding two VPS25 moieties.

## Discussion

Nanobodies, the isolated V<sub>H</sub>H domains of camelid antibodies, consist of as little as about 125 amino acids and are the smallest polypeptides, which specifically bind their respective antigens<sup>27</sup>. Since nanobodies can be translationally fused to cytosolic and membrane bound proteins, they allow for a plethora of *in vivo* applications, which are usable in basic research and applied sciences such as localization, reallocation and degradation of proteins<sup>28-30</sup>.

We have previously employed nanobodies in the endomembrane system to target the luminal binding domain of a vacuolar sorting receptor (VSR) to different compartments, which ultimately allowed for localization specific interaction studies of VSRs and a model ligand<sup>18</sup>. In this case, we determined the *in vivo* interaction of the two proteins via FRET-FLIM. For the analysis of ESCRT-II stoichiometry in living cells however, a FRET based readout was not feasible (**Fig. 4b**). This problem asked for a technique that allowed investigating direct and indirect protein-protein interactions, even if more than one moiety of a specific subunit might be present in a complex.

We solved those issues by exploiting a purely localization based read out. For this to work we had to specifically alter the localization of one ESCRT-II subunit and monitor the effect on the intracellular distribution of another fluorescently tagged subunit depending of the presence or absence of additional interactors. To ensure high specificity we employed the well-established Nb<sub>G</sub>-GFP antibody-epitope combination to recruit GFP-tagged ESCRT-II subunits onto a CNX-Nb<sub>G</sub> containing ER, without perturbing the integrity of the monitored cells (**Sup.Fig. 3**)<sup>17,18,26</sup>.

Applying this approach, we were able to show that the 1(VPS36):1(VPS22):2(VPS25) stoichiometry of ESCRT-II is also conserved in plants.

Even though fluorescent-3-hybrid and iVIP were brought into a plant system or respectively designed for this very case, they can be used in general to probe indirect interactions of soluble and even membrane recruited cytosolic proteins. However, their applicability is not restricted to protein-protein interaction, they can also be used to verify protein-membrane interactions. Both membrane associated proteins, VPS36-GFP and Box-GFP, but not completely cytosolic proteins as VPS25-GFP, were found to force the ER into close proximity to the PM when co-expressed with CNX-Nb<sub>G</sub>. They thereby induce a visually distinguishable, yet not functionally impaired, ER-phenotype (**Sup.Fig. 3**). Due to the variety of purposes these techniques are able to fulfill and the fact that they can be performed on a confocal microscope without the need of further upgrades, we envision fluorescent-3-hybrid and iVIP to be a viable addition to the toolbox of many plant cell biologists.

In addition to studying ESCRT-II composition, we also aimed at clarifying the localization of the endogenous ESCRT-II in living plants, since the almost exclusive presence of heterologously expressed VPS36 fusion proteins at this site, does not match with the endosomal function suggested by genetic evidence<sup>8,15</sup>. Interestingly, all three subunits were, indeed, detected at the PM and not just at endosomal structures of *Arabidopsis* root cells via immune electron microscopy (**Fig. 1k-q**). While the presence at endosomes can be explained by the involvement in the ‘classical’ ESCRT function, namely the sorting of ubiquitinated cargo into the intraluminal vesicles (ILVs) of the forming multivesicular bodies<sup>31</sup>, PM localization indicates an additional function at this very site.

ESCRT functions at the PM, which could also exist in plant cells and are described in other systems, include polar distribution of mRNA, PM repair and the formation of extracellular microvesicles<sup>32-35</sup>. Nevertheless, up to this point we do not know of any evidence supporting a role of ESCRT-II in these processes.

However, there is still the possibility of another function, which would also fit to the provided genetic evidence regarding VPS36: It has been shown that VPS36 is necessary for the formation of ILVs and that *vps36-1* mutant plants macroscopically phenocopy *amsh3* and *free1* seedlings (**Fig. 1b,c**)<sup>8,19,20</sup>, thus ESCRT-II might not be involved in an completely different process, but much rather play an additional earlier role in ubiquitin-dependent degradation of PM proteins. Even though Tom1-like proteins have been suggested for this function<sup>36</sup>, the identity of the initial ubiquitin receptor linking to-be-degraded proteins to endocytosis has not been finally resolved. Indeed, this role fits ESCRT-II not only localization wise, since specifically poly-ubiquitinated

proteins are endocytosed and VPS36 possesses more than one ubiquitin binding site, a property that has been associated with preferential binding to ubiquitin chains<sup>6,8,37</sup>. Furthermore, this would allow for an efficient interaction with FREE1/ESCRT-I and subsequent recruitment of ESCRT-III upon the arrival of a putative ESCRT-II-cargo complex at phosphoinositide-3-phosphate positive endosomes<sup>15,38-42</sup>.

## Methods

**Plant materials.** *Nicotiana tabacum* L. SR1 was grown on Murashige and Skoog medium additionally containing 2 % (w/v) sucrose, 0.5 g L<sup>-1</sup> MES and 0.8 % (w/v) Agar at pH 5.7 in 16/8 h light–dark cycles at 22 °C. *Arabidopsis thaliana* (L.) Heynh Col-0 was grown on MS medium supplemented with 1 % Agar at pH 5.7 in 16/8 h light–dark cycles at 22 °C. 2-week-old seedlings were transferred on soil and grown in 16/8 h light–dark cycles at 22 °C and 50 % relative humidity.

**Plasmid constructs.** Cloning strategies for all constructs are given in Supplementary Table 1. DNA manipulations were performed according to established procedures, using pGreenII<sup>6</sup>, pGEX-4T-3 (GE Healthcare Life Sciences) or pET-28b (EMD Biosciences) vectors and *Escherichia coli* MC1061. The sequences encoding the blue fluorescent fluorophore mTagBFP2 (GenBank AIQ82697.1) and *Gallus domesticus* lysozyme (NCBI Reference Sequence: P\_00698) were generated by reverse-translation of the amino acid sequence optimized for *Arabidopsis*-specific codon usage (EMBOSS Backtranseq), modified with an N-terminal HA-tag and chemically synthesized (GeneArt Gene Synthesis). The coding sequences of *AtVPS22*, *AtVPS25* and *AtVPS36* were PCR amplified from seedling cDNA. The coding sequence of *HRP* was amplified from pUC19-HRP-C<sup>42</sup>, which was a gift from Paul Ortiz de Montellano (Addgene plasmid # 40163).

**Protoplast isolation and gene expression.** Protoplasts were isolated by perforating leafs and incubating them in incubation buffer (3,05 g L<sup>-1</sup> Gamborg B5 Medium, 500 mg L<sup>-1</sup> MES, 750 mg L<sup>-1</sup> CaCl<sub>2</sub>·2H<sub>2</sub>O, 250 mg L<sup>-1</sup> NH<sub>4</sub>NO<sub>3</sub> adjusted to pH 5.7 with KOH) supplemented with 0.2 % w/v macerozyme and 0.4 % w/v cellulase) in the dark at 25 °C over-night. Three washing steps employing 50 mL of electrotransfection-buffer (137 g L<sup>-1</sup> sucrose, 2.4 g L<sup>-1</sup> HEPES, 6 g L<sup>-1</sup> KCl, 600 mg L<sup>-1</sup> CaCl<sub>2</sub>·2H<sub>2</sub>O adjusted to pH 7.2 with KOH), each, were used to rebuffer the

protoplasts. Per transfection 150  $\mu\text{L}$  of protoplasts were diluted in a total volume of 600  $\mu\text{L}$  electrotransfection-buffer containing 1–10  $\mu\text{g}$  of the employed plasmid DNA. Electrotransfection was performed using the square-wave pulse generator EPI-2,500 (Fischer) applying a single pulse at 130 V for 10 ms. Transfected protoplasts samples were then supplemented with 2 mL incubation buffer and incubated in the dark at 25 °C for 18-24 h.

**Production and characterization of antibodies.** spNb<sub>S</sub>-HRP was expressed in protoplasts and secreted into the culture medium. The fusion protein was rebuffed in TBS and 3 times enriched by using centrifugal filters with a cut-off of 10kDa (Merck UFC801024). GST- or 8xHis-tagged VPS22, VPS25 and VPS36 and GST-tagged HA-RFP-SYN were expressed for 3 h in *Escherichia coli* BL21 after induction with 1 mM IPTG. Expressed proteins were extracted from cells via incubation in TBS (6.06 g l<sup>-1</sup> Trizma base, 8.88 g l<sup>-1</sup> NaCl, 0.05 % (v/v)) supplemented with 0.4 g l<sup>-1</sup> Lysozyme on ice for 15 min. Solubilisation from inclusion bodies was achieved by addition of DTT, N-laurylsarcosine and Triton-X-100 at final concentrations of 0.5 mM, 1.5 % (v/v) and 4 % (v/v), respectively, followed by sonication on ice<sup>43</sup>. Affinity purification of extracts was performed with GST-Sepharose or Ni-NTA, respectively. Further purification of GST-tagged proteins destined for application in the immunization program was performed via SDS-PAGE and cutting of the bands of interest. Bands containing a total of 400  $\mu\text{g}$  of GST-tagged antigen were used for commercial immunization of rabbits (Eurogentec). Purified 8xHis-tagged antigen was used for the characterization of the resulting antibodies. GST-tagged HA-RFP-SYN was used for the characterization of Nb<sub>S</sub>-HRP.

**Immune-electron microscopy.** Root tips of 7-days-old wild type Arabidopsis seedlings were cut and immediately frozen in a high-pressure freezer (EM PACT2, Leica, Germany). This was followed by subsequent freeze substitution in dry acetone containing 0.1% uranyl acetate at -85 °C in an AFS freeze-substitution unit (Leica, Wetzlar, Germany). Infiltration with HM20, embedding and UV polymerization were performed stepwise at -35 °C<sup>37</sup>. Immunogold labeling was performed with anti-VPS22, anti-VPS25 and anti-VPS36 sera at a 1:60 dilution and gold-coupled secondary antibody at 1:50 dilution. Aqueous uranyl acetate/lead citrate poststained sections were examined in a Hitachi H-7650 transmission electron microscope with a CCD camera (Hitachi High-Technologies Corporation, Japan) operating at 80 kV.

**Confocal microscopy and statistical analysis.** Images were acquired using a Leica TCS-SP8 confocal laser-scanning microscope equipped with a x63 (1.2 numerical aperture) water immersion objective. HyDs were employed in sequential line scanning mode to detect the emission (em) of excited (ex) fluorophores: mTagBFP2 (ex/em, 405 nm/407-452 nm), GFP (ex/em, 488 nm/496–525 nm) and RFP (ex/em, 561 nm/589–636 nm). Pinholes were adjusted to 1 Airy unit for the emission of the individual fluorophores. For endosomal labelling FM4-64 (1:700 in ddH<sub>2</sub>O) was added 10 min prior to imaging. Post-acquisition image processing was performed with Adobe Photoshop CS3 and figures were assembled with CorelDraw X8. Line-intensity profiles were generated with LAS AF using the Line Profile tool.

### **Fluorescence lifetime imaging microscopy.**

Data was acquired with a Leica TCS-SP8. A PicoHarp 300 and a PDL 808 Sepia (both PicoQuant) were used as TCSPC module and diode laser driver, respectively. GFP was excited via a 470 nm laser (LDH-P-C-470B) at a pulse frequency of 40 MHz. Emission was detected at 496-525 nm by TCSPC employing a SMD Emission SPFLIM PMT. SymPhoTime 64 v2.1 (PicoQuant) was used for the analysis<sup>44</sup>. TCSPC was performed until a photon count per pixel of 500 was reached. The resulting histograms were deconvoluted using an instrumental response function before fitting them to a bi-exponential decay function. Fittings resulting in a chi-squared value between 1 and 2.5 were used for calculating the presented average values, for which at least 10 cells per experiment condition were considered. Sample size was estimated based on previously achieved effect sizes in our lab: Effect size  $f$  (ANOVA) for the data shown in Figure 3a<sup>18</sup> was 1.35; with our desired error values ( $\alpha=0.001$ ,  $(1-\beta)=0.95$ ) and 4 different groups of samples this computes to a minimum of 28 total samples or 7 samples per group. Calculation was performed using G\*Power Version 3.1.9.2. We chose to increase this number to 10 samples per group to accommodate for possible slightly weaker effect sizes or data point distributions, which would necessitate alternative non-parametric tests.

Shapiro-Wilk test for normality<sup>45</sup> was applied to analyse variances. Since several groups showed non-normal distribution, statistical significance was calculated using Dunn's method for multiple comparisons with a single control (JMP®, Version 13. SAS Institute Inc., Cary, NC, 1989-2017).

**Harvesting, protein extraction and immunoblotting.**

Cell-free culture media samples were harvested after flotation of electrotransfected tobacco protoplasts at 80 g for 5 min in sealed pre-punctured harvesting tubes, using insulin syringes.

Protoplast cell samples were prepared by transferring transfected protoplast samples into harvesting tubes adding 7.5 mL of 250 mM NaCl to them and sedimenting them at 80 g for 5 min. The resulting sediment was resuspended in a total of 250 mL extraction buffer (100 mM Tris, pH 7.8, 200 mM NaCl, 1 mM EDTA, 2 % (v/v)  $\beta$ -mercaptoethanol and 0.2 % (v/v) Triton X-100) and lysed via sonication. Media and cell samples were then cleared via centrifugation at 20,000 g and 4 °C for 15 min. Supernatants were diluted 1:1 with 2xXtreme Loading dye (900  $\mu$ L of sample buffer (0.1 % (w/v) bromophenol blue, 5 mM EDTA, 200 mM Tris-HCl, pH 8.8, 1M sucrose) supplemented with 300  $\mu$ L 10 % w/v SDS and 20  $\mu$ L of 1 M DTT)<sup>46</sup>, incubated at 95 °C for 5 min and loaded onto SDS-polyacrylamide gels. Electrophoretic separation was performed at 40 mA and followed by electroblotting of proteins onto nitrocellulose membranes at 200 mA for 60 min.

Purified 8xHis-tagged proteins and GST-tagged HA-RFP-SYN expressed in *E. coli* were diluted to the desired concentration in 1:1 TBS:2xXtreme Loading dye<sup>46</sup>, further electrophoretic separation and immunoblotting was performed as stated above for protoplast samples.

Nitrocellulose membranes were washed in TBS-T (TBS supplemented with 0.05 % (v/v) Tween-20), blocked in blocking solution (TBS-T supplemented with 5 % (w/v) BSA) and probed with the following antibodies in blocking solution:

Rat monoclonal anti-HA-Peroxidase (Roche 12013819001, 1:2.500), rabbit polyclonal anti-VPS22 (1:1000), rabbit polyclonal anti-VPS25 (1:1000), rabbit polyclonal anti-VPS36 (1:1000), rabbit polyclonal anti-GFP (Life Technologies A6455, 1:10,000) and spNb<sub>SYN</sub>-POD (1:100).

**Immunoprecipitation.** Cell samples were extracted in a total volume of 250  $\mu$ l Protoplast homogenization buffer (200 mM Tris/HCl, 300 mM NaCl, 1mM EDTA, 1 % (v/v) Triton X-100, pH 8) and then made up to 1.25 mL with NET-Gel buffer (50 mM Tris/HCl, 150 mM NaCl, 1mM EDTA, 0.25 % (w/v) Gelatine, 1% (v/v) Triton X-100, pH7.5). Immunoprecipitation was performed for 1 h using Dynabeads<sup>TM</sup> Protein A (invitrogen, 10001D), which were pre-coated with the indicated immune sera, at 4°C. Beads were washed four times with NET-Gel buffer. SDS-PAGE/WB was performed as described above.

**Replication.** All experiments were replicated at least twice.

## References

- 1 Noguchi, K. *et al.* bor1-1, an Arabidopsis thaliana mutant that requires a high level of boron. *Plant Physiol* **115**, 901-906, doi:115/3/901 [pii] (1997).
- 2 Zipfel, C. *et al.* Bacterial disease resistance in Arabidopsis through flagellin perception. *Nature* **428**, 764-767, doi:10.1038/nature02485 (2004).
- 3 Kasai, K., Takano, J., Miwa, K., Toyoda, A. & Fujiwara, T. High boron-induced ubiquitination regulates vacuolar sorting of the BOR1 borate transporter in Arabidopsis thaliana. *J Biol Chem* **286**, 6175-6183, doi:10.1074/jbc.M110.184929 (2011).
- 4 Lu, D. *et al.* Direct ubiquitination of pattern recognition receptor FLS2 attenuates plant innate immunity. *Science* **332**, 1439-1442, doi:10.1126/science.1204903 (2011).
- 5 Martins, S. *et al.* Internalization and vacuolar targeting of the brassinosteroid hormone receptor BRI1 are regulated by ubiquitination. *Nat Commun* **6**, 6151, doi:10.1038/ncomms7151 (2015).
- 6 Scheuring, D. *et al.* Ubiquitin initiates sorting of Golgi and plasma membrane proteins into the vacuolar degradation pathway. *BMC plant biology* **12**, 164, doi:10.1186/1471-2229-12-164 (2012).
- 7 Cai, Y., Zhuang, X., Gao, C., Wang, X. & Jiang, L. The Arabidopsis Endosomal Sorting Complex Required for Transport III Regulates Internal Vesicle Formation of the Prevacuolar Compartment and Is Required for Plant Development. *Plant Physiology* **165**, 1328-1343, doi:10.1104/pp.114.238378 (2014).
- 8 Wang, H. J. *et al.* VPS36-Dependent Multivesicular Bodies Are Critical for Plasmamembrane Protein Turnover and Vacuolar Biogenesis. *Plant Physiol* **173**, 566-581, doi:10.1104/pp.16.01356 (2017).
- 9 Bilodeau, P. S., Winistorfer, S. C., Kearney, W. R., Robertson, A. D. & Piper, R. C. Vps27-Hse1 and ESCRT-I complexes cooperate to increase efficiency of sorting ubiquitinated proteins at the endosome. *The Journal of cell biology* **163**, 237-243, doi:10.1083/jcb.200305007 (2003).
- 10 Katzmann, D. J., Babst, M. & Emr, S. D. Ubiquitin-dependent sorting into the multivesicular body pathway requires the function of a conserved endosomal protein sorting complex, ESCRT-I. *Cell* **106**, 145-155, doi:S0092-8674(01)00434-2 [pii] (2001).
- 11 Teo, H. *et al.* ESCRT-I core and ESCRT-II GLUE domain structures reveal role for GLUE in linking to ESCRT-I and membranes. *Cell* **125**, 99-111, doi:10.1016/j.cell.2006.01.047 (2006).
- 12 Wollert, T., Wunder, C., Lippincott-Schwartz, J. & Hurley, J. H. Membrane scission by the ESCRT-III complex. *Nature* **458**, 172-177 (2009).
- 13 Babst, M., Katzmann, D. J., Estepa-Sabal, E. J., Meerloo, T. & Emr, S. D. ESCRT-III: An endosome-associated heterooligomeric protein complex required for MVB sorting. *Developmental Cell* **3**, 271-282, doi:Doi 10.1016/S1534-5807(02)00220-4 (2002).
- 14 Tang, S. *et al.* ESCRT-III activation by parallel action of ESCRT-I/II and ESCRT-0/Bro1 during MVB biogenesis. *Elife* **5**, doi:10.7554/eLife.15507 (2016).
- 15 Richardson, L. G. *et al.* Protein-Protein Interaction Network and Subcellular Localization of the Arabidopsis Thaliana ESCRT Machinery. *Front Plant Sci* **2**, 20, doi:10.3389/fpls.2011.00020 (2011).



- 16 Herce, H. D., Deng, W., Helma, J., Leonhardt, H. & Cardoso, M. C. Visualization and targeted disruption of protein interactions in living cells. *Nat Commun* **4**, 2660, doi:10.1038/ncomms3660 (2013).
- 17 Kubala, M. H., Kovtun, O., Alexandrov, K. & Collins, B. M. Structural and thermodynamic analysis of the GFP:GFP-nanobody complex. *Protein Sci* **19**, 2389-2401, doi:10.1002/pro.519 (2010).
- 18 Künzli, F., Frühholz, S., Fäßler, F., Li, B. & Pimpl, P. Receptor-mediated sorting of soluble vacuolar proteins ends at the trans-Golgi network/early endosome. *Nature Plants* **2**, 16017, doi:10.1038/nplants.2016.17 (2016).
- 19 Gao, C. *et al.* A unique plant ESCRT component, FREE1, regulates multivesicular body protein sorting and plant growth. *Curr Biol* **24**, 2556-2563, doi:10.1016/j.cub.2014.09.014 (2014).
- 20 Isono, E. *et al.* The deubiquitinating enzyme AMSH3 is required for intracellular trafficking and vacuole biogenesis in *Arabidopsis thaliana*. *The Plant cell* **22**, doi:10.1105/tpc.110.075952 (2010).
- 21 Bolte, S. *et al.* FM-dyes as experimental probes for dissecting vesicle trafficking in living plant cells. *J Microsc* **214**, 159-173 (2004).
- 22 Wang, J., Ding, Y., Zhuang, X., Hu, S. & Jiang, L. Protein Co-localization Studies: Issues and Considerations. *Mol Plant* **9**, 1221-1223, doi:10.1016/j.molp.2016.05.011 (2016).
- 23 Lavy, M. & Yalovsky, S. Association of *Arabidopsis* type-II ROPs with the plasma membrane requires a conserved C-terminal sequence motif and a proximal polybasic domain. *Plant J* **46**, 934-947, doi:10.1111/j.1365-313X.2006.02749.x (2006).
- 24 Hierro, A. *et al.* Structure of the ESCRT-II endosomal trafficking complex. *Nature* **431**, 221-225, doi:10.1038/nature02914 (2004).
- 25 Guilliams, T. *et al.* Nanobodies Raised against Monomeric alpha-Synuclein Distinguish between Fibrils at Different Maturation Stages. *Journal of Molecular Biology* **425**, 2397-2411, doi:10.1016/j.jmb.2013.01.040 (2013).
- 26 Frühholz, S., Fäßler, F., Kolukisaoglu, Ü. & Pimpl, P. Nanobody-triggered lockdown of VSRs reveals ligand reloading in the Golgi. *Nature Communications* **9**, 643, doi:10.1038/s41467-018-02909-6 (2018).
- 27 Hamers-Casterman, C. *et al.* Naturally occurring antibodies devoid of light chains. *Nature* **363**, 446-448, doi:10.1038/363446a0 (1993).
- 28 Dmitriev, O. Y., Lutsenko, S. & Muyldermans, S. Nanobodies as Probes for Protein Dynamics in Vitro and in Cells. *J Biol Chem* **291**, 3767-3775, doi:10.1074/jbc.R115.679811 (2016).
- 29 Harmansa, S., Alborelli, I., Bieli, D., Caussin, E. & Affolter, M. A nanobody-based toolset to investigate the role of protein localization and dispersal in *Drosophila*. *Elife* **6**, doi:10.7554/eLife.22549 (2017).
- 30 Steeland, S., Vandenbroucke, R. E. & Libert, C. Nanobodies as therapeutics: big opportunities for small antibodies. *Drug Discov Today*, doi:10.1016/j.drudis.2016.04.003 (2016).
- 31 Campsteijn, C., Vietri, M. & Stenmark, H. Novel ESCRT functions in cell biology: spiraling out of control? *Current Opinion in Cell Biology* **41**, 1-8, doi:<http://dx.doi.org/10.1016/j.ceb.2016.03.008> (2016).
- 32 Irion, U. & St Johnston, D. bicoid RNA localization requires specific binding of an endosomal sorting complex. *Nature* **445**, 554-558,

- doi:[http://www.nature.com/nature/journal/v445/n7127/suppinfo/nature05503\\_S1.html](http://www.nature.com/nature/journal/v445/n7127/suppinfo/nature05503_S1.html) (2007).
- 33 Jimenez, A. J. *et al.* ESCRT machinery is required for plasma membrane repair. *Science* **343**, 1247136, doi:10.1126/science.1247136 (2014).
- 34 Wehman, Ann M., Poggioli, C., Schweinsberg, P., Grant, Barth D. & Nance, J. The P4-ATPase TAT-5 Inhibits the Budding of Extracellular Vesicles in *C. elegans* Embryos. *Current Biology* **21**, 1951-1959, doi:<https://doi.org/10.1016/j.cub.2011.10.040> (2011).
- 35 Nabhan, J. F., Hu, R., Oh, R. S., Cohen, S. N. & Lu, Q. Formation and release of arrestin domain-containing protein 1-mediated microvesicles (ARMMs) at plasma membrane by recruitment of TSG101 protein. *Proceedings of the National Academy of Sciences* **109**, 4146-4151, doi:10.1073/pnas.1200448109 (2012).
- 36 Korbei, B. *et al.* Arabidopsis TOL Proteins Act as Gatekeepers for Vacuolar Sorting of PIN2 Plasma Membrane Protein. *Current Biology* **23**, 2500-2505, doi:10.1016/j.cub.2013.10.036 (2013).
- 37 Hawryluk, M. J. *et al.* Epsin 1 is a Polyubiquitin-Selective Clathrin-Associated Sorting Protein. *Traffic* **7**, 262-281, doi:10.1111/j.1600-0854.2006.00383.x (2006).
- 38 Gao, C. J. *et al.* A Unique Plant ESCRT Component, FREE1, Regulates Multivesicular Body Protein Sorting and Plant Growth. *Current Biology* **24**, 2556-2563, doi:10.1016/j.cub.2014.09.014 (2014).
- 39 Babst, M., Katzmann, D. J., Snyder, W. B., Wendland, B. & Emr, S. D. Endosome-associated complex, ESCRT-II, recruits transport machinery for protein sorting at the multivesicular body. *Developmental Cell* **3**, 283-289, doi:S1534580702002198 [pii] (2002).
- 40 Shahriari, M. *et al.* The Arabidopsis ESCRT protein-protein interaction network. *Plant Mol Biol* **76**, doi:10.1007/s11103-011-9770-4 (2011).
- 41 Vermeer, J. E. M. *et al.* Visualization of PtdIns3P dynamics in living plant cells. *The Plant Journal* **47**, 687-700, doi:10.1111/j.1365-313X.2006.02830.x (2006).
- 42 Singh, Manoj K. *et al.* Protein Delivery to Vacuole Requires SAND Protein-Dependent Rab GTPase Conversion for MVB-Vacuole Fusion. *Current Biology* **24**, 1383-1389, doi:<https://doi.org/10.1016/j.cub.2014.05.005> (2014).

## Acknowledgments

We thank Diana Vranjkovic and Richard Gavidia for technical help. The financial support of the Deutsche Forschungsgemeinschaft (PI 769/1-2 and the Collaborative Research Centre SFB 1101 “Molecular Encoding of Specificity in Plant Processes” and TP A03) and the Deutscher Akademischer Austauschdienst (Project 57057314 & 57219822) is gratefully acknowledged.

## Author contributions

F.F., J.S.E., C.G., S.F., L.J and P.P. designed and analysed the experiments. F.F., Y.Z., J.S.E. performed experiments. F.F. and P.P. wrote the manuscript.

## Additional information

Correspondence and requests for materials should be addressed to P.P.

## Competing interests

The authors declare no competing financial interests.

## Figure legends

**Figure 1. ESCRT-II is essential and localizes at the PM.** **a**, Schematic structure of the *VPS36* gene and position of the T-DNA insertion. **b-d**, *vps36-1* individuals are not viable. Representative *vps36-1 Arabidopsis* seedlings compared to Col-0 of the same age (**b,c**). **d**, germination analysis of *vps36-1/+* offspring compared to Col-0. n = 1244, 129. **e,f**, *pVPS36::VPS36-GFP* rescues the *vps36-1* phenotype, 5 representative seedlings are shown in comparison to Col-0. n = 123, 178. **g,h**, *pVPS36* driven VPS36-GFP in the *vps36-/-* background (see **e**) co-localizes with FM4-64 at the PM and occasionally in punctae (highlighted by triangles, punctae solely labelled by FM4-64 are highlighted by arrows). **i,j**, biochemical characterization of generated antisera against the ESCRT-II subunits VPS36, VPS25 and VPS22. Western blot analysis demonstrating binding capability of all raised antisera to denatured antigens (**i**). Amounts of antigen is given in ng above the blot of the respective antiserum. **j**, immunoprecipitation analysis demonstrating binding capability of all antisera to native antigens. HA-tagged ESCRT-II subunits were expressed in tobacco protoplasts and total protein extracts (T) were subjected to immunoprecipitation (IP) using the antibodies as indicated. Uncoated beads (IP B) and extracts from mock transfected cells were used as controls. Precipitates were probed with  $\alpha$ HA-POD antibodies. **k-m**, immuno-gold localization of endogenous ESCRT-II subunits in *Arabidopsis* Col-0 roots using the respective antisera. Endogenous VPS36, VPS22 and VPS25 localize at the PM (10 nm gold particles are highlighted by arrowheads). **n**, co-expressed fluorescent ESCRT-II fusion proteins co-localize at the PM in tobacco mesophyll protoplasts. If not stated otherwise: scale bars, 10  $\mu$ m. Yellow line in the merged image indicates the region of interest (ROI) used for the line intensity profile of each fluorophore. Overlapping peaks of the fluorophores in the line intensity profile demonstrate co-localization.

**Figure 2. VPS36 recruits VPS22 and VPS25 to the PM.**

CLSM-based localization analysis of co-expressed fluorescent fusion proteins in tobacco mesophyll protoplasts. **a**, VPS36-GFP co-localizes with the PM marker Box-RFP at the PM. **b-e**, PM localization of VPS22 and VPS25 strictly depends on the presence of VPS36. VPS22-RFP alone is cytosolic when co-expressed with the PM marker Box-GFP (**b**) but is recruited to the PM in the presence of VPS36-GFP (**c**). Non-overlapping peaks of the fluorophores in the line intensity profile of the ROI shown in the enlargement demonstrate differential localization, while overlapping peaks demonstrate co-localization (compare **b** to **c**). The same is true for VPS25-RFP, respectively (**d,e**). **f**, FRET-FLIM analysis demonstrating interaction between co-expressed ESCRT-II subunits. Co-expression of VPS22-RFP or VPS25-RFP but not of cytRFP causes reduction of VPS36-GFP fluorescence lifetime. **g,h**, CLSM images showing both control protoplasts from the false color images given in (**f**), expressing VPS36-GFP alone (**g**) or in co-expression with cytRFP (**h**). Scale bars, 10  $\mu$ m. Yellow lines indicate ROIs used for line intensity profiles. FLIM charts depict the mean  $\pm$  SD fluorescence lifetime of  $n = 10$  measurements per group. Significance was calculated using Dunn's method for multiple comparisons with a single control (\*\*,  $p < 0.01$ ; \*\*\*,  $p < 0.001$  compared with the donor only control; NS, not significant)

**Figure 3. The C-terminus of VPS36 is necessary for the interaction with VPS22 and VPS25.**

**a-c**, FRET-FLIM analysis showing that deletion of the 33 C-terminal residues of VPS36 abolishes the VPS25-RFP dependent but not the VPS22-RFP dependent decrease in fluorescence lifetime of VPS36 $\Delta$ 33-GFP. **d-f**, deletion of 132 C-terminal residues abolishes the VPS22-RFP dependent decrease in fluorescence lifetime of VPS36 $\Delta$ 132-GFP. Reduction of lifetime is triggered by nanobody-mediated attachment of RFP upon co-expression of RFP-Nb<sub>G</sub> as positive control. **g-i**, VPS25-GFP fluorescence lifetime is reduced by VPS22-RFP or VPS36-RFP expression. Co-expression of cytRFP was used as non-interactor in negative controls, showing no effect on fluorescence lifetime of respective donors. **a,d,g**, representation of the complete FRET-FLIM data sets as bar charts. **b,e,h**, representative false color images, indicating measured GFP lifetimes. **c,f,i**, respective CLSM images of the protoplasts shown in **b,e,h**. Scale bars, 10  $\mu$ m. FLIM charts depict the mean  $\pm$  SD fluorescence lifetime of  $n = 10$  measurements per group. Significance was calculated using Dunn's method for multiple comparisons with a single control (\*\*,  $p < 0.01$ ; \*\*\*,  $p < 0.001$  compared with the donor only control; NS, not significant)

**Figure 4. Application of indirect *in vivo* precipitation (iVIP) to determine ESCRT-II stoichiometry.** **a**, schematic representation of the intra-complex interactions of ESCRT-II subunits demonstrated in this work. **b**, the putative ESCRT-II conformations explaining these results are depicted on the left. Discrimination between these models via standard co-localization studies is not feasible, since expression of the involved molecules in both cases leads to co-localization at the PM. FRET-FLIM measurements are also impaired: The upper putative conformation does not allow for FRET to occur. In the lower putative conformation 50% of donors, namely VPS25-GFP, are in complexes not containing an acceptor. This would largely mask possible FRET effects occurring in complexes containing a donor and an acceptor. **c,d**, CNX-NbG mediated recruitment of ESCRT-II complexes to the ER via an nanobody–epitope interaction with VPS25-GFP allows for discriminable outcomes: If ESCRT-II contains only one VPS25 moiety, no corecruitment of VPS25-RFP to the ER occurs, resulting in an VPS25-GFP and VPS22-BFP labeled ER (**c**). If ESCRT-II contains two VPS25 moieties VPS25-RFP is corecruited with the VPS25-GFP containing complexes to the ER resulting in an VPS25-GFP, VPS22-BFP and VPS25-RFP labeled ER (**d**). **e**, symbol legend for the panels mentioned above. **f**, schematic representation of spNB<sub>SYN</sub>-HRP. **g,h**, biochemical characterization of spNB<sub>SYN</sub>-HRP. Western blot analysis demonstrating binding capability of spNB<sub>SYN</sub>-HRP to purified denatured antigens (**g**). Amounts of antigen is given in ng above the blot. Western blot analysis showing detection of denatured antigens either extracted from protoplast (**h** RFP-TMD23-SYN, cytRFP-SYN) or precipitated from the respective culture medium (**h** secRFP-SYN).

**Figure 5. VPS22 and VPS36 co-precipitate with VPS25 *in vivo*.** **a,b**, cytosolic GFP but not cytosolic RFP is recruited to the surface of the ER when CNX-Nb<sub>G</sub> is co-expressed. **c,d**, the same is true for VPS25-GFP and VPS25RFP, respectively. **e,f**, VPS22-RFP and VPS36-RFP are recruited to the surface of the ER if CNX-Nb<sub>G</sub> and VPS25-GFP are co-expressed. Inlays show optical sections of nuclei and the surrounding nuclear envelopes (**a-f**). **g**, schematic representation of the predicted effect caused by co-expression of CNX-Nbs, VPS25-GFP and VPS36-RFP on the localization of the ER. **h**, co-expression of the constructs shown in **g** forces the ER into close proximity of the PM leading to a laminar ER phenotype. Scale bars, 10  $\mu$ m. Yellow lines indicate ROIs used for line intensity profiles.

### Figure 6. ESCRT-II contains two VPS25 moieties

**a-c**, if VPS22-BFP and VPS36-SYN are co-expressed CNX-NBG mediated ER-recruitment of VPS25-GFP coprecipitates VPS25-RFP. **d-j**, this is not the case if either VPS22-BFP or VPS36-SYN are not co-expressed. **a,d,g**, schematic representation of the expressed proteins and formed ESCRT-II complexes explaining the observed fluorescence patterns. **b,e,h**, cortical sections of protoplast expressing the indicated constructs. Lamellar ER patterns indicate expression of VPS36-SYN (**b,h**). **c,f,j**, equatorial sections of those protoplasts. Inlays show nuclei and surrounding nuclear envelopes. Line intensity plots indicate, that co-localization of VPS25-GFP and VPS25-RFP only occurs if VPS22-BFP and VPS36-SYN are co-expressed, this corresponds to the ER phenotype (compare to **a,d,g**). **i**, Western blot analysis detecting VPS36-SYN with spNB<sub>SYN</sub>-HRP. Sample labels correspond to the names of the panels, which explain the fluorescence patterns (**a,d,g**). Scale bars, 10  $\mu$ m. Yellow lines indicate ROIs used for line intensity profiles.

### Supplementary Figure 1. Protein-protein interactions can attach cisternal ER to the PM.

**a**, PM marker Box-RFP does not co-localize with ER marker RFP-HDEL. **b,c**, co-expression of CNX-NBG induces partial co-localization. Co-localization can only be observed in cortical lamellar cisternae, but not in reticular ER structures. **d,e,f**, the same can be observed for VPS36-GFP and RFP-HDEL. **g,h**, VPS36-GFP, but not ER marker BFP-CNX, co-localizes with FM4-64 at the PM. **i,j**, if also CNX-Nb<sub>G</sub> is co-expressed VPS36-GFP and BFP-CNX both co-localize with FM4-64 at the PM. **a-f**, cortical optical sections. **g-j**, equatorial optical sections. **h,j**, rotated enlargements of protoplasts shown in **g,i**, respectively. Lamella vary in size and shape, but can be clearly identified as such (compare **b,c,e,f** to **a,d**). Scale bars, 10  $\mu$ m. Yellow lines indicate ROIs used for line intensity profiles.

### Supplementary Figure 2. Localization in the nuclear lumen and the nuclear envelope are clearly distinguishable.

**a**, cytGFP is able to enter the nucleus. The GFP labeled nuclear lumen shows a completely different pattern in comparison to the RFP-HDEL labeled nuclear envelope. This is also evident in the line intensity plots showing sharp peaks for the RFP-HDEL and a plateau for the cytGFP. Scale bars, 10  $\mu$ m. Yellow lines indicate ROIs used for line intensity profiles.

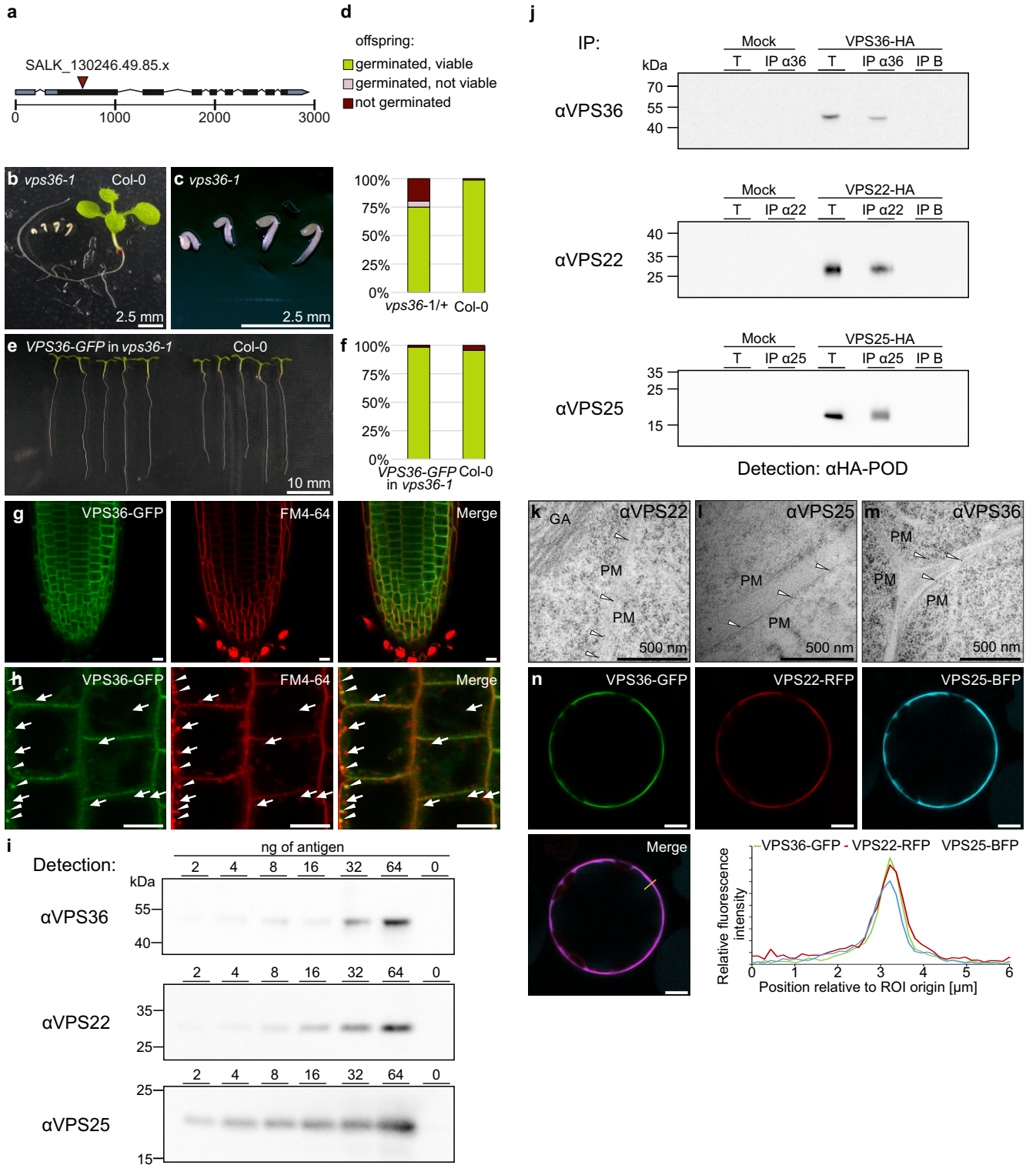
**Supplementary Figure 3. Attachment of cisternal ER to the PM does not impair ER functionality.** **a-d**, attachment of cisternal ER by co-expression of VPS36-GFP and CNX-NB<sub>G</sub> does not impair the export of soluble cargo from the ER. Vacuolar marker aleuRFP localizes to the vacuole and to dot-like structures representing MVBs independently of ER-PM attachment (compare **a,b** to **c,d**). **e-h**, iVIP mediated ER-PM attachment does still allow for ER export of membrane proteins. The cis-Golgi marker displays a punctate pattern when VPS36-GFP and CNX-NB<sub>G</sub> are co-expressed. The punctate pattern is comparable to the one produced by co-expression of ManI-RFP and VPS36-GFP (compare **e,f** to **g,h**). Equatorial optical sections (**a,c,e,g**) and cortical sections (**b,d,f,h**) are shown. Scale bars, 10  $\mu$ m.

**Supplementary Figure 4. Uncropped immunoblots.** **a**, biochemical characterization of generated antisera against the ESCRT-II subunits VPS36, VPS25 and VPS22 as shown (**1i**). Amounts of antigen is given in ng above the blot of the respective antiserum. **b**, immunoprecipitation analysis demonstrating binding capability of all antisera to native antigens as shown (**1j**). HA-tagged ESCRT-II subunits were expressed in tobacco protoplasts and total protein extracts (T) were subjected to immunoprecipitation (IP) using the antibodies as indicated. Uncoated beads (IP<sub>B</sub>) and extracts from mock transfected cells were used as controls. Precipitates were probed with  $\alpha$ HA-POD antibodies. **c,d**, biochemical characterization of spNB<sub>SYN</sub>-HRP as shown (**4f,g**). Western blot analysis demonstrating binding capability of spNB<sub>SYN</sub>-HRP to purified denatured antigens (**c**). Amounts of antigen is given in ng above the blot. Western blot analysis showing detection of denatured antigens either extracted from protoplast or precipitated from the respective culture medium (**d**). **e**, Western blot analysis detecting VPS36-SYN with spNB<sub>SYN</sub>-HRP as shown in (**6i**). Sample labels correspond to the names of the panels, which explain the fluorescence patterns (**6a,d,g**).

### **Supplementary Table 1. Cloning of expression vectors**

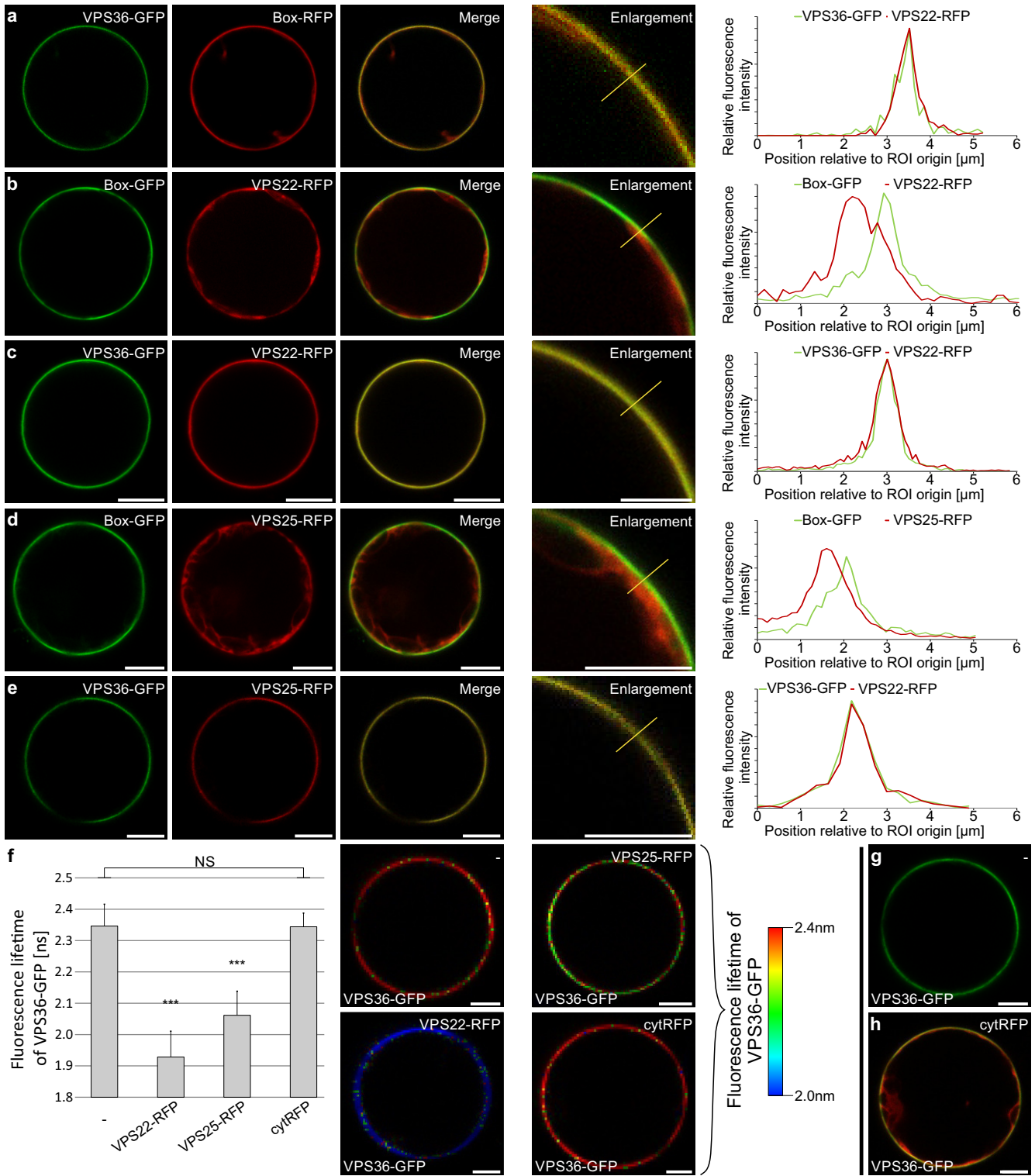
Composition/origin of vectors employed by this study.

Fäßler et al., Figure 1

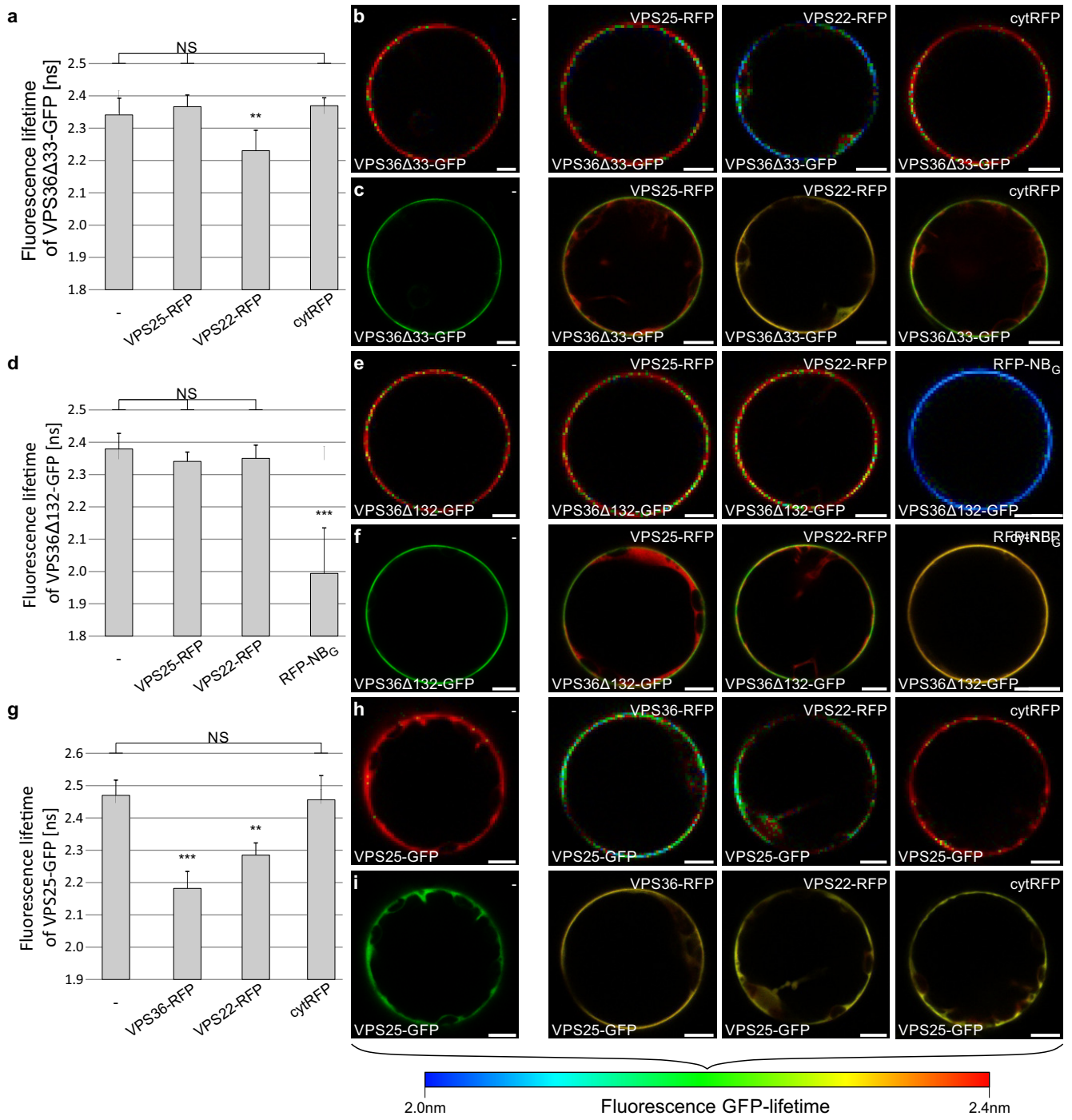




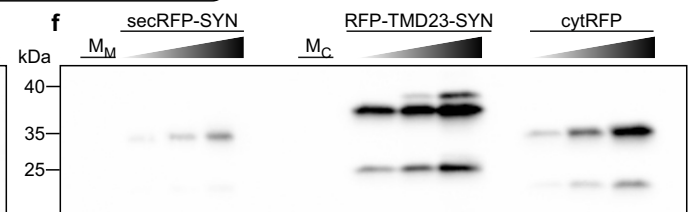
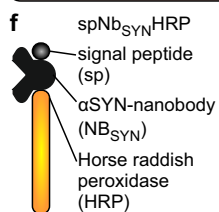
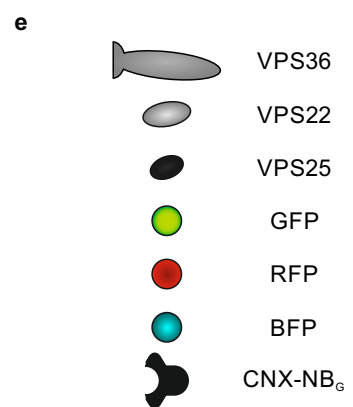
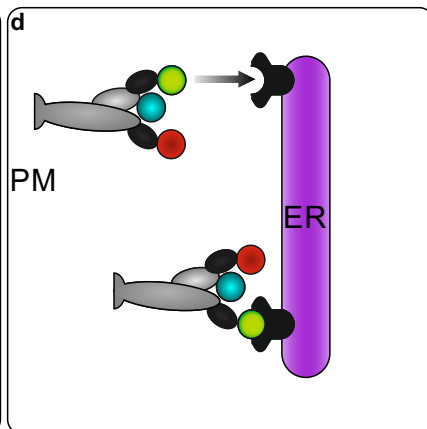
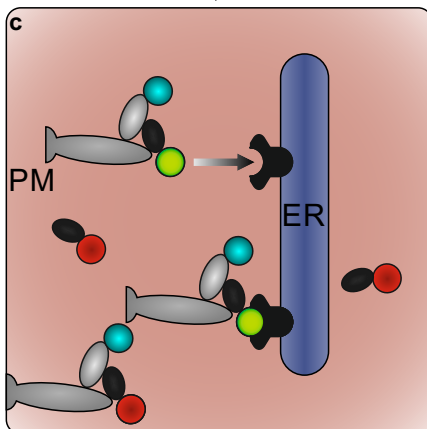
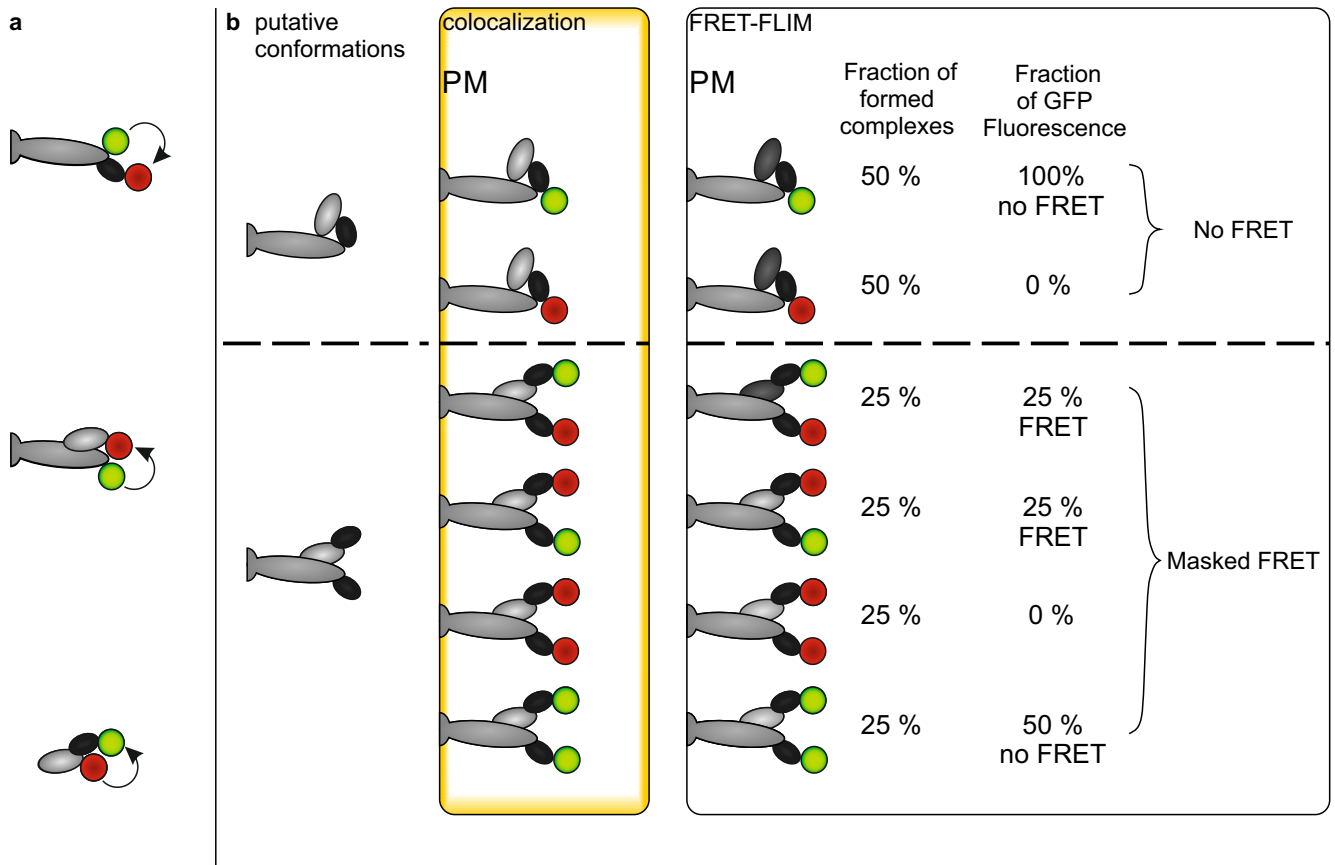
Fäßler et al., Figure 2



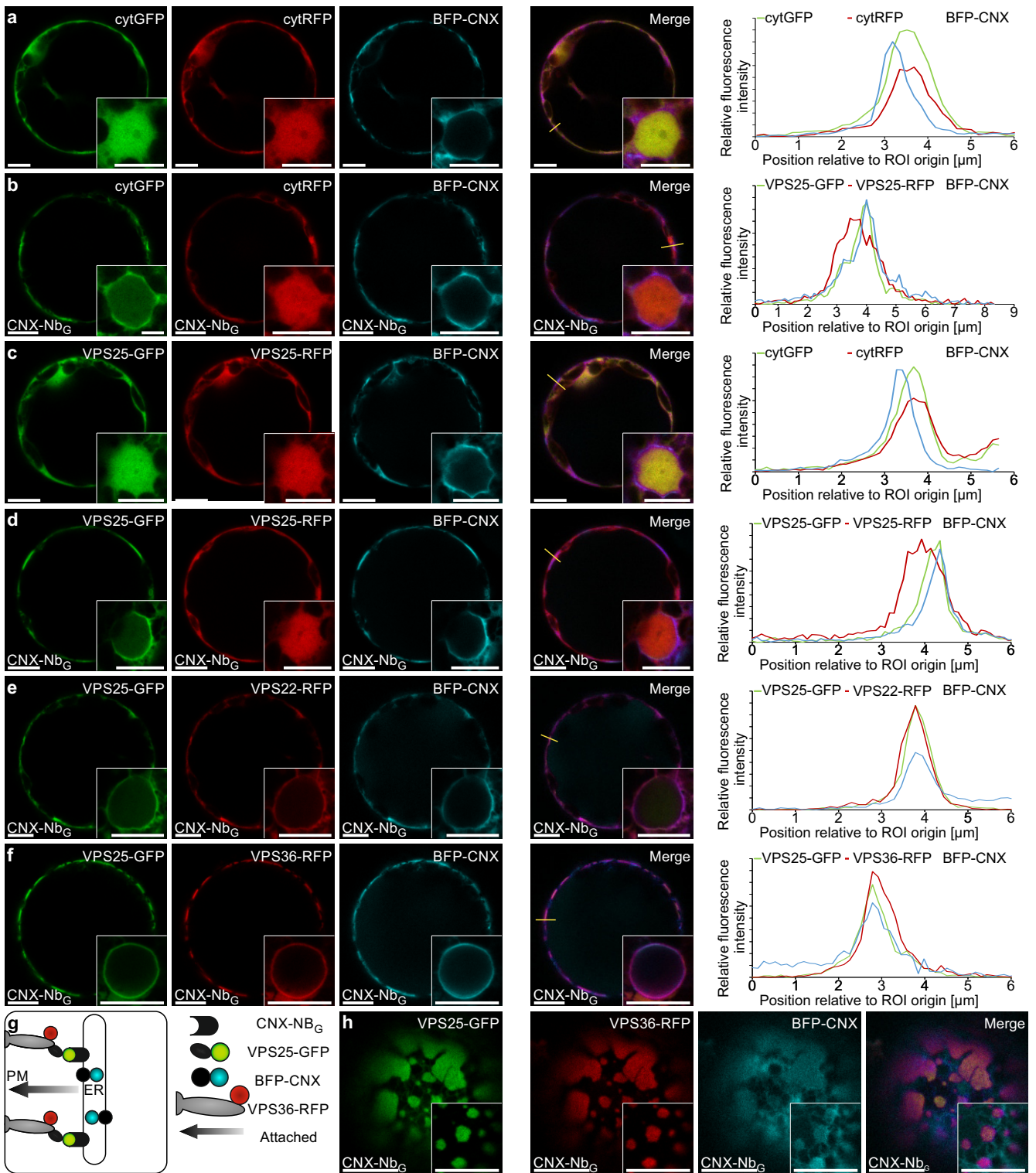
Fäßler et al., Figure 3



Fäßler et al., Figure 4

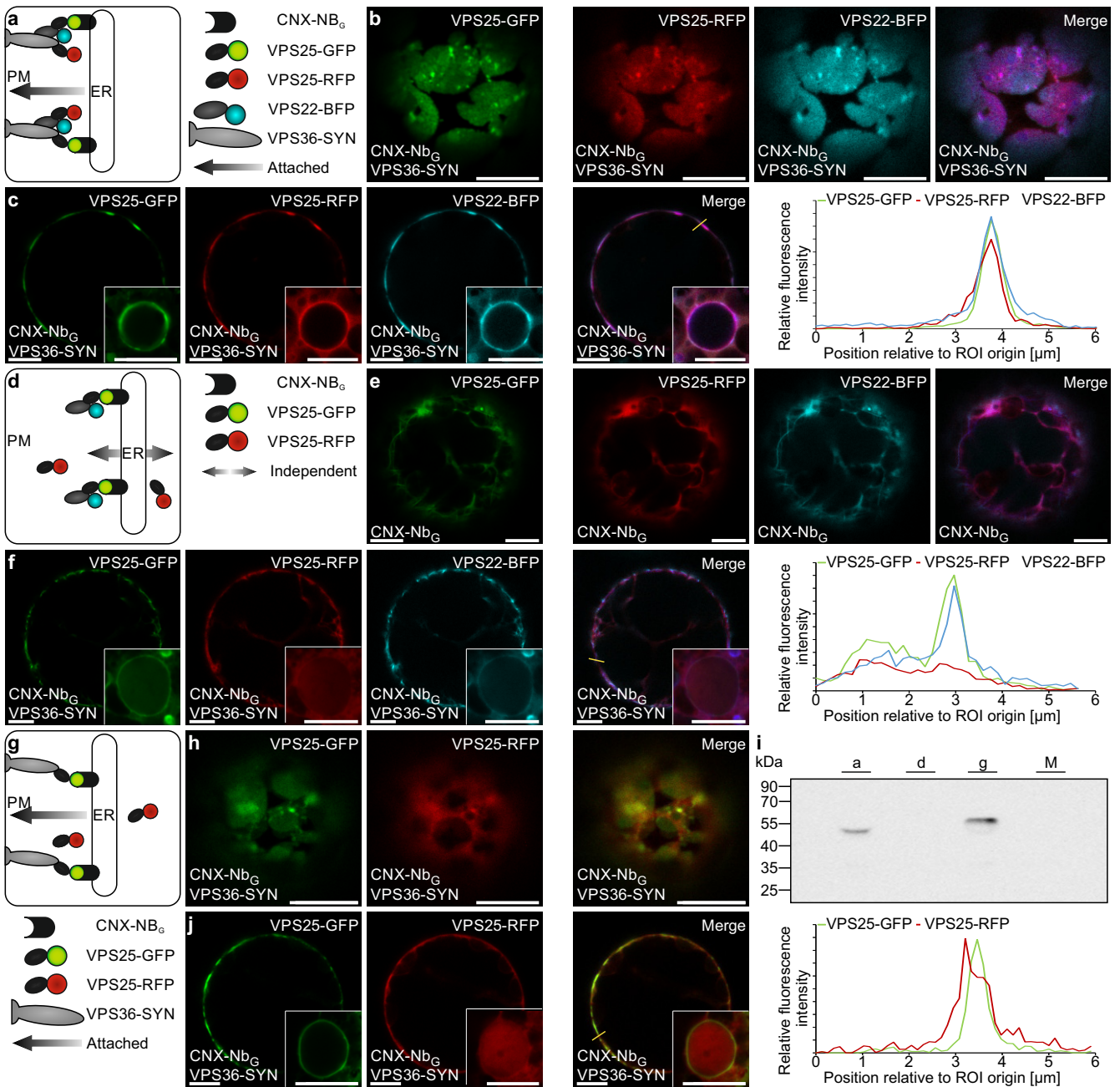


Fäßler et al., Figure 5

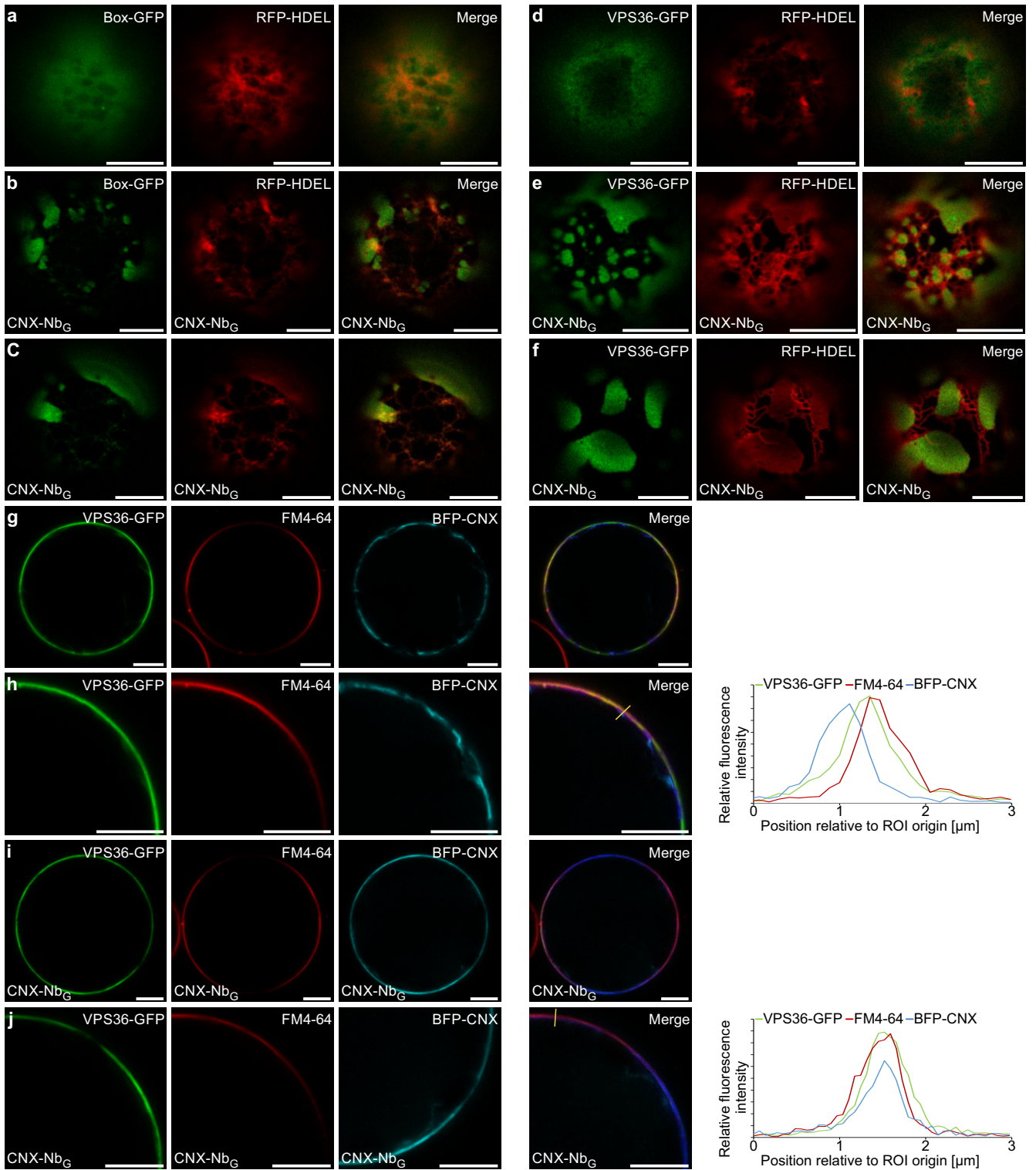




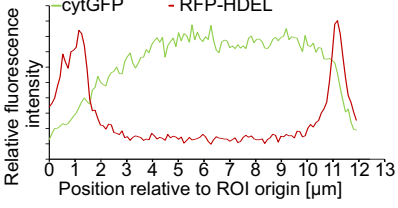
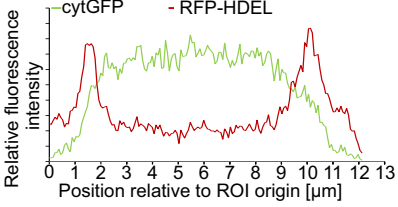
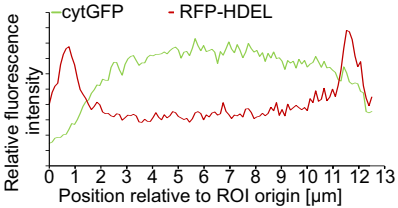
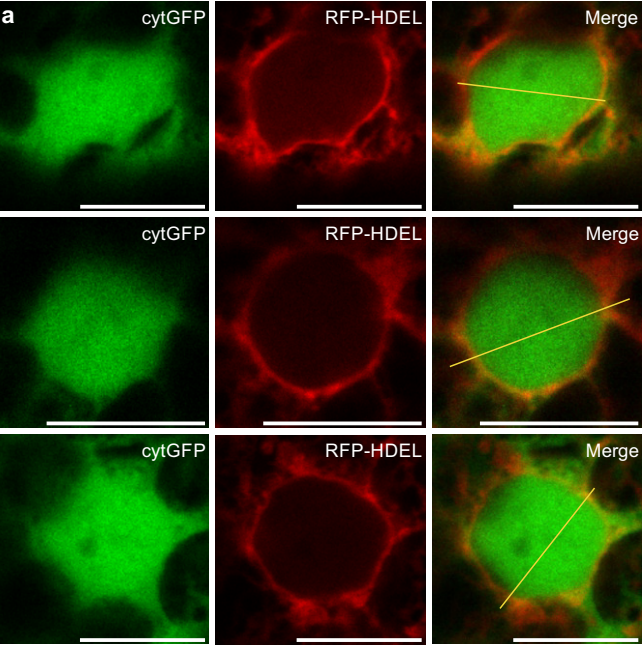
Fäßler et al., Figure 6



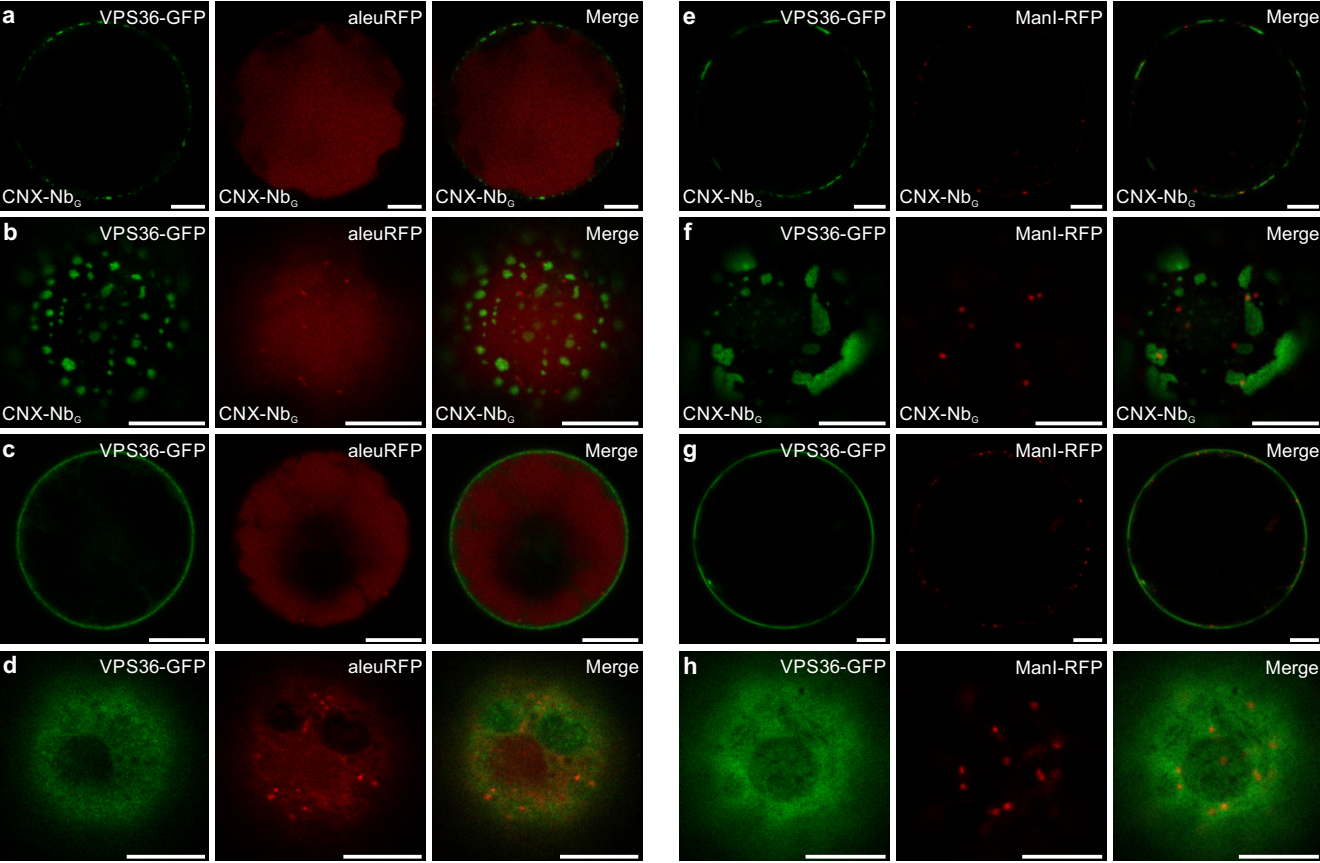
Fäßler et al., Supplementary Figure 1



Fäßler et al., Supplementary Figure 2

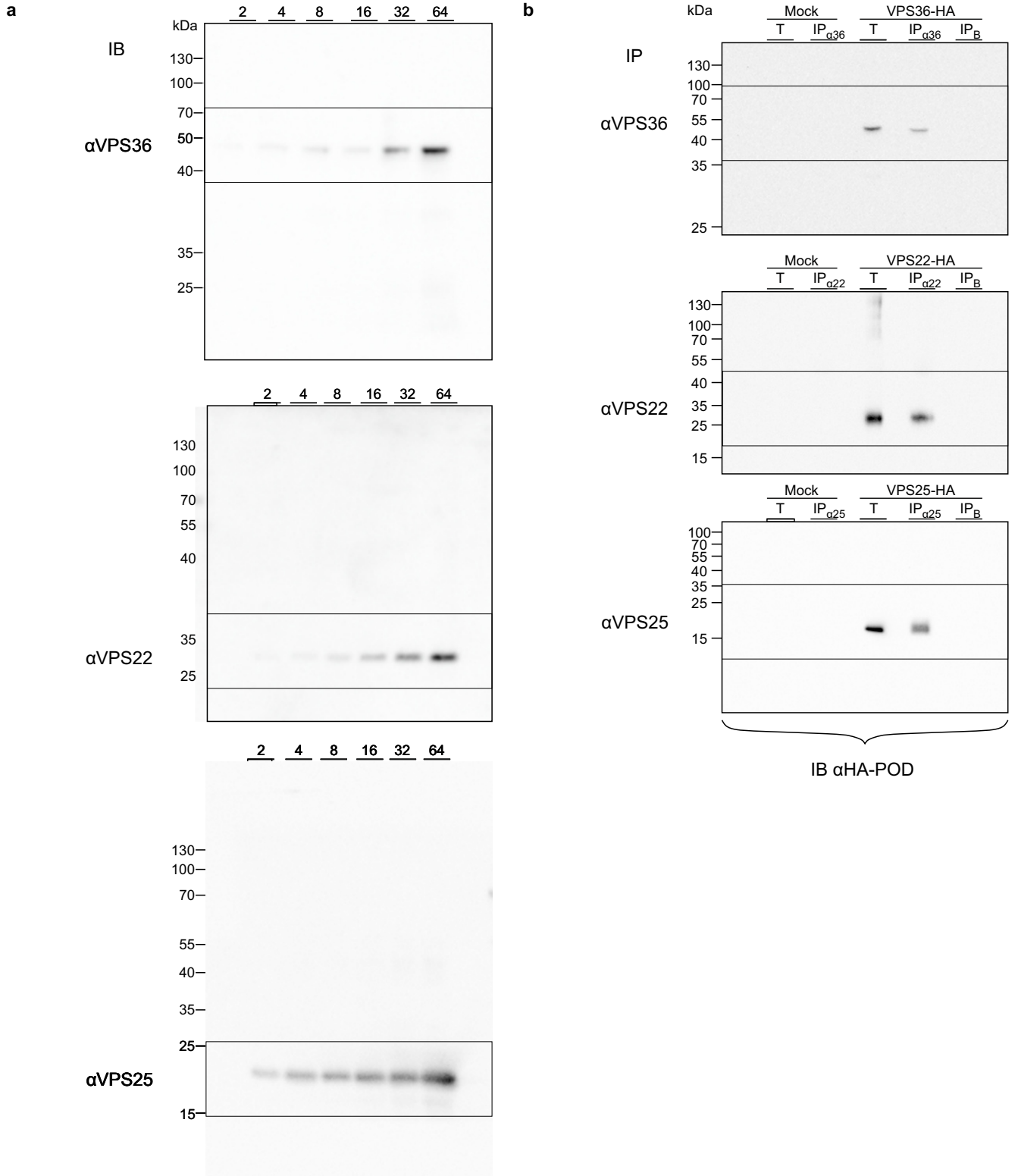


Fäßler et al., Supplementary Figure 3

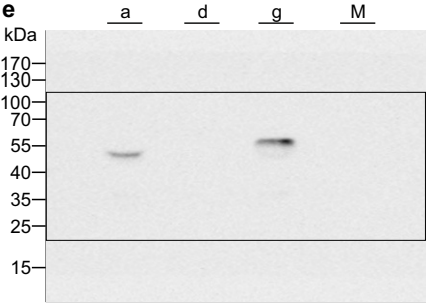
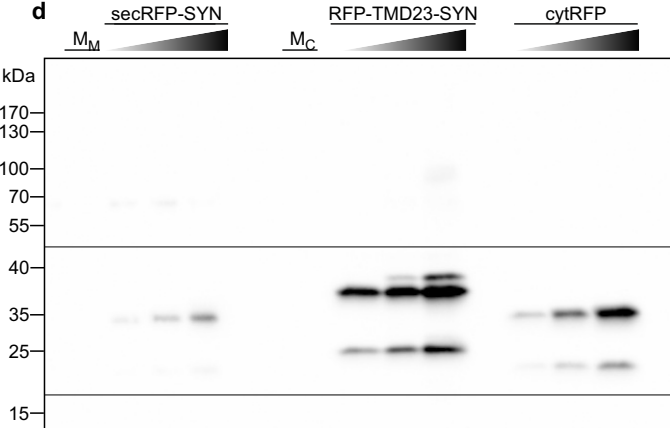
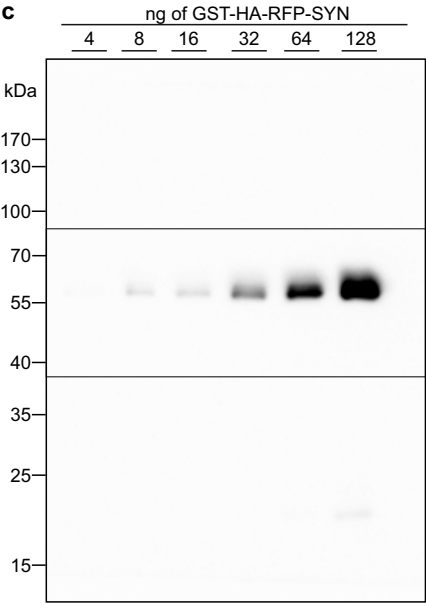




Fäßler et al., Supplementary Figure 4



Fäßler et al., Supplementary Figure 4



IB αHA-POD

Fäßler et al., Table 1

Construct	Primer	Primer Sequence	Template	Recipient vector
<b>GST-VPS22</b>	VPS22_EcoRI_S	AGACTAGAAATTCATGCGACGACG ACCAGGAAT	cDNA prepared from <i>Arabidopsis thaliana</i> seedlings	pGEX-4T-3
	VPS22_NotI_AS	AGTCTAGCGGCCGCTTAAGTATCA GATCCGATGG		cut <u>NotI/EcoRI</u>
<b>GST-VPS25</b>	VPS25_EcoRI_S	AGACTAGAAATTCATGCAGAAATT GGCTGATTTTC	cDNA prepared from <i>Arabidopsis thaliana</i> seedlings	pGEX-4T-3
	VPS25_NotI_AS	AGTCTAGCGGCCGCTCAGACAGA GAACTTGACGC		cut <u>NotI/EcoRI</u>
<b>GST-VPS36</b>	VPS36_EcoRI_S	AGACTAGAAATTCATGGCTAGTGG AAGCAGCAG	cDNA prepared from <i>Arabidopsis thaliana</i> seedlings	pGEX-4T-3
	VPS36_NotI_AS	AGTCTAGCGGCCGCTCATAACAGA CAACAAACTGG		cut <u>NotI/EcoRI</u>
<b>8His-VPS22-MYC</b>	8His-VPS22_NcoI_S	GATATACCATGGGTATCATCACC ACCACCACCATCATCTCGAGATGC GACGACGACC	GST-VPS22 (see above);	pET-28b
	VPS22-MYC_SalI_AS	GATCTGATACTGGCGGCCGCGAA CAAAAACCTTATTTCTGAAGAGGAT CTTTAAGTCGACAAGCTT		cut <u>NcoI/SalI</u>
<b>8HIS-VPS25-FLAG</b>	8HIS-VPS25_NcoI_S	GAGGACCCATGGGTATCATCAC CACCACCACCATCATCAGAAATTG GCTGATTTCAAGCTTCCTCAA	GST-VPS25 (see above);	pET-28b
	VPS25-FLAG_SalI_AS (new)	GTCCTCGTCGACTTACTTGTGCTC GTCGCTTTATAATCGACAGAGAA CTTGACGCCCTTCATCATCTGC		cut <u>NcoI/SalI</u>
<b>8His-VPS36-HA</b>	8HIS-VPS36_NcoI_S	GAGGACCCATGGGTATCATCAC CACCACCACCATCATGCTAGTGGA AGCAGCAGCATCGCAATCGGT	GST-VPS36 (see above);	pET-28b
	VPS36-HA_SalI_AS	GTCCTCGTCGACTTAAAGCATAATC AGGAACATCATAA		cut <u>NcoI/SalI</u>
<b>VPS36-mEGFP</b>	VPS36_XhoI_S	GAGGATCTCGAGATGGCTAGTGG AAGCAGCAG	GST-VPS36 (see above);	pFF15 (Künzl, 2016);
	VPS36_NotI_AS	CTCCTAGCGGCCGCTACAGACA ACAAACTGGTCGCTTTG		cut <u>SpeI/XhoI</u>
	GFP_NotI_S	GGAAGAGCGGCCGCTGGTGAGC AAGGGC	pSF72 (Frühholz, 2017)	
	GFP_STOP_SpeI_AS	ATCCTCACTAGTTTACTTGTACAG CTCGTCCATGC		
<b>VPS36Δ33-GFP</b>	VPS36_XhoI_S	GAGGATCTCGAGATGGCTAGTGG AAGCAGCAG	GST-VPS36 (see above);	VPS36-mEGFP (see above)
	pVPS36Δ33_XhoI_AS	GTCCTCTCGGCCGCCATAGAAT CGAAGCCCATCTG		cut <u>NotI/XhoI</u>
<b>VPS36Δ66-GFP</b>	VPS36_XhoI_S	GAGGATCTCGAGATGGCTAGTGG AAGCAGCAG	GST-VPS36 (see above);	VPS36-mEGFP (see above)
	pVPS36Δ66_NotI_AS	GTCCTCTCGGCCGCCAAAGCT GCATCCTAGCAG		cut <u>NotI/XhoI</u>
<b>VPS36Δ99-GFP</b>	VPS36_XhoI_S	GAGGATCTCGAGATGGCTAGTGG AAGCAGCAG	GST-VPS36 (see above);	VPS36-mEGFP (see above);
	pVPS36Δ99_NotI_AS	GTCCTCTCGGCCGCCCTTGT GGATGACCATCA		cut <u>NotI/XhoI</u>
<b>VPS36Δ132-GFP</b>	VPS36_XhoI_S	GAGGATCTCGAGATGGCTAGTGG AAGCAGCAG	GST-VPS36 (see above);	VPS36-mEGFP (see above)
	pVPS36Δ132_NotI_AS	GTCCTCTCGGCCGCCGAAATC AACTCTGTCCAC		cut <u>NotI/XhoI</u>
<b>pVPS36::VPS36-mEGFP</b>	pVPS36_EcoRI_S	AAAATGGAATTCATTTGATTTAATT G	GST-VPS36 (see above);	VPS36-mEGFP (see above)
	pVPS36_XhoI_AS	GTCCTCTCGAGGGAGACTCAATT CGGAAGCA		cut <u>XhoI/EcoRI</u>

<b>VPS36-RFP</b>	RFP_NotI_S	ATATTAGCGGCCGCATGGCCTCCT CCGAGGACG	pFF15 (Kuenzl, 2016);	VPS36-mEGFP (see above)
	RFP_STOP_SpeI_AS	CTGCAACTAGITTATGCTCCAGTA CTGTGGCGGC		cut <u>SpeI/NotI</u>
<b>VPS36-SYN</b>	p35S_EcoRI_S	GAGGACGAATTCAGGACTAATTGC ATC	VPS36-GFP (see above);	pSF72 (Frühholz, 2017)
	VPS36_NotI_AS	CTCCTAGCGGCCGCCTACAGACA ACAAACTGGTCGCTTTG		cut <u>NotI/EcoRI</u>
<b>VPS22-RFP</b>	VPS22_XhoI_S	GATGTA <del>CTCGAG</del> ATGCGACGACG ACCAGGAAT	GST-VPS22 (see above);	VPS36-RFP (see above)
	VPS22_NotI_AS	ATCCTC <del>GCGGCCGC</del> CAGTATCAG ATCCGATGGATG		cut <u>NotI/XhoI</u>
<b>VPS22-BFP</b>	mtagBFP_XhoI_S	GAGGACCTCGAGATGTCTGAACTT ATTAAGGA	PLUS: BFP2 codon-optimized and chemically synthesised	VPS22-RFP (see above)
	mtagBFP2-HA_SpeI_AS	GTCCTC <del>ACTAGIT</del> TAAGCATAATC AGGAACATCATAAGGATAATTCAA CTTATGTCCCAACTTAGAAGGAAG		cut <u>NotI/XhoI</u>
<b>VPS25-GFP</b>	VPS25_XhoI_S	GAGGATCTCGAGATGCAGAAATTG GCTGATTT	GST-VPS25 (see above);	VPS36-mEGFP (see above)
	VPS25_NotI_AS	GTCCTAGCGGCCGCAGACAGAGA ACTTGACGCCTTCATCA		cut <u>NotI/XhoI</u>
<b>VPS25-RFP</b>	VPS25_XhoI_S	GAGGATCTCGAGATGCAGAAATTG GCTGATTT	GST-VPS25 (see above);	VPS36-RFP (see above);
	VPS25_NotI_AS	GTCCTAGCGGCCGCAGACAGAGA ACTTGACGCCTTCATCA		cut <u>NotI/XhoI</u>
<b>VPS25-BFP</b>	mtagBFP_XhoI_S	GAGGACCTCGAGATGTCTGAACTT ATTAAGGA	PLUS: BFP2 codon-optimized and chemically synthesised	VPS25-RFP (see above)
	mtagBFP2-HA_SpeI_AS	GTCCTC <del>ACTAGIT</del> TAAGCATAATC AGGAACATCATAAGGATAATTCAA CTTATGTCCCAACTTAGAAGGAAG		cut <u>NotI/XhoI</u>
<b>Box-RFP</b>	RFP_ClaI_S	AGTCTAATCGATGGCCTCCTCCGA GGACGT	pFF15 (Kuenzl, 2016);	pDS09 (Scheuring, 2012)
	RFP_STOP_BamHI_AS	CTCGGCAGGATCCTCATGTCCA GTACTGTGGCGGC		cut <u>BamHI/ClaI</u>
<b>CNX-NbG</b>	p35S_EcoRI_S	GAGGACGAATTCAGGACTAATTGC ATC	pFF04 (Künzl, 2016);	pFF29 (Künzl, 2016);
	SP_NheI_AS	TTTTCTCCTACTGCTTTCTGCTAG CGGCATG		cut <u>KpnI/EcoRI</u>
	Lyso_NheI_S	ACTATTGCTAGCGGCATGAAGGTT TTTGGAAAGATGTGA	PLUS: Lysozyme codon-optimized and chemically synthesised	
	Lyso_NotI_AS	GCATATGCGGCCGCAAGTCTAC ATCCTCTAATCC		
	CNX_TMD-CT_NotI_S	ACAAGGGCGGCCGCGAACTGATT GAGAAAGC	pFF04 (Künzl, 2016);	
	CNX_TMD-CT_KpnI_AS	GTCCTCGGTACCATATCACGTCT CGGTTGCC		
<b>RFP-NbG</b>	RFP_ClaI_S	AGTCTAATCGATGGCCTCCTCCGA GGACGT	LBD-RFP-Nb (Künzl, 2016)	pFF04 (Künzl, 2016);
	NbG_STOP_BamHI_AS	TGCTTCGGATCCCTAATGATGATG ATGATGATGAGAAGAAACAGT		cut <u>BamHI/ClaI</u>
<b>BFP-CNX</b>	BFP2_NheI_S	CTTTCTGCTAGCGGCATGTCTGAA CTTATTAAGGA	PLUS: BFP2 codon-optimized and chemically synthesised	pFF04 (Künzl, 2016);
	BFP2_NotI_AS	CAGTTCGCGGCCGCCATTCAACTT ATGTCCCAACT		cut <u>NotI/NheI</u>
<b>spNbSYN-HRP</b>	HRP_NdeI_S	GAGGACCATATGATGCAGTTAACC CCTACATT	pUC19-HRP-C (Hartmann, 1992)	pFF04 (Künzl, 2016);
	HRP_STOP_BamHI_AS	GTCCTCGGATCCCTAAGAGTTGCT GTTGACCACTCTG		cut <u>NdeI/EcoRI</u>
	p35S_EcoRI_S	GAGGACGAATTCAGGACTAATTGC ATC	pSF64 (Frühholz, 2017)	
	NBD_NdeI_AS	GTCCTC <del>CATA</del> IGGCTGCTCACGGT CACCTGGG		

<b>cytRFP-SYN</b>	RFP_XhoI_S	GAGGATCTCGAGATGGCCTCTC CGAGGACGT	VPS25-RFP	VPS36-SYN (see above)
	RFP_NotI_AS	AGTCTAGCGGCCGCTGCTCCAG TACTGTGGCGGC		cut <u>NotI/XhoI</u>
<b>secRFP-SYN</b>	sp_ClaI_S	CTCTATATCGATGAGGCTTTGTAA ATTACAG	pFK13(Scheuring, 2012);	pSF74 (Frühholz, 2017);
	RFP_NotI_AS	AGTCTAGCGGCCGCTTAAGTATCA GATCCGATGG		cut <u>NotI/ClaI</u>
<b>RFP-TMD23-SYN</b>	sp_ClaI_S	CTCTATATCGATGAGGCTTTGTAA ATTACAG	pFK13 (Scheuring, 2012);	pSF74 (Frühholz, 2017);
	TMD23_NotI_AS	GTCCTCGCGGCCGCGCAGATCTCT TCCTGCCGACGA		cut <u>NotI/ClaI</u>
<b>GST-HA-RFP-SYN</b>	HA-RFP_EcoRI_S	ACGACTGAATTCCTATCCTTATGAT GTTCTGATTATGCTATGGCCTCC TCCGAGGACGTCATCA	RFP-TMD23-SYN (see above)	pGEX-4T-3
	SYN_SmaI_AS	AGTCGTCCGGGGCTAAGCCTCCG GTTCATAAT		cut <u>SmaI/EcoRI</u>
<b>GST-HA-RFP-SYN</b>	HA-RFP_EcoRI_S	ACGACTGAATTCCTATCCTTATGAT GTTCTGATTATGCTATGGCCTCC TCCGAGGACGTCATCA	RFP-TMD23-SYN (see above)	pGEX-4T-3
	SYN_SmaI_AS	AGTCGTCCGGGGCTAAGCCTCCG GTTCATAAT		cut <u>SmaI/EcoRI</u>
<b>cytGFP</b>	GFP_XhoI_S	GAGGACCTCGAGATGGTGAGCAA GGGC	VPS36-mEGFP (see above)	VPS36-mEGFP (see above)
	GFP_STOP_SpeI_AS	ATCCTCACTAGTTTACTTGTACAG CTCGTCCATGC		cut <u>SpeI/XhoI</u>

#### Markers

Box-GFP	Scheuring, 2012
RFP-HDEL	Künzl, 2016
aleuRFP	Künzl, 2016
ManI-RFP	Künzl, 2016

#### Accessions

GST	XXU13855
AtVPS22	NM_001341835
AtVPS25	NM_001341315
AtVPS36	NM_120574
mEGFP	BAQ19368
Box aus	NM_114673
Calnexin	NM_125573
HRP	J05552.1
SYN	XM_017008563
antiSYN	will be provided after publication
aleuRFP	U31094.1
antiGFP	KM396759
mTagBFP2	AIQ82697.1
mRFP	AF506027
Mani	XM_006584570